Functional characterization of Gpnmb in inflammatory and metabolic diseases

Dissertation

zur Erlangung des akademischen Grades
Doctor rerum naturalium
(Dr. rer. nat.)

eingereicht an der Lebenswissenschaftlichen Fakultät
der Humboldt-Universität zu Berlin

von

M.Sc., Bernadette Nickl

Präsidentin der Humboldt-Universität zu Berlin
Prof. Dr.-Ing. Dr. Sabine Kunst

Dekan der Lebenswissenschaftlichen Fakultät
Prof. Dr. Bernhard Grimm

Gutachter: Prof. Dr. Michael Bader
Prof. Dr. Karl Stangl
Prof. Dr. Thomas Sommer

Tag der mündlichen Prüfung: 28. Februar 2020

For Sayeeda

Summary

In 2018, the World Health Organization reported for the first time that "Overweight and obesity are linked to more deaths worldwide than underweight"[A]. Obesity increases the risk for the development of diabetes, atherosclerosis and cardiovascular diseases. Those metabolic diseases are associated with inflammation and the expression of **glycoprotein nonmetastatic melanoma protein b** (**Gpnmb**), a transmembrane protein that is expressed by macrophages and dendritic cells. We studied the role of Gpnmb in genetically- and diet-induced atherosclerosis as well as diet-induced obesity in *Gpnmb*-knockout and respective wildtype control mice. To this purpose, a mouse deficient in Gpnmb was created using Crispr-Cas9 technology.

Body weight and blood lipid parameters remained unaltered in both diseases. Gpnmb was strongly expressed in atherosclerotic lesion-associated macrophages. Nevertheless, the absence of Gpnmb did not affect the development of aortic lesion size. However, macrophage and inflammation markers in epididymal fat tissue were increased in *Gpnmb*-deficient mice. In comparison to atherosclerosis, the absence of Gpnmb elicited stronger effects in obesity. For the first time, we observed a positive influence of Gpnmb on insulin and glucose plasma levels. Obese *Gpnmb*-knockout mice displayed aggravated insulin resistance and liver fibrosis. The latter was associated with higher phosphorylated AKT levels and increased expression of lipogenic genes. Moreover, *Gpnmb*-knockout animals contained more macrophages in epididymal adipose tissue. Gpnmb was strongly expressed in adipose tissue macrophages in wildtype mice, suggesting an alleviating role of Gpnmb on adipose tissue inflammation.

This is corroborated by *in vitro* data where Gpnmb was mostly expressed in reparative macrophages stimulated with transforming growth factor β (TGFβ). However, this expression resulted only in a mild anti-inflammatory effect. Another important macrophage feature, autophagy, was not influenced by Gpnmb. This is surprising as Gpnmb expression, shedding and degradation was uniquely increased by bafilomycin. This is an inhibitor of the last step of autophagy and lysosomal degradation. Bafilomycin moreover altered the glycosylation of Gpnmb, which was highly variable throughout the study. Either bafilomycin-mediated Gpnmb induction might result from lysosomal overload or from a side effect of bafilomycin that is promotion of cell differentiation. This is supported by the observation that Gpnmb expression responded strongest to differentiation into mature macrophages. Differentiation from day 6 to day 7 *in vitro* increased *Gpnmb* transcript levels 100-fold, whereas treatment with TGFβ doubled and with bafilomycin tripled *Gpnmb* transcript levels in the same time span.

Taken together, Gpnmb expression is strongly induced in fully mature macrophages and can be further increased due to lysosomal inhibition. In obesity, the major risk factor for the development of diabetes type II, Gpnmb prevents the development of insulin resistance possibly by dampening adipose tissue inflammation.

[A] https://www.who.int/news-room/fact-sheets/detail/obesity-and-overweight

Zusammenfassung

Zum ersten Mal ist Übergewicht mit mehr Todesfällen weltweit verbunden als Untergewicht[B]. Übergewicht erhöht das Risiko für Diabetes, Arteriosklerose und Herz-Kreislauf-Erkrankungen. Diese gehen mit einer Entzündung und der Expression von **Glykoprotein nonmetastatic melanoma protein b** (**Gpnmb**) einher, einem Transmembranprotein, das hauptsächlich von Makrophagen und dendritschen Zellen exprimiert wird. Wir haben die Rolle von Gpnmb in genetisch- und ernährungsinduzierter Arteriosklerose sowie ernährungsinduzierter Adipositas bei Mäusen untersucht. Zu diesem Zweck wurden mit Hilfe der Crispr-Cas9-Technologie entsprechende Mauslinien ohne funktionales Gpnmb erzeugt.

Gpnmb-Knockout-Tiere zeigten ähnliches Körpergewicht und ähnliche Blutfettwerte in beiden Erkrankungen wie ihre Wildtyp-Kontrolltiere. Wie erwartet besaßen Makrophagen in arteriosklerotischen Läsionen eine hohe Expression von Gpnmb. Trotzdem war das Ausmaß der Aortenläsion in arteriosklerotischen *Gpnmb*-Knockout-Tieren unverändert. Allerdings wurden im epididymalen Fettgewebe von *Gpnmb*-Knockout-Tieren mehr Makrophagenmarker exprimiert. In Adipositas wurden mehr Auffälligkeiten durch die Abwesenheit von Gpnmb detektiert. Wir konnten erstmals einen positiven Einfluss von Gpnmb auf den Insulin- und Glukoseplasmaspiegel zeigen. Adipöse *Gpnmb*-Knockout-Mäuse besaßen eine ausgeprägte Insulinresistenz und verstärkte Leberfibrose. Letzteres war mit einer erhöhten AKT Phosphorylierung und einer höheren Expression lipogener Genen assoziiert. Darüber hinaus enthielten die *Gpnmb*-Knockout-Tiere, wie bereits im vorherigen Arterioskleroseexperiment, mehr Makrophagen im epididymalen Fettgewebe. Diese zeigten in Wildtyp-Tieren eine starke Gpnmb-Expression, was auf eine lindernde Rolle von Gpnmb auf die Entzündung des Fettgewebes hindeutet.

Dies wird durch *in vitro*-Daten bestätigt, wo Gpnmb am höchsten in Transforming growth factor β-(TGFβ)-stimulierten, reparativen Makrophagen exprimiert wurde. Allerdings war der entzündungshemmende Effekt von Gpnmb auf die Makrophagen gering. Zudem hatte Gpnmb keinen nachweisbaren Einfluss auf Autophagie, eine weitere wichtige Eigenschaft von Makrophagen. Das ist insofern überraschend, als dass wir eine Erhöhung der Gpnmb-Expression, seiner Abspaltung und seines Abbaus nach Stimulation mit Bafilomycin feststellen konnten. Dieser ist ein Inhibitor des letzten Schrittes der Autophagie und des lysosomalen Abbaus. Außerdem veränderte Bafilomycin die Glykosylierung von Gpnmb, welche durchgehend hochvariabel war. Somit wurde Gpnmb entweder durch lysosomalen Stress beeinflusst oder durch eine Nebenwirkung von Bafilomycin: der verstärkten Differenzierung von Zellen. Letzteres wird durch die Beobachtung bestätigt, dass die Expression von Gpnmb am stärksten auf die Differenzierung von Knochenmarkszellen hin zu reifen Makrophagen reagierte. Die *Gpnmb*-Trankriptlevel verdoppelten sich nach der Behandlung mit TGFβ innerhalb von 24 Stunden, verdreifachten sich mit Bafilomycin, aber verhundertfachten sich während der Differenzierung von Tag sechs zu Tag sieben *in vitro*.

[B] https://www.who.int/news-room/fact-sheets/detail/obesity-and-overweight

Zusammengefasst wird die Gpnmb-Expression in vollentwickelten Makrophagen stark induziert und durch lysosomale Überlastung weiter erhöht. In Adipositas, einer der Hauptrisikofaktoren für Diabetes mellitus Typ II, kann es die Entwicklung einer Insulinresistenz verhindern, möglicherweise durch die Dämpfung der einhergehenden Entzündung im Fettgewebe.

Table of Contents

1. Introduction

1.1. Metabolic syndrome

Metabolic syndrome is a term that fits to more than a third of the US and more than a half of the European population [1, 2]. Metabolic syndrome is not a disease per se, rather a conglomerate of clinical findings that occur often together and consist of two or more of the conditions visceral obesity, insulin resistance (disturbed glucose metabolism), high triglycerides, low high-density lipoprotein (HDL) levels and hypertension. Those conditions are often linked to each other (**Figure 1**). Patients with metabolic syndrome are generally at a higher risk for atherosclerosis, cardiovascular disease like ischemic heart disease and stroke, type II diabetes mellitus, neurological disorders like Parkinson's and Alzheimer's disease, nonalcoholic fatty liver disease and certain cancers [3]. The most effective treatment targeting this increased risk is a change of lifestyle [4–6].

The underlying mechanisms of the metabolic syndrome are (1) mitochondrial dysfunction, (2) the microbiome and/or (3) inflammation that slowly develops in either one or all of the organs liver, gut and adipose tissue [7, 8]. The release of inflammatory mediators like tumor necrosis factor α (TNFα), interleukin 1β (IL-1β) or C-reactive protein from one site might trigger inflammation in other tissues, resulting in a generalized tissue dysfunction.

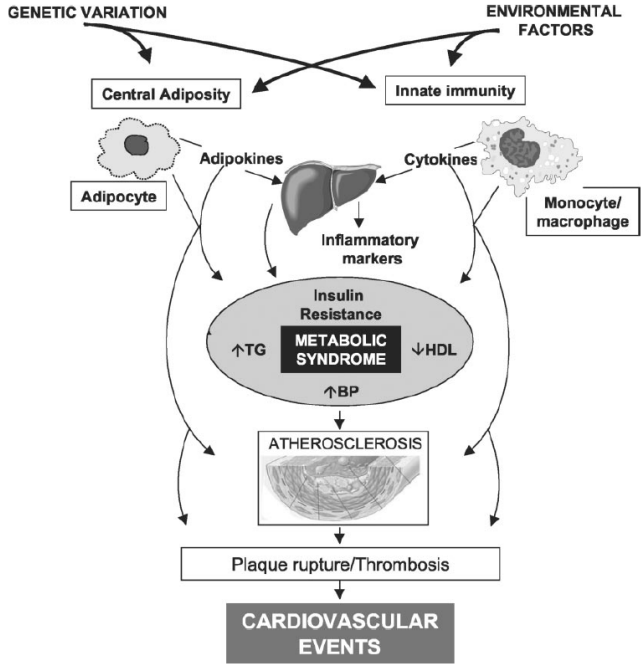

Figure 1: Pathophysiology of metabolic syndrome.
Environmental including lifestyle factors such as poor diet and sedentary behavior together with genetic predispositions lead to the development of metabolic syndrome. All factors like inflammation, blood triglyceride levels, hypertension, insulin resistance and obesity constantly influence each other. The clinical symptoms slowly progress in the development of atherosclerosis until a plaque rupture and concomitant thrombosis suddenly leads to a cardiovascular event like myocardial infarction or stroke. TG: triglycerides, BP: blood pressure. [9]

1.1.1. Obesity

The prevalence of obesity and its associated disorders has increased substantially worldwide over the last decades. In 2016, 39% of all adult men and woman were overweight[C]. Obesity can lead to a chronic, low-grade inflammation [10] and is the main risk factor for type II diabetes as it evokes insulin resistance, a state of pre-diabetes [11].

1.1.1.1. An inflammatory process

Inflammation is thought to be a critical contributor to pathogenesis of obesity. Epididymal adipose tissue shows the first signs of inflammation whereas subcutaneous adipose tissue shows the lowest and the latest age-associated insulin resistance and inflammation [12]. Macrophage-related genes were abundantly found in an approach to find genes causing obesity and metabolic syndrome in mouse and human [13, 14]. Adipose tissue macrophages play a major role in the immunological switch of adipose tissue in obesity that hence can lead to insulin resistance and diabetes type II [15, 16]. Residential macrophages in lean mice exhibit an "alternatively activated" M2 phenotype [17, 18]. Upon diet-induced obesity, expanding adipocytes release monocyte attracting molecules, TNFα, leptin and free fatty acids. The larger the adipocyte, the more monocytes are attracted from bone marrow and infiltrate the adipose tissue [15]. Thus, adiposity and macrophage content are directly correlated. In obese individuals, 40% of adipose tissue cells are composed of macrophages compared to 10% in lean individuals in both mice and humans [15]. The newly arrived macrophages acquire an inflammatory M1 phenotype and release a cocktail of pro-inflammatory cytokines like TNFα, IL-1β and IL-6 [17, 19]. More macrophages are recruited by the secreted chemokines, creating a loop of chronic inflammation [20]. Inflammation is especially caused by the uptake of palmitate that induces mitochondrial reactive oxygen species (ROS), autophagy signaling pathways and activation of the inflammasome [21]. In detail, serine kinases like c-Jun N-terminal protein kinase (JNK) and inhibitor of κB kinase β (IKKβ) are activated leading to phosphorylation of insulin receptor substrates (IRS) and locally promote inflammation via activator protein 1 (AP-1) and nuclear factor-κB (NF-κB) [20]. Drastic weight loss is able to return the polarization back to M2 [19]. Surprisingly, another study reports that macrophages in obesity are polarized in general more towards M2, stimulated by the uptake of free fatty acids released after lipolysis [22]. Others propose a third possibility with a macrophage activation that is distinct from the known M1-M2 axis and hence is called "metabolically activated" [23, 24]. Eventually, macrophages endocytose triacylglycerol-rich particles via scavenger receptor CD36 and store them as triacylglycerol droplets [22, 25]. Thereby, they turn into foam cells [22]. An inflammatory switch occurs also in T lymphocytes in adipose tissue that change from small amounts of T helper (T_H) 2/regulatory T cells to more and more inflammatory T_H1/CD8-T cells associated with obesity and insulin resistance [26].

The secreted pro-inflammatory cytokines can block insulin signaling on adipocytes, impairing insulin sensitivity of adipose tissue [17, 19, 21]. Inflammation affecting insulin response has evolutionary reasons. During bacterial infections, released inflammatory cytokines (TNFα, IL-6, IL-1β) promote insulin resistance to decrease the nutrient storage and increase its availability for effective, glycolysis-dependent immune response [27]. This emphasizes the theory that the pathology of obesity does not derive from excess nutrients but from its accompanying inflammation [28].

[C] https://www.who.int/gho/ncd/risk_factors/overweight/en/

1.1.1.2. Insulin signaling

Insulin induces uptake, metabolism and storage of glucose in muscle and adipose tissue and it suppresses glucose production and output of liver. Insulin is also able to stimulate the uptake of free fatty acids and lipid storage via lipogenesis and inhibition of lipolysis. In hyperglycemic individuals, pancreatic β-cells try to maintain normal blood glucose levels with compensatory insulin production. For some time, elevated insulin levels manage to overcome insulin resistance and retain normal glucose metabolism [20]. If insulin resistance cannot be overcome, diabetes mellitus type II is set on with a fatal triad of hyperinsulinemia, hyperglycemia, and hypertriglyceridemia [29]. Insulin resistance becomes mainly manifested in the three organs liver, muscle and adipose tissue [20].

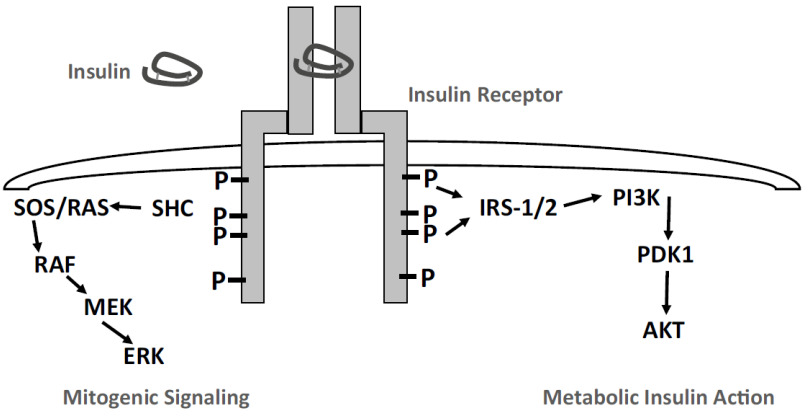

Figure 2: Insulin receptor activates two major intracellular signaling cascades.
The phosphoinositide 3' kinase (PI3K)/AKT pathway has a predominant metabolic effect and is activated by the insulin receptor mediated phosphorylation of insulin receptor substrates (IRS) 1/2. The RAS/RAF/MEK/ERK pathway has predominant mitogenic effects and is activated by the insulin receptor mediated phosphorylation of SHC. Figure and text adapted from [30].

After a meal, liver and pancreatic β-cells take up blood glucose via glucose transporter Glut2, a low-affinity transporter taking up glucose only in high concentrations [31]. Glucose is metabolized via glycolysis, which changes intracellular ATP/ADP ratio, inhibiting ATP-sensitive K^+ channels. The membrane potential of β-cells changes and voltage-gated Ca^{2+} channels are activated. A rise of cytosolic calcium triggers the exocytosis of insulin secretory vesicles. Insulin binds to its insulin receptor (Insr), a receptor tyrosine kinase, resulting in the activation of two cascades (**Figure 2**). The metabolic branch facilitates glucose transport by induction of glucose transporter Glut4 (Slc2a gene family) via proteinkinase B/AKT [11, 32]. The mitogenic branch promotes the RAS/mitogen-activated protein-extracellular signal-regulated kinase kinase (MEK)/extracellular signal-regulated kinases (ERK) signaling cascade [30]. Signaling of the metabolic branch is impaired in an insulin resistant state. A compensatory elevation of insulin levels maintains the metabolic homeostasis, however overstimulates the mitogenic branch. Thereby, high insulin levels are an important factor for the growth of cancers.

There is a tissue-specific expression of Glut isoforms. Whereas the brain takes up glucose via insulin-independent Gluts, insulin-dependent muscle and adipose tissue utilize Glut4 [33]. In comparison to other glucose transporters, Glut4 has the unique feature of being stored in an intracellular compartment and then quickly translocated to the cell membrane upon insulin stimuli, thereby being a major contributor to blood glucose homeostasis [34]. Balanced blood glucose levels are maintained mainly through glucose uptake by muscle and glucose production

by the liver. Glut2 is not only responsible for sensing blood glucose but also for releasing newly generated glucose from the liver into the bloodstream [32].

Adipocytes are another highly insulin-responsive cell type although accounting only for a small fraction of glucose uptake compared to muscle tissue [11]. The main action of insulin on adipose tissue is the uptake of fatty acids and the inhibition of lipolysis. In an insulin-resistant state, adipose tissue releases fatty acids that are stored ectopically in muscle or liver. Down-regulation of Glut4 in adipose tissue is a crucial step in development of insulin resistance, either directly or indirectly via endocrine molecules like leptin, resistin, retinol-binding protein 4 (RBP4) or TNFα [11, 20]. In muscle, insulin-mediated Glut4 translocation to the plasma membrane as well as glucose uptake is impaired in obese individuals [35]. Thus, they have a diminished overall glucose clearance from blood compared to non-obese ones, which is even more dramatic in diabetic patients, enhancing hyperglycemia [36]. Thus, a decrease of Glut4 in only one organ is sufficient to cause insulin resistance in other organs as well [34, 37, 38].

1.1.2. Atherosclerosis

In the 19th century, Rudolf Virchow described atherosclerosis as "entzündung" (inflammation). Half a century later, in 1913, Nikolai Anitschkow demonstrated that cholesterol feeding elicits atherosclerosis in rabbits and concluded that "without cholesterol, there is no atherosclerosis". [39]

Atherosclerosis is defined as a chronic inflammation of the arterial vessel wall caused by hypercholesterolemia. Rupture of atherosclerotic plaques and thrombi lead to ischemic heart disease and stroke, the leading causes of deaths in 2016[D]. Atherosclerotic lesions develop silently over decades with an interplay of lipids and inflammation until a certain threshold of symptoms is reached [5, 40]. It is debated whether atherosclerotic lesions are initiated by either crosstalk between accumulated low-density lipoproteins (LDL) in the vessel wall and resident immune cells or by a damaged endothelial layer [41, 42]. The latter can be caused by various factors like obesity, diabetes, hypertension, or smoking.

1.1.2.1. The aortic wall

A functional aortic wall consists of three layers. The innermost layer, *tunica intima*, consists of a thin endothelial and a subendothelial layer. It is separated with an internal elastic membrane from the second layer, *tunica media*, which is characterized by vascular smooth muscle cells with elastin. It can constrict and thereby regulate blood pressure. Adjacent to *tunica media*, the *tunica adventitia* consists largely of connective tissues. In bigger vessels, *tunica adventitia* also contains arterioles or perivascular adipose tissue. In atherosclerosis, immune cells invade the *intima* and *media* and the plaque is formed within or above the smooth muscle cells [43].

1.1.2.2. Development of a lesion

A healthy endothelium releases nitric oxide (NO). This multi-tasking molecule can regulate vascular tone, inhibit thrombosis, suppress vascular smooth muscle cell proliferation and leukocyte adhesion and transmigration [42, 44]. NO has even the capacity to inhibit oxidation of LDL [45]. However, LDL counteracts the bioactivity of NO. Uptake of LDL, reduced NO bioactivity and oxidative stress leads to inflammatory activation of endothelial cells, which produce leukocyte adhesion molecules and cytokines (vascular cell adhesion molecule 1 (VCAM-1),

[D] https://www.who.int/news-room/fact-sheets/detail/the-top-10-causes-of-death

interleukins, monocyte chemoattractant protein 1 (MCP-1), TNFα and interferons (IFN)). Apart from the impairment of normal endothelial functions, immune cells are recruited and activated [46]. Monocytes migrate to the intima and bind with their receptor CCR2 to abundant MCP-1. With macrophage colony-stimulating factor (M-CSF) and granulocyte-macrophage colony-stimulating factor (GM-CSF) being present, they differentiate to macrophages. Angiotensin II bound to its angiotensin type-1 receptor stimulates the NADH/NADPH oxidase of macrophages, endothelial cells and smooth muscle cells to produce reactive oxygen species (ROS) [47, 48]. ROS can lead to oxidation of intravascular LDL, proliferation of vascular smooth muscle cells, the expression of monocyte adhesion molecules on endothelial cells and scavenging of NO [48, 49]. All of those are pro-atherogenic factors contributing to its pathogenesis. LDL and very low-density lipoprotein (VLDL) enter the *intima* most easily. In plasma, LDL is protected against oxidation by circulating anitoxidants that are not present in arterial wall [50, 51]. Thus, LDL is therein oxidized to oxidized LDL (oxLDL), with ApoB being altered. ApoB is the ligand for the LDL receptor in liver. However, ApoB-modified oxLDL is no longer recognized by LDL receptor [52]. Instead, oxLDL and acetylated LDL (acLDL) are binding to scavenger receptors such as CD36 and CD68 expressed by macrophages (**Figure 3**) [53]. Upon uptake of oxLDL, macrophages and smooth muscle cells transform into foam cells [54].

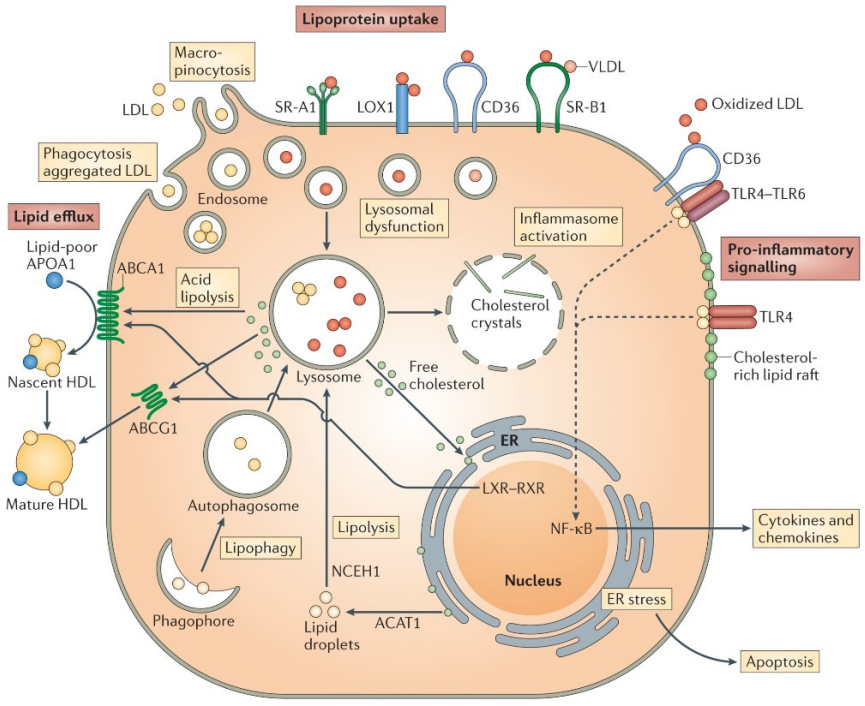

Figure 3: Lipophagy and lipid uptake/efflux in macrophages of atherosclerotic lesions.
Macrophages in atherosclerotic lesions contribute to the lipid metabolism by uptake of lipids via scavenger receptors such as CD36, storage of lipids, degradation by a specialized autophagy called lipophagy, and release of lipids mediated by efflux transporters. A central organelle is the lysosome whose capacity can influence the inflammatory status of the cell.
ABCA1: ABC transporter 1, ACAT1: acyl-coA cholesterol acyltransferase 1, ER: endoplasmic reticulum, HDL: high-density lipoprotein, LXR: liver-X-receptor / RXR: retinoid X receptor, LDL: low-density lipoprotein, nCEH: neutral cholesterol ester hydrolases, NF-κB : nuclear factor-κB, SRA: scavenger receptor A, TLR4: Toll-like receptor 4, VLDL: very low-density lipoprotein [55].

Moreover, tissue resident macrophages and mast cells are activated by oxLDL as well and secrete TNFα and histamine, respectively, promoting the expression of more monocyte-adhesion molecules like ICAM-1, VCAM-1, E-selectin on endothelial cells, which in turn leads to the retention and accumulation of more immune cells [56]. Like monocytes, T cells bind to VCAM-1

and migrate into the intima. oxLDL presents an antigen for T cells [57]. Activated T cells transform into T_H1 (releasing IL-1, IFNγ, TNF) or T_H2 (releasing IL-10, IL-4). They cross-talk with macrophages, endothelial cells and smooth muscle cells and further enhance the inflammatory milieu of the lesion [58]. Atherosclerotic lesions are associated with T_H1 predominance among plaque T cells. However, also T cells can switch from pro- to anti-inflammatory with lesion progression and display thus an important part of plasticity [57]. Resident mast cells degranulate and release heparin, TNFα, tryptase and chymase that activate pro-matrix metalloproteinases (Mmp). The latter convert angiotensin I into angiotensin II, completing the inflammatory circle. Eventually, plaques consist of lipids, cholesterol, immune cells, calcium, extracellular matrix and cellular debris.

Thus, LDL can start a vicious self-sustaining cycle of inflammation and deposition of cells, cell debris and extracellular matrix. Food containing excessive amounts of fat is a major risk factor for atherosclerosis, since it impairs endothelial function, enhances acute responses to cytokine stimulation and primes endothelial cells for enhanced monocyte recruitment. The main intervention to suspend the progression of atherosclerosis, remains the reduction of plasma LDL [4, 59].

1.1.2.3. Macrophages in atherosclerotic lesions

Different features of macrophages can influence the pathogenicity of atherosclerosis: (1) The first critical feature of macrophages is their inflammatory polarization [60]. In atherosclerotic lesions, all kinds of subsets are present, inflammatory, anti-inflammatory and specially activated by oxLDL [61]. Anti-inflammatory macrophages, similar to macrophages found in wound healing, contribute to matrix deposition and plaque stabilization. They are abundant in regressing plaques [62]. Pro-inflammatory macrophages on the other hand release retention factors and pro-inflammatory mediators, promoting inflammation by recruiting more leukocytes and secrete matrix degrading enzymes, de-stabilizing the plaque and increasing the risk of rupture [55]. Eventually, foam cells show signs of endoplasmatic reticulum (ER) stress, undergo apoptosis or die of necrosis and release their lipid content to form the necrotic, lipid core of the plaque [62]. (2) Macrophages, typically known for being resident, non-migrating cells, can reverse transmigrate and emigrate from plaques, a characteristic of regressing lesions [62]. This is possible by acquiring features of their closely related dendritic cells making them feasible to emigrate to lymph nodes [63, 64]. Thus, regulating expression of monocyte-adhesion molecules and macrophage trafficking means being able to regulate the pathogenesis of atherosclerosis [64]. (3) The same is true for regulating cholesterol efflux transporters in macrophages such as ATP-binding cassette subfamily A member 1 (Abca1), ATP-binding cassette sub-family G member 1 (Abcg1) and scavenger receptor class B member 1 (Srb1) [55, 64]. Cholesterol secreted by macrophages is gathered by HDL and carried back to the liver, an anti-atherogenic process called reverse cholesterol transport (**Figure 3**). (4) Autophagy is another crucial feature of macrophages in atherosclerotic plaques. In foam cells, lipids are degraded in a specialized process called lipophagy (**Figure 3**) [55]. Furthermore, autophagy clears apoptotic bodies that would otherwise form the necrotic core of the lesion and thus decreases NADPH oxidase-mediated oxidative stress [65]. Taken together, high plasticity of macrophages regarding inflammation, trafficking, lipid carrier expression and autophagy contributes to the fine-tuning of pathogenesis or regression of atherosclerosis.

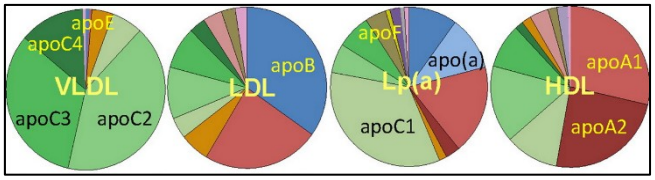

Figure 4: Frequencies of lipoprotein-associated proteins on different particle classes.
Very low-density lipoproteins (VLDL) are synthesized and secreted by the liver and transformed into the smaller and more cholesterol-rich, low-density lipoproteins (LDL). Human lipoprotein (a) [Lp(a)] is similar to LDL but contains additionally apolipoprotein(a) [apo(a)], which is attached to ApoB-100 by one disulfide bridge. High density lipoprotein (HDL) is the only non-ApoB-containing lipoprotein in circulation and has apoA1 as its major structural protein. Figure and text adapted from [66].

1.1.2.4. Lipoproteins and Apolipoproteins

Lipoproteins are water-soluble macromolecules whose main function is the transport of lipids between tissues. The main receiving organs are adipose tissue, muscle and liver, the latter being responsible for lipoprotein organization and re-distribution. Chylomicrons, VLDL, LDL and HDL are categories of lipoproteins that decrease in the listed order in size and triglyceride content, whereas protein content increases. Thus, HDL is the smallest of the lipoproteins with highest protein and smallest lipid content. The proteins in lipoproteins are called apolipoproteins and involve apolipoprotein (Apo) A, B, C, D, E and H (**Figure 4**). The recognition and uptake of lipids into cells is mediated mainly by ApoE and ApoB-100 [67]. Thus, their respective receptors in liver and other extrahepatic tissues regulate the levels of lipoproteins in plasma. ApoB-100 characterizes lipoproteins high in lipid content. Those lipoproteins are also called non-HDL and are highly atherogenic [68]. In a typical blood lipid panel, clinicians determine total cholesterol, LDL, HDL and triglyceride levels. A high ratio of LDL to HDL, but also low HDL levels by itself are considered as risk factors for the development of cardiovascular diseases and atherosclerosis.

1.1.2.5. Rupture

A plaque in the arterial wall is composed of several layers majorly involving a fibrous cap, a layer rich in immune cells and a necrotic lipid core. Morphologically, the pathogenicity of a plaque can be distinguished first by monocyte adhesion, then by the development of foam cells and lastly by the development of a fibrous cap [69]. A lipid core can manifest itself within a largely intact intima. In the pathological next step, the intima thickens with deposited extracellular matrix, mainly collagen, proliferation of smooth muscle cells and the development of a fibrous cap [40, 70]. The fibrous cap is the top layer of a plaque and consists of macrophages, T cells, smooth muscle cells and extracellular matrix components, mainly collagen. The thicker the fibrous cap with less immune cells and the smaller the lipid core, the more stable is the plaque and the less likely it is to rupture. Expression of Mmps, mainly collagenases, that degrade extracellular matrix, can lead to a thinning and thereby weakening of the fibrous cap, enhancing the risk of rupture [71]. A ruptured plaque releases its lipid core, which is highly thrombogenic, to the bloodstream. Platelets are activated, a coagulation cascade ensues and a thrombus is formed around the rupture site. After the rupture of a plaque with a following cardiovascular event, inflammatory markers such as C-reactive protein rise in blood, increasing the risk of further progressing atherosclerotic lesions [71].

1.2. Structure and function of Gpnmb

1.2.1. "Gpnmb"

Almost 25 years ago, Weterman *et al.* aimed to isolate a gene that is preferentially expressed in highly metastatic cells. Instead, they discovered the glycoprotein *nmb* that was expressed rather in lowly than in highly metastatic human melanoma cell lines [72], later designated "glycoprotein nonmetastatic melanoma protein b" (Gpnmb). A mouse orthologue correspondent to the human GPNMB was discovered several years later [73]. Simultaneously, a protein with 99.4% homology to mouse Gpnmb, only differing in 4 amino acids (aa), was described in mouse dendritic cells as "dendritic cell-associated, heparan sulfate proteoglycans-dependent integrin ligand" (DC-HIL) [74]. In detail, this protein was discovered when comparing genes expressed by a new dendritic cell line with macrophage cell lines J774 and RAW, as well as keratinocytes, dermal fibroblasts, T_H1, T_H2 and B cell lines. Today, only one version of Gpnmb is assumed to exist in mouse. Another independent discovery of Gpnmb was achieved in quail neuroretina cells that became pigmented after infection with a v-myc-encoding retrovirus, where the protein was called QNR-71 and had high homology to melanosomal proteins [75]. In chicken and quail, QNR-71 expression is restricted to pigmented retina and dermis [75]. The rat orthologue was called "osteoactivin" because of its upregulation in a *osteopetrotic*-knockout rat, a model disease for osteopetrosis [76]. Next, Gpnmb was independently discovered in human bone marrow fibroblasts, where it induces and interacts with the receptor neurokinin-1 and its high affinity ligand substance P, which regulates hematopoiesis [77]. This time, Gpnmb was called "hematopoietic growth factor-inducible neurokinin-1 type" (HGFIN). Although various names are still used, "Gpnmb" is most common for all species. Gpnmb orthologues have been identified in 261 organisms[E]. All of them except zebrafish share a polycystic kidney disease (PKD) domain[F]. The homology between the species is summarized in **Table 1**.

Table 1: Amino acid identity of Gpnmb across species.
Sequences from https://www.ncbi.nlm.nih.gov/ were blasted and the percentage of identical amino acids (aa) per two sequences were multiplied with query coverage. Similar amino acids were disregarded; thus, the protein similarity is eventually higher. Published similarity numbers are comparable [72–76, 78].

	GPNMB	Gpnmb	Gpnmb	Gpnmb	gpnmb	Pmel17
Species	human *(Homo sapiens)*	rat *(Rattus norvegicus)*	mouse *(Mus musculus)*	quail *(Coturnix japonica)*	zebrafish *(Danio rerio)*	human/ mouse
Alternative name	HGFIN	Osteoactivin	DC-HIL	QNR-71		gp100, SILV
Compared to human	**100%**	65%	67%	52%	30%	22%
Compared to mouse	67%	84%	**100%**	48%	28%	23%
Length	572 aa	572 aa	574 aa	559 aa	627 aa	626 aa

[E] https://www.ncbi.nlm.nih.gov/gene/107309209
[F] https://www.ncbi.nlm.nih.gov/homologene/1880

1.2.2. Structure of Gpnmb

Mouse, rat and human orthologues of Gpnmb are very similar in their structure. Gpnmb is a type I transmembrane protein that is heavily N-glycosylated and bears a short cytoplasmic and a major extracellular domain (**Figure 5**) [72, 79]. In detail, the murine Gpnmb protein of 574 aa consists of a long extracellular (aa 20-499), a transmembrane (aa 500-523) and a cytoplasmic domain (aa 524-574) [74]. In comparison, the rat Gpnmb transmembrane domain is located at aa 499-521 [79].

1.2.2.1. Motifs in the extracellular domain

The extracellular part of Gpnmb consists of different domains. The first 19-22 aa contain a signal peptide [72, 74, 79] that targets Gpnmb into the secretory pathway [80] and is cleaved at a NEC1/2 cleavage site (aa 23-25) [79]. A heparin-binding motif, the PKD domain (aa 250-384) [79] bearing an immunoglobulin-like folding structure [80] can bind and thus inhibit T cells [81]. An integrin-binding Arg-Gly-Asp (RGD)-motif (aa 64-66) [74, 79, 80] can form a complex with $\alpha_5\beta_1$ integrin, the receptor for fibronectin [82, 83]. A proline-rich region forms a hinge that resembles immunoglobulin A [74]. A kringle-like domain (KLD), a structural domain found in blood clotting and fibrinolytic proteins [80], is important for the migratory function of Gpnmb [84]. With its heparin and integrin binding domains, Gpnmb has the capacity to bind several cell types like vascular endothelial cells, keratinocytes, melanoma cells and fibroblasts [74, 78].

1.2.2.2. Motifs in the cytoplasmic domain

The cytoplasmic tail of Gpnmb contains an immunoreceptor tyrosine-based activation motif (ITAM, aa 529–532) [74]. This motif is important for signal transduction in immune cells and part of CD3, the T cell receptor, and some Fc receptors [79]. Additionally, there are several predicted functional motifs including a substrate recognition site for cyclin 1, an interaction motif for molecules of the mitogen-activated protein kinase (MAPK) cascade, a class III PDZ domain-binding motif, a glycogen synthase kinase (GSK)-3 phosphorylation recognition site, a phosphorylase kinase phosphorylation site and a sorting signal responsible for the interaction with adaptor protein (AP) complex [79]. Furthermore, there are two sorting and internalization di-leucine motifs targeting Gpnmb from the trans-Golgi network to the lysosomal-endosomal or melanosomal compartments [74, 79, 80].

Within the molecular function, phosphate binding yielded the highest score [79]. And indeed, Gpnmb is phosphorylated by epidermal growth factor receptor (EGFR) at Y529 of its intracellular ITAM-like motif after binding to the dermatophyte *Trichophyton rubrum* or syndecan-4 [85, 86 p.; 87].

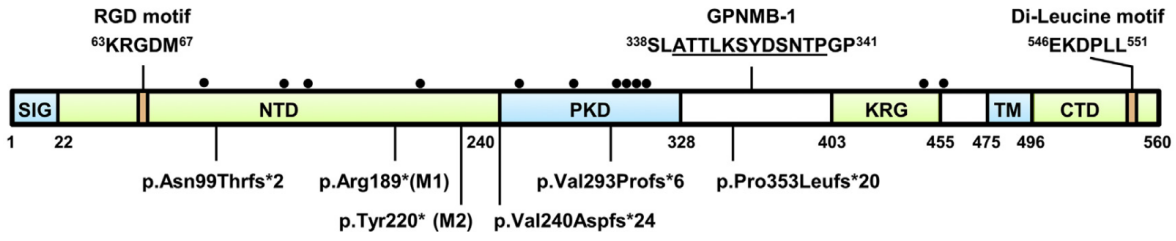

Figure 5: Structure and mutations of human GPNMB.
Solid circles represent N-glycosylation sites. A splice isoform of GPNMB (GPNMB-1) was identified only in humans with an in-frame 12-amino acid deletion. Figure and text adapted from [88].

1.2.3. Splicing

The length of human GPNMB is either 560 aa [72] or 572 aa [80]. Alternative splicing at the exon 6/7 results in a full length or a truncated version lacking 36 nucleotides/12 aa after aa 339, which is not reported for mouse or rat Gpnmb [89, 90]. The splice site is located in the proline-rich region. The shorter version can exhibit higher potency of inhibiting activated T cells [89]. Mouse and rat Gpnmb permanently contain the proline-serine rich insertion of 14 or 16 aa, respectively, which might account for improved melanosome handling [76].

1.2.4. Glycosylation

Gpnmb is a protein heavily modified and glycosylated in Golgi apparatus [80]. Human GPNMB has 12 reported N-linked glycosylation and a phosphoserine site [80]. Murine Gpnmb/DC-HIL contains only 11 N-glycosylation [74, 78] and several putative O-glycosylation sites [74]. The 12th glycosylation site might be the reason why Gpnmb has a bigger influence on pigmentation in humans than in mouse iris [88, 91]. Rat Gpnmb contains 13 predicted N-glycosylation sites [76] and 3 glycosaminoglycan attachment site [79]. Glycosylation leads to a deviation of the actual size of Gpnmb in Western blot compared to its predicted size of 58-64 kDa [75]. At least two bands appear in Western blot that could display a premature around ~100 kDa and a slower running, more mature and heavier glycosylated form of Gpnmb around ~110kDa [80]. Gpnmb contains high mannose type N-linked glycosylation [92], in contrast to hybrid or complex type glycosylations. Furthermore, Gpnmb can be modified by attachment of sialic acids [80] and by mannosylation, which can be altered by retinoic acid [93].

Glycosylation of Gpnmb is essential for binding to the dermatophytes *Trichophyton rubrum* [85]. Gpnmb can bind to T cells which depends on the glycosylation of the receptor syndecan-4 [94]. Syndecan-4 bearing special heparan sulfate moieties binds Gpnmb with higher affinity. Additionally, abundant transforming growth factor β (TGFβ) can protect those moieties from degradation, enhancing the effect of Gpnmb [94]. Heparan sulfate moieties vary strongly between cell types and might be the reason why syndecan-4 expression alone for example on B cells is not sufficient for Gpnmb binding [94, 95].

1.2.5. Mutations of Gpnmb

In humans, different homo- or heterozygous mutations in *GPNMB* exist that result in C-terminally truncated versions of GPNMB (**Figure 5**). Affected people develop a disease called amyloidosis cutis dyschromica, which is characterized by a hyperpigmentation [88]. The only human homozygous mutation known is R189* (stop codon instead of arginine 189) and results in a truncated protein that is moreover lowly expressed probably due to nonsense mediated decay of its mRNA. This mutated version mislocalizes in the cytoplasm and shows increased co-localization with calnexin compared to the wildtype version, suggesting ER-associated degradation. The epidermal layers of the *Gpnmb*-"knockout" individual are characterized by a deposition of fibrillary amyloids probably from apoptotic keratinocytes and an increased infiltration of macrophages. A similar, homozygous nonsense mutation (R150*) in the *Gpnmb* gene in DBA/2J mice is used as a *Gpnmb*-knockout mouse model. Interestingly, in contrast to humans, those mice develop pigmentary glaucoma but retain unaltered skin color [96]. Glaucoma is rescued when the same mutation is inserted into an albino mouse that has an abolished pigment production. Murine melanocytes in contrast to human melanocytes are

restricted to hair follicles, but not present in the epidermis of the skin, possibly accounting for the discrepancy of the phenotype between mouse and human [88].

It is debated whether mutations in the loci rs199347 and rs156429, that can influence *GPNMB* gene methylation and expression, are associated with an increased risk for Parkinson's disease [97–102], amyotrophic lateral sclerosis and multiple system atrophy [103]. However, major differences occur between Caucasian, Taiwanese, Chinese and Han Chinese populations [103]. [104, 105], making it difficult to predict a risk allele or a function of Gpnmb in those diseases.

Point mutations of *Gpnmb* occur in breast and colorectal cancers as well. Six percent of breast cancer tumors contain one of two heterozygous missense mutations of Gpnmb, A110D or S519I [106]. A role of Gpnmb in promoting metastasis was suggested in an ovarian cancer p53null patient [107]. Here, Gpnmb was not found in primary tumors, but in extrapelvic recurrent cancers where Gpnmb contains the missense mutation P561S in the intracellular domain [107].

1.2.6. Interaction

1.2.6.1. Interactions with proteins within the cell

Gpnmb interacts with β1 integrin as shown by co-immunoprecipitation [82], with Na^+/K^+-ATPase α subunits in human and murine glioma/glioblastoma [108], with the ER chaperones calnexin [109], and binding immunoglobulin protein (BiP) [110]. Although Gpnmb interacts with two ER chaperones, it does not induce the general unfolded protein response. It rather ameliorates ER stress by enhancing *BiP* pre-mRNA splicing in the nucleus [110]. Gpnmb and neurokinin 1 share amino acid residues within the binding pocket of neurokinin 1 [77, 111]. Thus, Gpnmb noncovalently interacts with a high affinity ligand of neurokinin 1, substance P.

1.2.6.2. Receptor syndecan-4

The heparan sulfate proteoglycan syndecan-4 was identified as a receptor for Gpnmb and binding inhibits activated T cells [112–114, 81]. Surprisingly, although B cells constitutively express syndecan-4 [115] and negative regulation of B cell activation was predicted for Gpnmb function [79], B cells do not bind Gpnmb [114]. Fibroblasts potentially express syndecan-4, being a possible target of Gpnmb binding. Syndecan-4 [74] and another unknown factor [116] are receptors for Gpnmb on endothelial cells, facilitating trans-endothelial migration.

1.2.6.3. Receptor CD44

CD44 is another receptor for Gpnmb [117]. Gpnmb acts via CD44 on astrocytes [98], white adipocytes [118], mesenchymal stem cells [119] and osteoclasts, which can be abolished by hyaluronan, the major ligand of CD44 [120]. CD44 is upregulated by phorbol esters such as phorbol 12-myristate 13-acetate (PMA) [121] and bears heparan sulfate sugars [95].

1.2.6.4. Heterodimer formation

Gpnmb can also form heterodimers with $\alpha_5\beta_1$ integrin, the receptor for fibronectin [82, 83, 122], facilitating adhesion, migration and cancer metastasis.

EGFR and Gpnmb form a hetero-dimer upon heparin-binding EGF-like growth factor (HB-EGF) stimulation [86]. Gpnmb is phosphorylated by EGFR at the intracellular domain (Y525). This leads to the recruitment of a long non-protein coding RNA and two proteins, resulting in the

phosphorylation and stabilization of hypoxia-inducible factor (Hif)-1α and the transcription of Hif-1α target genes. This plays a role in triple-negative breast cancer, where Gpnmb is part of a pathway activating Hif-1α target genes that are normally activated upon hypoxia. This results in the promotion of the tumor glycolysis reprogramming and tumorigenesis.

1.2.7. Shedding

Soluble, extracellular Gpnmb is produced by proteolytic ectodomain shedding [80]. Soluble Gpnmb found in plasma might exert different functions than the full-length, transmembrane version. Gpnmb ectodomain shedding is tightly regulated [80] and can be induced by IL-12 [123], phorbol ester PMA and calmodulin inhibitors [80]. Apparently, activation of intracellular calcium pathways are involved in shedding of Gpnmb [80]. Four extracellular N-arginine dibasic convertase cleavage sites are predicted for rat Gpnmb [79]. Gpnmb is mostly shed at R459-R460 close to the transmembrane domain [92] by ADAM10 [92, 118, 124], possibly ADAM8 [118], but not by ADAM12 and 17 [124]. A special cleavage of Gpnmb has been observed exclusively in a specific M1 type subset of microglia in the brain, not in other cell types or organs [123]. In detail, furin-like proteases shed Gpnmb at K170, which results in the generation of a unique Gpnmb antigen for this microglia subset.

1.2.8. The homologue Pmel17

Apart from its orthologues, the closest homologous protein to Gpnmb is melanocyte protein Pmel (Pmel17) (**Table 1**). Studying Pmel17 might give insight into the functional properties of Gpnmb. Melanin, the molecule responsible for color of skin, hair and eye, is produced and stored in small vesicular compartments closely related to lysosomes called melanosomes that undergo several maturation steps. In an attempt to identify all proteins of early melanosomes and thus providing a tool for discrimination between lysosomes and platelets, 68 proteins were identified, among them Gpnmb and Pmel17 [125]. Pmel17 is one of the 12 proteins that were melanosome-specific, in contrast Gpnmb was detected in both categories. Another approach identified 1500 melanosome-specific proteins of all melanosomal stages in human melanoma cells [126]. GPNMB was identified in all stages of melanosomes and is therefore considered as a constituent/resident protein of melanosomes [126]. Pmel17 expression is limited to melanocytes and its mutation causes a silver fur color in mice [127], explaining its original gene name s*ilver* in mice. Mutations in Pmel17 causes the white color of chicken and the silver color of horses [128]. Although a complete knockout of Pmel17 dramatically disrupts melanosomes in mice, fur color is only slightly altered [128]. Pmel17 is a specific melanosomal protein that is necessary for the successful synthesis of melanin [129].

Pmel17 expression levels are reduced when Gpnmb is knocked down and expression of both increases after irradiation thus expression levels might be linked [91]. Like Gpnmb in other cell types, Pmel17 co-localizes with β_1 integrin [82, 126] and with ER marker BiP in melanosomes [110, 125]. Pmel17 is targeted by its PKD domain towards lysosome-associated membrane glycoprotein 1 (Lamp1)-positive lysosomes. In contrast, 6 additional N-glycosylation sites disrupt this targeting information in the PKD domain of Gpnmb, which rather localizes to early endosomal/recycling vesicles, ER and Golgi [130]. Glycosylation also nullifies the intrinsic capacity of Gpnmb to form amyloid fibrils, which is a characteristic of Pmel17 [129, 131]. Thus, glycosylation of Gpnmb contributes greatly to its function, which thus differs from Pmel17.

1.2.9. Tissue expression of Gpnmb

Gpnmb has a very low endogenous expression in all tissues[G] [132–134]. Summarizing several, mostly contradicting screenings, the top organs that endogenously express Gpnmb are retina, iris, fat and skin whereas brain, liver, kidney and heart are mostly not expressing it [73, 74, 76, 77, 134–137]. Gpnmb expression is especially abundant in retinal pigmented epithelium and melanoblasts in embryonic development [73, 138], which is why DBA/2J mice with a functional *Gpnmb*-knockout develop glaucoma [135].

Whereas Gpnmb expression in healthy tissue is comparably low [134], it is heavily induced in inflammatory diseases [79, 137, 139–141], in tissues with aggressive cancers [142, 143] or in muscles of rats that stayed in space for 16 days in the space shuttle Columbia [144].

1.2.10. Cell types with Gpnmb expression

1.2.10.1. Immune cells

Gpnmb expression is low in peripheral blood cells or bone marrow but can be increased dramatically with treatment of GM-CSF and/or M-CSF, which promotes the differentiation into antigen-presenting cells [77, 134, 137, 145]. The first group of antigen-presenting cells are macrophages. Gpnmb is expressed in mature macrophages from bone marrow [77, 81, 119, 134, 137, 146, 147], in kidney 7 days after kidney injury [137], in liver with fibrosis [109, 136] and in adipose tissue after high fat high sugar diet [109]. Gpnmb is furthermore expressed in other, tissue-specific macrophages such as some subsets of brain microglia [123, 141], glioblastoma associated microglia and macrophages [133, 148] as well as in thioglycolliate-induced peritoneal macrophages [85], which excel native bone marrow-derived macrophages (BMDM) roughly 10-fold in Gpnmb expression [134].

Apart from macrophages, the second group of antigen-presenting cells are dendritic cells. Gpnmb is highly expressed in almost all subsets of dendritic cells of several species [74, 85, 89, 132, 134, 145, 146, 149, 150].

There is a another specific subset of cells that exhibits a very high Gpnmb expression, called myeloid-derived suppressor cells (MDSCs) [146]. MDSCs are characterized in humans as $CD14^+$ [151] or $CD14^+HLA\text{-}DR^{no/low}$ MDSCs [152] and in mouse as $CD11b^+$ [146] or $CD11b^+Gr1^+$ cells [153]. MDSCs are a relatively immature population of bone marrow-derived cells, potent inhibitors of T cell function, and might play a role in autoimmune diseases [146]. In cancer, Gpnmb expression derives often from MDSCs within tumor or spleen, blood and bone marrow [151, 153, 154]. In other diseases such as psoriasis [152] or experimental autoimmune encephalomyelitis (EAE), a mouse model for multiple sclerosis [146], Gpnmb was discovered in MDSCs as well.

Only once, Gpnmb was mentioned in differentiating and mature eosinophils [155]. Gpnmb is not expressed in B or T cells [132, 145]. Taken together, Gpnmb is mainly expressed by macrophages and dendritic cells as well as by tissues infiltrated by those [134].

[G] http://www.immgen.org/databrowser/index.html

1.2.10.2. Cancer cells

The expression of Gpnmb in cancer cells can exceed the expression in endogenously Gpnmb-expressing cells. For example, primary osteosarcoma tumor cells contain more Gpnmb than osteoblasts [156]. It is debated whether Gpnmb expression in cancer derives from the cancer itself or tumor-stromal cells. In both, Gpnmb can exert pro-tumor effects (see chapter 1.2.16 and 1.3.2).

1.2.10.3. Melanocytes

Gpnmb is heavily expressed in skin, potentially by all cell types within it [78]. Reports argue whether Gpnmb is expressed in keratinocytes [78, 81, 88] or not [80]. Other cell types that express Gpnmb are epidermal $CD1a^+$ Langerhans cells (immature dendritic cells) [78, 88, 89] and melanoblasts during embryonic development [138]. Eventually, all reports agree that the major source of Gpnmb expression in skin derives from melanocytes [78, 80, 88, 89].

Gpnmb is potentially mapped to mouse fur color [126]. Hoashi *et al.* suggest a role of Gpnmb rather in late (stage II /IV) than in early melanogenesis (stage I/II) [80]. However, Gpnmb expression is rather expressed in low or non-pigmented cells [80] and does not affect melanin production [157]. Gpnmb expression is even negatively correlating with iris pigmentation of mice [158]. Unlike other melanosomal proteins, Gpnmb has not been associated with albinism. In contrast to those negative data regarding mouse melanosome function, *GPNMB*-knockdown in human melanocyte cell line highly affects melanosome number and genes such as *tyrosinase* (*Tyr*), *tyrosinase-related protein 1* (*Trp1*), *Pmel17* [91, 159]. This species discrepancy might derive from one glycosylation site that is not present in mouse [74, 78].

1.2.11. Localization within the cell

Gpnmb is frequently detected in small vesicles in the cytoplasm [73, 85]. Mostly, those vesicles are not further characterized. Others report a co-localization of Gpnmb with lysosomal enzyme arylsulfatase B (Arsb) [160], with lysosomal markers Lamp-1 [78, 123] and cathepsin D [92], with lysosomal/endocytic marker Lamp-2 [147], or with early endosome marker early endosome antigen (EEA) [130]. Gpnmb localizes to vesicles that are major basic protein 1 (MBP1)-positive, a marker for granules in eosinophils [155] or vesicles that are transferrin-positive [88, 130]. In melanocytes, Gpnmb is mostly localized to melanosomes but not exclusively [72, 80]. Although Gpnmb is found preferentially in the melanosomal fraction, it also localizes to Lamp1-positive lysosomes, especially if the cells are not pigmented [78, 80]. Taking together, Gpnmb mostly resides in the lysosomal/endocytic pathway.

Additional to vesicles in the perinuclear area, substantial Gpnmb signal is detected in the ER and Golgi [130] and on the cell surface [74, 81, 137, 147]. However, Gpnmb can change its localization under TNFα treatment from lysosomes to the cell surface [78] and the opposite occurs, relocation to small peri-nuclear vesicles, when treating cells sequentially with IFNγ and LPS [134]. Upon chloroquine treatment, Gpnmb localized to autophagosomal compartments [137] and upon thapsigargin treatment, Gpnmb even re-locates to the nucleus, enhancing BiP splicing [110]. Gpnmb was also reported to change its localization from β-COP-positive Golgi [134, 147] to Lamp-2 positive late endosomes and lysosomes upon 7 days of receptor activator of NF-κB ligand (RANKL) treatment in osteoclasts [147]. Gpnmb was also found in rough ER marker in osteoblasts in early differentiation and can be then labeled in small secretory vesicles in the cell periphery [93].

1.2.12. Induction of Gpnmb

1.2.12.1. Cytokines

As Gpnmb is expressed in antigen-presenting cells, its expression reacts to exposure of cytokines [77, 85, 89, 153]. However, this is a controversial topic that is outlined in more detail in chapter 1.2.15.2 regarding the association of Gpnmb with the inflammatory polarization of macrophages.

1.2.12.2. Transcription factors

Microphthalmia-associated transcription factor (MITF) is an established transcription factor for *Gpnmb* [132, 138, 147, 160] and other melanosomal genes such as *Pmel17, Ty and, Trp1* [161]. There is a conserved element with two MITF consensus sites in the 5'-untranslated region (UTR) of human *GPNMB* sequence [138]. Gpnmb expression in an MITF-independent manner was also reported [91, 148], suggesting the use of other transcriptional regulators.

For instance, *Gpnmb* is also a target of the transcription factor Hif-1α [162]. Hif-1α and its subsequent target gene expression improves bone formation, angiogenesis and increases vascular endothelial growth factor (VEGF) expression [162, 163]. In contrast, a lack of Hif-1α promotes soft tissue, adipose tissue and fibrosis instead. Gpnmb in turn leads to Hif-1α stabilization and transcription of its target genes involved in metabolism [86].

The 5' region of human *GPNMB* contains consensus sequences for transcription factors linked to cycle quiescence (EBP, Myb, Rb and 8 times p53), to cycling (8 times AP-1, SP1, CREB), and to differentiation (MyoD and ETS-1) [164]. The regulation by AP-1, relevant in iris pigmentation, has been also considered elsewhere [158]. Eight potential p53 binding sites are a unique phenomenon in the human genome [164]. Indeed, p53 was proven to be a transcription factor of GPNMB and induces *GPNMB* gene expression in several human prostate cell lines [165]. Like p53, Gpnmb is proposed as a tumor suppressor [166]. The lower the transcription of Gpnmb, the more aggressive is the cancer cell line. In the most aggressive cell line, MDA-MB-231, Gpnmb transcription cannot be activated unless p53 is present. Lastly, the transcription factor Sox9 regulates the expression of extracellular matrix genes like osteopontin, fibronectin and Gpnmb in activated hepatic stellate cells [167].

1.2.12.3. Others

Gpnmb expression is induced by various conditions like knockdown of the lysosomal enzyme Arsb in normal human bronchial epithelial cells [160]**,** by bone morphogenetic protein 2 (Bmp-2) via Smad1 in osteoblasts [168], irradiation in melanocytes and melanoma cells [78, 91], α-melanocyte-stimulating hormone (MSH) in melanoma cells [78], culture medium buffering agent HEPES in a RAW264.7 macrophage cell line [169], lysosomal stress induced by ammonium chloride, bafilomycin, concanamycin A, palmitate, chloroquine and Torin1 in RAW264.7 macrophages [170, 171], ER stress like thapsigargin in NSC-34 motor neuron-like cells [110], basic fibroblast growth factor (bFGF) and platelet-derived growth factor (Pdgf) in C_2C_{12} mouse myoblastic cells [172] or retinoic acid in osteoblasts [93].

1.2.13. Proteins induced by Gpnmb

Gpnmb induces a wide variety of genes, including inflammatory [85], lipogenic [118] as well as lipid-associated genes [83, 85, 148].

Gpnmb is also known for inducing pro-fibrotic [173] or anti-fibrotic genes [174]. Thus, it might play a role in degeneration and regeneration of the extracellular matrix. Proteins well-known to be influenced by Gpnmb are the Mmps. Treating cell lines from different stages of head and neck squamous cell carcinoma with recombinant human GPNMB or siRNA targeting GPNMB alters expression levels of Mmp2, -3, -9, -10, -11 [175] and -13 [175, 176]. However, this was not consistent across cell lines, so upregulation still depends on other conditions.

In detail, Mmps that are repeatedly described to be induced by Gpnmb are Mmp3 [92, 172, 174, 177, 178] and Mmp9 [82, 172, 176, 179]. Additionally, tissue inhibitor of metalloproteinase (Timp) 1 but not Timp2 and -3 are induced [176, 179], whereas lowering effect of Gpnmb on Timp1 and -2 expression was also reported [173].

1.2.14. Signaling of Gpnmb

MAP kinase cascades are important transducers of external stimuli. Whereas ERK1/2 transduces signals from mitogens, p38 or JNK transduce stress or cytokine signals [180]. Both can interfere with the pathway of phosphoinositide 3′ kinase (PI3K)/AKT, which is another central signaling pathway. Gpnmb can influence those pathways in any possible way.

1.2.14.1. Mitogen-activated protein kinases

p38 and JNK are two MAP kinases that are involved in inflammation, apoptosis, proliferation and differentiation [181]. In the absence of a functional Gpnmb in osteoclasts, the two MAP kinases p38 and JNK show higher phosphorylation levels [182]. However, Gpnmb was reported to induce p38 phosphorylation [92] via MITF [160]. Gpnmb was also reported to have no effect on phosphorylation of JNK, p38 or $I_K\beta$ in differentiating osteoclasts [120], JNK and IκB in macrophages [183] or p38 in human dendritic cells [149].

Apart from p38 and JNK, studies about Gpnmb focused more on third MAP kinase involved in proliferation, differentiation and survival, ERK1/2 [181]. Circulating Gpnmb can induce ERK1/2 phosphorylation in NSC34 hybrid neuroblastoma/spinal cord cell line [184], by binding to β_1 integrin receptor in neutrophils of cystic fibrosis patients [82], Na^+/K^+-ATPase α subunits in human and murine glioma/glioblastoma [108, 185], or CD44 receptor on mesenchymal stem cells [119]. Gpnmb-mediated ERK phosphorylation can be dependent on VEGF in breast cancer cells [83] or LPS in BV-2 microglia [177]. Gpnmb-dependent ERK phosphorylation can lead to Mmp9 [82] or Mmp3 expression [92, 177]. On the other hand, Gpnmb was also reported to inhibit ERK phosphorylation in a CD44-dependent manner in differentiating osteoclasts [120, 182]. By inhibiting p38 and ERK1/2 signaling pathways, Gpnmb can induce an anti-inflammatory phenotype in macrophages [183].

ERK phosphorylation can in turn influence Gpnmb expression. In some cancer cell lines, activation of ERK was inversely associated with Gpnmb expression [186, 187]. The opposite, phosphorylation of ERK increasing Gpnmb expression, is reported as well. Phosphorylated ERK activates MITF and the transcription of MITF-dependent target gene *Gpnmb*, which enhances pigmentation and/or tumor growth [161]. However, in one case Gpnmb expression does not respond to ERK, Raf or MEK1/2 inhibitors [132].

1.2.14.2. AKT

AKT is a central kinase that can phosphorylate a series of substrates, thereby affecting a variety of central cellular processes such as survival [188]. AKT phosphorylation is either inversely related to Gpnmb expression. When Gpnmb is present, survival, pAKT (active) and pGSK-3β (inactive) is lower in osteoclasts [182]. Inhibition of AKT signaling in immature human monocyte-derived dendritic cells results in activated GSK-3β, which promotes MITF phosphorylation and thus *Gpnmb* expression [132]. Gpnmb can be strongly induced by tyrosine kinase inhibitors imatinib, nilotinib and dasatinib commonly used in chronic myeloid leukemia, where they inhibit the kinase activity of the fusion protein of breakpoint cluster region protein (Bcr) and tyrosine-protein kinase Abl1 (Abl) [132, 189, 190]. LPS counteracts those tyrosine kinase inhibitors by promoting phosphorylation of AKT. Thus, nilotinib together with LPS abrogates Gpnmb induction. LPS alone has no effect on Gpnmb expression [132].

Alternatively, AKT phosphorylation correlates to Gpnmb expression. Phosphorylated AKT (pAKT) is consistently higher in Gpnmb-expressing cancer cells [83]. In osteosarcoma cell lines [191] and breast cancer [192], Gpnmb enhances the canonical Wnt signaling pathway and acts on PI3K/AKT/mammalian target of rapamycin (mTOR) pathway. This pathway is completed to CD44/PI3K/AKT/mTORC1/sterol regulatory element-binding protein 1c (SREBP-1c) pathway in adipocytes; thus, Gpnmb binding to CD44 stimulates lipogenesis [118]. Similar data were obtained in mesenchymal stem cells [119]. Soluble Gpnmb can also activate the AKT pathway in glioblastoma or [108, 185] or a neural cell line [184].

1.2.15. Macrophage-related functions

Apart from its massive overexpression in diseases, the function of Gpnmb is quite diverse. Several biological processes were predicted for rat Gpnmb by computer modeling [79] that are listed here in order from high to low score: Heme catabolism, endothelial cell differentiation, establishment of protein localization, negative regulation of B cell activation, melanin biosynthesis from tyrosine, regulation of blood pressure, response to light, lung development, antigen processing, endogenous antigen via major histocompatibility complex (MHC) class I. Some of those predictions should be later reported to be true. However, research focused more on the influence of Gpnmb on typical features of antigen-presenting cells, such as phagocytosis, inflammation and interaction with T cells.

1.2.15.1. Phagocytosis and autophagy

Autophagy is a Greek word that means “self eating”, which literally summarizes the process it describes. It is a topic that gained public interest by the 2016 Nobel Prize in Physiology or Medicine to Yoshinori Ohsumi[H]. A cell can degrade and recycle its own contents by enclosing it in membranes. It is a degradation and recycling process independent of proteasomal degradation. Thirty highly conserved genes called Atg (AuTophaGy-related genes) tightly regulate the steps of autophagy [193]. Organelles or cell debris that are to be degraded are surrounded by pre-autophagosomes. These are loose membranes that fuse together to a larger vesicle. Pre-autophagosomes mature to autophagosomes, characterized by microtubule-associated protein 1 light chain 3 (Atg8/LC3) B-II. Endosomal vesicles can join to form an amphisome. The latter and the lysosome fuse together to form the autophagolysosome characterized by Lamp1 and Lamp2. The lysosome carries the transmembrane proton pump vacuolar H^+-ATPase (V-ATPase) that

[H] https://www.nobelprize.org/prizes/medicine/2016/ohsumi/facts/

lowers the luminal pH and allows proteases to degrade the vacuolar content. The transmembrane protein Atg22 facilitates the efflux of macromolecules and amino acids. Enhanced autophagy is often considered as beneficial because it clears misfolded protein and damaged organelles like mitochondria, peroxisomes or ER, which is called mitophagy, pexophagy or reticulophagy, respectively [194–196]. Thereby, autophagy can influence both growth and ageing on the cellular and organism level.

Autophagy is utilized in macrophages to degrade phagocytosed particles like viruses and bacteria. Gpnmb binds the dermatophytes *Trichophyton rubrum* with high affinity and to *Microsporum audouinii* with lower affinity, but not to *Candidal pseudohyphae, Staphylococcus aureus*, group A streptococci, *Pseudomonas aeruginosa* or *Escherichia coli* [85]. Upon binding, Gpnmb is phosphorylated, which promotes maturation and potency of the Gpnmb-expressing cell [85]. Additionally, Gpnmb has been connected to autophagy because of its upregulation in the lysosomal storage diseases like Gaucher and Niemann-Pick-disease and based on its localization to lysosomes [137, 197]. Gpnmb expression is correlated reversely to phosphorylation levels of mTOR, an inhibitor of autophagy [149]. On the other hand, soluble Gpnmb might inhibit autophagy by activating mTORC1 [118, 192]. Gpnmb was described as an important molecule for the uptake of apoptotic bodies [137, 176]. Gpnmb-expressing macrophages exhibit the double phagocytic capability compared to cells lacking Gpnmb expression [176]. However, the role of Gpnmb in autophagy has never been thoroughly followed up.

1.2.15.2. Polarization

Macrophages display a high degree of plasticity in adjusting their phenotype to their respective environment [198]. Pro- and anti-inflammatory macrophages are only the two far ends of a wide axis of polarization. Even *in vitro*, a simplified *in vivo* simulation, a wide variety of activators can make comparisons between studies difficult [198].

Several publications report an induction of Gpnmb in anti-inflammatory conditions. However, extracting the basic information from several publications reveals a very heterogeneous picture of Gpnmb induction (**Table 2**). Important additional variables are species, cell type and time period of treatment. However, Gpnmb seems to be induced rather in later time points [149], suggesting it not being an acute protein.

In vivo, it is difficult to assign the polarization of macrophages that express Gpnmb to one of the categories pro- or anti-inflammatory. Gpnmb expression is found in restorative macrophages in liver fibrosis [199] and correlates with infiltration of M2 macrophages in wound healing [200] and human glioblastomas [201]. However, Gpnmb is also expressed in an inflammatory microglia subtype [123]. And one study reports that Gpnmb is expressed in glioblastoma-associated microglia/macrophages that cannot be assigned to one of the two categories [133].

Expression of Gpnmb can in turn influence the polarization of the Gpnmb-expression cell. Here, literature is more consistent. Gpnmb expression boosts expression of anti-inflammatory marker genes, whereas Gpnmb-knockdown or -knockout results in the expression of rather pro-inflammatory genes [98, 134, 158, 170, 202]. Additionally, Gpnmb induces signal transducer and transcription activator 6 (STAT6) phosphorylation, a protein involved in IL-4-induced macrophage polarization [202]. Only one report shows that Gpnmb is responsible for the induction of the pro-inflammatory molecules TNFα, IL-1β, iNOS, and NO in activated BV-2 microglia [177].

Table 2: Influence of inflammatory or anti-inflammatory molecules on the expression of Gpnmb.
The effect of indicated stimulants on Gpnmb expression ranges from several degrees of induction (↑↑,↑,↗) to no effect (↔) or a downregulation (↓). MDDC: monocyte-derived dendritic cells, BMDM: bone marrow-derived macrophages, PBMC: peripheral blood mononuclear cells, PBMC-DDC: peripheral blood mononuclear cell-derived dendritic cells. Asterisk (*): Differentiation into dendritic cells additionally requires the survival factors GM-CSF and IL-4.

Inducer	Gpnmb	Cell type	Source
IL-2	↗	human PBMCs	[89]
IL-4	↗	human PBMCs	[89]
	↔	murine RAW264.7 macrophages	[170]
	↑	murine BMDM	[119]
	↔	murine BMDM	[179]
	↑	murine BMDM	[202]
	↑	murine primary astrocytes	[98]
	↔	murine RAW264.7 macrophages	[169]
IL-4 + IL-13	↔	murine RAW264.7 macrophages	[170]
IL-10	↗	human PBMCs	[89]
	↑	human PBMC-DDC	[149]
	↑↑	human MDDC*	[150]
	↔	murine BMDC	[153]
IL-11	↗	human PBMCs	[89]
IL-12	↗	human PBMCs	[89]
	↔	murine BMDC*	[153]
IL-13	↔	murine BMDC*	[153]
PGE2	↔	murine BMDC*	[153]
TGFβ	↔	rat Kupffer cells from liver fibrosis	[136]
	↑↑	human PBMCs	[89]
	↔	murine BMDC*	[153]
IL-6	↗	human PBMCs	[89]
	↔	murine BMDC*	[153]
IFNγ	↔	rat Kupffer cells from liver fibrosis	[136]
	↑	murine BMDC	[81]
	↑	murine keratinocytes	[81]
	↗	human PBMCs	[89]
	↔	murine B16-F10 melanoma cells	[157]
	↔	human MDDC*	[150]
	↑	murine BMDC*	[153]
	↔	murine RAW264.7 macrophages	[170]
	↓	murine BMDM	[179]
IL-1β	↑	murine BMDC*	[153]
TNFα	↗	human PBMCs	[89]
	↔	human MDDC*	[150]
	↑	murine BMDC*	[153]
	↑	porcine primary chondrocytes	[203]
IFN-γ + LPS	↑	murine RAW264.7 macrophages	[134]
	↑	murine BMDM	[134]
	↔	murine RAW264.7 macrophages	[170]
	↔	murine BMDM	[119]
	↓	murine BMDM	[202]
IL-1β, IFNγ, TNFα	↑	murine BMDC*	[153]
	↔	murine primary astrocytes	[98]
IL-1β, PGE2, TNFα	↑	human PBMC-DDC*	[89]
LPS	↓	rat Kupffer cells from liver fibrosis	[136]
	↔	human immature MDDC	[81]
	↑	murine BMDCs	[81]
	↔	human PBMCs	[89]
	↓	human MDDC*	[150]
	↔	murine RAW264.7 macrophages	[170]
	↑	murine BV-2 microglia	[177]
	↓	human PBMC-DDC*	[132]
	↔	murine BV-2 microglia	[148]
	↓	murine RAW264.7 macrophages	[169]

1.2.16. Impact on cancer via inhibition of T cells

Based on its structure, a negative regulation of B cells was predicted for Gpnmb [79]. Instead, a negative influence on T cell activation was revealed, which has major implications for cancer progression.

1.2.16.1. Inhibition of T cells

T cells are activated when antigens bind their unique and specific T cell receptor (TCR). A T cell receptor complex is formed by TCR, CD3 and co-receptors CD4 or CD8 that bind MHC class II or MHC class I, respectively. Recruitment of CD4 or CD8 in turn leads to the differentiation into a T helper cell or cytotoxic T cell, respectively. The extent of T cell activation however is determined by binding of its accessory molecules. Fine-tuning of T cell responses are mediated in inhibitory manner by programmed death (PD)-1, a receptor expressed by activated T cells, B cells and myeloid cells. PD-1 ligands (PD-L1, PD-L2) are expressed by antigen-presenting cells [204, 205]. Interaction of PD-1 and PD-L1 subsequently reduces T cell activation. Other famous accessory molecules are members of the B7 family (CD80 and CD86) that bind T cell receptors CD28 (stimulatory) and cytotoxic T-lymphocyte protein 4 (CTLA-4) (inhibitory) [206–208]. The idea of blocking co-inhibitory molecules on T cells and thus boosting the immune anti-tumor response received the Nobel Prize in 2018[I].

The "next" co-inhibitory couple is proposed to be Gpnmb on antigen-presenting cells and syndecan-4 on T cells [114]. Chung *et al.* propose this interaction to be similar to the PD-1/PD-L1 response [81]. Roughly 35% of $CD4^+$ and 10% of $CD8^+$ cells but not naïve T cells can be bound by Gpnmb [81, 114]. Gpnmb binds T cells on a later stage in T cell activation, when early activation marker CD69 starts to decline [89]. Gpnmb reduces proliferation as well as IL-2, IFNγ and TNFα secretion of activated mouse and human CD4 and CD8 T cells [81, 89, 114]. This is dependent on the receptor of Gpnmb, syndecan-4, which is induced on mouse and human activated T cells [89, 114]. A characteristic of the leukemic variant Sézary syndrome is high syndecan-4 expression in clonal malignant T cells, whereas syndecan-4 is hardly expressed in CD4 T cells of healthy controls [94].

Binding of human T cells to Gpnmb recruits CD148 to a syndecan-4/syntenin complex [209]. CD148 is phosphorylated, which increases its protein tyrosine phosphatase activity, mediating the inhibitory function of Gpnmb [209]. TCR, CD3 and the co-inhibitory molecule PD-1 or CTLA-4 are typically located in the immunological synapse, the interface between T cells and the antigen-presenting cell [209]. However, with binding to an antigen-presenting cell, syndecan-4 and CD148 are moving away from CD3 and the immunological synapse, suggesting a delayed time of action [209, 210]. Not much is known about the intracellular cascade that is initiated upon ligand-binding of syndecan-4. For instance, syndecan-4 is autophosphorylated at serine and tyrosine residues [89]. It was also reported that Gpnmb binding to activated T cells leads to its internalization [117], which is important for Gpnmb as a therapeutic target. For instance, antibodies targeting Gpnmb coupled to a cytotoxic agent are used in cancer therapy (chapter 1.3.2).

When Gpnmb expressed by antigen-presenting cells binds to syndecan-4 on T cells, it not only changes T cell activation, but also promotes dendritic cell maturation, resulting in highly potent antigen-presenting cells able to activate naïve T cells [85]. Binding of Gpnmb on dendritic cells

[I] https://www.nobelprize.org/prizes/medicine/2018/summary/

results in phosphorylation of Gpnmb at Y529 in its intracellular ITAM-like motif. This promotes secretion of IL-1β and TNFα and changes gene expression of dendritic cells in a way that they activate T cells stronger [85]. In contrast, the same research group reports later that phosphorylation of Gpnmb is necessary for the production of IFNγ, NO, and TNFα in MDSCs that convey the immune suppressive effect of antigen-presenting cells to T cells [146, 153]. IL-1β and IFNγ in serum is necessary for the induction of Gpnmb and thus T cell suppressive MDSCs [153]. Taken together, pro-inflammatory cytokines induce Gpnmb expression, which upon binding leads to the secretion of more pro-inflammatory cytokines by the Gpnmb-expressing cell that in turn activates T cells, whereas certain pro-inflammatory cytokines suppress T cell activity. Thus, Gpnmb might balance immune responses in a dual manner, or might promote different actions as soluble and full-length protein. The group of Arizumii first concentrated on Gpnmb-expressing dendritic cells, specified the T cell inhibiting cell type later to $CD11b^{+}Gr1^{+}$ cells/MDSCs and concluded that Gpnmb on macrophages and dendritic cells was not able to inhibit T cell activation [153]. $CD11b^{+}Gr1^{+}$ progenitors usually differentiate in healthy individuals but expand in cell numbers in cancer patients, conferring their immunosuppressive action [153].

1.2.16.2. Impact on angiogenesis

Gpnmb expression level correlates with tumor growth of mammary carcinoma cells in both immunocompetent and immunocompromised mice [124]. Thus, Gpnmb-containing tumor cells promote tumor growth in a way other than inhibition of T cells. Those additional effects of Gpnmb are inhibition of apoptosis and promotion of angiogenesis. Gpnmb-containing tumors display enhanced vascular density and CD31 recruitment [83, 124]. Promoted angiogenesis occurs in many different ways, both directly and indirectly via VEGF upregulation [116, 124]. Soluble Gpnmb attracts endothelial cells at a level equal to VEGF but not as high as fibroblast growth factor 2 (FGF2) [124]. Gpnmb induced neuropilin-1, a co-receptor for VEGF, and this induction is necessary for increased survival and proliferation of breast cancer cells [83]. By disrupting the vascular endothelial cadherin-β-catenin complex and thus the barrier function of endothelial cells, Gpnmb increases permeability and allows transmigration of tumor cells [116]. Taking together, Gpnmb is a potent stimulator of angiogenesis and thus a tumor-enhancing factor.

1.2.16.3. Impact on migration

As Gpnmb is a heparin-mediated integrin ligand for endothelial cells, it is responsible for trans-endothelial migration of dendritic cells [74], mesenchymal stem cells [119] and other bone marrow progenitors as well as tumor cells, while sabotaging migration of T cells [116]. This function promotes tumor growth after injecting breast cancer cells into mice [83]. Not only the heparin-binding PKD domain but also the integrin-binding RGD-motif and phosphorylation at its intracellular tail as well as the KLD domain of Gpnmb are important for migration, invasion and metastasis of cancer cells [83, 84, 87]. About 10% of endothelial cells express an unknown interaction partner for Gpnmb, which melanoma cells use as sites for invasion [116]. On the other hand, it was reported that Gpnmb is able to inhibit migration, matrigel invasion and the ability to grow in soft agar of a cancer cell lines [165, 166].

1.2.16.4. Impact on proliferation

The influence of Gpnmb on proliferation, cell survival and apoptosis is controversial.

Overexpression of Gpnmb increases proliferation and blocking Gpnmb with an antibody decreases proliferation in eosinophils [155]. Extracellular Gpnmb induces proliferation and cell survival in mesenchymal stem cells [119] and in NSC34 motor neuron cells [184]. Injecting breast cancer cells into immunocompromised mice, Gpnmb-mediated neuropilin 1 induction increases survival and proliferation [83]. The number of tumor-infiltrating macrophages increased as well being a result from either enhanced recruitment or increased proliferation. On the other hand, Gpnmb was also reported to inhibit [165, 166] or not affect [124, 157] proliferation of various cancer cell lines.

Gpnmb decreases apoptosis in breast cancer cells [83, 124]. Furthermore, Gpnmb was shown to protect from apoptosis when added to M1 conditioned medium usually inducing apoptosis in mesenchymal stem cells [119]. Gpnmb protects from cell death and neuronal degeneration in amyotrophic lateral sclerosis and cerebral ischemia by inducing ERK and AKT phosphorylation and ameliorating ER stress [110, 184]. Anti-apoptotic properties of Gpnmb could be conferred by the Gpnmb-target gene *stanniocalcin 1* [158]. However, cell death was not influenced by Gpnmb in non-tumorigenic mammary gland epithelial MCF12A cell line [166] and soluble Gpnmb binding and inhibiting T cells is achieved by cell cycle arrest rather than apoptosis indicated by fewer cells in the S-phase [81].

1.3. Gpnmb in diseases

1.3.1. Biomarker

Whereas the function of Gpnmb in diseases is not quite clear, its upregulation in various diseases implies a potential as a biomarker that has been emphasized multiple times. Gpnmb can be used as a marker to recognize immunosuppressive $CD11b^{+}Gr1^{+}$ cells/MDSCs in immune-evading melanomas [153], which can be used to detect melanoma recurrence [154]. In one case where the $DC\text{-}HIL^{+}CD14^{+}HLA\text{-}DR^{no/low}$ cells (the human equivalent for mouse $CD11b^{+}Gr\text{-}1^{+}$ cells) reappeared, a new melanoma was discovered [154]. Gpnmb expression was debated but is now rather excluded as a biomarker for melanoma [143]. Instead, Gpnmb is suggested as prognostic marker for shorter recurrence time and poor outcome in breast cancer, especially in triple-negative breast cancers [142] and discussed for hepatocellular carcinoma [211]. Still, soluble Gpnmb levels in serum of melanoma patients may provide clinical utility to monitor the response to MAPK inhibitor therapy [161]. Searching for a blood-based biomarker for AMPK activation to measure therapy success, Gpnmb was proposed [212]. Gpnmb was proposed as a biomarker for frailty in age [213], progressive renal injury [214], Niemann-Pick disease [215, 216], Gaucher disease [217–219], and nonalcoholic steatohepatitis in obesity [109], to monitor disease progression. In humans infected with the hepatitis C virus, Gpnmb can serve as a biomarker to detect late stages of liver fibrosis [167] as well as the late, chronic cardiac remodeling phase in viral myocarditis [220], and as a putative biomarker for wound healing and remodeling in myocardial infarction [179]. Gpnmb is upregulated in cardiac diseases [179], but in one study, Gpnmb plasma levels are reduced compared to healthy controls in mice and humans [221]. Thus, soluble Gpnmb levels were even proposed to serve as a biomarker to identify healthy, unaffected patients [221]. In patients suffering from heart failure, Gpnmb levels

in plasma are independent of pro brain natriuretic peptide (proBNP) levels, a common marker for cardiac damage, thus Gpnmb might predict other factors or derive from other conditions than proBNP [221]. Thus, Gpnmb was proposed so often as a biomarker that its specificity and useful application is debatable.

1.3.2. Cancer

Gpnmb was discovered in cancer cells [72], and this research field is to this point the broadest spectrum of knowledge about Gpnmb, which might help finding the endogenous role of Gpnmb.

1.3.2.1. Melanoma

Searching for genes that are highly expressed in melanoma, Tse *et al.* found a high Gpnmb expression in 15 out of 17 melanoma cell lines and melanoma clinical specimens, but relatively low expression in other tumor types [90]. The expression profile of Gpnmb in melanoma is more consistent than other melanosomal proteins used for targeted therapy [171]. Melanoma can be treated with an anti-Gpnmb antibody linked to the cytotoxic agent MMAE, called CDX-011 *glembatumumab vedotin*. Upon binding to Gpnmb presented on Gpnmb-expressing cells, the antibody-drug conjugate is internalized, the linker is cleaved inside the cell and the cytotoxic agent kills the cell [90]. In pre-clinical trials, treating Gpnmb-expressing melanoma cell lines or mice with a human melanoma SK-MEL-2 and SK-MEL-5 xenograft model with this antibody-drug conjugate strongly reduced tumor growth [90, 222]. Interestingly, anti-mitotic drugs or the unconjucated antibody alone had less effect than the conjugate [222], clearly showing that the conjugate is targeting the tumor cells directly and not the T cells. The antibody-based drug is currently in phase II study in patients with advanced melanomas [223].

Cancer cells not only benefit from Gpnmb expression through immune evasion (chapter 1.2.16.1), it also can confer drug resistance in response to treatment with BRAF/MEK inhibitors [161]. A typical sign of drug resistance in melanoma cells is the upregulation of Gpnmb and other MITF-mediated melanosomal genes like *Pmel17, Tyr, Trp1.* Combined therapy with MEK inhibitor and Gpnmb-targeting CDX-011 disrupts resistance to MEK inhibitor and reduces tumor growth in comparison to either drug alone [161]. Gpnmb is not only expressed by melanoma cells but also by immune suppressing MDSCs that lower the activation of tumor-reactive T cells and syndecan-4 containing T cells are necessary for this effect [153, 157]. MDSCs are an early indicator of cancer relapse, being potential biomarker and therapeutic target for melanoma [154]. Knockdown of Gpnmb leads to a substantial increase in survival of mice and to a decrease in tumor volume and growth [157]. The latter effect was absent in immune-deficient mice, suggesting the involvement of T cells. This effect on reducing tumor growth exceeds the effect of knocking down PD-L1 [157]. Whereas melanoma benefits from Gpnmb expression, EL-4 lymphoma and LL2 lung carcinoma do not differ in growth when injected into either wildtype or *Gpnmb*-knockout mice [153]. Their respective MDSCs have less suppressive effect than B16 melanoma-associated immune cells [153]. IL-1β and IFNγ, cytokines that are only released by B16 melanomas not by the other two tumor types, in serum are necessary for the induction of Gpnmb and thus functional MDSCs [153]. Suppressive activity of Gpnmb varies also between other cancers; MDSCs from colorectal and pancreatic cancer are able to suppress T cell activity, those from prostate cancers not [151].

1.3.2.2. Breast cancer

Like melanoma, breast cancers expressing Gpnmb are killed very efficiently by CDX-011 in mice [142]. Phase I/II clinical trial with CDX-011 in heavily pre-treated female patients with metastatic breast cancer resulted in longest progression-free survival (18 weeks) in patients with Gpnmb-positive tumors [224]. Phase II trial with heavily pre-treated patients with refractory breast cancer was conducted to evaluate whether treatment success depends on Gpnmb expression [225]. The primary end point of this study was not met, however, unexpected improvement was detected in a subgroup with triple-negative breast cancer that did not react to other treatments at all [225]. This cancer type is especially difficult to treat because it lacks therapeutic targets. Gpnmb however can serve as a marker for the most aggressive subtypes of triple-negative breast cancers and its expression correlates with enhanced metastasis and lower survival [142]. A second phase II trial specifically with Gpnmb-overexpressing, triple-negative breast cancer is in progress [225, 226]. More studies are planned concerning other Gpnmb-positive cancers including cutaneous and uveal melanomas, pediatric osteosarcoma, and squamous cell lung cancer.

Apart from tumor epithelium and stroma [142], especially the cancer stem cells might be a source of Gpnmb expression [227]. EGFR-mediated phosphorylation of Gpnmb at Y529 transduces dedifferentiation, invasiveness, and tumorigenesis induced by the oncogene MAFK [227]. A second effect of EGFR and Gpnmb interaction is the stabilization of Hif-1α and transcription of its target genes [86]. This increases the tumor glycolysis reprogramming and tumorigenesis. Other pro-tumor functions of Gpnmb in breast cancer include promotion of metastasis [142], angiogenesis [124] and proliferation, angiogenesis and metastasis as well as a decrease in apoptosis [83]. Unfortunately, the last study was not conducted in mice with intact immune system, so the impact of T cells remains unclear.

1.3.2.3. Other solid tumors

Gpnmb expression has been reported in multiple other tumors as well with differing findings about the role and expression site of Gpnmb. Most solid tumors like bladder, breast, colorectal, kidney, lung, melanoma, pancreatic, or prostate cancer exhibit high expression of Gpnmb in MDSCs [151]. In osteosarcoma however, high expression of Gpnmb derives directly from the tumors itself [156]. Gpnmb can promote glioblastoma growth directly [108] or indirectly via immune evading strategies [201]. Here, Gpnmb is upregulated in post-treatment glioblastomas that were resistant to therapies and were marked by an infiltration of M2 macrophages. In head and neck squamous cell carcinoma, Gpnmb belongs to the highest upregulated genes and was thus proposed to be a therapeutic target for the antibody-drug-conjugate, however its role in this cancer type is still debated [175, 228, 229]. Analogous to other diseases described below, Gpnmb levels quickly decrease with cancer treatment [187].

An anti-tumor role was rarely proposed for Gpnmb. It was suggested as a tumor suppressor gene because it decreases proliferation, invasion, migration and the ability to grow in soft agar *in vitro* [165, 230]. The *GPNMB* gene is hypermethylated in human adenoma and colon and hence Gpnmb is lower expressed in more aggressive tumors. Metz *et al.* consider Gpnmb as a tumor suppressor as well and report an inverse relationship of Gpnmb expression and aggressiveness of the cancer cell line [166].

1.3.3. Autoimmune diseases

The T cell inhibitory effect was also studied in diseases where overreactive T cells are detrimental. In contrast to cancer, the immune-suppressing role of Gpnmb is beneficial. Surprisingly, in a T cell-mediated skin inflammation (contact hypersensitivity), Gpnmb injection before and after challenge into sensitized mice promotes a worse allergic response [81]. The authors explain that injected Gpnmb prevents the interaction of Gpnmb and syndecan-4, thus disrupting the inhibitory effect on T cells [81]. Depleting syndecan-4 positive T cells with Gpnmb that is coupled to a ribosomal inhibitor 3 h before immune challenge reduces swelling and infiltrating leukocytes, an effect that lasted 3 weeks [117]. Like the novel cancer treatment with anti-PD-1 or CTLA-4 antibodies, blocking syndecan-4 with an antibody during challenge boosted the immune system and thus the allergic reaction in contact hypersensitivity [114].

In cancer, the immunosuppressive activity of Gpnmb is not consistent among all cancer types and in autoimmune diseases it is similar. Whereas Gpnmb exerts an immune-suppressive and protective role in EAE, a model disease for multiples sclerosis, [146], its role in psoriasis is limited [152]. In EAE, Gpnmb and syndecan-4 knockout have the same effect that is a more severe and prolonged disease of EAE with more autoreactive T cells [146]. Psoriasis is marked by hyperproliferative keratinocytes and massive infiltration of leukocytes into the epidermis. Patients exhibit more MDSCs that express more Gpnmb and T cells with higher expression of syndecan-4 than healthy controls [152]. Although levels of Gpnmb-containing MDSCs are higher than in melanoma [152, 154], the immune-suppressive capacity of psoriasis-associated MDSCs are lower than melanoma-associated MDSCs [152]. Therefore, even with high levels of Gpnmb-containing cells, psoriasis is not a disease where Gpnmb function is crucial [152].

1.3.4. Inflammatory diseases

Transcriptomic upregulation of rat Gpnmb is detected in several diseases like hypertension, autoimmune encephalomyelitis, tumors, liver cirrhosis, diabetes [79] as well as in an *in vitro* model of osteoarthritis [203] and in leprotic patients [231]. Colitis is a representative disease of Gpnmb function, because Gpnmb expression is increased in colitis and increases with severity and levels of pro-inflammatory cytokines [183]. Especially the macrophages in the mucosa are a source of Gpnmb. DBA/2J mice lacking Gpnmb have a worse outcome with higher levels of pro-inflammatory cytokines IL-1β and IL-6, suggesting an anti-inflammatory effect of Gpnmb [183].

1.3.5. Bone remodeling

Gpnmb was discovered in a osteopetrosis rat model [76], a disease with defective osteoclasts. Overexpression of Gpnmb in rats leads to higher bone volume, density and thickness compared to wildtype mice [232]. Gpnmb increases osteoblast numbers and bone mineralization and decreases osteoclast numbers and bone resorption. Thus, the balance between bone biogenesis and degradation is disturbed [182, 232]. Osteoblasts from DBA/2J mice show a reduced alkaline phosphatase staining and activity as well as calcium deposition, suggesting that Gpnmb is a positive regulator of osteoblastogenesis and matrix mineralization [93, 233]. Bmp-2 induces Gpnmb via Smad1, which in turn increases alkaline phosphatase activity [168]. Gpnmb influences signaling by either reducing TGFβ receptors and phosphorylated levels of Smad2/3 [93, 233] or increasing Col1a1, TGFβ1 as well as TGFβ receptor (TGFβR) 1 and 2 levels in osteoblasts [232]. Interestingly, serum of DBA/2J mice increases osteoblast proliferation but serum from DBA/2J-Gpnmb^{+} mice has no effect. The difference might be RANKL, a factor for

osteoclast differentiation and activation, whose expression and concentration in serum is reduced by Gpnmb [182, 232]. Thus, Gpnmb not only promotes osteoblastogenesis but also reduces osteoclast size, proliferation, fusion capability and activity, possibly due to aberrant cytoskeleton reorganization [120, 182]. Gpnmb inhibits osteoclast differentiation by binding to CD44 on their surface and downregulating ERK phosphorylation [120]. An increased bone resorption capacity of osteoclasts by Gpnmb is hypothesized to be a result of hyperresponsiveness to RANKL [120, 182]. Additionally, Gpnmb influences the differentiation of mesenchymal stem cells that can differentiate into either the osteoblast or the adipocyte lineage. Gpnmb might shift the differentiation towards an osteoblast fate, thereby decreasing adiposity and enhancing bone formation rather than bone resorption [234]. Concluding, Gpnmb has an anabolic role in bone formation.

1.3.6. Heart diseases

Screening for differentially activated genes after myocardial infarction, our group discovered Gpnmb, whose expression was highly elevated after myocardial infarction [179]. Approximately 7 days after myocardial infarction, *Gpnmb* mRNA peaks in murine peri-infarct heart tissues, showing a 300-fold increase compared to sham controls. Gpnmb expression derives from infiltrated macrophages into the heart as it is not expressed by resident macrophages [137, 179]. This timing coincides with the infiltration of reparative macrophages, suggesting a role in remodeling of the heart injury [235]. Corresponding results were reported by Li *et al.* [137]. In acute kidney injury, Gpnmb expression peaks after 7 days as well and is co-expressed with macrophage markers [137]. Here, Gpnmb is important for the uptake of apoptotic cell debris. In viral myocarditis, Gpnmb is upregulated in the third phase of cardiac remodeling after the acute viral and the subacute immune phase, which occurs approximately two months after infection [220]. Gpnmb has been proposed as a biomarker for myocardial infarction and heart failure with however contradicting data. Lin *et al.* report an increase of cardiac *Gpnmb* mRNA levels and a decrease in soluble Gpnmb in blood, whereas we found an increase of Gpnmb in both blood and heart of infarcted patients and mice [179, 221].

1.3.7. Fibrosis

Fibrosis is involved in the scarring process after an acute injury and involves the deposition of extracellular matrix. A balance must be maintained between fibrosis induction and resolution, thus fibrosis can be beneficial or detrimental. A common organ affected by fibrosis is the liver. Non-alcoholic liver diseases can be divided into the more common non-alcoholic fatty liver disease (NAFLD) that is defined as steatosis/fatty liver without liver damage and little or no hepatic inflammation, and the progressive form non-alcoholic steatohepatitis (NASH) with hepatitis/inflammation of the liver and liver cell damage with concurrent fibrosis. NASH may lead to cancer or cirrhosis [236, 237].

Gpnmb is highly expressed in fibrosis induced by eight weeks of carbon tetrachloride injections (CCl_4), two week bile duct ligation in mice [167] or renal interstitial fibrosis in unilateral kidney ureter obstruction in rats [238]. In humans infected with hepatitis C virus, Gpnmb is induced especially in later stages of liver fibrosis [167]. Furthermore, Gpnmb levels are elevated in cystic fibrosis patients [82], in NAFLD patients and even more in NASH patients [109]. In the latter, Gpnmb serum levels correlated with liver damage [109].

1.3.7.1. Liver fibrosis

Liver fibrosis can be induced by CCl_4 injection for several weeks. Liver damage marker alanine aminotransferase (ALT) peaks early after two days and has returned to baseline levels when macrophage infiltration peaks and resolution of injury commences [176]. Half of the mice die when liver fibrosis is prevented by depleting macrophages from day 2. As a result, ALT levels stay high, whereas fibrotic gene (*Tgfβ*, *Col1a1*, *Mmp9*, *Mmp13*) and cytokine (*Il1β*, *Il10*, *Ccl2*) expression as well as fibrosis (Sirius red and α-smooth muscle actin (SMA) staining) of liver tissue is decreased [176]. Gpnmb mRNA and protein levels increase successively until day six and fall down abruptly at day eight [176]. Conducting the same experiment in rats, Gpnmb peaks already after 48 h [136]. Thus, Gpnmb is induced especially in the recovery phase in a subset of CD68-positive macrophages [136, 176]. Some of the Gpnmb-positive cells phagocytose apoptotic bodies, a feature that is enhanced by Gpnmb [176]. In this study, Gpnmb promotes fibrosis as shown by increased Sirius red staining and increased expression of Mmp9, -13 and Timp1 after 6-8 days when Gpnmb is maximally expressed [176]. Here, Gpnmb does not influence ALT levels; however, the impact of Gpnmb on liver damage markers remains controversial. For instance, five days of liver-specific Gpnmb overexpression is not enough to alter both ALT or aspartate aminotransferase (AST) levels [118]. A lowering effect of Gpnmb on ALT levels was reported in mice fed a high fat high sugar diet [109] whereas an elevation of ALT levels was reported in liver fibrosis in choline-deficient diet-fed rats [173]. In the last two mentioned disease models, liver fibrosis is ameliorated by Gpnmb [109, 173] and Gpnmb reduces expression of fibrotic genes like *Col1a1*, *Timp1* and *-2* [173].

An important contributor to liver fibrosis are hepatic stellate cells that are activated upon liver injury and regulate the production of extracellular matrix components [167]. Gpnmb can be induced in activated compared to quiescent hepatic stellate cells [167] and either increases [176] or decreases [173] α-SMA, a marker for activated hepatic stellate cells in liver fibrosis.

1.3.7.2. Muscle fibrosis

In muscle, Gpnmb has a beneficial role on resolving fibrosis by inducing Mmps. This effect was observed after denervation of the gastrocnemius muscle of mice. *Gpnmb* expression peaks at day ten after denervation, which coincides with the peak of *Mmp2*, *-3*, *-9* and *-14* expression [172]. Likely, the soluble form of Gpnmb induces Mmp expression, because Gpnmb is expressed by sarcolemma of myofibers and S-100-positive Schwann-like cells in denervated skeletal muscle, whereas Mmp3 is expressed by infiltrated fibroblasts [172]. Mmp3 is basally not induced in muscle of Gpnmb-overexpressing mice but is further enhanced compared to wildtype mice when the muscle is denervated [172]. Thus, induction of Mmps by Gpnmb requires a specific context. In this short term experiment, Gpnmb overexpression had no major impact on muscle function [172]. After long term denervation for 70 and 90 days, Gpnmb prevents the degeneration of myofibers by inducing the expression of anti-fibrotic genes [174]. Thus, muscle fibrosis hinders regeneration and full strength recovery, which is prevented by Gpnmb overexpression [174].

No effect of Gpnmb on fibrosis was detected after myocardial infarction up to 4 weeks, although Gpnmb as well as Mmp9 and Timp1 is induced [179]. The same is true in osteotomy, despite elevated Mmp3 and -9 levels, no major effect on muscle function was detected in Gpnmb overexpressing mice [178]. Thus, Gpnmb is likely to play a role in the promotion or resolution of fibrosis, however the exact mechanism remains unclear.

1.3.8. Neurodegenerative diseases

Patients with Parkinson's disease have a reduced glucocerebrosidase activity [239], which is the same enzyme defective in patients with Gaucher disease. Analogous to Gaucher disease, Parkinson's disease is associated with the accumulation of glycosphingolipids in the substantia nigra. Whereas a Parkinson's disease mouse model with mutated glucocerebrosidase exhibit high Gpnmb levels (see chapter 1.3.9), mice modeling Parkinson's disease by synucleinopathy show neither altered glucocerebrosidase activity nor elevated Gpnmb levels. Thus, Gpnmb reacts to accumulated lipids and not to α-synuclein [239]. Gpnmb expression attenuates neuroinflammation in a third model of Parkinson's disease induced by the neurotoxin MPTP [98]. Here, Gpnmb is preferentially expressed by anti-inflammatory astrocytes, whereas its receptor CD44 is rather expressed by inflammatory astrocytes. Gpnmb shifts the environment in the brain to the anti-inflammatory side by reducing NO, ROS and IL-6 levels secreted by astrocytes in a CD44-dependent manner [98].

In two of three mouse models for Alzheimer's disease and in patients with sporadic Alzheimer's disease, *Gpnmb* mRNA levels increase time-dependently in brain tissue [148]. Gpnmb signal localizes to microglia, especially those surrounding amyloid β plaques, around vessel walls and in cells reminiscent of lipid-loaded macrophages. Treatment with amyloid β can even induce Gpnmb expression *in vitro* [148].

Gpnmb was detected as a protective factor in patients with amyotrophic lateral sclerosis (ALS) [184]. A mutation of superoxide dismutase ($SOD1^{G93A}$) induces neurotoxicity that mimics ALS in mice. Among 26 000 differentially regulated genes, Gpnmb belonged to the genes with the most dramatic increase in spinal cord of diseased mice. Gpnmb is expressed only at a late time point of 20 weeks and is expressed in motor neurons and astrocytes but not in microglia. In healthy wildtype mice, interaction with $SOD1^{G93A}$ inhibits glycosylation of Gpnmb, leading to poly-ubiquitination of Gpnmb and its proteasomal degradation. Activated astrocytes on the other hand can secrete the intact extracellular fragment of Gpnmb, which prevents the $SOD1^{G93A}$-induced cell death of motor neurons. By maintaining surrounding motor neurons, Gpnmb attenuates the pathogenicity of ALS. Muscle atrophy could be prevented by a simple Gpnmb injection into the gastrocnemius muscle of mice with mutated SOD1 [240].

1.3.9. Lysosomal storage diseases

Glycosphingolipids are important membrane components in the outer leaflet of the plasma membrane. The basic components of glycosphingolipids are palmitoyl-CoA and serine (**Figure 6**). Palmitate is known to induce Gpnmb [170]. However, induction of Gpnmb is caused rather by palmitate metabolites, because Gpnmb expression is abrogated when an enzyme metabolizing palmitate (serine palmitoyltransferase) is inhibited. Palmitate is converted to ceramide, which is the basis for several products like sphingolipids glucosylceramide (GlcCer) and lactosylceramide (LacCer), phosphoethanolamine, sphingosines, sphingomyelin and glycosylphosphatidylinositol (GPI) anchors for proteins [241, 242]. In two diseases, accumulation of ceramide metabolites induces Gpnmb expression.

Niemann-Pick disease is characterized by the accumulation of cholesterol and glycosphingolipids because the enzyme mediating intracellular cholesterol trafficking is defective. Lipid accumulation exceeds lysosomal capacity of macrophages that turn into foam cells. Gpnmb is expressed in those macrophages in patients and a mouse model for Niemann-

Pick disease, Npc1$^{nih/nih}$ [215, 216]. *Gpnmb* belongs to the highest upregulated genes in all three tested organs brain, liver and kidney of Npc1$^{nih/nih}$ mice. In kidney, it is the second highest upregulated gene after *V-ATPase V0 subunit d2* (*Atp6v0d2)*, encoding the lysosomal proton pump [216, 243]. *Gpnmb* expression and release correlates to the accumulation of glycosphingolipids, especially GlcCer and LacCer, but not to cholesterol or ceramide [216]. Other markers of lysosomal stress such as *cathepsin D* and *C-C motif chemokine 3* (*Ccl3*) react the same way as *Gpnmb*, suggesting not a Gpnmb-specific effect but an effect derived from unspecific lysosomal stress [216].

The second lysosomal storage disease, Gaucher disease, is characterized by the accumulation of the glycosphingolipid GlcCer because the enzyme degrading it to ceramide is defective, thereby resembling Niemann-Pick disease. GlcCer is converted by the alternative enzyme acid ceramidase to glucosylsphingosine, which accumulates in lysosomes and leads to chronic metabolic inflammation and the pathology of Gaucher disease [244]. A characteristic are lipid-loaded lysosomes of macrophages. Gpnmb is elevated in spleen, plasma and cerebrospinal fluid of patients and mice with Gaucher disease [217, 219]. Severity of Gaucher disease and production of GlcCer correlates with plasma Gpnmb levels [218].

Ceramide levels are elevated in obesity, simply because of the elevated levels of palmitate and amino acids, which are the basic elements for ceramide synthesis [245]. Inflammatory environment and toll-like receptor (TLR) 4 activation promote ceramide accumulation. Enhanced ceramide degradation to sphingosine-1-phosphate (S1P) has been shown to both protect against and promote insulin resistance. Thus, the role of S1P is controversial [242, 245–247]. S1P was also shown to transmit the beneficial effects of adiponectin whereas blockage of the ceramide degradation pathway and subsequent accumulation of ceramide induces apoptosis [248]. Ceramide can inhibit AKT independent of PI3K and thereby reduce Glut4 expression and insulin-mediated glucose uptake [248]. Lowering glycosphingolipid synthesis improves insulin sensitivity and hyperinsulinemia, reduces *de novo* hepatic lipogenesis and steatosis [249]. Treating hypercholesteremic mice with an inhibitor of glycosphingolipid synthesis, AMP-DNM, improves insulin resistance and liver steatosis. Concomitantly, GlcCer and LacCer in liver and blood as well as Gpnmb expression and macrophage markers in liver are lowered [250]. Treating leptin-deficient mice with AMP-DNM lowers GlcCer, but not ceramide in plasma [251]. Thus, not ceramide but GlcCer might account for Gpnmb induction.

Elevated ceramide levels affect insulin resistance. Ceramide can be generated through *de novo* synthesis or by sphingomyelin hydrolysis (**Figure 6**) [242, 245]. A third way to produce ceramides is the salvage/recycling pathway in acidic lysosomes [252]. The final product S1P is converted back to sphingosine that can re-enter the cytosol where it is transformed to ceramide and to complex sphingolipids. Interestingly, the pathology of Gaucher disease, caused by a mutation in the enzyme (gluco)cerebrosidase (GBA) can be rescued when additionally disabling GBA2, the second isoform of GBA (**Figure 6**). GBA but not GBA2 deficiency leads to the accumulation of sphingosine and S1P, which are implicated in inflammatory diseases [244]. GBA/GBA2 double knockout mice have elevated GlcCer but low Gpnmb levels. Only Gaucher disease suffering animals (GBA knockout) show high Gpnmb levels [218]. Thus, not circulating GlcCer levels but degradation products like glucosylsphingosine, sphingosine, S1P or lysosomal stress might induce Gpnmb.

Taken together, Gpnmb is shown to be induced by cholesterol, ceramide and GlcCer accumulation, however the most likely cause for Gpnmb upregulation are alternative degradation products of GlcCer such as glucosylsphingosine, sphingosine or S1P. Another

possibility is that overload of lysosomes induce Gpnmb expression as Gpnmb is required to mediate macroautophagy [137].

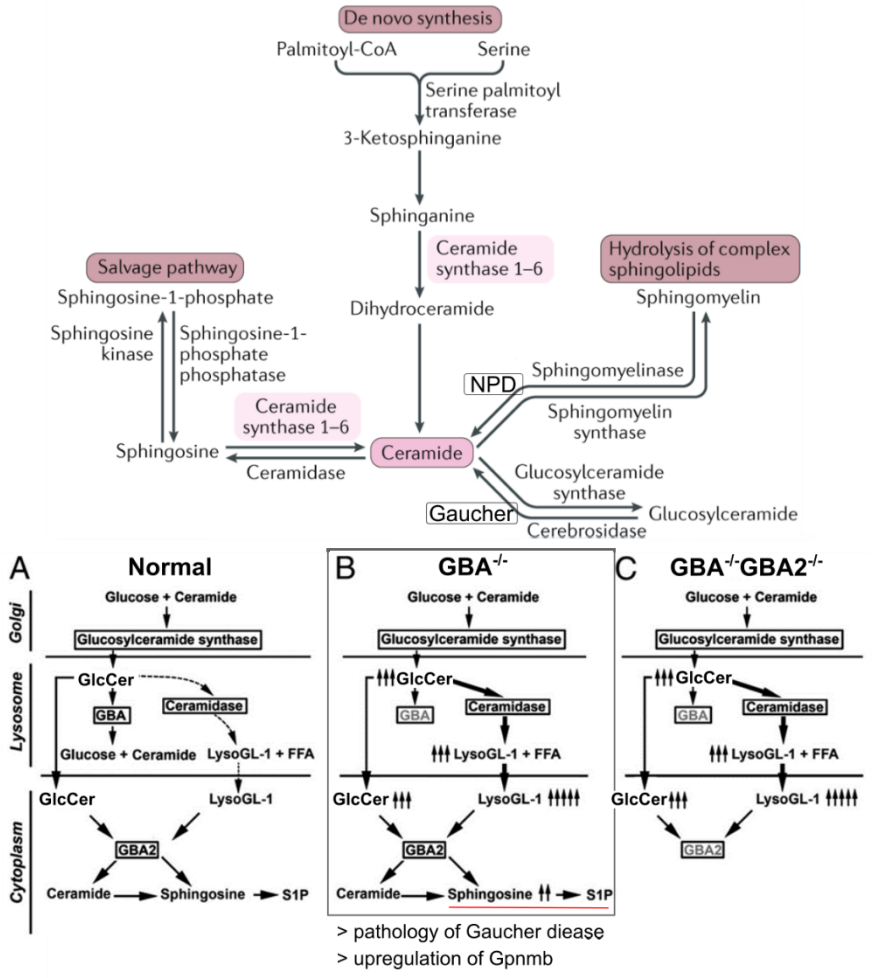

Figure 6:Glycosphingolipid pathways involved in Gpnmb upregulation. ***Above:*** *Palmitate and ceramide metabolism: Impaired conversion of sphingomyelin to ceramide results in Niemann-Pick disease (NPD) and impaired conversion of glucosylceramide to ceramide results in Gaucher disease. Both have highly upregulated Gpnmb levels. Figure adapted from [242] who reviews metabolites as regulators of insulin sensitivity.* ***Below:*** *Elevated glucosylceramide (GlcCer) levels can be degraded to sphingosine and sphingosine-1-phosphate in an alternate pathway, which is the regular salvage pathway of ceramide (see above).* **A)** *In normal mice, the lipid substrate glucosylceramide (GlcCer) is converted by the lysosomal glucocerebrosidase (GBA) to ceramide.* ***B)*** *Lysosomal GBA deficiency cause the pathology of Gaucher disease. Accumulating GlcCer and glucosylsphingosine (LysoGL-1) spill over into the cytoplasm, where the extralysosomal neutral glucocerebrosidase GBA2 converts them to ceramide and sphingosine, respectively.* ***C)*** *The pathology is rescued when GBA2 is mutated as well. Gpnmb upregulation might be caused by elevated sphingosine and sphingosine-1-phosphate (S1P) levels. FFA: free fatty acids. Figure and text adapted from [244].*

1.3.10. Obesity

Adipose tissue releases adipokines and is thereby an active endocrine organ. Adipokines control the balance between lipolysis and adipogenesis, immune cell infiltration and remodeling, and additionally, they are communicating the state of the organ to other tissues [253, 254]. Recently, Gpnmb was identified as a novel adipokine [255]. In screenings for differentially expressed genes induced by high fat diet, Gpnmb was found among the highest expressed genes in mice and humans [140, 255]. Among 45 000 genes influenced by high fat diet, *Gpnmb* was within the top three upregulated genes in the epididymal white adipose tissue of mice [140]. In genetically obese mice with leptin-deficiency, Gpnmb is upregulated as well [249].

Dahlman *et al.* show a differential expression of Gpnmb dependent on both obesity and adipose depot in humans [255]. There is a higher Gpnmb expression in inguinal than in visceral adipose tissue. Thereby, Gpnmb might contribute to the metabolic differences of those two fat depots.

Surprisingly, the opposite is true for mice. High fat diet highly induced Gpnmb production only in epididymal adipose tissue but not in inguinal or other fat depots in mice [170]. In obese OLETF rats, an animal model for metabolic syndrome and type II diabetes, *Gpnmb* transcript increases in all adipose tissues in obese compared to lean rats and increases with body weight [109]. In mice [170] and humans [118], Gpnmb expression correlates to body weight as well. Liver-specific Gpnmb overexpression is even able to increase white adipose tissue weight [118]. In humans, GPNMB serum levels are associated and contribute to obesity and metabolic parameters such as hip circumference, body mass index and insulin resistance [118]. Blocking Gpnmb even rescues obesity in mice by increasing thermogenic expenditure. Patients with type II diabetes exhibit elevated Gpnmb plasma levels compared to patients with normal glucose tolerance [109].

Overexpression of Gpnmb by the adipocyte fatty-acid–binding protein (aP2) promoter in epididymal adipose tissue and macrophages [256] but not in liver causes amelioration of hepatic fat deposition and fibrosis, suggesting an endocrine role of Gpnmb from adipose tissue to liver [109]. An endocrine effect was also proposed by Gong *et al.* but in the other direction. Hepatic Gpnmb is secreted and has a negative effect on fat accumulation and insulin sensitivity of white adipose tissue [118]. Gpnmb is upregulated by inhibition of SREBP pathway, which promotes biosynthesis of fatty acids. Both high fat diet and fasting increases and refeeding lowers Gpnmb expression. Surprisingly, Gpnmb was reported to derive mainly from hepatocytes and not from liver-associated Kupffer cells, which presents a deviation from other literature. Moreover, Gpnmb dramatically increases lipogenic genes and Glut1 and Glut4 expression in adipose tissue as well as fat mass [118]. However, overexpression of Gpnmb in adipose tissue macrophages does not improve adipose tissue weight [109]. Thus, an effect of Gpnmb directly on adipocytes is questionable.

In adipose tissue, Gpnmb is mainly expressed in the stromal vascular fraction and not in adipocytes [109, 170]. Gpnmb is abundantly expressed in 3T3-L1 pre-adipocytes but expression is downregulated during differentiation to adipocytes [109]. The expression of Gpnmb in adipose tissue correlates to the signal of macrophage markers around apoptotic adipocytes [170]. This formation is called “crown-like structures”, because the macrophages are arranged in a way that resembles the shape of a crown. Lysosomal stress, caused by palmitate, induces Gpnmb expression *in vitro* [170]. Thereby, Gpnmb might be important for metabolically activated macrophages. Due to its upregulation especially in adipose tissue macrophages, Gpnmb was proposed to play an important role in the development of low-grade inflammation in obesity, which enhances the pathogenicity of obesity [140, 170, 255]. However, another study did not find a difference in Gpnmb expression between metabolically activated macrophages (activated with glucose, palmitate and insulin), M1 (LPS and IFNγ) or basal macrophages [23]. Moreover, the positive effect of Gpnmb on adipocytes and fat mass occurs in a macrophage-independent manner [118]. Taken together, the effect of Gpnmb expression on adipose tissue remains elusive. We hypothesize that Gpnmb influences the development of obesity by reducing the inflammatory state of the adipose tissue.

1.3.11. Atherosclerosis

The chronic, low-grade inflammation of atherosclerosis is determined by macrophages that take up more and more lipids until they develop to foam cells. High cholesterol as well as LDL levels are the most important risk factor for the development of atherosclerosis. Gpnmb lowers cholesterol and LDL levels in mice fed a high fat high sugar diet [109], but elevates triglycerides

and cholesterol levels in serum of mice fed a choline-deficient, L-amino acid-defined diet [173]. A proteomics approach investigating atherosclerotic lesions of rabbits fed a high cholesterol diet detected Gpnmb as the protein with the most dramatic upregulation after high cholesterol diet [257]. The second and third protein were Apolipoprotein E and B, respectively, which have been associated with atherosclerosis before. In rabbits fed a normal chow, Gpnmb was hardly detectable in the ascending aorta. Gpnmb can disrupt the endothelial barrier and increase its permeability [116]. A leaky endothelial layer facilitates the deposition of LDL in the arterial wall and the transmigration of immune cells [41, 258]. Gpnmb-induced Mmp expression [175] could further destabilize the plaque [71]. Additionally, Gpnmb is expressed by a diverse array of macrophages that are united by a lipid overload. For instance, Gpnmb is expressed by lipid-loaded macrophages of Gaucher and Niemann-Pick disease [197], obesity [170] as well as Alzheimer disease [148]. Gpnmb is upregulated in renal tissue after acute kidney damage and even here, it localizes to vesicles containing cholesterol [137]. Thus, foam cells of atherosclerotic plaques should express Gpnmb as well, which was indeed shown in mice [137]. A role of Gpnmb in the vesicular transport and procession of lipids and thus in the development of foam cells is likely. However, a proof-of-concept study for the role of Gpnmb in atherosclerosis with a knockout control has not yet been conducted. We seek to prove that the presence Gpnmb can influence the plaque formation and thereby the disease progression of atherosclerosis.

1.4. Summary

In many diseases, Gpnmb levels are accurately able to reflect disease burden, with a decrease of Gpnmb after functional therapy. Its upregulation is mostly associated to the infiltration of antigen-presenting cells into the diseased tissue. In a first conclusion, the high upregulation is often deduced as disease-related and thus detrimental. However, the upregulation of Gpnmb might derive from macrophages that exert anti-inflammatory and immune-balancing effects, possibly via T cells. Cancer cells might utilize this immune-dampening function of Gpnmb to progress more efficiently. Eventually, most studies report more on the changes in Gpnmb expression rather than on its function. With potentially different functions of full-length cell-bound and soluble Gpnmb, its role in different diseases remains complicated and very often controversial findings are published.

2. Materials

2.1. Chemicals and Reagents

Table 3: Chemicals and Reagents

Chemicals and reagents	Company (Location)
0.05% Trypsin-EDTA (1x) (Gibco)	Thermo Fisher Scientific (Waltham, USA)
1,4-Dithiothreitol (DTT; 0.1M) (Invitrogen)	Thermo Fisher Scientific (Waltham, USA)
β-Mercaptoethanol	Sigma-Aldrich (St. Louis, USA)
3-Methyladenine (3-MA)	Cayman Chemical (Ann Arbor, USA)
8-Hydroxy-5-nitrochinoline (NQ)	Sigma-Aldrich (St. Louis, USA)
Acetone	Carl Roth (Karlsruhe, Germany)
Acetylated low density lipoprotein, human	Alfa Aesar (Haverhill, USA)
Acrylamide and bisacrylamide stock solution Rotiphorese® Gel 30 (37,5:1)	Carl Roth (Karlsruhe, Germany)
Agarose	Biozym (Oldendorf, Germany)
Agarose-TUBE1 (Tandem Ubiquitin Binding Entity) #UM401	Lifesensors (Malvern, USA)
Ammoniumperoxydisulfate	Sigma-Aldrich (St. Louis, USA)
Ampicillin Ampicillin	Serva (Heidelberg, Germany) or Life Technologies (Carlsbad, USA)
Bafilomycin A1 Bafilomycin A1	Calbiochem/Merck (Darmstadt, Germany) or Cayman Chemical (Ann Arbor, USA)
Bovine Serum Albumin (BSA)	Sigma-Aldrich (St. Louis, USA)
Bromphenol blue	Sigma-Aldrich (St. Louis, USA)
Butylated hydroxytoluene	MP Biomedicals (Eschwege, Germany)
Chloroform	Merck (Darmstadt, Germany)
Chloroquine diphosphate crystalline	Sigma-Aldrich (St. Louis, USA)
Complete protease inhibitor cocktail tablets	Roche (Basel, Schweiz)
Copper (II) sulfate solution	Sigma-Aldrich (St. Louis, USA)
D(+)-Saccharose	Carl Roth (Karlsruhe, Germany)
Deoxycholate	Serva (Heidelberg, Germany)
Deoxyribonucleotide (dNTP)	Bioline (London, UK)
Diethylpyrocarbonate (DEPC) Diethylpyrocarbonate (DEPC)	Serva (Heidelberg, Germany) Sigma-Aldrich (St. Louis, USA)
Dimethyl sulfoxide (DMSO)	Sigma-Aldrich (St. Louis, USA)
Disodium phosphate (Na_2HPO_4)	Sigma-Aldrich (St. Louis, USA)
DNase I recombinant	Roche (Basel, Schweiz)
Dulbecco's Modified Eagle Medium (DMEM), high glucose, GlutaMAX, pyruvate (#31966)	Thermo Fisher Scientific (Waltham, USA)
Dulbecco's Modified Eagle Medium (DMEM), low glucose, Glutamine, pyruvate (#31885)	Thermo Fisher Scientific (Waltham, USA)
Eosin Y solution	Sigma-Aldrich (St. Louis, USA)
Ethanol	Berkel AHK (Berlin, Germany)
Ethidium Bromide	Carl Roth (Karlsruhe, Germany)
Ethylenediaminetetraacetic acid (EDTA)	Serva (Heidelberg, Germany)

Chemicals and reagents	Company (Location)
Ethylenediaminetetraacetic acid (EDTA)	Carl Roth (Karlsruhe, Germany)
Eukitt® Quick-hardening mounting medium	Sigma-Aldrich (St. Louis, USA)
Exo 1	Sigma-Aldrich (St. Louis, USA)
Fetal bovine serum	Sigma-Aldrich (St. Louis, USA)
First Strand buffer (5x) (Invitrogen)	Thermo Fisher Scientific (Waltham, USA)
FRAP/mTOR Inhibitor (Rapamycin)	Cell Signaling Technology (Danvers, USA)
Gel loading dye Purple (6x)	New England Biolabs (Ipswich, USA)
Glacial acetic acid	Carl Roth (Karlsruhe, Germany)
Glycerol	Carl Roth (Karlsruhe, Germany)
Glycine	Carl Roth (Karlsruhe, Germany)
GM6001	Santa Cruz Biotechnology (Dallas, USA)
Golgicide A	Merck (Darmstadt, Germany)
GoTaq® qPCR Master Mix	Promega (Fitchburg, USA)
Hematoxylin Solution	Sigma-Aldrich (St. Louis, USA)
Heparin-Sodium (5 000UI/mL)	B.Braun Melsungen (Melsungen, Germany)
High cholesterol diet (HCD): EF TD88137 mod. Western Type Diet, E15721-34 10 mm pellets	ssniff (Soest, Germany)
High fat diet (HFD): MD.06414 Adjusted Calories Diet	Envigo (Huntingdon, United Kingdom)
HyClone Hank's 1X Balanced Salt Solutions (HBSS) without calcium and magnesium	GE Healthcare Life Sciences (Chicago, USA)
Hydrochloric acid (HCl)	Carl Roth (Karlsruhe, Germany)
IFN-γ (recombinant, murine)	Peprotech (Rocky Hill, USA)
IGPAL-CA-630	Sigma-Aldrich (St. Louis, USA)
IL-13 (recombinant, murine)	Peprotech (Rocky Hill, USA)
IL-4 (recombinant, murine)	Peprotech (Rocky Hill, USA)
Isoflurane	Abbott (Chicago, USA)
Isopropyl	Carl Roth (Karlsruhe, Germany)
Ketavet (100 mg/ml)	Pfizer (New York, USA)
LB Agar (Luria/Miller),	Carl Roth (Karlsruhe, Germany)
LB Broth (Luria/Miller)	Carl Roth (Karlsruhe, Germany))
Leupeptin	Sigma-Aldrich (St. Louis, USA)
Lipofectamine 2000 Transfection Reagent (Invitrogen)	Thermo Fisher Scientific (Waltham, USA)
Lipopolysaccharides from Escherichia coli O55:B5	Sigma-Aldrich (St. Louis, USA)
Macrophage colony-stimulating factor (M-CSF) (murine, recombinant)	Peprotech (Rocky Hill, USA)
Magnesium chloride ($MgCl_2$; 50mM)	Sigma-Aldrich (St. Louis, USA)
Methanol	Chemsolute/ Th.Geyer (Renningen, Germany)
MG132	Sigma-Aldrich (St. Louis, USA)
MicroAmp Optical Adhesive Film	Applied Biosystems (Foster City, USA)
Moloney Murine Leukemia Virus Reverse Transcriptase (M-MLV)	Promega (Fitchburg, USA)
Moloney Murine Leukemia Virus Reverse Transcriptase (M-MLV) (Invitrogen)	Thermo Fisher Scientific (Waltham, USA)
Mouse GPNMB/Osteoactivin Protein (His Tag) 50475-M08H	Sino Biological (Wayne, USA)
Nonidet P40 (NP-40) Nonidet P40 (NP-40)	USB United States Biochemicals (Cleveland, USA), Amersham Life Science (Little Chalfont, UK)
Normal donkey serum	dianova Jackson ImmunoResearch (West Grove, USA)

Chemicals and reagents	Company (Location)
Odyssey® Blocking Buffer	LI-COR Bioscience (Lincoln, USA)
Odyssey® two-color protein molecular weight marker	LI-COR Bioscience (Lincoln, USA)
OilRedO	Sigma-Aldrich (St. Louis, USA)
One Shot™ TOP10F' Chemically Competent E. coli (Invitrogen)	Thermo Fisher Scientific (Waltham, USA)
Palmitic acid	Sigma-Aldrich (St. Louis, USA)
Paraffin	Carl Roth (Karlsruhe, Germany)
Paraformaldehyde (PFA) $%, buffered	Fischar (Saarbrücken, Germany)
Penicillin-streptomycin (100x) (Gibco)	Thermo Fisher Scientific (Waltham, USA)
Pentobarbital	Release
Phosphatase inhibitor cocktail tablets PhosStop	Roche (Basel, Schweiz)
Phosphate buffered saline (PBS, 10x, for ELISA) (Gibco)	Thermo Fisher Scientific (Waltham, USA)
Phosphate buffered saline (PBS, cell culture)	Sigma-Aldrich (St. Louis, USA)
Phosphoric acid (H_3PO_4)	Sigma-Aldrich (St. Louis, USA)
pHrodo E.coli Bioparticles conjugate for phagocytosis	Life Technologies (Carlsbad, USA)
pHrodo Green zymosan A Bioparticles conjugate for phagocytosis	Life Technologies (Carlsbad, USA)
Potassium Acetate	Merck (Darmstadt, Germany)
Potassium chloride (KCl)	Sigma-Aldrich (St. Louis, USA)
Potassium dihydrogenphosphate (KH_2PO_4)	Merck (Darmstadt, Germany)
Precision plus protein™ standards all blue	Bio-Rad Laboratories (Hercules, USA)
Prestained protein marker, broad range 7-175 kDa	New England Biolabs (Ipswich, USA)
Protein A/G PLUS-Agarose Immunoprecipitation Reagent #sc-2003	Santa Cruz Biotechnology (Dallas, USA)
Proteinase K	Carl Roth (Karlsruhe, Germany)
Pvu II digestion enzyme	New England Biolabs (Ipswich, USA)
pX330-U6-Chimeric_BB-CBh-hSpCas9 plasmid #42230; RRID:Addgene_42230 http://n2t.net/addgene:42230	Addgene (Watertown, USA)
Quick-Load© 100 bp DNA ladder	New England Biolabs (Ipswich, USA)
Quick-Load© 1 kb DNA ladder	New England Biolabs (Ipswich, USA)
Random primers p(dN)6	Roche (Basel, Schweiz)
Red Blood Cell Lysis buffer (10x)	Biolegend (San Diego, USA)
RedTaq ® DNA Polymerase	Sigma-Aldrich (St. Louis, USA)
Revert Total Protein Stain	LI-COR Bioscience (Lincoln, USA)
RIPA Buffer (10X)	Cell Signaling Technology (Danvers, USA)
RNAse A	Promega (Fitchburg, USA)
RNAsin® Ribonuclease Inhibitor (Rnasin) RNAsin® Ribonuclease Inhibitor (Rnasin)	Promega (Fitchburg, USA) EURx (Gdansk, Poland)
Rompun 2% (Xylazin)	Bayer (Leverkusen, Germany)
Roswell Park Memorial Institute (RPMI) 1640 medium, GlutaMAX (#61870)	Thermo Fisher Scientific (Waltham, USA)
Roti-load 1 protein loading buffer	Carl Roth (Karlsruhe, Germany)
Rotiphorese 50x TAE Buffer	Carl Roth (Karlsruhe, Germany)
Saline (NaCl 0.9%)	B.Braun Melsungen (Melsungen, Germany)
Sirius red F3B (Direct Red 80)	Sigma-Aldrich (St. Louis, USA)
Sodium acetate	Sigma-Aldrich (St. Louis, USA)

Chemicals and reagents	Company (Location)
Sodium chloride/ NaCl	Sigma-Aldrich (St. Louis, USA)
Sodium citrate	Calbiochem/Merck (Darmstadt, Germany)
Sodium desoxycholate	Merck (Darmstadt, Germany)
Sodium dihydrogenphosphate	Merck (Darmstadt, Germany)
Sodium dodecyl sulfate (SDS)	Serva (Heidelberg, Germany)
Sodium hydrogencarbonate	Merck (Darmstadt, Germany)
Sodium hydroxide (NaOH)	Carl Roth (Karlsruhe, Germany)
Staurosporine	Cayman Chemical (Ann Arbor, USA)
Streptavidin-HRP	R&D Systems (Minneapolis, USA)
Taq DNA Polymerase with ThermoPol Buffer	New England Biolabs (Ipswich, USA)
Temed	Carl Roth (Karlsruhe, Germany)
Tet-O-FUW-EGFP plasmid #30130	Addgene (Watertown, USA)
Thapsigargin	Cayman Chemical (Ann Arbor, USA)
Thermus Aquaticus (Taq) DNA Polymerase (Invitrogen)	Thermo Fisher Scientific (Waltham, USA)
Transforming Growth Factor β1 (TGF-β1, mouse)	Cell Signaling Technology (Danvers, USA)
TriFast peqGOLD	peqlab (Erlangen, Germany)
Tris(hydroxymethyl)aminomethane	Carl Roth (Karlsruhe, Germany)
Triton X-100	Sigma-Aldrich (St. Louis, USA)
Trizol® (Invitrogen)	Thermo Fisher Scientific (Waltham, USA)
Tween-20	Sigma-Aldrich (St. Louis, USA)
Vectashield® Mounting Medium with DAPI (Hard Set)	Vector Laboratories (Burlingame, USA)
Xylene	Carl Roth (Karlsruhe, Germany)

2.2. ELISA, Kits

Table 4: ELISAs and Kits

ELISA	Company (Location)
Murine IL-1β Standard ABTS ELISA Development Kit # 900-K47	Peprotech (Rocky Hill, USA)
Murine IL-6 Standard ABTS ELISA Development Kit # 900-K50	Peprotech (Rocky Hill, USA)
Murine TNFα Standard ABTS ELISA Development Kit # 900-K54	Peprotech (Rocky Hill, USA)
Duo-Set ELISA Development System mouse Osteoactivin/GPNMB # DY2330	R&D Systems (Minneapolis, USA)
Rat/Mouse Insulin ELISA Kit #EZRMI-13K	Merck Millipore (Burlington, USA)
Mouse C-Peptide ELISA #80-CPTMS-E01	ALPCO (Salem, USA)
Kit	**Company (Location)**
ApoTox-Glo Triplex Assay	Promega (Fitchburg, USA)
Bicinchoninic Acid (BCA) Protein Assay Kit	Sigma-Aldrich (St. Louis, USA)
Cyto-ID Autophagy Detection Kit 2.0	Enzo Life Sciences (Farmingdale, USA)
PureYield™ Plasmid Maxiprep System	Promega (Fitchburg, USA)
TMB Microwell Peroxidase Substrate System	KPL (Maryland, USA)
Wizard ® SV Gel and PCR Clean-Up System	Promega (Fitchburg, USA)

2.3. Antibodies

Table 5: Primary and secondary antibodies.
ICC: Immunocytochemistry, IHC: Immunohistochemistry, WB: Western blot. mAb monoclonal antibody; pA: polyclonal antibody.

Protein	Antibody	Host	Method	Dilution	Company (Location)
Primary antibodies					
Adipophilin	Adipophilin pAb # 20R-AP002	guinea-pig	IHC	1:500	Fitzgerald (North Acton, USA)
AKT	AKT(pan) (C67E7) mAb # 4691	rabbit	WB	1:1000	Cell Signaling Technology (Danvers, USA)
AKT	pAKT (Ser473) (D9E) XP mAb #4060	rabbit	WB	1:2000	Cell Signaling Technology (Danvers, USA)
ATP6a2	ATP6ap2	rabbit	WB	1:1000	Sigma-Aldrich (St. Louis, USA)
CD31	CD31 pAb # ab28364	rabbit	IHC	1:160	Abcam (Cambridge, UK)
Gapdh	Gapdh 14C10, mAb #2118	rabbit	WB	1:1000	Cell Signaling Technology (Danvers, USA)
GM130	GM130 (H-7) mAb # sc-55590	mouse	ICC	1:100	Santa Cruz Biotech-nology (Dallas, USA)
Gpnmb	Osteoactivin/Gpnmb antibody #MAB2330 ➢ Not specific	rat	ICC WB	1:1000	R&D Systems (Minneapolis, USA)
Gpnmb	GPNMB pAb # 20338-1-AP ➢ No signal detected	rabbit	WB	1:1000	Proteintech (Rosemont, USA)
Gpnmb	Human Osteoactivin/GPNMB Antibody polyclonal IgG #AF2550	goat	IHC ICC	1:100 1:100	R&D Systems (Minneapolis, USA)
Gpnmb	Mouse Osteoactivin/Gpnmb pAb IgG #AF2330	goat	WB	1:1000	R&D Systems (Minneapolis, USA)
IRS1	IRS1 (D23G12) mAb #3407	rabbit	WB	1:1000	Cell Signaling Technology (Danvers, USA)
IRS1	pIRS1 (Tyr612) pAb IgG #44-816G	rabbit	WB	1:1000	Thermo Fisher Scientific (Waltham, USA)
LC3B	LC3B pAb #L7543	rabbit	WB	1:1000	Sigma-Aldrich (St. Louis, USA)
Mac-2	Mac-2 (Galectin-3) # CLO49P	rat	IHC	1:200	Acris (Herford, Germany)
Ubiquitin	Mono- and polyubiquitinylated conjugates mAb (FK2) IgG1 # BML-PW8810-0100	mouse	WB	1:1000	enzolifescience (Farmingdale, USA)
Secondary antibodies:					
	IRDye®-conjucated anti-mouse/rabbit pAb IgG (H+L)	donkey	WB	1: 10,000	LI-COR Bioscience (Lincoln, USA)
	Cy3-conjugated anti-rat	donkey	IHC ICC	1:300 1:200	dianova Jackson ImmunoResearch (West Grove, USA)
	AlexaFlour 488-conjugated	donkey	IHC	1:300	dianova Jackson

Protein	Antibody	Host	Method	Dilution	Company (Location)
	anti-guinea pig				ImmunoResearch (West Grove, USA)
	Cy3-conjugated anti-goat	donkey	IHC ICC	1:300 1:200	dianova Jackson ImmunoResearch (West Grove, USA)
	Cy3-conjugated anti-mouse	goat	ICC	1:200	dianova Jackson ImmunoResearch (West Grove, USA)
	AlexaFluor 488-conjugated anti-goat	donkey	ICC	1:200	Life Technologies (Carlsbad, USA)

2.4. Lab equipment

***Table 6: Lab equipment**.*
Imaging systems, instruments and devices as well as expendables.

Instruments and Materials	Company (Location)
Imaging systems	
Binocular CKX31 (cell culture)	Olympus (Tokio, Japan)
Binocular MZFLIII	Leica (Wetzlar, Germany)
Fluorescence microscope BZ-9000	Keyence (Neu-Isenburg, Germany)
Fluorescence stereo microscope M205 FA	Leica (Wetzlar, Germany)
Inverted microscope DMI6000B	Leica (Wetzlar, Germany)
Microplate Reader Infinite® M200	Tecan (Männedorf, Schweiz)
Odyssey® infrared imaging system	LI-COR Bioscience (Lincoln, USA)
Instruments and devices	
ACCU-Chek glucometer	Aviva/ Roche (Basel, Schweiz)
Agarose gel electrophoresis chamber	Biometra (Göttingen, Germany)
Centrifuge Biofuge 13	Heraeus (Hanau, Germany)
Centrifuge Labofuge 400e	Heraeus (Hanau, Germany)
Centrifuge Sorvall RC 5C	Heraeus (Hanau, Germany)
Cooling centrifuge 5804 R	Eppendorf (Hamburg, Germany)
Electronic multichannel pipettes Xplorer	Eppendorf (Hamburg, Germany)
Electronic multistep pipettes Xplorer	Eppendorf (Hamburg, Germany)
Electroporator 2510	Eppendorf (Hamburg, Germany)
FACS ARIA III cell sorter	BD (Franklin Lakes, USA)
FastPrep™-24 instrument	MP Biomedicals (Eschwege, Germany)
Fine balance	Kern&Sohn GmbH (Balingen, Germany)
Gel Imager C200	Azure Biosystems (Dublin, USA)
Gel Imager Transilluminator MultiImage™Light Cabinet	Alpha Innotech (San Leandro, USA)
Incubator Heracell vas160i CO_2 incubator (cell culture)	Thermo Fisher Scientific (Waltham, USA)
Incubator Heraeus Instruments Function Line	Heraeus (Hanau, Germany)
Incubator Labotect C60 Inkubator (cell culture)	Heraeus (Hanau, Germany)
Instruments for surgery and organ collection	FST Fine Science Tools (Heidelberg, Germany)
LSR Fortessa cell analyzer	BD (Franklin Lakes, USA)
Microbalance	Sartorius (Göttingen, Germany)
Microm modular tissue embedding center EC350-2	Thermo Fisher Scientific (Waltham, USA)
Microm STP 120 spin tissue processor	Thermo Fisher Scientific (Waltham, USA)

Instruments and Materials	Company (Location)
Microwave 8020	Privileg (Fürth, Germany)
Nalgene Mr. Frosty containers	Thermo Fisher Scientific (Waltham, USA)
NanoDrop™ 1000 spectrophotometer	Peqlab (Erlangen, Germany)
Nucleofactor® 2b device	Lonza (Cologne, Germany)
pH Meter pH Level 1	WTW (Weilheim, Germany)
Pipetboy acu	Integra Biosciences (Zizers, Switzerland)
Pipettes	Discovery Abimed (Langenfeld, Germany)
Power supply PowerPac™ HC	Bio-Rad Laboratories (Hercules, USA)
Pipettes Gilson Disposable CellstarR	Gilson (Middleton, WI, USA)
Precision balance 440-43N	Kern & Sohn GmbH (Balingen, Germany)
Real time PCR system 7900HT AbiPrism	Applied Biosystems (Foster City, USA)
Real-Time PCR System QuantStudio 5	Applied Biosystems (Foster City, USA)
Roller mixer SRT1	Snijders (Tilburg, Netherlands)
Roller mixer SU1400	sunlab (Mannheim, Germany)
Rotable platform Polymax 1040	Heidolph Instruments (Schwabach, Germany)
Rotary microtome HM 355 S	Microm (Walldorf, Germany)
SDS-PAGE gel electrophoresis chamber	Bio-Rad Laboratories (Hercules, USA)
Single channel Transferpette® micropipettes	Brand (Wertheim, Germany)
Sonicator Bioruptor plus	diagenode (Seraing, Belgium)
Sonicator Ultrasound Sonoplus	Bandelin electronic (Berlin, Germany)
Sterile laminar flow work bench safe 2020	Thermo Fisher Scientific (Waltham, USA)
Sterile laminar flow work Laminair®HB2448	Heraeus (Hanau, Germany)
Tank blotter	Bio-Rad Laboratories (Hercules, USA)
Thermocycler C1000	Bio-Rad Laboratories (Hercules, USA)
Thermocycler Master cycler nexus GX2	Eppendorf (Hamburg, Germany)
Thermocycler peqSTAR	Peqlab (Erlangen, Germany)
Thermomixer 5437	Eppendorf (Hamburg, Germany)
UV Stratalinker 1800	Stratagene (La Jolla, USA)
Vacuum pump BVC 21	vacuubrand (Wertheim, Germany)
Vacuum pump BVC professional	vacuubrand (Wertheim, Germany)
Water bath	GFL (Burgwedel, Germany)
Expendables	
384-well optical plate MicroAmp	Applied Biosystems (Foster City, USA)
Beads for tissue homogenization	MP Biomedical
Cell culture dishes and plates Cellstar®	Greiner AG (Kremsmünster, Austria)
Cell scraper	TPP (Trasadingen, Switzerland)
Cryogenic vial	Corning (Corning, USA)
Disposable pipettes Cellstar®	Greiner AG (Kremsmünster, Austria)
Falcon® 40µm Cell Strainer	Corning (Corning, USA)
Falcon tubes (15 and 50 ml)	Greiner AG (Kremsmünster, Austria)
FastPrep™ lysing matrix tubes and caps	MP Biomedicals (Eschwege, Germany)
Filter tips (10, 20, 200 and 1000 ml) Surphob	Biozym (Oldendorf, Germany)
GenePulse® electroporation cuvettes	Bio-Rad Laboratories (Hercules, USA)
Hypodermic needle Sterican 23G 1 ¼'' ø 0,60 x 30 mm	B.Braun Melsungen (Melsungen, Germany)
KOVA Glasstic® Slide 10 with grids	Hycor Biomedical (Garden Groove, USA)
Latex gloves	Sänger (Schrozberg, Germany)
Micro-slide 8 well ibi-treat	Ibidi (Gräfelfing, Germany)
Microvette Lithium/heparin-coated tubes	Sarstedt (Nümbrecht, Germany)
MiniCollect® K3EDTA-coated tubes	Greiner AG (Kremsmünster, Austria)

Instruments and Materials	Company (Location)
Nitrile gloves	Cardinal Health (The Hague, The Netherlands)
Normal chow (0.25%sodium)	Ssniff (Soest, Germany)
NUNC Maxisorp 96well ELISA plate	Sigma-Aldrich (St. Louis, USA)
Nunc™ 4-Well dishes for IVF	Thermo Fisher Scientific (Waltham, USA)
Pasteur pipettes	Carl Roth (Karlsruhe, Germany)
PCR strip tubes + caps Axygen	Corning (Corning, USA)
Plastipak™ Plastic Concentric Luer-Lock 50 mL Syringe	BD (Franklin Lakes, USA)
PVDF membranes	Amersham Life Science (Little Chalfont, UK)
Save-Lock Tubes	Eppendorf (Hamburg, Germany)
Serological pipettes	Sarstedt (Nümbrecht, Germany)
SuperFrost® Plus slides	Menzel Gläser (Braunschweig, Germany)
Syringe filters Whatman FP30/0.2CA-S	GE Healthcare life sciences (Chicago, USA)
Syringe filters Whatman FP30/0.45CA-S	GE Healthcare life sciences (Chicago, USA)
Syringes Luer Injekt® Solo	B.Braun Melsungen (Melsungen, Germany)
Syringes Omnifix® Solo 1mL	B.Braun Melsungen (Melsungen, Germany)
Syringes Single Use Luer	Herny Schein (New York, USA)
Whatman paper (3 mm)	Whatman (Maidstone, UK)

3. Methods

3.1. Genotyping of mouse lines

3.1.1. DNA Isolation for Genotyping

To determine the genotype of mouse lines, biopsies of ear, toe nail, or tail were incubated with 25 µL (toe nail) or 100 µL (ear, tail) of Ear buffer (**Table 7**) shaking overnight at 55 °C. The buffer contained the broad-spectrum serine protease Proteinase K for digestion of proteins and hair, hence making the DNA accessible. To inactivate Proteinase K activity, the samples were heated to 95 °C for 10 min. 250 µL (toe nail) or 750 µL (ear, tail) of Tris-EDTA (TE) buffer (**Table 7**) were added. RNase A in the TE buffer degraded RNA, resulting in genomic DNA in solution. Cellular debris was removed by centrifugation at full speed for 5 min. The supernatant contained the isolated genomic DNA of the respective animal. Samples were stored at 4 °C until usage.

Table 7: Solutions to isolate genomic DNA from animal biopsies.

	Ingredient	End concentration
Ear buffer (pH 7.0)	NaCl	200 mM
	Tris-HCl pH 8.5	100 mM
	EDTA pH 8.0	0.1 mM
	SDS	1%
	Proteinase K	1 mg/mL
TE buffer (pH 8.0)	Tris-HCl pH 7.4	10 mM
	EDTA pH 8.0	1 mM
	RNase A	20 µg/ml

3.1.2. Primers for genotyping of mouse lines

Primer sequences that were used to genotype animals are listed in **Table 8**. All oligonucleotides were synthetized by Biotez Berlin Buch GmbH and delivered in a lyophilized state. The primers were diluted in double-distilled water (ddH_2O) to a concentration of 50 pmol/µL and stored at -20 °C.

Table 8: Oligonucleotide sequences used for genotyping the indicated mouse lines.

Mouse line	Target gene	Primer name	Sequence (5' to 3')
C57BL/6N-Gpnmb$^{-/-}$	*Gpnmb*	86c gRtest3 fw	5'-CATAAAACAGAGCGGATCGCA
C57BL/6N-ApoE$^{-/-}$/Gpnmb$^{-/-}$		87 Gpnmb gRtest bl rv	5'-TGGGTCAACGAGTGTAAGCG
C57BL/6N-ApoE$^{-/-}$/Gpnmb$^{-/-}$	*ApoE*	ApoE_3:	5'-CGAAGCCAGCTTGAGTTACAG
		ApoE_WT5:	5'-TATCTAAACAGACTCCACAGC
		ApoE_KO5:	5'-GACTGGGCACAACAGACAATC
DBA/2J and DBA/2J-Gpnmb^{+}	*Gpnmb*	mGpnmb7F	5'-CTACAACTGGACTGCAGGGG
		mGpnmb8R	5'-AGCTCCATTTCTTCCATCCA

3.1.3. Polymerase Chain Reaction (PCR)

Genotyping was performed to distinguish wildtype from transgenic animals. PCR was performed according to the manufacturer's instructions. PCR efficiency was optimized by adjusting the concentration of primers, deoxyribonucleotides (dNTPs), magnesium chloride ($MgCl_2$) and genomic DNA as well as duration and temperature for annealing and elongation. The standard steps of the PCR can be seen in **Table 9**.

Table 9: General steps of a PCR to genotype animals.

PCR steps	Time	Temperature	Cycles
Initial denaturation	3 min	94 °C	1x
Denaturation	20-30 sec	94 °C	
Annealing	30 sec	55-65 °C	34x
Elongation	30-60 sec	68/72 °C	
Final elongation	5-10 min	68/72 °C	1x

3.1.4. Agarose gel electrophoresis

PCR amplicons were visualized by gel electrophoresis. Agarose was dissolved in tris-acetate-EDTA (TAE) buffer, diluted from Rotiphorese 50x TAE Buffer. To enable visualizing DNA in UV light, 5 µL 0.2% ethidium bromide was added to 35 mL of dissolved agarose. The PCR amplicon was mixed with gel loading dye and loaded onto an agarose gel. PCR products were electrophoretically separated at constant voltage (80-110 V) for 20-40 min. Fluorescing bands were visualized with UV light using a gel imager Transilluminator MultiImage™Light Cabinet or gel imager C200. A Quick-Load 100 bp DNA ladder served as molecular weight reference.

3.1.5. Genotyping of mouse lines

3.1.5.1. Genotyping the mouse lines DBA/2J and DBA/2J-Gpnmb$^+$

Table 10: PCR protocol for genotyping the mouse lines DBA/2J and DBA/2J-Gpnmb$^+$.

Stock conc.	Ingredient	Volume [µL]
10x	10x Selfmade PCR Puffer (Table 11)	2.5
50 mM	$MgCl_2$	1
5 mM	dNTP	2
7.1 µM	Primer mGpnmb7F	1
7.1 µM	Primer mGpnmb8R	1
	ddH_20	15.375
5000 U/mL	*Taq* DNA Polymerase (NEB)	0.125
	Genomic DNA	2
Enzymatic digestion		
	PCR amplification product	5 µL
	Pvu II	0.4 µL
	ddH_2O	4.6 µL

Time	Temperature	Cycles
2 min	94 °C	1x
20 sec	94 °C	
30 sec	58 °C	35x
30 sec	72 °C	
4 min	72 °C	1x
infinite	4 °C	

1.5 h	37 °C	1x
infinite	4 °C	

The two strains DBA/2J and DBA/2J-Gpnmb$^+$ were genotyped with the protocol in **Table 10**. The product was loaded onto a 3% agarose gel. The point mutation at *Gpnmb* R150* that can be found in DBA/2J mice presents a motif for the restriction enzyme Pvu II. Digestion resulted in two bands of the sizes 75 and 50 base pairs (bp) when the point mutation was present. *Gpnmb*

wildtype allele was marked by a single 125 bp band. The two strains were kept separately, however a heterozygous animal would be visualized by three bands at 50, 75 and 125 bp.

Table 11: Ingredients for 10x Self-made buffer.

	Ingredient	End concentration for 10x
10x Self-made PCR Buffer	KCl	500 mM
	Tris HCL pH 8.4	200 mM

3.1.5.2. Genotyping the mouse lines C57BL/6N-Gpnmb$^{-/-}$ and C57BL/6N-ApoE$^{-/-}$/Gpnmb$^{+/-}$

To determine the genotype of the *Gpnmb* alleles, a PCR mix of 25 µL in total was prepared and run with its respective PCR program (**Table 12**). A part of the amplicon mixture was visualized with a 3% agarose gel at 245 bp. The Wizard SV Gel and PCR Clean-Up System was used to purify the fragment from the rest of the PCR mix (20 µL). The DNA was eluted from the column with 100 µL ddH_2O and the concentration was measured using a Nanodrop 1000. The concentration of about 20 ng/µL was diluted to 5 ng/µL. This is a concentration applicable for sequencing at LGC Genomics GmbH (Berlin, Germany) using primer 87 Gpnmb gRtest bl rv (**Table 8**), resulting in a sequence like the one in **Table 13** and **Figure 11 A**. Ab1 files were analyzed with the Sequence Scanner Software 2 (2012, Applied Biosystems, Foster City, USA). **Table 14** shows the PCR protocol to discriminate between knockout (850 bp) and wildtype *ApoE* (560 bp) alleles that were visualized on a 2% agarose gel.

Table 12: PCR protocol for genotyping the **Gpnmb** *alleles in the mouse lines C57BL/6N-Gpnmb$^{-/-}$ and C57BL/6N-ApoE$^{-/-}$/Gpnmb$^{+/-}$.*

Stock conc.	Ingredient	Volume [µL]
10 x	ThermoPol Buffer (NEB)	2.5
5 mM	dNTP	1
5 µM	Primer 86c	1
5 µM	Primer 87	1
	ddH20	18.075
5000 U/mL	*Taq* DNA Polymerase (NEB)	0.125
	Genomic DNA	1.3

Time	Temperature	Cycles
30 sec	95 °C	1x
22 sec	95 °C	34x
30 sec	60.5 °C	
50 sec	68 °C	
5 min	68 °C	1x
infinite	4 °C	

Table 13: Genomic **Gpnmb** *sequence that is sequenced for genotyping.*
Capitals: untranslated region, red: start codon of translation, fat: deleted base.

CTGGGGAGTCAGAGTCAAGCCCTGACTGGTTGCAGGCGCTCGGAGTCAGCatg**g**aaagtctctgcggggtcctgggatttctgctgctg
gctgcaggactgcctctccaggctgccaagcgtgagtcccgtcctctctgggcgcttacactcgttgacccaaatgatgggccaggccctttgactggagtt

Table 14: PCR protocol for genotyping the ApoE alleles in the mouse lines C57BL/6N-Gpnmb$^{-/-}$ and C57BL/6N-ApoE$^{-/-}$/Gpnmb$^{+/-}$.

Stock conc.	Ingredient	Volume [µL]
10 x	ThermoPol Buffer (NEB)	2.5
5 mM	dNTP	2
50 mM	$MgCl_2$	1
10 µM	Primer ApoE3	0.75
10 µM	Primer ApoEWT5	0.75
10 µM	Primer ApoEKO5	0.75
	ddH20	15.625
5000 U/mL	*Taq* DNA Polymerase (NEB)	0.125
	Genomic DNA	1.5

Time	Temperature	Cycles
3 min	95 °C	1x
20 sec	95 °C	34x
20 sec	56 °C	
1 min	68 °C	
5 min	68 °C	1x
infinite	4 °C	

3.2. Animal experiments

The animal experiments were approved by Landesamt for Gesundheit und Soziales (LaGeSo, Berlin, Germany) and are listed with the animal license G 0018/16.

3.2.1. Atherosclerosis

3.2.1.1. Diet induced atherosclerosis

Feeding *ApoE*-knockout animals a high cholesterol diet (HCD) is a way to accelerate the development of atherosclerotic plaques in the aortic vessels accompanied by a chronic, low-grade inflammation. Therefore, 8-12 weeks old, female C57BL/6N-ApoE$^{-/-}$/Gpnmb$^{-/-}$ mice and their *Gpnmb* wildtype controls were fed a HCD (TD.88137) with 42% calories from fat (21% milkfat, 0.21% cholesterol per weight) for 8 and 12 weeks. Only 3-4 mice were held per cage to minimize stress. Body weight, consumed chow and water were measured twice a week. Once a week, the health status of each mouse was evaluated individually with the aid of a score sheet. At the end of the feeding period, body composition was measured of 4 h fasted mice as described in chapter 3.2.3.1.

3.2.1.2. Organ collection of atherosclerotic mice

Mice were anesthetized intraperitoneally with 100-150 mg/kg pentobarbital (Release, 500 mg/mL), diluted with saline, using a 1 ml syringe and a 23 G needle. All subsequent injections were conducted with a 23 G needle. Mouse abdomen and thorax were opened and the heart was exposed to take blood from the right ventricle with a heparin-flushed 1 mL syringe. 500 µL of blood were collected in a lithium/heparin-coated tube and kept on ice until centrifugation at 2000*g for 5 min at 4 °C. The plasma was stored at -80 °C for Enzyme-linked Immunosorbent Assays (ELISA) (chapter 3.5.5) and measurement of clinical parameters (chapter 3.2.3.2). The mouse was perfused with 1 mL of ice-cold Solution 1 (**Table 15**) in the left ventricle. Vena cava was cut and the mouse was perfused with 3 mL of ice-cold Solution 2. The gallbladder was removed to avoid contaminations. A piece from the tail for re-genotyping, heart, lung, liver, epididymal fat, perirenal fat, thymus, adrenal gland, pancreas, spleen, muscle, and skin of the ear were collected in FastPrep Tubes for RNA and protein analysis as well as in 4% buffered paraformaldehyde (PFA) solution for histology. The aorta was dissected using a binocular and fixed in 4% PFA. The mouse was perfused with 2 mL of Solution 3 and kidneys, brain and brown fat were dissected and fixed in 4% PFA solution for histology. Relevant organ weights (liver, epididymal fat, brown fat) were measured.

Table 15: Ingredients for solutions to perfuse mice.

	Component	End concentration
Solution 1: Saline/heparin	NaCl 0.9%	
	Heparin (5 000 UI/mL)	0.005% / 25 UI/mL
Solution 2: PBS/ BHT/ EDTA (pH 7.4)	PBS	
	EDTA	2 µM
	Butylated hydroxytoluene	20 µM
Solution 3: PFA (pH 7.4)	Paraformaldehyde 4%	
	EDTA	2 µM
	Butylated hydroxytoluene	20 µM
	D(+)-Saccharose	5%

3.2.2. Obesity

3.2.2.1. Diet-induced obesity

To induce obesity, 10-12 weeks old, male C57BL/6N-Gpnmb$^{-/-}$ mice and their wildtype controls were fed a high fat diet (HFD), with 60% calories (MD.06414) from fat for 16 weeks. To minimize stress and the risk of rivalry fights, only 3-4 mice were held per cage. Body weight, consumed chow and water was measured twice a week. Once a week, the health status of each mouse was evaluated with the aid of a score sheet. At the end of the 16 week-feeding period, body composition was measured of 4 h fasted mice as described in chapter 3.2.3.1.

3.2.2.2. Glucose Tolerance Test

After body composition measurement, an oral glucose tolerance test was conducted in now 6 h fasted mice to detect changes in glucose metabolism. This is a common test for pre-diabetes. The tail was anesthetized with a 0.25% bupivacaine solution to prevent pain. Then, a blood sample was collected from the tail vein with the ACCU-Chek glucometer to determine glucose levels. Mice were given one dose of glucose (3 g/kg at a concentration of 0.5 mg/µL) with an oral gavage and blood glucose was measured after 15, 30, 60, and 120 min.

3.2.2.3. Organ collection of obese mice

For anesthesia, a solution with 2 mL of 10% ketamine and 0.8 mL of 2% xylazine per 10 mL 0.9% saline was prepared. Each animal was injected intraperitoneally with 100 µL of this solution per 10 g body weight using a 1 ml syringe. Thus, each animal received 200 mg ketamine and 16 mg xylazine per kg body weight. All injections were conducted with a 23 G needle. Mouse abdomen and thorax were opened and the heart was exposed to take blood from the right ventricle with a heparin-flushed syringe. 500 µL blood was collected in a K_3EDTA-coated tube and kept on ice until centrifugation at 5000*g for 10 min at 4 °C. The plasma supernatant was stored for further analysis at -80 °C. The mouse was perfused with 5 mL of ice-cold Solution 1 (**Table 15**) containing saline with heparin in the left ventricle. A biopsy from the tail was collected for verification of the genotype. Heart, lung, liver, epididymal fat, thymus, kidney, pancreas, perirenal fat, spleen, muscle, skin of the ear, brain and brown fat were collected in FastPrep Tubes for RNA and protein analysis as well as in 4% buffered paraformaldehyde solution for histology. Relevant organ weights (liver, epididymal fat, brown fat) were measured.

3.2.3. Analysis of animal parameters

3.2.3.1. Body composition analysis

After the feeding period, mice were fasted for 4 h. A non-invasive body composition analysis was conducted to determine the percentage of water, fat and dry substance of the mice. In collaboration with Stefanie Schelenz and Martin Taube of the Max Delbrück Centrum for Molecular Medicine in the Helmholtz Association (MDC) Pathophysiology core facility, the measurement was performed with a nuclear magnetic resonance (NMR) spectrometer (LF90II, Bruker, Billerica, USA). Each measurement lasted about 3 min in a warm-temperate chamber, rendering anesthesia unnecessary.

3.2.3.2. Measurement of lipids and liver parameters in plasma

Plasma samples from mice were diluted in ddH_2O and triglycerides, cholesterol, HDL, LDL, alkaline phosphatase (ALP), aspartate aminotransferase (AST) and alanine aminotransferase (ALT) levels were analyzed in the MDC Pathophysiology core facility by Patrick Langner with an AU480 Chemistry Analyzer (Beckman Coulter, Brea, USA).

3.3. Cell Culture

3.3.1. Primary murine bone-marrow derived macrophages

Mice were sacrificed by cervical dislocation without anesthesia. The skin was incised ventrally and peeled from the lower trunk and hind limbs. The legs were dissected from the mouse. Femur and tibia were cleaned from muscles and tissue with paper and stored on ice until further use. The bones were transferred to a laminar hood, sterilized with 70% ethanol for 1 min and washed with DMEM containing penicillin/streptomycin. The epiphysis were cut off and the diaphysis was flushed with DMEM with a 23 G needle and a 5 ml syringe until the cavity became transparent. The bone marrow was filtered through a 40 µm cell strainer to remove bone particles, transferred to a 15 ml Falcon tube and centrifuged for 5 min at 800 rpm. The supernatant was discarded and the cells were incubated in Red Blood Cell Lysis buffer for 1 min at room temperature. Osmotic pressure led to explosion of erythrocytes. The reaction was stopped by adding 10 mL of DMEM. Cells were centrifuged and resuspended in 5 mL complete RPMI1640 medium (RPMI1640 containing GlutaMAX, 100 U/ml penicillin/streptomycin, 10% fetal bovine serum and 30 ng/mL recombinant macrophage colony stimulating factor (M-CSF) or 33% L929 conditioned medium). A sample was extracted and diluted 1:50 to determine the cell number. Cells were seeded at a number of 10 x 10^3 per well of a µ-Slide 8-Well, 10 x 10^3 per well of a 96-well plate, 1.5 – 2 x 10^6 per well of a 6-well plate or 10 x 10^6 per 10 cm dish and cultured at 37 °C and 5% CO_2 under water-saturated atmosphere. After three days, half of the medium was replaced by fresh complete medium. On day six, the former floating cells were now attached and branching, appearing like old tree trunks, a visual sign that the stem cells and monocytes differentiated to mature macrophages.

3.3.2. Cell lines

B16-F10, NIH-3T3 or L929 cells, stored in liquid nitrogen, were thawed quickly at 37 °C, diluted 1:10 in their respective medium to dilute the dimethyl sulfoxide (DMSO) from the freezing mix. After centrifugation, the pelleted cells were resuspended in their respective complete medium (see below) and plated in a culture dish. All centrifugation steps were conducted at 800 rpm for 5 min at room temperature.

Cell lines were kept in mycoplasma-free conditions in incubators with 37 °C and 5% CO_2 under water-saturated atmosphere. Cells were maintained by changing the medium every 2-3 days and splitting before reaching confluency. In detail, the cells were washed both carefully and thoroughly two times with pre-warmed phosphate buffered saline (PBS) to remove bivalent cations that would inhibit trypsin activity. The cells were detached by incubation with pre-warmed 0.05% trypsin-EDTA at 37 °C for 3-6 min. Trypsin activity was stopped by adding 10 mL of complete medium. After pelleting the cells, they were resuspended in complete medium and plated appropriately.

To freeze cells for long-term storage, cells were trypsinized, centrifuged, and resuspended in freezing mix containing 50% fetal bovine serum, 10% DMSO and 40% DMEM without antibiotics. In each cryogenic vial, 1 mL of cells was carefully pipetted. They were placed in a Nalgene Mr. Frosty container at -80 °C for 24 h to ensure slow freezing. Eventually, the vials were transferred to a liquid nitrogen container.

B16-F10 cells are skin melanoma cells from the C57BL/6J mouse strain. Melanocytic cells are an established source of Gpnmb expression [74, 78, 80] and were used additionally to primary macrophages to study Gpnmb function. The cells were kept in DMEM (4.5 g/L glucose, pyruvate, GlutaMAX), 1x penicillin-streptomycin and 10% fetal bovine serum.

NIH-3T3 are murine embryonic fibroblasts and were used to test the efficiency of the sgRNA to knockout *Gpnmb*. The cells were kept in DMEM (1 g/L glucose, pyruvate, glutamine), 1x penicillin-streptomycin and 10% fetal bovine serum.

L929 cells are murine fibroblasts that were a kind gift from the group of Prof. Kettenmann. They overexpress M-CSF and can be used to condition medium for differentiation of monocytes to macrophages [259, 260]. The cells were kept in DMEM (4.5 g/L glucose, pyruvate, GlutaMAX), 1x penicillin-streptomycin and 10% fetal bovine serum. The cells were cultured in T75 flasks. On day 1, cells were seeded in 25 mL medium. On day 4, the medium was filtered with a 0.2 µm syringe filter and stored at -20 °C. The confluent cells were incubated with 25 mL of fresh medium for another 3 days and the medium was filtered and stored at -20 °C. Two separate dishes were kept: (1) cells at high density to obtain conditioned medium and (2) cells that were maintained at pre-confluency to keep the cells in optimal growth state.

3.3.3. Starvation-induced autophagy

BMDMs were seeded in 6-well plates and differentiated as described in chapter 3.3.1. On day six, cells were washed twice with PBS to remove dead cells and traces of nutrients. The cells were starved for 1 – 4 h with Hanks balanced salt solution (HBSS), a solution with glucose but without amino acids, lipids, serum, magnesium and calcium. Cells were treated with bafilomycin A1 as a positive control for induction of autophagy. After indicated times, cells were washed 1-2 times with ice-cold PBS, lysed and scraped in TriFast or TriZol for RNA extraction or in 1x radioimmunoprecipitation assay (RIPA) lysis buffer for protein extraction.

3.3.4. Analysis of lysosomes

Fluorescently labelled conjugates that can be eaten by phagocytic cells are a useful tool to study phagocytosis. BMDMs were seeded in a 96-well or 4-well plate. Differentiated macrophages were washed 1-2 times with PBS and incubated in triplicates with pHrodo green zymosan A bioparticles or pHrodo red *E. coli* bioparticles for 30 min to 6 h. The substances were solved according to the manufacturer's instructions and due to previous tests further diluted 1:10 in complete RPMI1640 medium. After the incubation time, cells were washed with PBS, measured with a microplate reader with excitation wavelength at 560 nm or 509 nm and emission wavelength at 585 nm or 533 nm for *E. coli* or zymosan A bioparticles, respectively. Cells were fixed with 4% PFA for 20 min and stained with Hoechst 33342, diluted 1:1000 in PBS to a final concentration of 2 µM, to determine the cell number. Representative pictures were obtained from cells in 4-well plates with the fluorescence microscope BZ-9000.

3.3.5. Pull-down of ubiquitinated proteins

Tandem Ubiquitin Binding Entity (TUBE) is a protein that exhibits an up to 1000-fold increased affinity for poly-ubiquitin chains compared to traditional ubiquitin binding proteins [261]. Coupled to agarose, TUBEs can be used to purify ubiquitinated proteins. Binding and stabilization of poly-ubiquitin chains renders inhibitors for deubiquitination and protein degradation unnecessary. The pull-down was conducted according to the manufacturer's instructions.

3.3.6. Co-Immunoprecipitation for interaction proteomics

The protocol for co-immunoprecipitation was adapted from Hubner *et al.* [262]. BMDMs from femur and tibia were cultured in 10 cm dishes as described in chapter 3.3.1. On day six, cells were treated with vehicle (0.1% DMSO), 33 µM bafilomycin or 10 ng/mL TGFβ. Cells were scraped on ice and lysed with 100-200 µL IP Lysis Buffer (**Table 16**), vortexed and incubated on ice for 30 min with occasional vortexing. Unsolved cell debris was removed by centrifugation at 14 000*g for 10 min at 4 °C. Protein concentration was determined using a bicinchoninic acid kit (chapter 3.5.2). One aliquot per samples was removed for quality control on Western blotting ("Input"). The samples were adjusted with IP Lysis Buffer to the same volume. Anti-Gpnmb antibody (AF2330, R&D) was added according to the protein concentration. 1 mg of protein was matched with 10 µL (= 5 µg) of antibody. Proteins were incubated with the antibody for 3 h on a rotating wheel at 4 °C. To equilibrate agarose beads, 1.1 mL of A/G PLUS-Agarose Immunoprecipitation Reagent were washed three times with IP Lysis Buffer and centrifuged at 1400*g for 5 min at 4 °C. For 1 mg of protein, 40 µL of beads slurry were added. The protein/antibody/beads mixture was incubated for another 3 h on a rotating wheel at 4 °C. The samples were centrifuged at 1400*g for 5 min at 4 °C. The unbound proteins present in the supernatant were collected ("Flow through"), the pelleted bound proteins were washed 3 times with IP Wash Buffer (**Table 16**) and 3 times with PBS. The pellets were handed over to Dr. Philipp Mertins and Dr. Daniel Hernandez of the MDC Proteomics core facility who performed an on-bead protein digest with urea. After Tandem Mass Tag (TMT) labeling, the Gpnmb-binding proteins were measured with a mass spectrometer.

Table 16: Solutions for co-immunoprecipitation of Gpnmb-binding proteins.

IP Lysis Buffer	
NaCl	150 mM
Tris pH 7.5	50 mM
Glycerol	5%
IGPAL-CA-630	1%
NP40	1%
Deoxycholate	0.5%
SDS	0.1%
Protease inhibitor	1x
Phosphatase inhibitor	1x

IP Wash Buffer	
NaCl	150 mM
Tris pH 7.5	50 mM
Glycerol	5%

3.4. RNA expression analysis

3.4.1. RNA isolation

Organs were collected in FastPrep tubes containing 5 beads and stored at -80 °C until RNA isolation. On the day of the RNA isolation, samples were homogenized with 1 mL of TriFast or TRIzol Reagent twice for 40 sec at speed level 4 using the FastPrep™-24 instrument with a 5 min resting period in between. Thereafter, the manufacturer's instructions of TRIzol or TriFast were followed.

Cells were lysed in the cell culture dish with 1 mL TRIzol or TriFast, scraped, transferred to a FastPrep tube containing 5 beads, homogenized for 20 sec using the FastPrep machine and stored at -80 °C until RNA isolation. On the day of the RNA isolation, samples were thawed and the manufacturer's instructions of TRIzol or TriFast were followed.

RNA concentration and purity was assessed using a Nanodrop 1000 spectrophotometer and stored at -80 °C until use.

3.4.2. Complementary DNA synthesis

First, remaining DNA in the RNA sample was degraded to avoid amplifying genomic DNA that would infer a higher gene expression of the respective gene. Therefore, 1.5-4 µg of RNA were

Table 17: Protocol for DNA digestion of RNA samples.

Ingredient	Volume [µL]
10X buffer	1,5
Rnasin	1
DNase I	1
RNA	1,5-4 µg
ddH_2O	ad 15 µL

DNA digestion steps	Time	Temperature
DNA digestion	20 min	37 °C
Inactivation of DNase enzyme activity	10 min	75 °C
		directly on ice

Table 18: Protocol for reverse transcription of RNA samples.
The protocols for different brands of reverse transcriptase and respective buffer differ slightly. RT: Reverse transcription.

Ingredient (Invitrogen)	Volume [µL]
5X First-strand buffer (Inv.)	4
DTT (0.1 M)	2
Random primers	1
dNTP (5mM)	2
RNase inhibitor	1
M-MLV (Invitrogen)	1
RNA	1 µg
ddH_2O	ad 20 µL

RT steps	Time	Temperature
Priming	10 min	26 °C
Transcription	50 min	42 °C
Enzyme inactivation	5 min	95 °C
Conservation	infinite	4 °C

Ingredient (Promega)	Volume [µL]
5x M-MLV Buffer (Promega)	4
Random primers	1
dNTP (5mM)	2,5
RNase inhibitor	0,5
M-MLV (200U, Promega)	0,8
RNA	1 µg
ddH_2O	ad 20 µL

RT steps	Time	Temperature
Priming	10 min	26 °C
Transcription	60 min	37 °C
Enzyme inactivation	10 min	75 °C
Conservation	infinite	4 °C

treated with DNase digestion mix (**Table 17**). After heat-inactivating the enzyme, the mix was quickly chilled on ice to avoid re-formation of RNA secondary structures. Secondly, 1 µg of RNA was reverse transcribed into complementary DNA (cDNA) according to **Table 18**. The cDNA samples were stored at -20 °C until use.

3.4.3. Quantitative Real-Time PCR (qRT-PCR)

Gene expression on RNA level of cells or tissues was determined using qRT-PCR. The quantification was performed using a 384-well plate format in the qRT-PCR system 7900HT or the QuantStudio 5 with GoTaq® qPCR Master Mix, fluorescent DNA-binding BRYT Green® Dye and CXR as reference dye. The qRT-PCR program is shown in **Table 19**. Primers were designed to amplify fragments smaller than 200 bp, obviating the need for an elongation time. All primers exhibit a similar melting point in order to perform all reaction at the same annealing temperature of 60 °C. Diluting the template to 9 ng cDNA per reaction was sufficient in most quantifications (**Table 20**). However in some cases, gene expression was too low to reach the cycle threshold within 40 cycles, so the amount of cDNA was increased to 20 or 50 ng. A melting curve was carried out at the end of the qRT-PCR program as a quality control for the amplicon. Reactions with signs of unspecific fragments or primer dimers were excluded. All samples were quantified in duplicates. SDS2.4.1 or QuantStudio™ Design & Analysis Software v1.3.1 (both Applied Biosystems, Foster City, USA) was used for analysis. Cycle threshold was set manually in the exponential phase of amplification. The expression of the gene of interest was normalized to the expression of the housekeeping gene TATA-binding protein (Tbp). Relative gene expression between groups was calculated using the 2^{-dCt} method that results in the fold change of gene expression compared to the housekeeping gene.

Table 19: Protocol for qRT-PCR with GoTaq enzyme.

Stock conc.	qRT-PCR steps	Volume [µL]
	cDNA (1:50)	9
2x	GoTaq® master mix	10
5 µM	Primer Forward	0.4
5 µM	Primer Reverse	0.4
100x	CXR reference dye	0.2

Steps	Time	Temperature	Cycles
Initial denaturation	10 min	95 °C	1x
Denaturation	15 sec	95 °C	40x
Annealing and elongation	60 sec	60 °C	
Dissociation curve		60-99-60 °C	

Table 20: Overview of standard RNA/cDNA concentrations that were used to quantify mRNA expression.

Amount of reverse transcribed RNA	1 µg
Volume of reverse transcription	20 µL
Concentration of reverse transcription	50 ng/µL
Dilution for qRT-PCR	1:50
Concentration of cDNA used for qRT-PCR	1 ng/mg
Volume of cDNA used for qRT-PCR	9 µL
Total amount of cDNA used in one qRT-PCR reaction	9 µg

3.4.4. Oligonucleotide sequences used for qRT-PCR

Table 21: Oligonucleotide sequences used for qRT-PCR.
All oligonucleotides were synthetized by Biotez Berlin Buch GmbH and delivered in a lyophilized state. The primers were diluted in ddH_2O to a concentration of 50 pmol/µL and stored at -20 °C. For qRT-PCR reactions, primers were diluted to a working concentration of 5 pmol/µL. The primers are specific for the respective mouse gene.

Abbreviation	Gene	Sequence from 5' to 3'
Abca1	*ATP-binding cassette transporter*	CCCAGAGCAAAAAGCGACTC GGTCATCATCACTTTGGTCCTTG
Acc	*Acetyl-CoA carboxylase*	ATCCGCCTCTTCCTGACAA TGCCTGGAACCTCTTTGATT
Arg1	*Arginase 1*	CTCCAAGCCAAAGTCCTTAGAG AGGAGCTGTCATTAGGGACATC
Cd36	*Cluster of differentiation 36*	TTTCCTCTGACATTTGCAGGTCTA AAAGGCATTGGCTGGAAGAA
Col1a1	*Collagen, type I, α 1*	GACATGTTCAGCTTTGTGGACCTC GGGACCCTTAGGCCATTGTGTA
Col3a1	*Collagen, type III, α 1*	GGTGGTTTTCAGTTCAGCTATGG CTGGAAAGAAGTCTGAGGAATGC
Cpt1	*Carnitine Palmitoyltransferase 1A*	GTTCCCCGCGAGTCCCTCCA GCTTGACATGCGGCCAGTGGT
F4/80	*F4/80*	CATCCAGCCAAAGCAGAAGT CAGCTGCAGACTGTGTGTGT
Fasn	*Fatty-acid synthase*	GCAAGCTGTCCCCTGATG GAACCAGCCCCATCACAC
Fibronectin	*Fibronectin*	TCGCACTGGTAGAAGTTCCA ATCATTTCATGCCAACCAGTT
Foxo1	*Forkhead box protein O1*	ATGCTCAATCCAGAGGGAGG ACTCGCAGGCCACTTAGAAAA
Glut1/ Slc2a1	*Solute carrier family 2, facilitated glucose transporter member 1*	GCTGTGCTTATGGGCTTCTC CACATACATGGGCACAAAGC
Glut2/ Slc2a2	*Solute carrier family 2, facilitated glucose transporter member 2*	TGTGCTGCTGGATAAATTCGCCTG AACCATGAACCAAGGGATTGGACC
Glut3/ Slc2a3	*Solute carrier family 2, facilitated glucose transporter member 3*	TTCTGGTCGGAATGCTCTTC AATGTCCTCGAAAGTCCTGC
Glut4/ Slc2a4	*Solute carrier family 2, facilitated glucose transporter member 4*	ACATACCTGACAGGGCAAGG CGCCCTTAGT-TGGTCAGAAG
Glut6/ Slc2a6	*Solute carrier family 2, facilitated glucose transporter member 6*	TTGGTGCTGTGAGGCT TGGCACAAACTGGACGTA
Glut8/ Slc2a8	*Solute carrier family 2, facilitated glucose transporter member 8*	TTCATGGCCTTTCTAGTGACC GAGTCCTGCCTTTAGTCTCAG
Glut10/ Slc2a10	*Solute carrier family 2, facilitated glucose transporter member 10*	ACCAAAGGACAGTCTTTAGCTG ATCTTCCAAGCAGACGGATG
Glut12/ Slc2a12	*Solute carrier family 2, facilitated glucose transporter member 12*	GGGTGTCAACCTTCTCATCTC CCAAAGAGCATCCCTTAGTCTC
Gpnmb	*Glycoprotein nonmetastatic melanoma protein b*	GAAGCCAGCATCTCAGGTTC CTGAACACCGACCCAGTTTT
Gsk-3β	*Glycogen synthase kinase-3β*	CCCCACACATCTGCTAAGGT TACACACACGGTCGGAGAAG
Gyg1	*Glycogenin-1*	TCTTACCCCTGCTCCAACAC CTGACAAGGCTCCTGAGACA

Gys2	*Glycogen [starch] synthase, liver*	GGAAGAAACTCTATGACGGGTTATT TCATCGATCATATTGTGAGTGGTC
Igf-1r	*Insulin-like growth factor 1 receptor*	CATGTGCTGGCAGTATAACCC TCGGGAGGCTTGTTCTCCT
IL-6	*Interleukin-6*	CTGCAAGAGACTTCCATCCAGTT GAAGTAGGGAAGGCCGTGG
InsR	*Insulin receptor*	TTTGTCATGGATGGAGGCTA CCTCATCTTGGGGTTGAACT
Mmp-9	*Matrix metalloproteinase-9*	CCATGCACTGGGCTTAGATCA GGCCTTGGGTCAGGCTTAGA
Nos2	*Nitric oxide synthase, inducible*	GTTCTCAGCCCAACAATACAAGA GTGGACGGGTCGATGTCAC
ObRa	*Leptin receptor*	GAAGTCTCTCATGACCACTACAGATGA TTGTTTCCCTCCATCAAAATGTAA
ObRb	*Leptin receptor*	GCATGCAGAATCAGTGATATTTGG CAAGCTGTATCGACACTGATTTCTTC
Pparγ	*Peroxisome proliferator-activated receptor γ*	GAAAGACAACGGACAAATCACC GGGGGTGATATGTTTGAACTTG
Scd1	*Acyl-CoA desaturase 1*	CGTTCCAGAATGACGTGTACGA AGGGTCGGCGTGTGTTTC
Syndecan-4	*Syndecan-4*	CTCCTGGAAGGCAGATACTTCTC GTGTCATCCAGATCTCCAGAACC
Tbp	*TATA box-binding protein-like protein 1 (Tbpl1)*	CCCTATCACTCCTGCCACACC CGAAGTGCAATGGTGTTTAGGTC
Tgfβ1	*Transforming growth factor β-1 proprotein*	TGCGCTTGCAGAGATTAAAA CTGCCGTACAACTCCAGTGA
Tnfα	*Tumor necrosis factor α*	CCCTCACACTCAGATCATCTTCT GCTACGACGTGGGCTACAG

3.5. Protein expression analysis

3.5.1. Protein isolation

Organ tissues were collected in FastPrep tubes containing 5 beads (skin: 10 beads) and stored at -80 °C until protein isolation. On the day of the protein isolation, samples were homogenized with an adequate volume of RIPA buffer containing protease and phosphatase inhibitors for 40 sec several times at speed level 4 with a 5 min resting period in between, in which the samples were stored on ice, using the FastPrep-24 instrument. Sample homogenates were sonicated for 30 sec to disrupt double membranes and incubated at 4 °C or on ice for 30 min with intermittent mixing. Cell debris was removed by centrifugation at 13 000*g for 10 min at 4 °C. The supernatant with the dissolved proteins was transferred to a new 1.5 mL tube and stored at -20 °C until usage.

To extract proteins from cells, culture plates were washed twice with ice-cold PBS and scraped with an adequate volume of RIPA buffer containing protease and phosphatase inhibitors. For the well of a 6-well plate, 20-30 µL RIPA buffer was used, for a 10 cm dish 100-200 µL RIPA buffer. Cell homogenates were sonicated, centrifuged and stored as described above.

3.5.2. Determination of protein concentration

The concentration of proteins was determined using a bicinchoninic acid kit. Protein bonds reduce copper^{2++} to copper^{+}, which reacts with bicinchoninic acid. This complex has a purple color; therefore the color intensity correlates to the amount of protein in the reaction. Samples were measured in duplicates pure and in a 1:10 dilution. A standard series of bovine serum albumin (BSA) solved in RIPA buffer was used as reference. A 7-fold 1:2 dilution series was made starting from 1 mg/mL BSA downwards. In a 96-well plate, 5 µL of sample or standard and 100 µL working solution containing bicinchoninic acid and 4% (w/v) copper sulfate at a ratio of 50:1 were mixed. After 30 min at 37 °C, the colorimetric biochemical reaction was quantified at 562 nm using a microplate reader. The protein concentration was calculated using Excel 2013 (Microsoft, Redmond, USA).

3.5.3. SDS-polyacrylamide gel electrophoresis (SDS-PAGE)

SDS-PAGE was performed to separate proteins according to their size. Denaturing gels with 1 mm thickness were casted using the Bio-Rad electrophoresis system. Separating gels containing 8-15% acrylamide (**Table 22**, detection of IRS and phosphorylated IRS (pIRS) with 8%, detection of Gpnmb with 10%, detection of LC3B with 15% acrylamide gel) were casted and overlaid with isopropyl to straighten the separating gel-stacking gel interface. After polymerization, the isopropyl was removed with Whatman paper and the stacking gel containing 5% acrylamide and an appropriate comb were added. The polymerized gels were stored in a humid bag at 4 °C overnight.

Table 22: Ingredients for separating and stacking gels.
The volumes are sufficient for 2 gels.

	8% separating gel	10% separating gel	15% separating gel	5% stacking gel
ddH_2O	9.36 mL	7.9 mL	6.54 mL	5.5mL
1.5 M Tris pH 8.8	5.0 mL	5.0 mL	5.0 mL	
1 M Tris pH 6.8				1.0mL
SDS 10%	200 µL	200 µL	200 µL	80 µL
Acrylamide	5.44 mL	6.8 mL	8.16 mL	1.3 mL
APS	100 µL	100 µL	100 µL	50 µL
Temed	20 µL	20 µL	20 µL	20 µL

Table 23: Ingredients for SDS-PAGE and Western blot buffers.

Electrophoresis buffer	
Glycine	196 mM
Tris-HCl (pH 8.4)	20 mM
SDS	0.1%

Transfer buffer	
Glycine	200 mM
Tris	20 mM
Methanol	20%

TBST buffer	
NaCl	150 mM
Tris	50 mM
Tween-20	0.05%

Protein samples were adjusted to an equal amount of 10-50 µg protein with ddH_2O and one part of 4x Roti-load reducing loading buffer in a total volume of 20-30 µL. Samples were denatured at 95 °C for 5 min. Gels were immersed in electrophoresis buffer (**Table 23**) and 20 µL of the protein samples and 5 µL of a molecular weight marker (either Precision plus protein™ standards all blue, Odyssey® two-color protein molecular weight marker, or for the detection of LC3B: Prestained protein marker broad range 7-175 kDa) were loaded onto the gel. Empty wells

were filled with 20 µL of 1x loading buffer. Electrophoresis was performed first at 80 mV until the proteins migrated from the stacking into the separating gel, followed by 100-110 mV until the dye front migrated out of the gel.

3.5.4. Western blotting

Electrophoretically separated proteins were transferred from the SDS-PAGE gel onto a polyvinylidene difluoride (PVDF) membrane using a wet transfer system from Bio-Rad. The membrane was activated for 5 min with methanol. The stacking gel was removed and the separating gel was placed in a "sandwich" next to the activated membrane in between one sponge and two Whatman papers on each side. Air bubbles between the gel and the membrane were removed carefully. The blotting was performed in ice-cold transfer buffer (**Table 23**) at 0.28 mA for 2.5 h (LC3B: 1.5 h) at 4 °C.

The blotted membrane was blocked with Odyssey blocking buffer for a minimum of 30 min at room temperature. The primary antibody was diluted accordingly (**Table 5**) in a mix of 2.5 mL Tris-buffered saline containing 0.5% Tween-20 (TBST, **Table 23**) and 2.5 mL of Odyssey blocking buffer, and incubated at 4 °C overnight under constant rolling. Unbound primary antibody was removed with 3-4 washes 10 min each with 20 mL TBST. The membrane was incubated with Odyssey IRDye secondary antibody, diluted 1:10,000 in TBST, for 2 h at room temperature under constant rolling. After 3-4 washes 10 min each with 20 mL TBST, the membrane was scanned using an Odyssey infrared imaging system. The signals were analyzed using Image Studio Lite Software Version 5.2.5 (2015, LI-COR Bioscience, Lincoln, USA). The same membrane was incubated with anti-glyceraldehyde-3-phosphate dehydrogenase (Gapdh) antibody to normalize the signal on the membrane. Alternatively, the whole protein staining solution Revert was applied directly after blotting and before blocking according to the manufacturer's instructions.

3.5.5. Enzyme-linked immunosorbent assay (ELISA)

Gpnmb, Insulin, C-Peptide and cytokine levels in plasma as well as Gpnmb and cytokine levels in cell culture supernatants were determined with respective commercially available ELISAs (**Table 4**). If no pre-coated plate was included in the kit, a NUNC Maxisorp 96well ELISA plate was covered overnight with the capture antibody. The protocol was then conducted according to the manufacturer's instructions. The TMB Microwell Peroxidase Substrate System was used as a substrate for the horseradish peroxidase reaction. The reaction was stopped with an equal volume of 1 M phosphoric acid (H_3PO_4). Interpolation of unknown samples into the standard curve values was conducted with GraphPad Prism 5 software (San Diego, CA, USA) with the RIA/nonlinear regression (curve fit) tool.

3.6. Immunofluorescence

3.6.1. Immunocytochemistry

B16-F10 cells or BMDMs were seeded on µ-Slide 8-Well slides and cultured until the appropriate density or maturity was reached, respectively. The cells were washed twice with PBS and fixed with 4% PFA for 20 min. Cells were permeabilized with PBS containing 0.1% Triton X-100 (PBST) for 15 min, followed by blocking of unspecific antibody binding sites with 5% normal

donkey serum/PBS for 30 min. The first antibody was applied 1:100 in 1% normal donkey serum/PBS in a humid box on a rocking platform overnight at 4 °C. After 5 washes with PBST, the secondary antibody was applied diluted 1:200 in PBS and incubated in the dark for 2 h. The antibody was removed and replaced by Hoechst 33342, diluted 1:1000 in PBS to a final concentration of 2 µM. Hoechst 33342 was incubated in the dark for 10 min. After 5 more washes with PBST and 2 washes with PBS, the cells were observed with the confocal fluorescence microscope LSM710 of the MDC Advanced Light Microscopy core facility.

3.6.2. Immunohistochemistry

Organs were fixed in 4% PFA for several days to ensure thorough fixation. Then, samples were washed twice in PBS and dehydrated in a series of alcohol (2x 70% ethanol 30 min, 2x 80% ethanol 30 min, 2 x 96% ethanol 60 min, 2x isopropyl 60 min, 2x xylene 90 min). Organs were infiltrated with paraffin twice for 90 min and embedded in fresh paraffin. Then, the organs were cut with a rotary microtome, placed on a microscope slide and air-dried overnight at room temperature.

Paraffin sections were deparaffinized and rehydrated as follows: 3x xylene, 3x 100%, 1x 90%, 1x 80%, 1x 70%, 1x 60%, 1x 50%, 1x 40%, 1x 30% ethanol and 2x ddH_2O, each for 5 min. Antigens were unmasked by boiling the sections in sodium citrate buffer (10 mM sodium citrate, 0.05% Tween-20, pH 6.0) for 20 min. Sections were washed twice in PBS (diluted to 1x, **Table 24**) for 5 min and blocked with 10% normal donkey serum/PBS for 10 min. The primary antibody diluted in PBS was incubated in a humid chamber overnight at 4 °C. The next day, sections were washed 3 times for 5 min with PBS. If two different antigens were stained, the second primary antibody was applied again for one night and washed 3 times for 5 min with PBS. The respective secondary antibodies diluted in PBS were applied separately in the dark at room temperature for 2 h each and washed 3 times for 5 min with PBS. Sections were mounted with nuclei staining 4, 6-diamidino-2-phenylindole (DAPI) in Vectashield mounting medium and covered with a cover slip.

Table 24: Ingredients of 10x phosphate-buffered saline (PBS).

	Ingredient	End concentration of 10x
10 x PBS pH 7.4	NaCl	137 mM
	KCl	2.7 mM
	Na_2HPO_4	10 mM
	KH_2PO_4	1.7 mM

3.6.3. Analysis of atherosclerotic plaques

3.6.3.1. Analysis of lesion size in whole aorta with OilRedO

The aortas were dissected from mice from the ischiatic branches up to the heart with the three principal branches of the thoracic aorta. They were fixed in 2 mL Solution 3 (**Table 15**) for at least 2 days. Then, the fixative was replaced by Solution 2. The perivascular fat and adventitia were carefully removed under a binocular microscope (**Figure 7**). The plaques were visualized indirectly by the fat-staining OilRedO solution that was prepared by mixing 60 mL OilRedO stock solution with 40 mL ddH_2O. The solution was incubated for 1 h and filtered first through 2 filter papers and then through a 0.45 µm sterile filter. The aorta was placed 10 min in 60% isopropyl, 20 min in OilRedO staining solution, 10 min in 60% isopropyl and then several minutes in tap water.

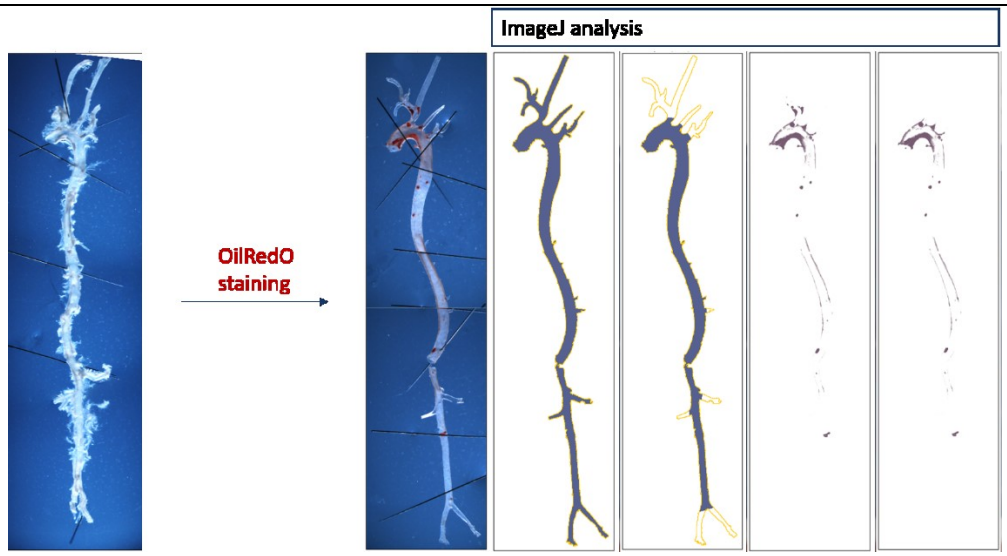

Figure 7: Analysis of plaque size with OilRedO staining and ImageJ.

The aorta was pinned down on 1% agarose and two pictures were taken per aorta with a Leica M205 FA microscope. The two pictures were merged with Photoshop CS V8 (Adobe, San Jose, USA). The plaques were analyzed with ImageJ 1.52i (Wayne Rasband, National Institute of Health, USA) (**Figure 7**). The tool "Colour Deconvolution" was used to separate the color of the picture into three new pictures with the vectors [r1]=0.53073084 [g1]=0.64286375 [b1]=0.5523142 [r2]=0.6582442 [g2]=0.61842936 [b2]=0.4292549 [r3]=0.6702717 [g3]=0.51439077 [b3]=0.53491867. The first color was closed, the second was used for whole area of aorta, and the third was used for the area of the plaques. To measure the areas, a threshold was set individually for each color (color 2/whole aorta: [0, 4], color 3/plaque area: [0, 33]) and identical for all aortas. A selection was created that included only positive signals. Branches that were varying between animals were excluded (**Figure 7**). The ratio of area of plaques versus area of whole aorta was used to create graphs.

3.6.3.2. Analysis of lesion size in aortic roots with hematoxylin and eosin

Hematoxylin and eosin staining was used to quantify lesion size. Sections were deparaffinized and rehydrated as described above (chapter 3.6.2) and washed with tap water for 10 min. Nuclei were stained with hematoxylin for 5 min and washed with tap water for 3 times 10 min each. Differentiation was achieved with a hydrochloric acid solution (0.11% HCl, 67.2% ethanol) for 3 sec. Sections were washed thoroughly with tap water, and an eosin solution was incubated for 5-10 sec. Sections were dehydrated in increasing alcohol series (shortly in 80%, 90%, 100% ethanol, isopropyl, and finally xylene for 30 min), mounted with Eukitt mounting medium and covered with a cover slip. Pictures were obtained with the light microscope BZ-9000.

ImageJ 1.52i was used to manually draw a selection around the plaques. Plaque size per section was calculated as average of the three lesions within one aortic root, one for each valve. The average of 4 sections in an interval of 45 µm of 3 different animals per strain was analyzed.

3.6.3.3. Analysis of fibrosis in aortic roots with Sirius red

Sirius red staining was used to visualize fibrosis in aortic root sections. Sections were deparaffinized and rehydrated as described above (chapter 3.6.2) and washed with tap water for

10 min. Section were incubated with Picro-Sirius Red Solution for 60 min in the dark and rinsed with 5% glacial acetic acid diluted in tap water. The sections were shortly dipped into 100% ethanol and left in xylene for 30 min. The sections were mounted with Eukitt mounting medium and covered with a cover slip. Pictures were obtained with the light microscope BZ-9000.

ImageJ 1.52i was used to manually draw a selection around the plaques. Sirius Red is differently intense within one lesion, the severeness of fibrosis equals gray area. The sum of gray area of all lesions per section was determined with the tool "Integrated density" that describes the product of the selected area (the plaques) and mean gray value (the intensity of the signal) and is therefore a product of size and magnitude of fibrosis. The average of 4 sections in an interval of 45 µm of 3 different animals per strain was analyzed.

3.7. Statistics

All data were subjected to statistical analysis using the GraphPad Prism 5 or 6 software (San Diego, CA, USA). Results in this study are presented as mean ± SEM (standard error of mean). The Student's t-test was applied for comparisons between independent pairs of means. Three or more groups with one variable of interest were analyzed using One-way analysis of variance (ANOVA) with Bonferroni post-test. Two variables of interest were analyzed by a Two-way ANOVAs with Bonferroni post-test. All variables were not considered to be normally distributed and thus a nonparametric version of each statistical test was chosen. Differences between two groups with a p-value of < 0.05 were considered to be statistically significant. The following categorization applies to all displayed graphs in this study: * $p < 0.05$; ** $p < 0.01$; *** $p < 0.001$; **** < 0.0001; and in the same way for all other symbols.

4. Animals

4.1. Animal husbandry

All mouse lines were kept in pathogen-free conditions in the MDC animal facility according to the German Animal Protection Law. Mice were housed in individually ventilated cages at a temperature of 21-23 ˚C, with a light/ dark cycle of 12 h each. Chow (0.25% sodium) and water were provided *ad libitum.* Breeding consisted of 1-2 female and one male mouse. The offspring was weaned 21 days after birth (p21). The genotype was determined from isolated DNA from either toe nail (p5-9) or ear (after p14), or, at the end of an animal experiment, DNA from the tip of the tail for verification of the genotype. Dependent on the weight, up to six animals of the same sex were hold in one cage. The animal experiments were reviewed and approved by the LaGeSo (Berlin, Germany).

The DBA/2J strain contains a naturally occurring point mutation in the *Gpnmb* gene, resulting in a premature stop-codon at R150* and thereby a functional *Gpnmb* knockout [96]. A co-isogenic control strain was created by crossing DBA/2J and C57BL/6J, backcrossing the progenies with DBA/2J mice for 10 generations and selecting for wildtype *Gpnmb* allele [263], resulting in the DBA/2J-Gpnmb^{+}/SjJ strain that is called DBA/2J-Gpnmb^{+} strain from now on. DBA/2J-Gpnmb^{+} (*Gpnmb* wildtype) and DBA/2J (*Gpnmb* mutant) mouse strains were ordered from The Jackson Laboratory and kept as inbred strains.

C57BL/6N-Gpnmb$^{-/-}$ and C57BL/6N-ApoE$^{-/-}$/Gpnmb$^{-/-}$ mice were generated in cooperation with Prof. Ralf Kühn's core facility in MDC (chapter 4.3). C57BL/6N-Gpnmb$^{-/-}$ mice were held homozygously knockout for *Gpnmb* alleles and were compared to the C57BL/6N wildtype strain in animal experiments. C57BL/6N-ApoE$^{-/-}$/Gpnmb$^{-/-}$ mice were kept homozygously knockout for *ApoE* and heterozygous for *Gpnmb* alleles. Thus, *Gpnmb* homozygous knockout and wildtype siblings were compared in animal experiments.

The wildtype control C57BL/6N mice were ordered from The Jackson Laboratory and kept as inbred strains.

ApoE is synthesized by liver, macrophages, and in nervous system [67]. It is part of lipoprotein particles and binds to the LDL receptor. ApoE is essential in the clearance of lipoprotein particles by liver and peripheral tissues [66]. ApoE deficiency in mice results in diminished LDL uptake by the liver and thus increasing circulating LDL levels. As a consequence, LDL is increasingly deposited in the arterial wall, leading to atherosclerotic lesions. A mouse deficient in ApoE was created in 1992 and is since a useful model to study atherosclerosis in mouse [264]. Even though mice are naturally high HDL and low LDL animals and differ in that way from humans, similar plaque development can be induced with the *ApoE*-knockout mouse model [69, 70].

4.2. DBA/2J mouse line

The DBA/2J strains are commercially available and a convenient animal model to study Gpnmb function. *Gpnmb* mRNA of DBA/2J mice, which theoretically should be equally abundant as in DBA/2J-Gpnmb^{+} mice, is downregulated, probably due to nonsense mediated decay [135, 265]. We used DBA/2J and DBA/2J-Gpnmb^{+} mouse strains to study Gpnmb function, however there are some reasons why we decided to change to a new mouse model. Although no functional Gpnmb protein should be present, uncertainty remains about the influence of the truncated remnant of Gpnmb in DBA/2J mice. The truncated version was discovered as a punctate, perinuclear pattern in the ER [233], although most other reports treated DBA/2J as a complete *Gpnmb*-knockout or use C57BL/6 mice with the R150* mutation from DBA/2J mice as knockout control [109]. Additionally, comparisons of the DBA/2J strain to the commonly used C57BL/6 strain are difficult. Even genetically identical mouse strains are known to exhibit differences in behavior and phenotype dependent on diet and environment, thus the phenotype of different inbred strains are even further apart. Therefore, we aimed for a complete *Gpnmb*-knockout on a C57BL/6 background.

4.3. Generation of C57BL/6N-Gpnmb$^{-/-}$ and C57BL/6N-ApoE$^{-/-}$/Gpnmb$^{-/-}$ mouse line with Crispr-Cas9

C57BL/6N-Gpnmb$^{-/-}$ and C57BL/6N-ApoE$^{-/-}$/Gpnmb$^{-/-}$ were generated on the C57BL/6N and C57BL/6N-ApoE$^{-/-}$ background strain, respectively. The first base after the start codon ATG of the gene *Gpnmb* was deleted with Crispr (Clustered regularly interspaced short palindromic repeats)-Cas9 (Crispr-associated) technology.

4.3.1. The technology Crispr-Cas9

Crispr-Cas9 is a technology that uses sequence-specific nucleases and serves as a method to mutate the target locus of interest in living organisms. Cas9 is an endonuclease that cleaves DNA on both strands and is directed to a DNA locus that is complementary to the RNA sequence of the single-guide RNA (sgRNA) within the Crispr-complex. The sgRNA contains normally about 20 complementary nucleotides. A protospacer-adjacent motif (PAM, 5'-NGG-3') must exist on the 3' end of the targeted DNA locus, which is the only strict limitation when selecting the sgRNA. The PAM serves as a binding site for Cas9. A double strand break occurs 3-4 bp upstream of the PAM sequence. Injecting Crispr-Cas9 into zygotes will lead to cleavage of the target locus in the zygote and continuously in all progeny cells. Classical repair mechanisms like nonhomologous end joining (NHEJ) will ligate the break if there is no template present, otherwise, with appropriate donor DNA, homology-directed repair (HDR) might fix the break. Injecting synthetic single-stranded DNA (ssDNA) is a tool to direct the repair mechanism towards homology-directed repair, thus minimizing variation in the resulting mutations [266].

4.3.2. Design of sgRNA to target Gpnmb

First, the website http://Crispr.mit.edu/[J] was used to check off-target sites and efficiency (**Figure 8**). Next, the website CRISPOR http://crispor.tefor.net/ was used to "design, evaluate and clone guide sequences for the Crispr-Cas9 system" (**Figure 9**). It was used to check for efficiency, off-target effects and PAMs close to the sgRNAs. Guide #5 of **Figure 8** was selected as sgRNA to target the *Gpnmb* locus.

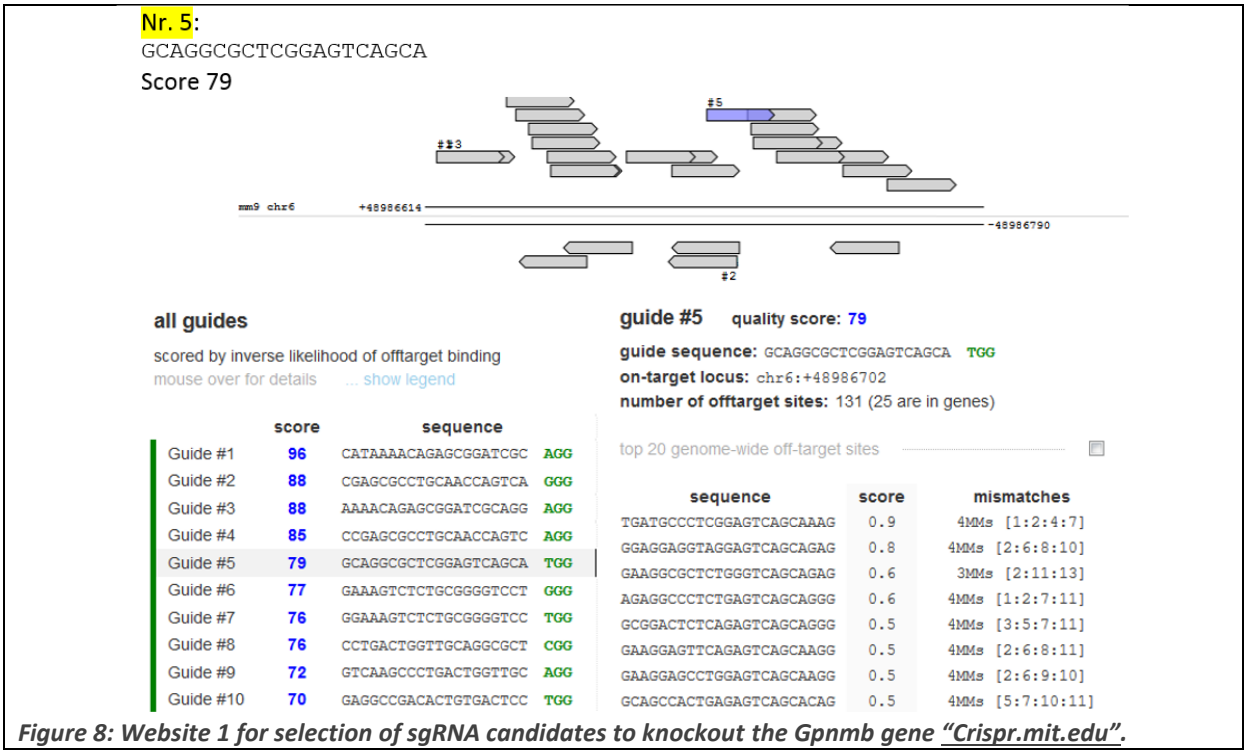

Figure 8: Website 1 for selection of sgRNA candidates to knockout the Gpnmb gene "Crispr.mit.edu".

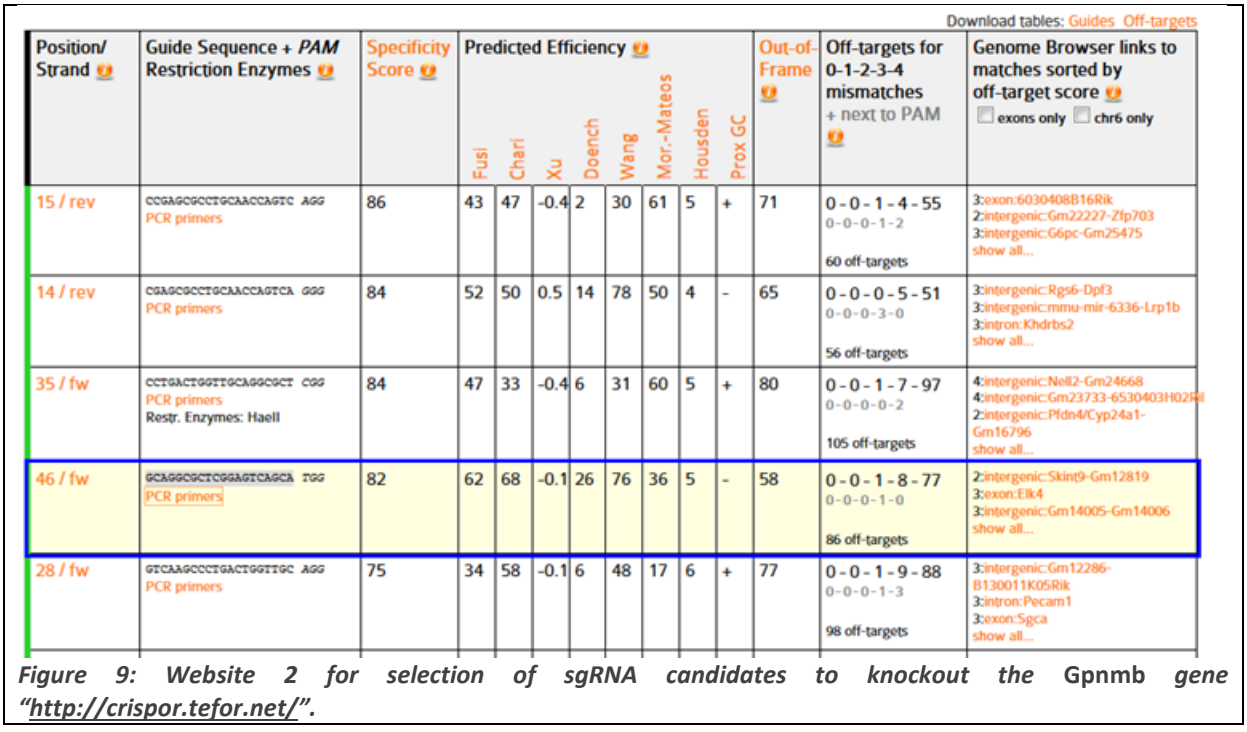

Figure 9: Website 2 for selection of sgRNA candidates to knockout the Gpnmb gene "http://crispor.tefor.net/".

[J] currently: https://zlab.bio/guide-design-resources

We implemented a donor ssDNA as template to aim for homology-directed repair. The 99 bp ssDNA template (**Table 25**) is homologous to a part of genomic mouse *Gpnmb* DNA except one base, with the locus of the sgRNA not in the middle but asymmetrically around the sgRNA sequence (the 5' homologous arm being twice as long as the 3' homologous arm). Four bases at the 5'- and 3'-end contained phosphorothioate modifications, respectively, to increase efficiency [267]. We aimed to delete the first base after the translational start codon ATG, a guanine. Within the sequence 5'-ATGG, the first three bases are the start codon of *Gpnmb*, the last three bases served as PAM for Cas9 recognition. By deleting the second guanine, the PAM was destroyed. Thereby, the Crispr-Cas9 machinery was rendered inactive on alleles with the desired deletion.

4.3.3. Cloning of sgRNA targeting Gpnmb locus

The sgRNA targeting *Gpnmb* was inserted as double-stranded DNA-oligonucleotide into the pX330 vector (**Figure 10**) that contains guide RNA and Cas9 expression cassettes. Two complementary oligonucleotides with the sgRNA sequence were ordered (**Table 25**). Attached were four bases at the 5'-end that enabled the integration into the pX330 vector (official name pX330-U6-Chimeric_BB-CBh-hSpCas9, Addgene plasmid #42230) [268].

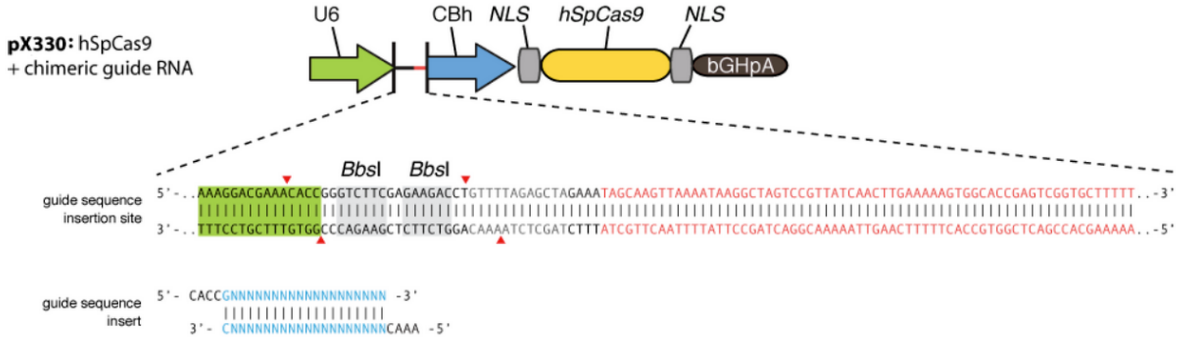

Figure 10: Scheme of pX330 vector pX330-U6-Chimeric_BB-CBh-hSpCas9.
NLS: nuclear localization signals, U6-promotor, human codon–optimized Streptococcus pyogenes SpCas9[K]

First, the two complementary oligos gRGpnmb (**Table 25**) were aligned by heating and slow cooling (**Table 26**). The vector pX330 (**Figure 10**, **Table 25**) was digested with the restriction enzyme BbsI. The larger fragment was purified with the Wizard SV Gel and PCR Clean-Up System, leaving sticky ends that are complementary to the sticky ends of the aligned double stranded gRGpnmb. The smaller fragment of pX330 vector contained the recognition sites for BbsI, rendering cutting of pX330 with BbsI impossible. Vector and aligned oligonucleotides were ligated (**Table 27**) and test-digested again with BbsI (**Table 28**).

10 µL of the digested vector (where positive vectors could not be digested anymore) with integrated sgRNA were transformed into One Shot™ TOP10F' Chemically Competent *E. coli*. The bacteria were kept on ice for 30 min followed by a heat shock at 42 °C for 45 sec and 3 min on ice. After adding 1 mL LB medium (25 g LB Broth Luria/Miller, solved in 1 L ddH_2O) without antibiotics, the bacteria were cultured in a shaking thermomixer at 37 °C for 45 min. This was followed by growth overnight on an agar dish (40 g of LB Agar Luria/Miller, solved in 1 L ddH_2O) at 37 °C, selected by ampicillin resistance (100 µg/mL, solved in 120 mM NaOH). The next day, seven clones were picked and each clone was cultured in 5 mL LB medium with ampicillin

[K] https://media.addgene.org/data/40/15/0c6b1494-b811-11e2-bd71-003048dd6500.png

selection overnight in a shaking 37 °C incubator. Bacterial DNA was isolated from 4 mL of the overnight culture.

Table 25: Oligonucleotide sequences used to create and validate Crispr-Cas9-mediated Gpnmb-knockout mouse.
gRGpnmb: *Oligonucleotides of sgRNA targeting Gpnmb locus for insertion into the pX330 vector,* ***X330seq****: oligonucleotide used to proof-read the vector by sequencing,* ***86/87 Gpnmb gRtest bl****: oligonucleotides used to validate the successful cleavage in the genome,* ***ssDNA template****: oligonucleotide that served as a template to create Crispr-Cas9-mediated Gpnmb knockout mouse lines. Underlined is the sequence of the sgRNA. *= phosphorothioate rest at the respective base. Grey shaded is the transcriptional start codon of* Gpnmb*. Bold are the two nucleotides that frame the guanine that is present in the genome but not here anymore.* ***sgRNA "T7gRGpnmb" and gRNA_31****: Oligonucleotides used to create an amplicon from pX330 vector that is then processed to Crispr-RNA, which is injected into zygotes. "T7gRGpnmb" comprises of T7 promotor plus the sgRNA for Gpnmb, underlined is the sequence of the sgRNA. All oligonucleotides were synthesized and ssDNA template was additionally HPLC-purified by Biotez Berlin Buch GmbH.*

Name of the oligo	Sequence	Function
gRGpnmb fw gRGpnmb rev	5'- CACC GCAGGCGCTCGGAGTCAGCA 5'- AAAC TGCTGACTCCGAGCGCCTGC	CACC gRNA AAAC ANRg
X330seq	5'- GGCCTATTTCCCATGATTCC	Sequencing of pX330 vector
86 Gpnmb gRtest bl fw 87 Gpnmb gRtest bl rv	5'- GGAGTCAGAGTCAAGCCCTG 5'- TGGGTCAACGAGTGTAAGCG	Validation of successful deletion
ssDNA template	5'- C*T*G*T*GACTCCTGGTGGATGGGACTGGGGAGT CAGAGTCAAGCCCTGACTGGTTGCAGGCGCTCGGAGT CAGCATGAAAGTCTCTGCGGGGTCCTG*G*G*A*T	Injected donor DNA
sgRNA "T7gRGpnmb" gRNA_31	5'- TAATACGACTCACTATAGGCAGGCGCTCGGAGTCA GCA 5'- AAAAGCACCGACTCGGTGCC	Replacement of U6 by T7 promotor

Table 26: Step 1 in cloning sgRNA for Gpnmb into pX330 vector.
Annealing of the complementary sgRNAs "gRGpnmb" to each other.

Oligo annealing	Volume [µL]
gRGpnmb fw (100 µM)	1
GRGpnmb rv (100 µM)	1
T4 Kinase buffer	1
T4 Poly Kinase NEB #B0201S	0.5
ddH_2O DEPC	6.5

Time	Temperature
30 min	37 °C
5 min	95 °C
	Cool slowly at room temperature

Table 27: Step 2 in cloning sgRNA for Gpnmb into pX330 vector.
Ligation of pX330 vector and the annealed oligos of step 1.

Ligation of vector	Volume [µL]
pX330 DNA (Maxi #362, 937 ng/µL, "pX330-U6-Chimeric_BB-Cbh-hSpCas9", cut with BbsI	1
Annealed Oligos, 1:250 diluted	2
T4 Ligase (Promega #M180B)	1
T4 Buffer (Promega #C126A)	1
ddH_2O DEPC	5

Time	Temperature
overnight	16 °C

For mini-preparation of DNA from the bacteria, 4 mL of the bacterial culture were pelleted for 5 min at 6000*g. The pelleted cells were solved in 250 µl of Solution A (**Table 29**). To lyse the cells, 250 µl of Solution B were added and mixed gently by inversion. After incubation for 3-5 min at room temperature, 250 µl of Solution C were added to neutralize the sample and stop the lysis. The mixture of precipitated DNA, protein and SDS was gently mixed, incubated on ice for 10-30 min and centrifuged for 10 min at 13 000*g. The supernatant was transferred to a new 1.5 ml tube, 500 µL 99% isopropyl were added and mixed by inversion. After an incubation step for 10 min at room temperature, the DNA was pelleted by centrifugation for 15 min at 13 000*g. The pellet was washed with 500 µL 70% ethanol and centrifuged for 15 min at 13 000*g. The pellet was air-dried and resuspended in 50 µL H_2O DEPC.

To visualize positive clones, 2 µL DNA were linearized with BbsI analogous to **Table 28** and loaded onto a 1% agarose gel. The BbsI restriction site was removed by insertion of the gRGpnmb oligonucleotide. Negative bacterial clones, transformed with an empty vector, were visualized by one band, positive clones could not be linearized with BbsI and showed two bands of open-circle and supercoiled versions of the vector. Bacteria of one positive clone were expanded with 250 mL LB medium at 37 °C in a shaking incubator overnight. DNA ("Maxi #406") was isolated with a PureYield™ Plasmid Maxiprep System and send to sequencing with primer X330seq (**Table 25**) to LGC genomics (**Table 30**).

Table 28: Step 3 in cloning sgRNA for Gpnmb into pX330 vector.
Digestion of pX330 vector with BbsI enzyme.

Linearization of vector pX330	Volume [µL]
Ligation product	10
BbsI	1
Buffer 2	2
ddH_2O DEPC	7

Time	Temperature
1 h	37 °C

Table 29: Ingredients of solutions to isolate DNA from small bacterial cultures.

	Ingredient	End concentration
Solution A	Glucose	50 mM
	EDTA pH 8	10 mM
	Tris pH 8	25 mM
	RNase (4 mg/mL)	1%
Solution B	NaOH	0.2 M
	SDS	0.1%
Solution C	Kaliumacetat pH 5.5	3,1 M

Table 30: Sequence of vector pX330 with inserted sgRNA to target Gpnmb.
Underlined is the sgRNA recognition site.

>gRGpnmb_4.pX330seq
TGGAATTAATTTGACTGTAAACACAAAGATATTAGTACAAAATACGTGACGTAGAAAGTAATAATTTCTTGGGTAGTTTGCAGTTTTAAAATTATGTTTTAAAATGGACTATCATAT
GCTTACCGTAACTTGAAAGTATTTCGATTTCTTGGCTTTATATATCTTGTGGAAAGGACGAAACACC**GCAGGCGCTCGGAGTCAGCA**GTTTTAGAGCTAGAAATAGCAAGTTAAAA
TAAGGCTAGTCCGTTATCAACTTGAAAAAGTGGCACCGAGTCGGTGCTTTTTTGTTTTAGAGCTAGAAATAGCAAGTTAAAATAAGGCTAGTCCGTTTTTAGCGCGTGCGCCAATT
CTGCAGACAAATGGCTCTAGAGGTACCCGTTACATAACTTACGGTAAATGGCCCGCCTGGCTGACCGCCCAACGACCCCCGCCCATTGACGTCAATAGTAACGCCAATAGGGACTT
TCCATTGACGTCAATGGGTGGAGTATTTACGGTAAACTGCCCACTTGGCAGTACATCAAGTGTATCATATGCCAAGTACGCCCCCTATTGACGTCAATGACGGTAAATGGCCCGCC
TGGCATTGTGCCCAGTACATGACCTTATGGGACTTTCCTACTTGGCAGTACATCTACGTATTAGTCATCGCTATTACCATGGTCGAGGTGAGCCCCACGTTCTGCTTCACTCTCCCCA
TCTCCCCCCCCTCCCCACCCCCAATTTTGTATTTATTTATTTTTTAATTATTTTGTGCAGCGATGGGGGCGGGGGGGGGGGGGGGGGGCGCGCGC

4.3.4. Test of sgRNA efficiency in cell culture

Before creating transgenic animals, the efficiency of the sgRNA was tested in NIH-3T3 cells. NIH-3T3 cells were cultured in a 12-well plate and one well was transfected with DNA of the *Gpnmb*-sgRNA (gRGpnmb, Maxi #406) and an enhanced green fluorescent protein (EGFP) control plasmid (**Table 31**). First, 0.4 µL EGFP plasmid were mixed with 500 µL Opti-Mem. 100 µL of this mix were transferred to a new tube and 1.1 µL of gRGpnmb plasmid were added. Secondly, 7 µL of Lipofectamine 2000 were gently mixed with fresh 100 µL Opti-MEM. Then, 100 µL of Opti-MEM with Lipofectamine 2000 was combined with 100 µL of Opti-MEM with the two plasmids, mixed gently and incubated at room temperature for 5 min. The growth medium of NIH-3T3 cells was replaced by 1 mL of 37 °C pre-warmed Opti-MEM, 200 µL of the Lipofectamine/plasmid mix were added and mixed by gentle rocking. The cells were allowed to take up the plasmid for 24 h, then the medium was changed back to normal growth medium (chapter 3.3.2). Two days later, the cells were washed and detached with trypsin. The cells were resuspended in 500 µL PBS and transferred to a flow cytometry tube. The cells were sorted for green fluorescence (561 nm), emitted from EGFP transfected cells, with a BD Aria II sorter into fresh medium. EGFP-positive cells were plated in one well of a 24-well plate.

About five days later, genomic DNA was isolated by adding 300 µL of Ear buffer (**Table 7**, chapter 3.1.1), shaking at 55 °C for 3-4 h, inactivating the digestion enzymes at 95 °C for 5 min, adding first 30 µL of 3 M sodium acetate and then 900 µL of isopropyl. The sample was thoroughly mixed and precipitated at -20 °C overnight. The sample was centrifuged at 13 000*g for 20 min and the pellet was washed with 500 µL 70% ethanol. After centrifugation at 13 000*g for 10 min, the pelleted DNA was air-dried. The DNA was resuspended in 50 µL ddH_2O at 55 °C for 5 min. PCR was performed according to **Table 32** with DNA from Crispr-Cas9 transfected NIH-3T3 cells and with DNA from a DBA/2J-Gpnmb$^+$ biopsy as control. The 157 bp fragments were purified from the 3% agarose gel with the Wizard SV Gel and PCR Clean-Up System and sent for sequencing to LGC Genomics GmbH (Berlin, Germany) with primers 86 Gpnmb gRtest bl fw and 87 Gpnmb gRtest bl rv (**Table 25**). Multiple overlapping peaks in the sequence proved that the sgRNA had caused several mutations in the amplified area. Therefore, the test in NIH-3T3 cells was concluded positively and the sgRNA could be utilized in animals.

Table 31: Plasmids for transfection of NIH-3T3 cells with Gpnmb-sgRNA to test mutation efficiency.

Plasmid	Concentration	Amount of plasmid	Volume for transfection
gRGpnmb (Maxi #406)	803 ng/µL	0.9 µg	1.1 µL
EGFP (Maxi # 228, Tet-O-FUW-EGFP [269])	1.5 µg/µL	0.1 µg	0.07 µL

Table 32: Protocol for the amplification of the Gpnmb locus the sgRNA was supposed to target.
Test of sgRNA efficiency in NIH-3T3 cells.

Stock conc.	Ingredient	Volume [µL]
2x	RedTaq	12.5
5 µM	Primer86 Gpnmb gRtest bl fw	0.9
5 µM	Primer 87 Gpnmb gRtest bl rv	0.9
	ddH_2O	8.7
	Genomic DNA	2

Time	Temperature	Cycles
5 min	95 °C	1x
20 sec	95 °C	34x
30 sec	60 °C	
30 sec	72 °C	
5 min	72 °C	1x
infinite	4 °C	

4.3.5. Injection of Crispr-Cas9 into zygotes

Vector pX330 with integrated sgRNA to target *Gpnmb* was used as a DNA template for the transcription to RNA, which is subsequently injected into animals. First, the U6 promotor was replaced by a T7 promotor that could be used for *in vitro* transcription. The PCR protocol is shown in **Table 33**, the primer sequences in **Table 25**. Then, RNA was synthesized by *in vitro* transcription with a T7 polymerase. We collaborated with Prof. Ralf Kühn and Andrea Leschke of the MDC Transgenic core facility from this point. The resulting Crispr RNA targeting *Gpnmb* was microinjected together with *Cas9* mRNA and the ssDNA template (**Table 25**) into the pronucleus of C57BL/6N and C57BL/6N-ApoE$^{+/-}$ zygotes. Those were subsequently implanted into foster mothers and the offspring was genotyped. The protocol for genotyping is described in detail in chapter 3.1.5.2. We deleted one guanine after ATG. Sequencing the DNA with the 3' primer showed two cytosine peaks in *Gpnmb*$^{+/+}$ animals, one cytosine peak in *Gpnmb*$^{-/-}$ animals and a double peak in *Gpnmb*$^{+/-}$ heterozygous animals (**Figure 11 A**). Note the phase shift and overlap of the two alleles present in the heterozygous animal starting from the mutation. Validation of

Table 33: PCR protocol for replacing U6 promotor of Crispr-DNA by a T7 promotor that can be used for* in vitro *transcription.

Stock conc.	Ingredient	Volume [µL]
5x	Phusion Buffer	12.5
50 mM	$MgCl_2$	1
7 µM	Primer sgRNA "T7gRGpnmb"	0.9
7 µM	Primer gRNA_31	0.9
5 mM	dNTP	2
	Phusion Taq	0.5
	ddH_2O	27.5
1 ng/mL	gRGpnmb (Maxi #406)	2

Time	Temperature	Cycles
30 sec	95 °C	1x
30 sec	95 °C	34x
30 sec	60 °C	
1 min 10 sec	72 °C	
5 min	72 °C	1x
infinite	4 °C	

Gpnmb-knockout on protein level was difficult as Gpnmb is hardly expressed in a healthy condition. Bone marrow was extracted from respective animals and differentiated *in vitro* into highly Gpnmb expressing macrophages (chapter 3.3.1). There are several antibodies available to detect Gpnmb. Three were tested (#20338-1-AP/Proteintech, #MAB2330/R&D, #AF2330/R&D) and only one (#AF2330/R&D) was able to detect the characteristic bands about 100 kDa in wildtype animals that were absent in both DBA/2J and C57BL/6N-Gpnmb$^{-/-}$ animals (**Figure 11 B**). The downside of the antibody is the detection of a plethora of unspecific bands. Thus, every experiment using Western blot was conducted using a *Gpnmb*-knockout control and only signals were considered that were absent in a *Gpnmb*-knockout model. Taken together, we succeeded in the generation of a *Gpnmb*-knockout strain called C57BL/6-Gpnmb^{tm1Bdr}, in this study called C57BL/6N-Gpnmb$^{-/-}$.

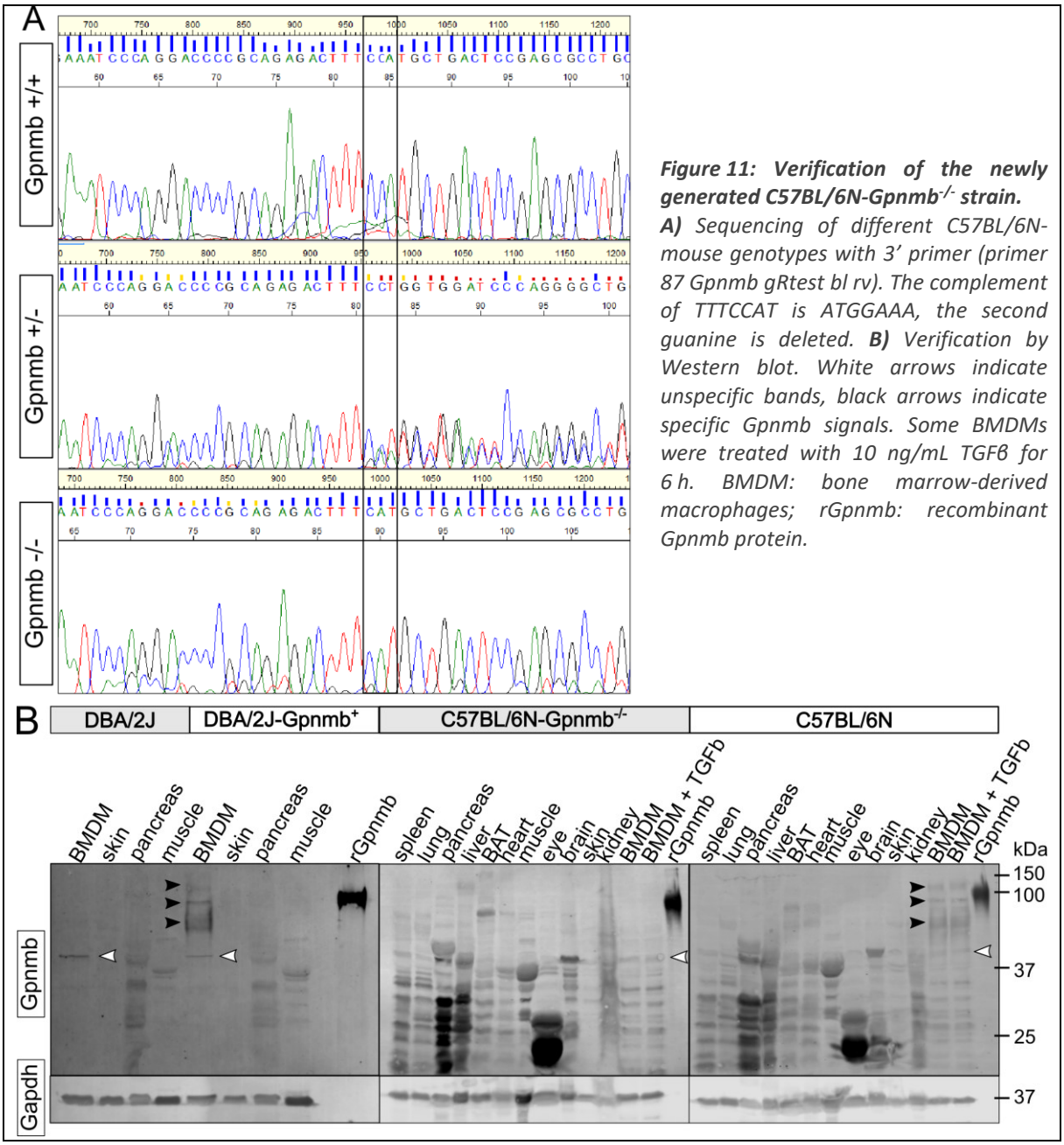

Figure 11: Verification of the newly generated C57BL/6N-Gpnmb$^{-/-}$ strain.
A) *Sequencing of different C57BL/6N-mouse genotypes with 3' primer (primer 87 Gpnmb gRtest bl rv). The complement of TTTCCAT is ATGGAAA, the second guanine is deleted.* ***B)*** *Verification by Western blot. White arrows indicate unspecific bands, black arrows indicate specific Gpnmb signals. Some BMDMs were treated with 10 ng/mL TGFß for 6 h. BMDM: bone marrow-derived macrophages; rGpnmb: recombinant Gpnmb protein.*

5. Aim of the Thesis

Gpnmb is highly expressed in several diseases but the reason for its upregulation and its role in the pathogenesis of the diseases remain mostly unknown. It is established that Gpnmb is upregulated in most diseases because of its expression in macrophages and dendritic cells. To elucidate actions and functions of Gpnmb, we aimed to study Gpnmb in macrophages both in cell culture and in model diseases in which macrophage function is critical for the pathogenesis. We chose atherosclerosis and obesity, both are lipid storage diseases that go along with a chronic, low-grade inflammation.

The study is split into three parts. The first part is addressing basic cellular functions of Gpnmb *in vitro.* For the second part, atherosclerosis was induced in high cholesterol diet-fed ApoE-deficient mice to find an influence of Gpnmb on the development of lesions in the aortic wall. In the third part, the role of Gpnmb in obesity was studied in high fat diet-fed mice, expecting to detect an impact of Gpnmb on body weight. Gpnmb was reported to be upregulated in both atherosclerosis and obesity, but the impact of Gpnmb on their progression remains unclear. Therefore, a *Gpnmb*-knockout mouse model was newly generated that was applied in all three parts.

6. Results

6.1. Cellular functions

6.1.1. Gpnmb exerted a mild anti-inflammatory effect

Macrophages can fulfill a variety of functions dependent on their environment. They adapt their expression status accordingly within an axis spanning from inflammation to anti-inflammation. *In vitro*, those categories are mimicked in a simplified manner. Having a knockout animal model available, we aimed to investigate the influence of Gpnmb on the inflammatory state of macrophages. Mature macrophages derived from C57BL/6N and C57BL/6N-Gpnmb$^{-/-}$ bone marrow were polarized with cytokines IL-4 and IL-13 (anti-inflammatory M2a phenotype), or IFNγ and LPS (pro-inflammatory M1 macrophages) for 4, 24 or 48 h, respectively. Chung *et al.* showed a very high Gpnmb expression induced by TGFβ (reparative M2c macrophages), an important cytokine in macrophages for suppression of immune response and tissue remodeling, therefore this cytokine was included in the studies [89].

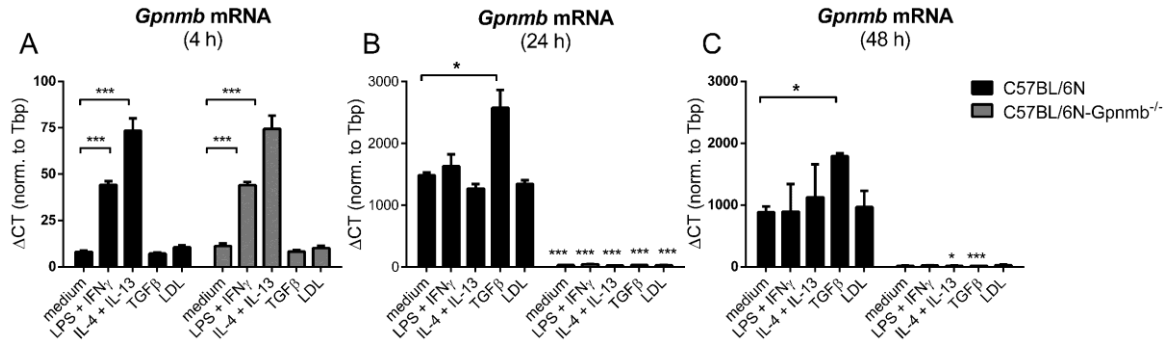

Figure 12: Gpnmb mRNA levels of differently polarized C57BL/6N- and C57BL/6N-Gpnmb$^{-/-}$-derived macrophages.

*Cells were treated with 20 ng/mL IL-4 and 20 ng/mL IL-13, or 20 ng/mL TGFβ, or 50 ng/mL LPS and 20 ng/mL IFNγ, or 20 µg/mL LDL. Transcript levels were measured by qRT-PCR after 4 h (**A**), 24 h (**B**) or 48 h (**C**). n=3. Statistical differences were determined by a Two-way ANOVA with Bonferroni posttests. Stars without bars indicate genotype differences; * p<0.05; *** p<0.001.*

First, the expression of Gpnmb was studied on mRNA and protein level. On mRNA level, *Gpnmb* was upregulated in M1 macrophages and even higher in M2a macrophages after 4h (**Figure 12**). *Gpnmb* mRNA was still detectable in C57BL/6N-Gpnmb$^{-/-}$ mice. This changed at 24 and 48 h, when *Gpnmb* mRNA was highly induced in wildtype bone marrow-derived macrophages (BMDMs). At these time points, *Gpnmb* was induced especially in TGFβ-polarized M2c macrophages, which was confirmed on protein level by Western blot (**Figure 13 A, B**). The extracellular fragment of Gpnmb in the supernatant was measured at 48 h by ELISA; here a different picture was observed: most of Gpnmb protein was shed by inflammatory M1 macrophages whereas reparative M2c macrophages showed reduced Gpnmb shedding

(**Figure 13 C**). Thus, the macrophages with the highest Gpnmb expression retained the protein. Therefore, Gpnmb expression and shedding might underlie different regulatory mechanisms.

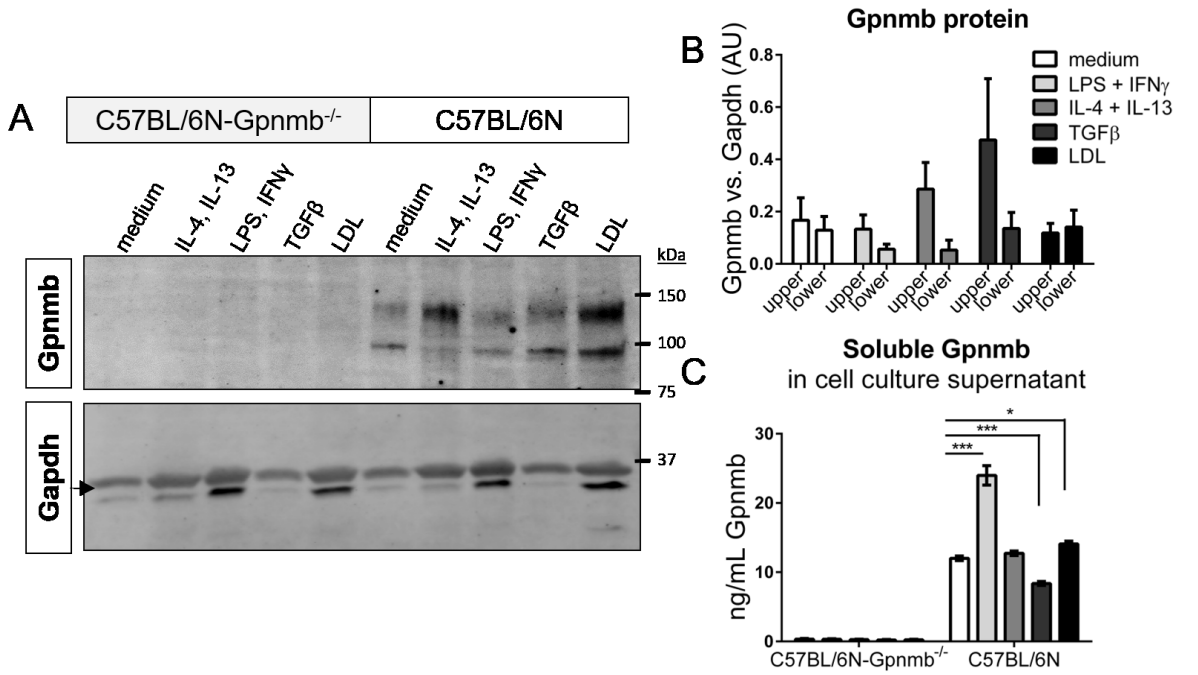

Figure 13: Gpnmb protein expression and release of differently polarized C57BL/6N- and C57BL/6N-Gpnmb$^{-/-}$-derived macrophages.

Cells were treated with 20 ng/mL IL-4 and 20 ng/mL IL-13, or 20 ng/mL TGFβ, or 50 ng/mL LPS and 20 ng/mL IFNγ, or 20 µg/mL LDL for 48 h. ***A)*** *Western blot of stimulated cell extracts. Undiluted lysates were loaded onto a gel without determination of protein concentration. Therefore, normalization to a loading control was crucial.* ***B)*** *Quantification of the two characteristic Gpnmb bands.* ***C)*** *Quantification of released soluble Gpnmb in cell culture supernatant by ELISA. n=3. Statistical differences were determined by a Two-way ANOVA with Bonferroni posttests; * p<0.05; *** p<0.001.*

In the second part of the experiment, the effect of Gpnmb on the expression of marker genes was assessed in these macrophages. Looking for mRNA expression of M1/M2a/M2c marker genes, most genes (*Il1β*, *Nos2*, *Cd86*, *Cd206*, *Abca1*, *Arginase 1 (Arg1)*, *Cd36*) were not affected by the presence of Gpnmb (data not shown). Other genes (*Il6*, *Tnfα, Ym1* and *Il10*) revealed an anti-inflammatory influence of Gpnmb (**Figure 14**). To measure the release of cytokines, TNFα, IL-6 and IL-1β in cell culture supernatant were measured by ELISA. None of these molecules could be detected in cell culture supernatants of BMDMs that were stimulated with TGFβ or in unstimulated macrophages. IL-1β remained at the lower detection limit throughout the stimulation panel (data not shown). TNFα and IL-6 showed a strong induction after pro-inflammatory M1 stimulation. By tendency, the secretion of inflammation markers was suppressed by the presence of Gpnmb (**Figure 15**), confirming mRNA data.

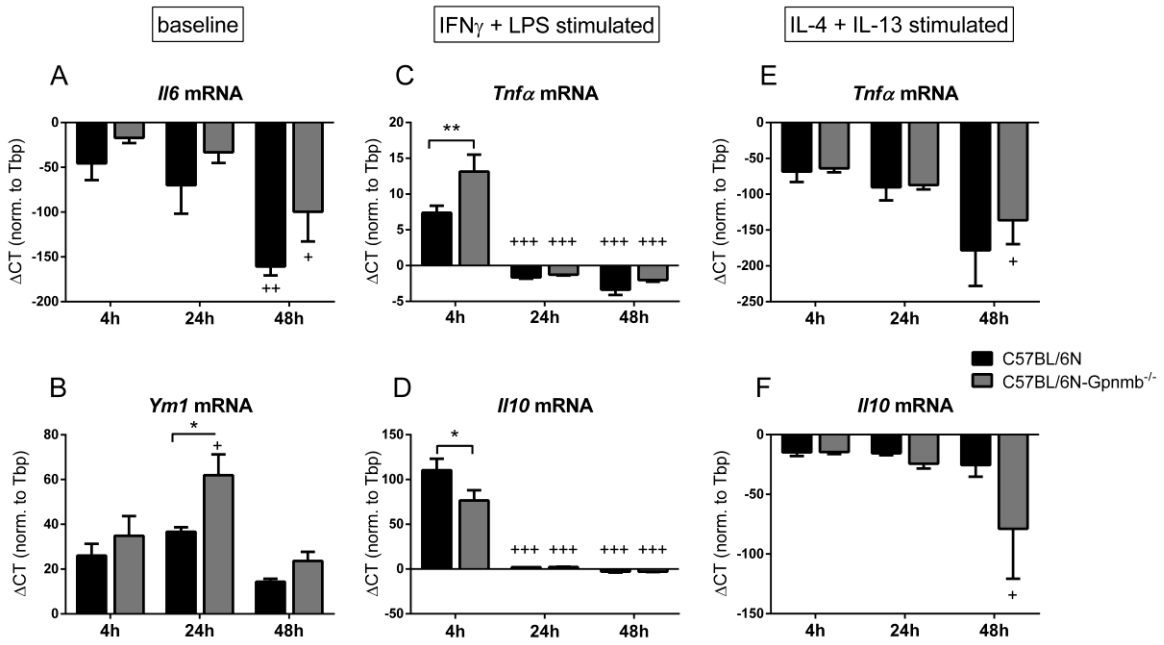

Figure 14: Inflammation status of C57BL/6N- and C57BL/6N-Gpnmb$^{-/-}$-derived macrophages.
*Cells were stimulated with 20 ng/mL IL-4 and 20 ng/mL IL-13, or 50 ng/mL LPS and 20 ng/mL IFNγ for 48 h. mRNA levels were measured by qRT-PCR. The upper panels **(A, C, E)** show pro-inflammatory marker genes, the lower panels **(B, D, F)** show anti-inflammatory marker genes. n=3. Statistical differences were determined by a Two-way ANOVA with Bonferroni posttests. * Genotype differences within one time point; * p<0.05; ** p<0.01; + time differences within one genotype; + p<0.05; ++ p<0.01; +++ p<0.001.*

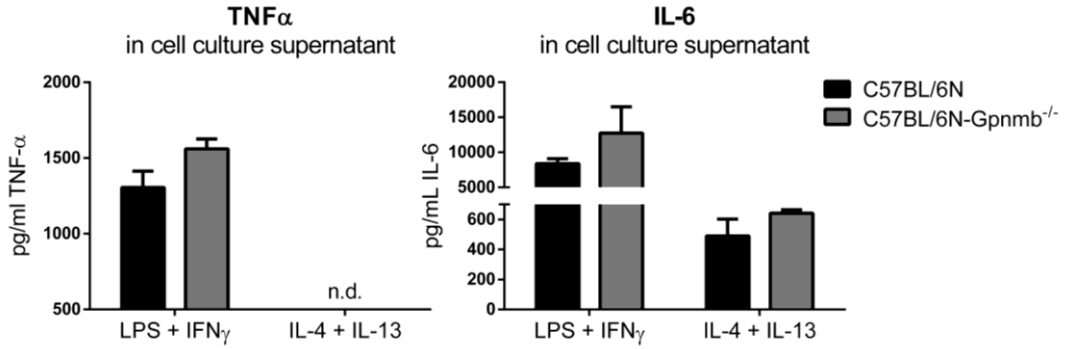

Figure 15: Cytokine release of C57BL/6N- and C57BL/6N-Gpnmb$^{-/-}$-derived macrophages.
Cells were stimulated with 20 ng/mL IL-4 and 20 ng/mL IL-13, or 50 ng/mL LPS and 20 ng/mL IFNγ for 48 h. TNFα and IL-6 were measured in the cell culture supernatant by ELISA. n.d.: not detected. n=3. No statistical difference was detected between genotypes using a non-parametric t-test/Mann Whitney test.

6.1.2. Gpnmb did not affect phagocytosis and autophagy

Another profound task of macrophages is phagocytosis, that is, the uptake and digestion of extracellular particles. Gpnmb was reported to localize to lysosomes and to have an impact on lysosomal storage diseases like Gaucher and Niemann-Pick-disease [78, 137, 170, 197], so we studied the functions of lysosomes. pHrodo *E. coli* and pHrodo zymosan are particles from bacteria or yeast, respectively, coupled to a fluorescent dye that emits light only at low pH present in lysosomes. Thus, uptake and degradation of those particles can be measured over time. Both particles were tested for different time periods, with 2 h being the peak of

incorporated pHrodo *E. coli* and zymosan. However, there was no effect by the absence of Gpnmb in macrophages from DBA/2J mice (**Figure 16**).

To study the role of Gpnmb in autophagy, BMDMs from C57BL/6N-Gpnmb$^{-/-}$ and wildtype control mice were starved with a buffered salt solution (HBSS) for 1 and 4 h and cell extracts were examined by Western blot. Autophagy can be monitored by the transformation of LC3BI to LC3BII, a protein found in either cytoplasm (LC3BI) or autophagosomes (LC3BII). However, neither the ratio of the two LC3B isoforms nor the ratio LC3BII/Gapdh revealed an influence of Gpnmb on autophagy (**Figure 17 A-C**). This was confirmed using a commercial CYTO-ID® Autophagy Detection Kit (**Figure 17 E-G**).

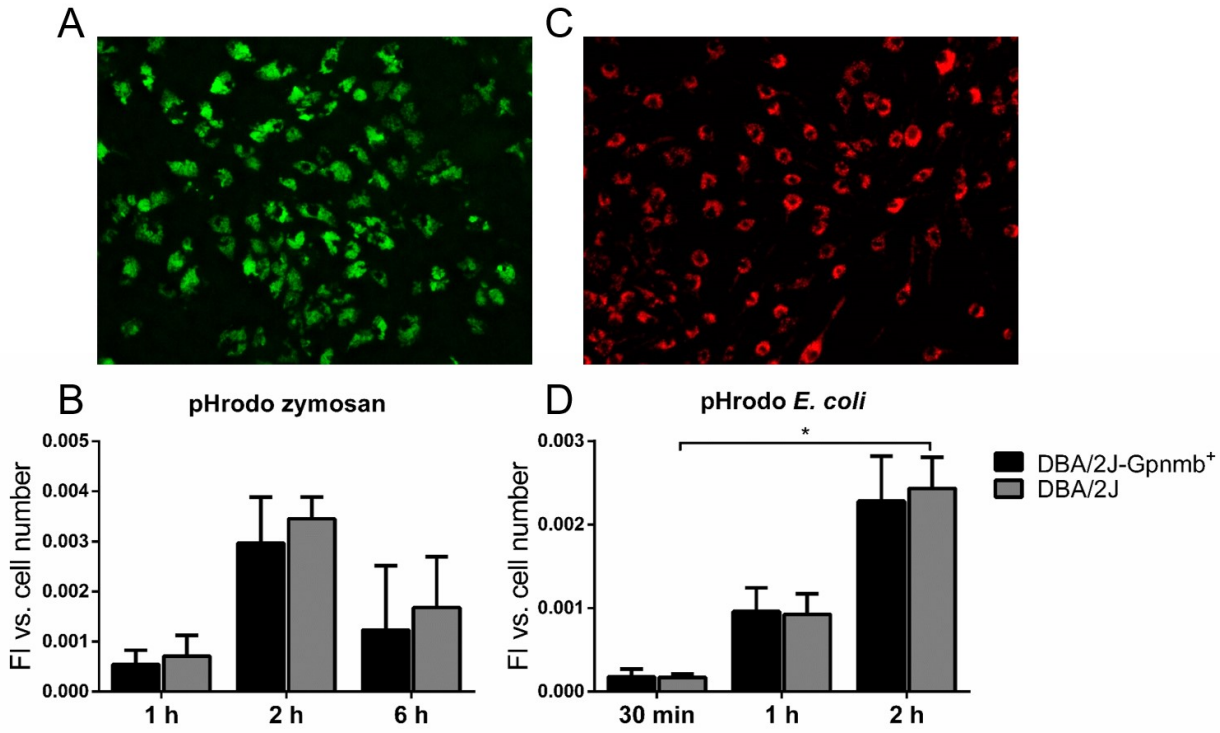

Figure 16: Uptake of labelled yeast (A, C) or bacterial (B, D) particles by DBA/2J or DBA/2J-Gpnmb^{+} derived macrophages.

A, D) *For representative pictures, cells were cultured in a 4 well plate and treated with pHRodo zymosan or E. coli.* ***B, D)*** *Cells were cultured in a 96 well plate, treated accordingly and measured with a microplate reader. FI: fluorescence intensity. n=2-4. Statistical differences were determined by a Two-way ANOVA with Bonferroni posttests; * p<0.05.*

Surprisingly, a high induction of Gpnmb was detected treating the cells with the positive control for autophagy experiments, bafilomycin A1 (**Figure 17 A, C**). Bafilomycin blocks the fusion of lysosomes with phagosomes and the resolution of autophagy by inhibiting the V-ATPase [270, 271]. The induction of Gpnmb could be either due to a lower level of lysosomal degradation that is stopped by bafilomycin, or by newly synthesized Gpnmb. Increased *Gpnmb* mRNA levels after bafilomycin treatment suggested that bafilomycin induces *de novo* Gpnmb expression (**Figure 18**). Upregulation of Gpnmb was also visible by immunocytochemistry. Localization of Gpnmb in the Golgi apparatus (**Figure 19**) seemed unaltered after bafilomycin treatment (**Figure 18 C**).

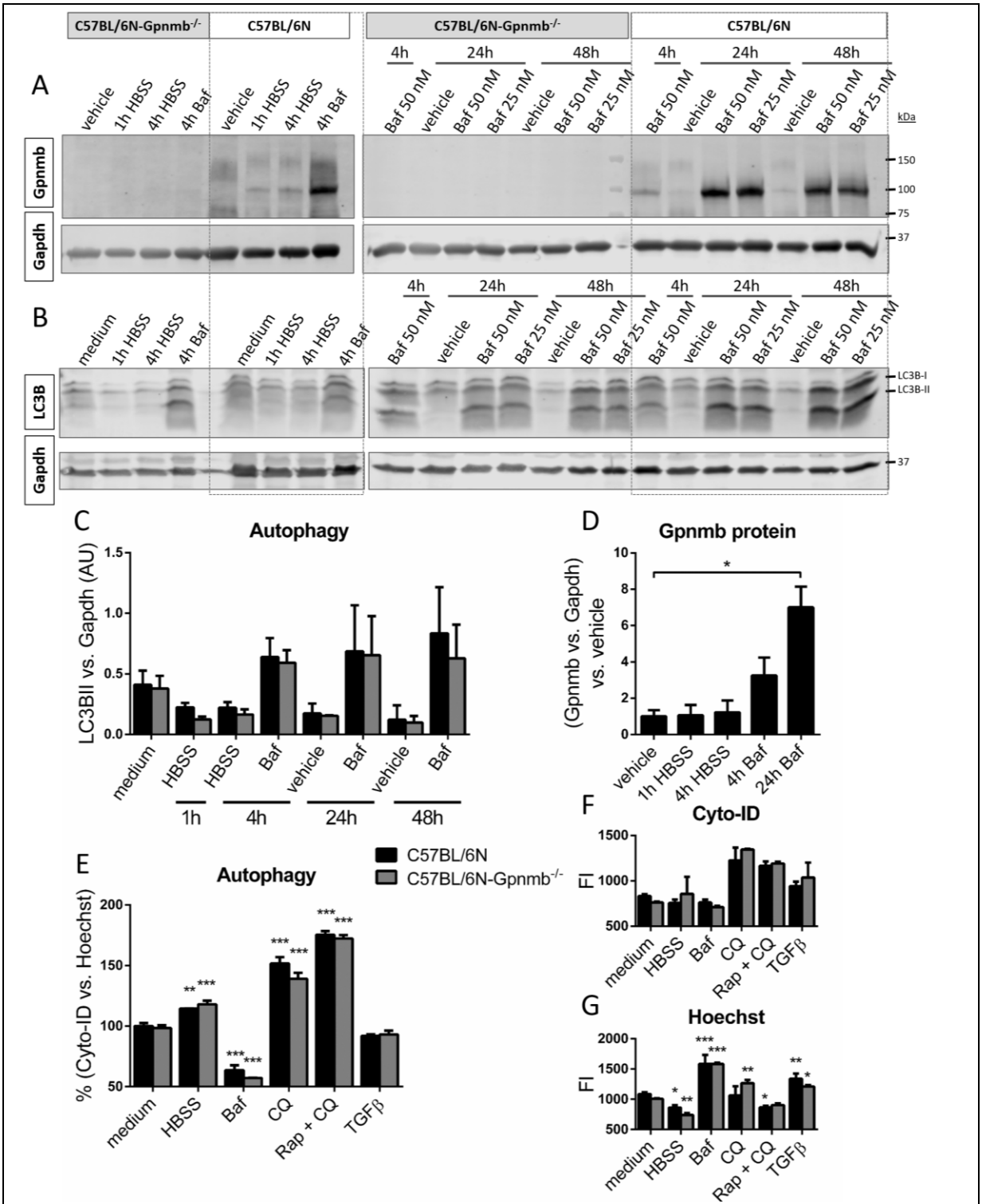

Figure 17: Autophagy in C57BL/6N- and C57BL/6N-Gpnmb$^{-/-}$-derived macrophages.
Cells were treated with 50 nM bafilomycin (Baf). ***A-B)*** *Analysis of Gpnmb expression and autophagy on the basis of LC3BI and II levels in Western blot.* ***C*** *and* ***D*** *shows the respective quantifications of B and A. n=2-5.* ***E-G)*** *Autophagy analysis by CYTO-ID® Autophagy detection kit. Cells were cultured in a 96 well plate and either starved with HBSS for 2 h, treated with 50 nM bafilomycin, 20 ng/mL TGFβ, 75 µM chloroquine (CQ) or 0.5 µM rapamycin (Rap) for 24 h.* ***F)*** *The cationic amphiphilic tracer dye (Cyto-ID) stains pre-autophagosomes, autophagosomes, and autophagolysosomes.* ***G)*** *Hoechst 33342 stains nuclei and was used to measure cell number.* ***E*** *shows the ratio of* ***F*** *and* ***G****. AU: arbitrary units. FI: fluorescence intensity. n=3. Statistical differences in D were determined by One-way ANOVA/ non-parametric Kruskal-Wallis test with Dunn's Multiple Comparison posttest. Statistical differences in C, E, G were determined by a Two-way ANOVA with Bonferroni posttests * significant relative to the respective "medium" condition of the same genotype; * p<0.05; ** p<0.01; *** p<0.001. No statistical difference was detected between genotypes.*

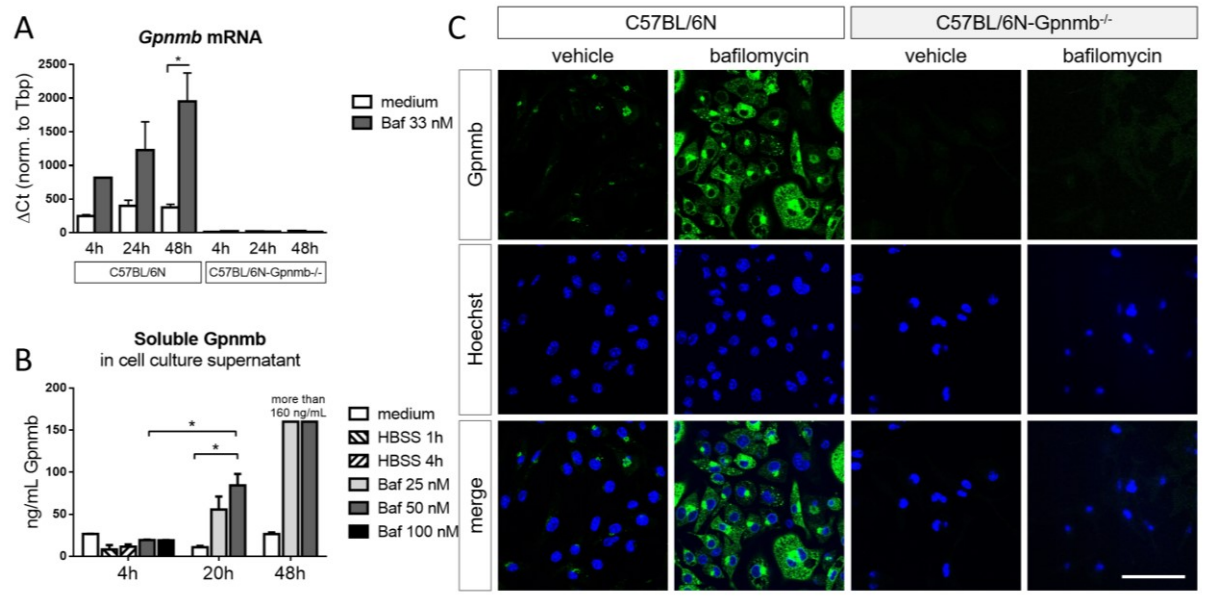

Figure 18: Bafilomycin induced Gpnmb expression and release in C57BL/6N- and C57BL/6N-Gpnmb$^{-/-}$-derived macrophages.

A) *Gpnmb mRNA levels were measured by qRT-PCR. n=3 for C57BL/6N, n=1 for C57BL/6N-Gpnmb$^{-/-}$.* ***B)*** *Soluble Gpnmb in the supernatant of wildtype macrophage cultures starved with HBSS or treated with bafilomycin (Baf) for indicated time periods was measured by ELISA. n=2. Scale bar: 50 µm. Statistical differences within the C57BL/6N-group were determined by a Two-way ANOVA with Bonferroni posttests; * p<0.05.*

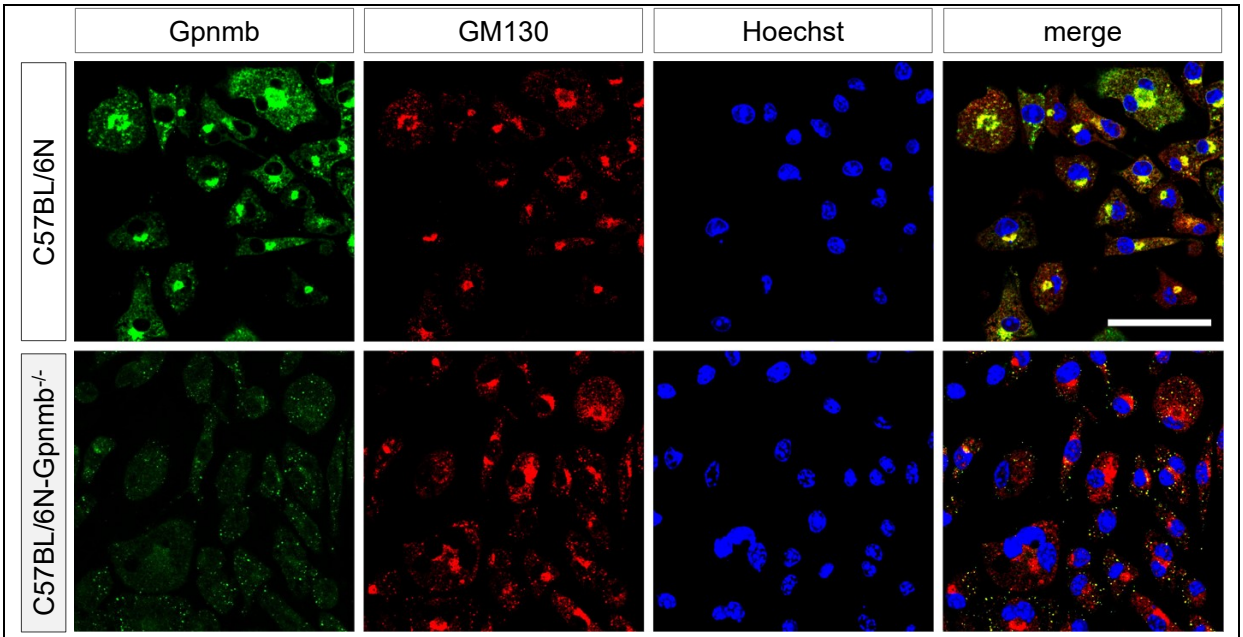

Figure 19: Localization of Gpnmb to the Golgi apparatus.

Anti-130 kDa cis-Golgi matrix protein (GM130) antibody was used to label Golgi apparatus. Hoechst 33342 was used to label nuclei. Scale bar: 50 µm.

6.1.3. Post-translational modifications of Gpnmb were highly variable

Whereas an influence of Gpnmb on autophagy could not be detected in common assays, Gpnmb itself exhibited a highly variable phenotype based on size and concentration under the influence of starvation as well as bafilomycin treatment. Western blots for Gpnmb showed several bands. Two bands around 100 kDa were the most pronounced. The upper one looked based on the fuzzy appearance like a strongly glycosylated protein, the lower one looked distinct. The latter was greatly enhanced by bafilomycin treatment, so we concluded that this is the premature, newly synthesized form of Gpnmb. Under HBSS treatment, the upper form increased in size rather than concentration. We wanted to find out, if Gpnmb is post-translationally modified in the cell upon starvation and bafilomycin treatment.

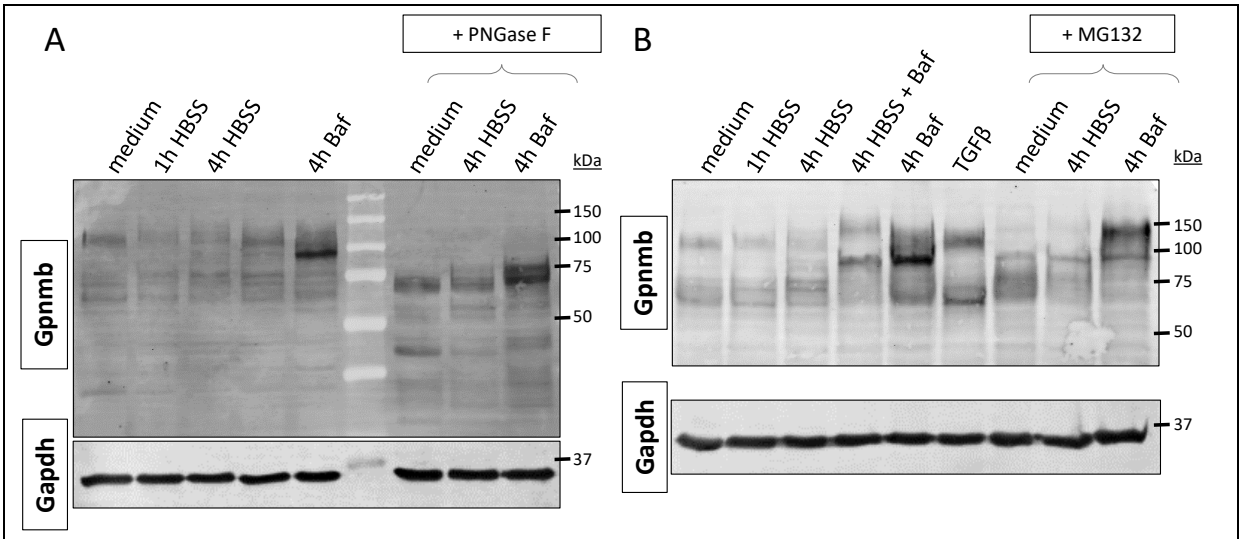

Figure 20: Glycosylation and degradation of Gpnmb by the 28S proteasome in C57BL/6N-derived macrophages.

Western blot of cells that were either starved with HBSS for indicated times, starved for 4 h and added serum for 30 additional minutes, treated with 100 nM bafilomycin (Baf), 10 ng/mL TGFβ, or 15µM MG132 for 4 h. ***A)*** *Comparison of cell lysates and cell lysates treated with the amidase PNGase F that removes N-linked glycans.* ***B)*** *Influence of proteasomal inhibitor MG132.*

To check the glycosylation status of Gpnmb in different conditions, whole protein lysates where stripped of N-linked oligosaccharides attached to asparagine residues using the amidase PNGase F. Gpnmb was in fact strongly glycosylated (**Figure 20**). In all conditions, de-glycosylation led to decreased size and to a more distinct shape of the band. However, the de-glycosylated size pattern of Gpnmb under medium, starvation (HBSS) and bafilomycin conditions remained different from each other. De-glycosylation did not strip the protein to a core protein of the same weight (**Figure 20 A**), meaning that other post-translational modifications must exist in those conditions.

A stress condition like starvation might lead to an increased degradation of the protein. So we looked next into ubiquitination to check Gpnmb degradation. Therefore, the 28S proteasome was blocked using the inhibitor MG132. We expected the upper band of Gpnmb in Western blot, which increased in size, to increase in intensity and the lower band to decrease. This happened only under bafilomycin treatment (**Figure 20 B**). Pull-down of ubiquitinated proteins showed that bafilomycin treatment did increase the ubiquitination of Gpnmb (**Figure 21**). Especially the upper form of Gpnmb was hardly visible in whole cell lysates but was concentrated in the

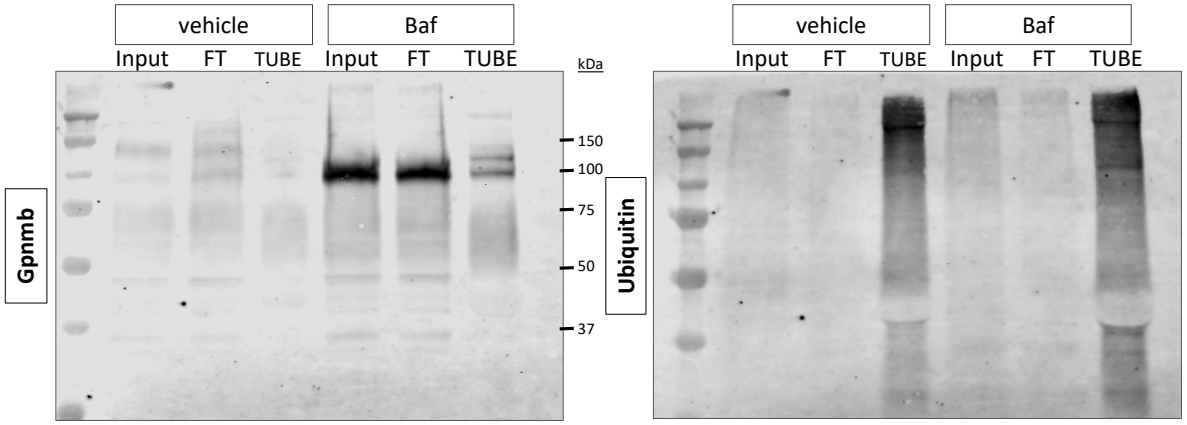

Figure 21: Ubiquitination of Gpnmb in C57BL/6N-derived macrophages.
*Western blot for Gpnmb **(left)** and ubiquitin **(right)** of an co-immunoprecipitation with Tandem Ubiquitin Binding Entity (TUBE), a protein binding ubiquitin chains with high affinity. Cells were treated with 100 nM bafilomycin (Baf) for 24 h. Input: whole cell lysate, FT: Flow-through/unbound proteins, TUBE: co-immunoprecipitated proteins with TUBE.*

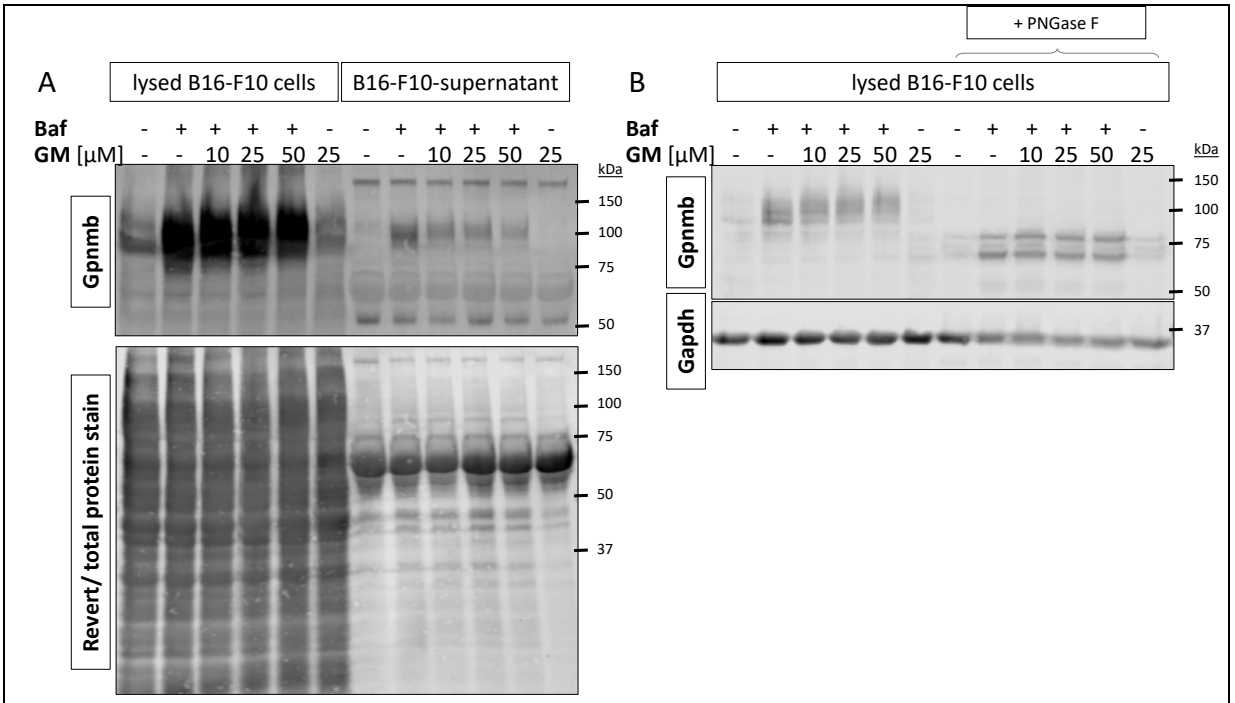

Figure 22: Gpnmb glycosylation and shedding in B16-F10 cells.
*Cells were treated with 33 nM bafilomycin (Baf) or various concentrations of Mmp9-inhibitor GM6001 (GM) in serum-free medium for 24 h. **A)** Comparison of Gpnmb in the cell lysates and soluble Gpnmb released into the supernatant. For loading control, the whole protein stain "Revert" was used. **B)** Comparison of cell lysates and cell lysates treated with amidase PNGase F that removes N-linked glycans. The left halves of Western blot A and B show the identical protein lysates. They differ only in amount of protein that was loaded onto the gel and exposure time during image acquisition.*

pulled-down fraction. However, the size of the ubiquitinated forms were smaller than the glycosylated form visible in vehicle-treated macrophages. Staining with an anti-ubiquitin antibody showed that ubiquitin chains were attached to proteins of all sizes, as expected.

Next, we wondered if shedding is specifically associated with the glycosylated form of Gpnmb. Shedding of Gpnmb increased significantly upon bafilomycin treatment (**Figure 18 B**). It increased time and dose-dependently until the upper detection limit of the ELISA was reached.

Gpnmb expression under bafilomycin treatment is always characterized by a definite band below 100 kDa and a smeary band above 100 kDa. We suspected that one of the bands might be the one that is shed and treated cells with GM6001, a broad-spectrum inhibitor of Mmps. At 10 to 25 µM, GM6001 was reported to inhibit Gpnmb shedding [80, 92, 171]. We aimed to accumulate one form of Gpnmb that is normally shed. GM6001 attenuated bafilomycin-induced Gpnmb signal in the cell culture medium, proving inhibition of shedding (**Figure 22 A**). With increasing GM6001 concentration, Gpnmb increased in size, which is due to N-glycosylation (**Figure 22 B** right). Surprisingly, both bafilomycin-induced forms were detected in the supernatant, even though the lower band was very faint. The upper, glycosylated form of Gpnmb was preferably released. However, although cellular Gpnmb differed in its glycosylation status, the soluble form did not. Soluble Gpnmb has therefore always the same set of glycans attached. Thus, the goal of this experiment, to assign one size of Gpnmb in Western blot to the shed version, was not finally reached. Of note, cellular Gpnmb stripped of N-glycans still consists of several bands as observed before (**Figure 20 A**).

Summarizing, bafilomycin increases the turn-over of Gpnmb: it induces its *de novo* synthesis, increases shedding and release as well as proteasomal degradation. Gpnmb that cannot leave the cell is increasingly glycosylated. Other post-translational modifications of Gpnmb under starvation as well as its function for the cell needs to be further checked.

6.1.4. Bafilomycin had a unique effect on Gpnmb expression

The upregulation and release of Gpnmb could be either a unique effect of bafilomycin or a general effect of a cellular stressor. It was already reported, that other ER and lysosomal inhibitors like chloroquine induce Gpnmb expression and release [170, 171]. Therefore, several molecules were compared to bafilomycin at two different incubation times (4 and 48 h) and doses (high and low). Targeting the lysosomes, additional to bafilomycin, chloroquine and leupeptin was used. Whereas bafilomycin stops the acidification of lysosomes and autophagosomes by inhibition of the V-ATPase [270, 271], the lysosomotropic agent chloroquine is doing the same via neutralizing the low pH of acidic organelles [272]. Thereby, they have similar effects but act in different ways. Leupeptin is a lysosomal protease inhibitor, also stopping degradation of lysosomal content. Three-methyladenine (3-MA) was used to block autophagy from a very early start [273], when autophagic vacuoles form from ER. 3-MA is an inhibitor of PI3K and acts differently on different steps of autophagy [274]. In detail, 3-MA persistently blocks PI3K type I, which blocks autophagy via PIP3, AKT and mTOR. On the other hand, it transiently blocks PI3K type III that leads to PIP production and enhanced autophagy. Thus, 3-MA inhibits autophagy in short term and starving conditions but promotes autophagy in nutrient environment and long term (~more than 9 h). Palmitate was added because it promotes autophagic flux [275] and induces Gpnmb expression [170]. Therefore, palmitate was coupled to 11% BSA in RPMI1640. Autophagy was in some conditions further enhanced by rapamycin, an inhibitor of mTOR which leads to enhanced autophagy [276]. So far, the agents interact both with the cell organelle lysosome and with the process autophagy. As mentioned before, Gpnmb is known to be upregulated by ER stressors [110], so the ER-inhibitor thapsigargin was included in the panel. Thapsigargin blocks sarco/endoplasmic reticulum Ca^{2+}-ATPase as well as the fusion of autophagosomes with lysosomes and has therefore similarities with bafilomycin. Brefeldin A (BFA) fuses ER and Golgi and blocks vesicular transport from ER/Golgi and is hence a stressor for both cell organelles [277]. Golgicide A (GCA) disrupts the Golgi apparatus where Gpnmb was localized (**Figure 19**). Exo1 inhibits exocytosis and hence the release of vacuoles.

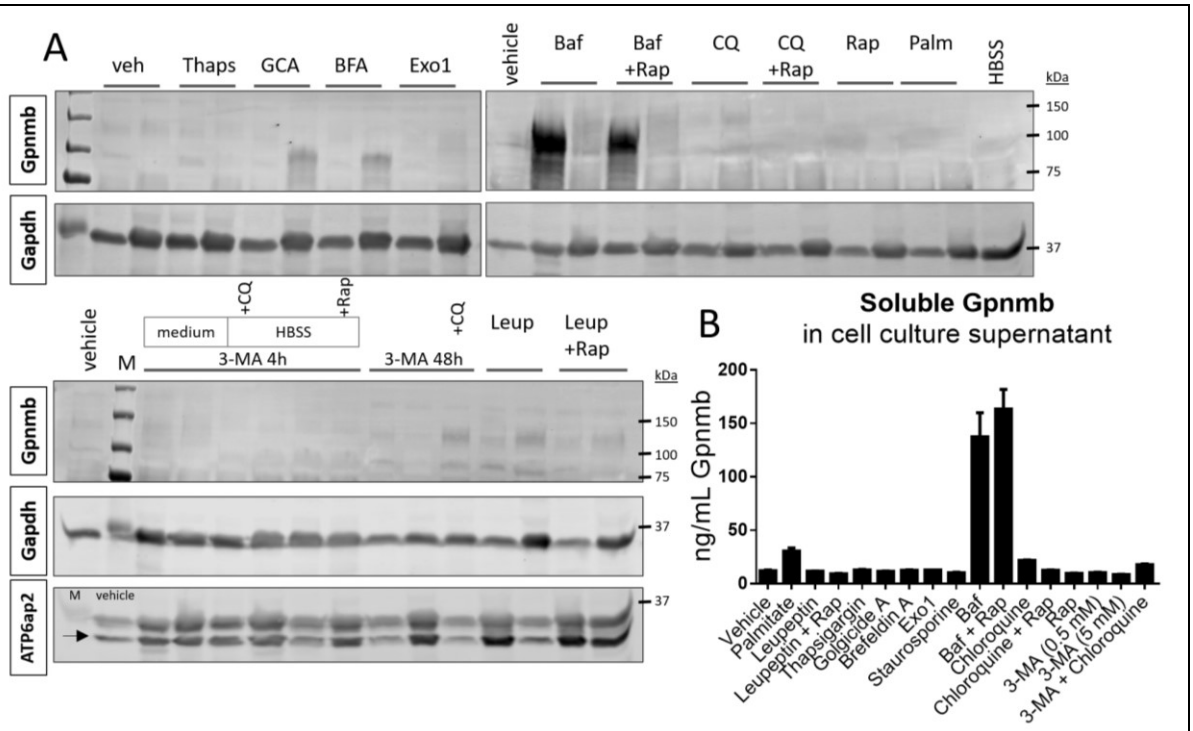

Figure 23: Influence of cellular stressors on Gpnmb size and shedding in C57BL/6N- and C57BL/6N-Gpnmb$^{-/-}$-derived macrophages.

A) *Two conditions of a stimulant were tested, the first line shows, if not otherwise indicated, the lower dose for longer period of time, the second line shows the higher dose for a short period of time. Baf: bafilomycin [33 nM 48 h, 100 nM 4 h], BFA: brefeldin A [50 ng/mL 48 h, 5 µg/mL 4 h], CQ: chloroquine [20 µM 48 h, 50 µM 4 h], Exo1 [50 µM 48 h, 50 µM 1 h] GCA: golgicide A [2 µM 48 h, 10 µM 2h], Leup: leupeptin [10 µM in combination, 10 µM 48 h, 100µM 4h], M: marker, 3-MA: 3-methyladenine [0.5 mM in combination, 0.5 µM and 5 mM 48 h, 1 mM in combination, 1 mM and 10 mM 3 h, the concentration of 3-MA is indicated in small digits in the figure as well], Palm: palmitate [200 µM 48 h, 200 µM 4 h], Rap: rapamycin [0.3 µM in combination, 0.2 µM 48 h, 0.3 µM 4 h], Thaps: thapsigargin [0.5 µM 48 h, 1 µM 4h], veh: vehicle [0.1% DMSO].**B)** Influence of cellular stressors on Gpnmb shedding. Soluble Gpnmb in the supernatant of macrophage cultures stimulated with different agents for 48 h, measured by ELISA. n=1, two technical replicates.*

ER stressors did not influence the appearance of Gpnmb in Western blot (**Figure 23**). Lysosomal stressors like leupeptin increased the small form of Gpnmb after 4 h. Golgi stressors like GCA and BFA did the same after 4 h. We expected to see an expression of Gpnmb by chloroquine treatment comparable to bafilomycin treatment. Although there was an induction after 48 h, the levels were not matched with bafilomycin-induced induction. Gpnmb shedding showed similar results (**Figure 23 B**). Treatment with BFA and staurosporine can abrogate Gpnmb shedding [80] and can thus serve as negative controls. Chloroquine and palmitate doubled the levels of soluble Gpnmb as expected from other reports [170, 171]. However, no agent was close to induce similar Gpnmb shedding levels as bafilomycin. To examine if treatment with bafilomycin altered immediate binding partners of the V-ATPase as well, V-ATPase associated protein 2 (ATP6ap2) expression was blotted. This protein is directly associated with the V-ATPase and necessary for its function [278–280]. However, ATP6ap2 expression was neither affected by V-ATPase inhibition nor by other stimuli (**Figure 23 A**). In contrast, it was expressed similar to the housekeeping protein Gapdh. To summarize, Gpnmb size and level reacts to cellular stress, however, there seems to be a unique effect of bafilomycin on Gpnmb.

Wondering about the effect of bafilomycin-induced Gpnmb expression, we observed that cell growth is enhanced by bafilomycin treatment (**Figure 17 G**) and suspected an influence of

Gpnmb. Therefore, an assay quantifying cell survival, apoptosis and necrosis ("ApoToxGlow") was conducted. Surprisingly, bafilomycin decreased cell survival and increased apoptosis (**Figure 24**). It was reported before that treatment with bafilomycin inhibits cell growth and induces apoptosis [281]. It explains the results, however contradicts our observation and measurement (**Figure 17 G**) of cell growth under bafilomycin or chloroquine treatment. A high signal for apoptosis and a low signal for cell viability might be due to accumulating stress response metabolites after exceeding growth in a limited space and nutrients. TGFβ on the other hand increased cell viability and did not affect apoptosis. Staurosporine induces apoptosis [282] and was used as a positive control. Anyway, no impact of Gpnmb on cell growth or apoptosis could be measured. To find the bafilomycin-mediated Gpnmb function, we collaborated with the MDC Proteomics core facility.

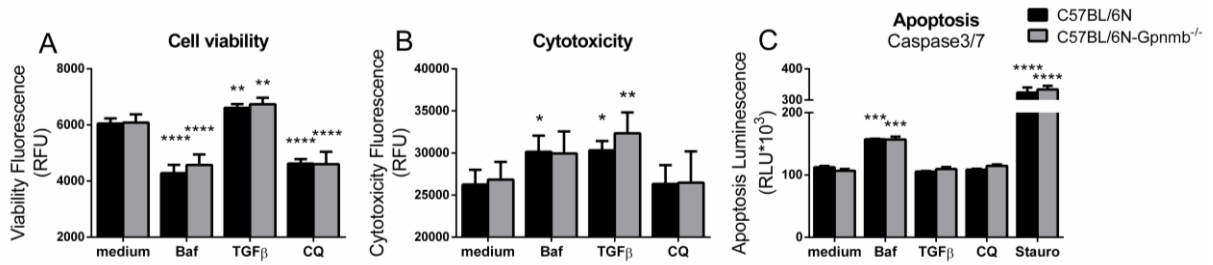

Figure 24: Apotox Glow assay for cell viability, cytotoxicity and apoptosis in C57BL/6N- and C57BL/6N-Gpnmb$^{-/-}$-derived macrophages.
*Cells were treated with 50 nM bafilomycin (Baf), 20 ng/mL TGFβ or 75 µM chloroquine (CQ) for 24 h. 10 µM staurosporine for 4 h was used as a positive control for apoptosis induction. n=3. Statistical differences were determined by a Two-way ANOVA with Bonferroni posttests, * significant relative to the respective "medium" condition of the same genotype; * p<0.05; ** p<0.01; *** p<0.001; **** p<0.0001.*

6.1.5. Interaction proteomics

Together with Dr. Daniel Hernandez and Dr. Philipp Mertins from the MDC Proteomics core facility, we decided to conduct interaction proteomics of untreated, TGFβ- [10 nM], as well as bafilomycin [33 nM]-treated C57BL/6N-Gpnmb$^{-/-}$ and wildtype-derived macrophages. These were the most promising molecules based on the above described experiments. Gpnmb was immunoprecipitated in mild conditions with anti-Gpnmb antibody to find proteins that are bound to Gpnmb by mass spectrometry. The results confirmed published interaction partners of Gpnmb such as the ER chaperones calnexin [109] and BiP [110] that were detected in our experiment as well, verifying the results. Moreover, new potential interaction partners were detected. Most proteins were bound in bafilomycin-treated condition, both vehicle and TGFβ-treated conditions were similar and did not have as many detected proteins. In pathways revealed with Kyoto Encyclopedia of Genes and Genomes (KEGG) analysis software (Kyoto, Japan, 2000), more proteins within one pathway could be detected after treatment with bafilomycin (**Table 34**), suggesting an enhancing effect. Some of the most promising pathways are illustrated in **Figure 25**. Selected for illustration were pathways where several proteins accumulated in close spatial proximity to each other in the KEGG picture, such as "phagosome" or "antigen and protein processing". Surprisingly, in all conditions, mostly ribosome-associated proteins were bound to Gpnmb. The whole list of detected binding partners is shown in **Table 36** in the appendix.

Table 34: Pathway search results of KEGG analysis tool "KEGG Mapper – Search&Color".
Listed are the amount of proteins that are bound to Gpnmb and are found in a specific pathway. In the first box, general pathways and in the second box, infections are listed. Underlined are processes that are illustrated in ***Figure 25****.*

Pathway	vehicle	TGFβ	Baf
Ribosome	12	12	12
Phagosome	5	5	9
Regulation of actin cytoskeleton	4	4	5
Axon guidance	4	3	5
Leukocyte transendothelial migration	3	2	4
Endocytosis	3	3	7
Pathways in cancer	3	3	4
Tight junction	3	2	4
Gap junction	3	2	3
Fc γ R-mediated phagocytosis	3	3	3
Human immunodeficiency virus 1 infection	3	2	8
Antigen processing and presentation	2	3	8
Protein processing in endoplasmic reticulum	2	3	5
Ras signaling pathway	2	2	3
Platelet activation	2	1	3
Sphingolipid signaling pathway	2	2	3
Fluid shear stress and atherosclerosis	2	3	3
Thyroid hormone synthesis	2	3	3
Human cytomegalovirus infection	2	2	8
Human T-cell leukemia virus 1 infection	2	3	7
Human papillomavirus infection	1	1	3
Herpes simplex virus 1 infection	0	0	5
Epstein-Barr virus infection	0	0	5
Herpes simplex virus 1 infection	0	0	5

A

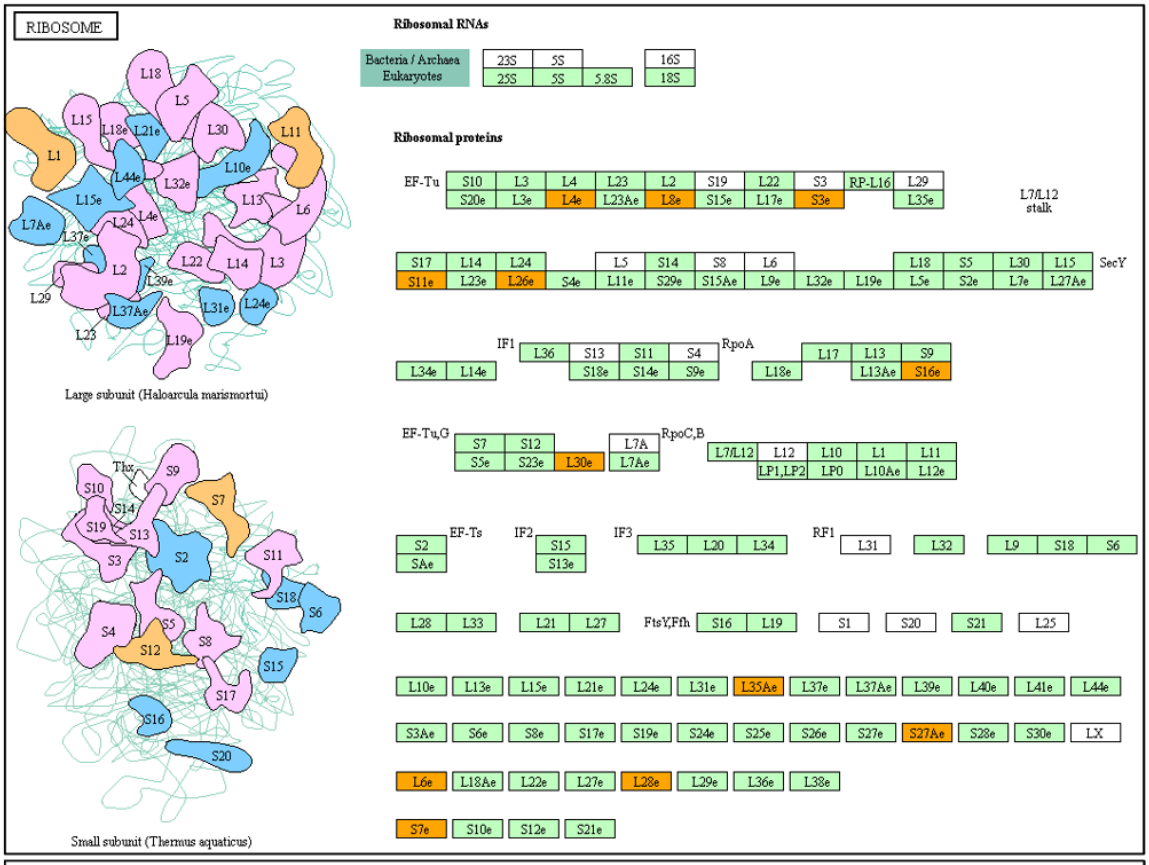
RIBOSOME
Ribosomal RNAs
Bacteria / Archaea
Eukaryotes
23S 5S 16S
25S 5S 5.8S 18S
Ribosomal proteins
EF-Tu
RP-L16
L7/L12 stalk
SecY
IF1
RpoA
EF-Tu,G
RpoC,B
EF-Ts
IF2
IF3
RF1
FtsY,Ffh
Large subunit (Haloarcula marismortui)
Small subunit (Thermus aquaticus)

B

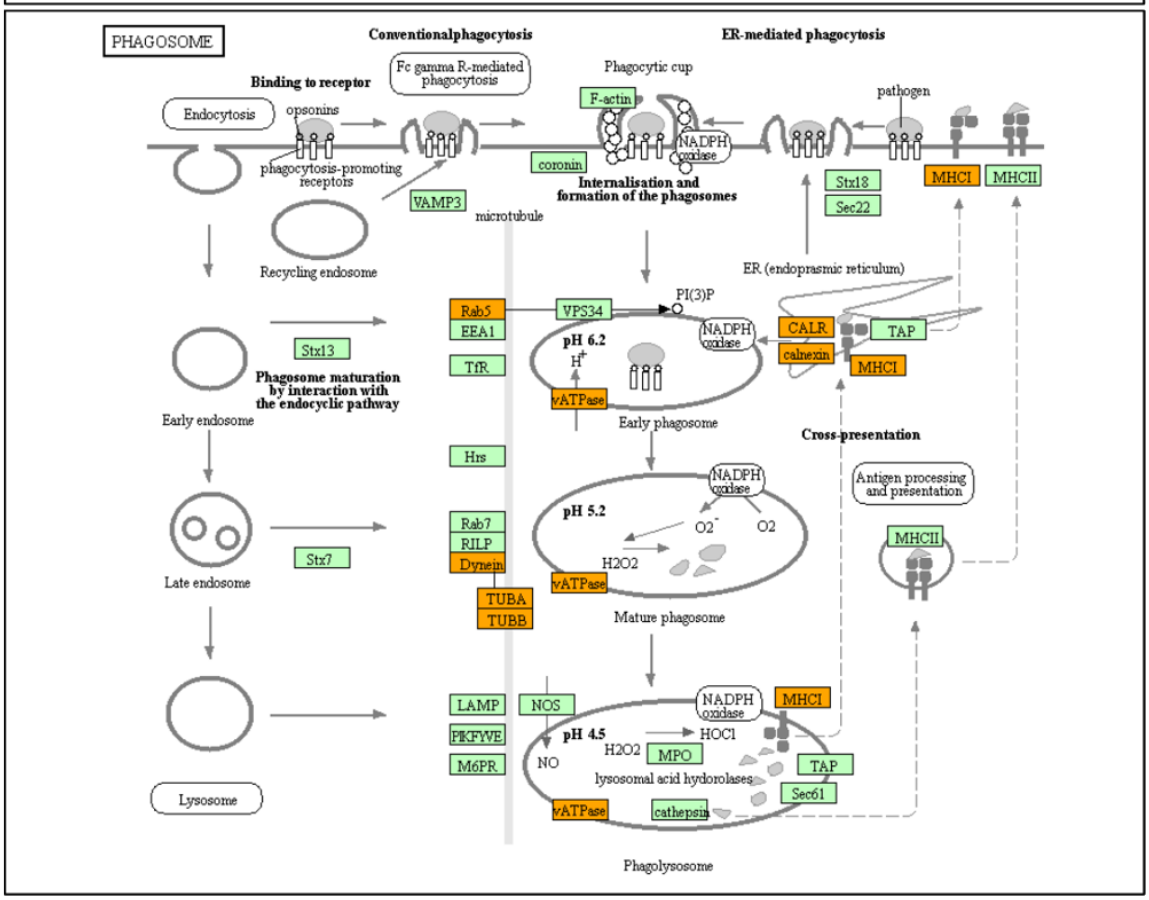
PHAGOSOME
Conventionalphagocytosis
ER-mediated phagocytosis
Binding to receptor
Fc gamma R-mediated phagocytosis
Phagocytic cup
pathogen
Endocytosis
opsonins
F-actin
NADPH oxidase
phagocytosis-promoting receptors
coronin
Internalisation and formation of the phagosomes
Stx18
Sec22
MHCI
MHCII
VAMP3
microtubule
Recycling endosome
ER (endoprasmic reticulum)
Rab5
EEA1
VPS34
PI(3)P
pH 6.2
H+
vATPase
CALR
calnexin
TAP
TfR
Stx13
Phagosome maturation by interaction with the endocyclic pathway
Early endosome
Early phagosome
Cross-presentation
Hrs
pH 5.2
O2-
O2
H2O2
Antigen processing and presentation
Rab7
RILP
Dynein
Stx7
Late endosome
TUBA
TUBB
Mature phagosome
LAMP
PIKFYVE
M6PR
NOS
NO
HOCl
MPO
lysosomal acid hydorolases
cathepsin
Sec61
Lysosome
Phagolysosome

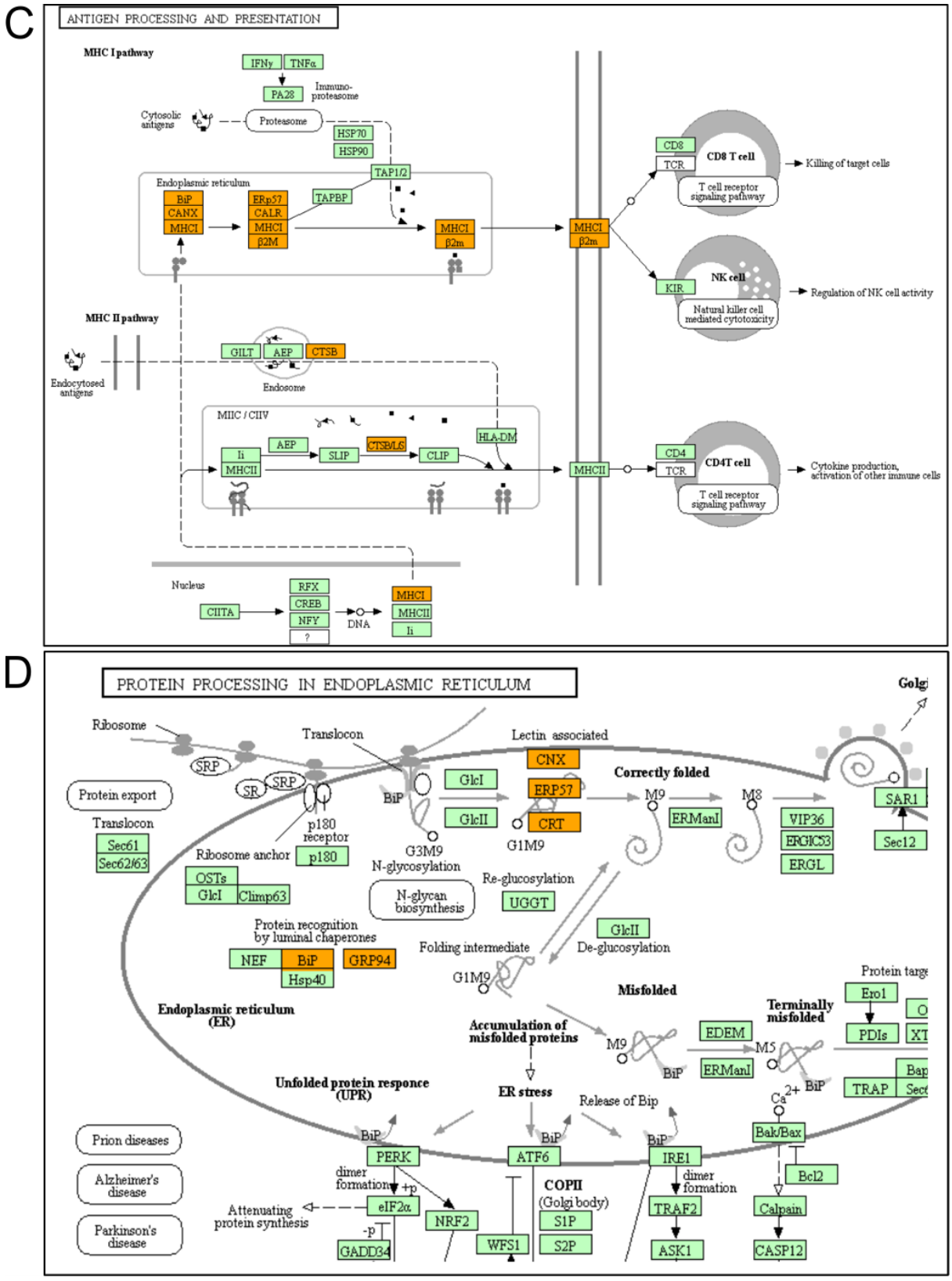

Figure 25: KEGG analysis[L] with tool "KEGG Mapper – Search&Color" Pathway[M] based on results detected with interaction proteomics.

Proteins were entered that bound Gpnmb upon bafilomycin treatment. Proteins bound by Gpnmb are depicted in orange, unbound proteins in green.

[L] https://www.genome.jp/kegg-bin/color_pathway_object

[M] https://www.genome.jp/kegg/tool/map_pathway2.html

An interesting interaction partner was the cysteine protease cathepsin B. It bound Gpnmb in bafilomycin-treated cells that secrete high levels of Gpnmb. Cathepsin B has both endopeptidase and exopeptidase activity and is localized to lysosomes. We hypothesized that Gpnmb is already shed in vesicles by cathepsin B and released upon request, additionally to the reported shedding at the plasma membrane. Using 8-hydroxy-5-nitrochinoline (NQ), an inhibitor of cathepsin B, the amount of soluble Gpnmb in the cell culture supernatant should be reduced. If Gpnmb is shed but not released, different sizes of Gpnmb should be detected by Western blot. However, the amount of extracellular Gpnmb in the supernatant was not decreased and Western blot dod not show altered Gpnmb sizes (**Figure 26**). This renders cathepsin B as a sheddase of Gpnmb unlikely.

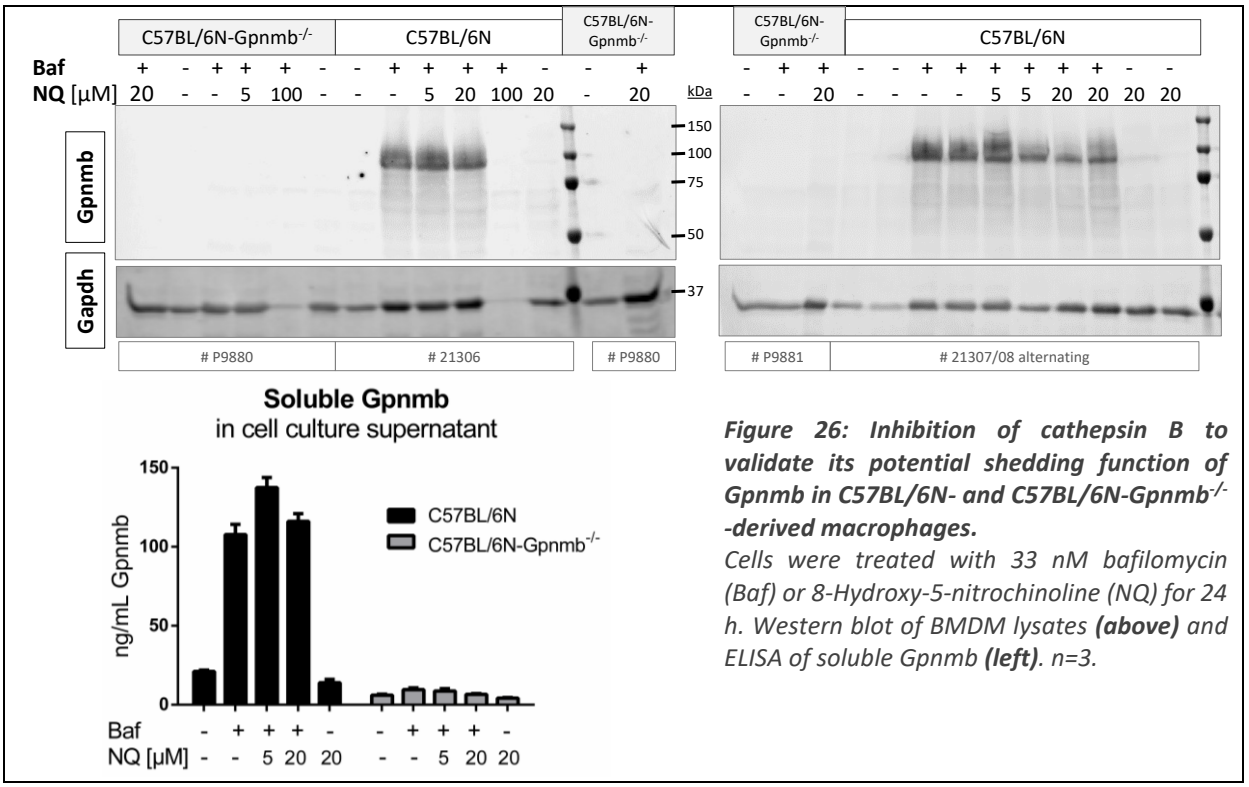

Figure 26: Inhibition of cathepsin B to validate its potential shedding function of Gpnmb in C57BL/6N- and C57BL/6N-Gpnmb$^{-/-}$-derived macrophages.
Cells were treated with 33 nM bafilomycin (Baf) or 8-Hydroxy-5-nitrochinoline (NQ) for 24 h. Western blot of BMDM lysates ***(above)*** *and ELISA of soluble Gpnmb* ***(left)****. n=3.*

6.2. Atherosclerosis

6.2.1. Gpnmb did not affect lipid metabolism

To assess the role of Gpnmb in inflammatory lipid-storage diseases, atherosclerosis was induced in female mice based on diet and genotype. We fed littermates of the genotype C57BL/6N-ApoE$^{-/-}$/Gpnmb$^{-/-}$ and C57BL/6N-ApoE$^{-/-}$/Gpnmb$^{+/+}$ a high cholesterol diet (HCD) consisting of 42% calories from fat and 0.21% (w/w) cholesterol for 8 and 12 weeks. In *Gpnmb*-knockout mice, Gpnmb could be hardly detected on mRNA level in epididymal adipose tissue and liver as well as the soluble form in plasma (**Figure 27 A-C**). The mRNA for the Gpnmb receptor *syndecan-4* was increased in liver of *Gpnmb*-knockout animals (**Figure 27 D-E**).

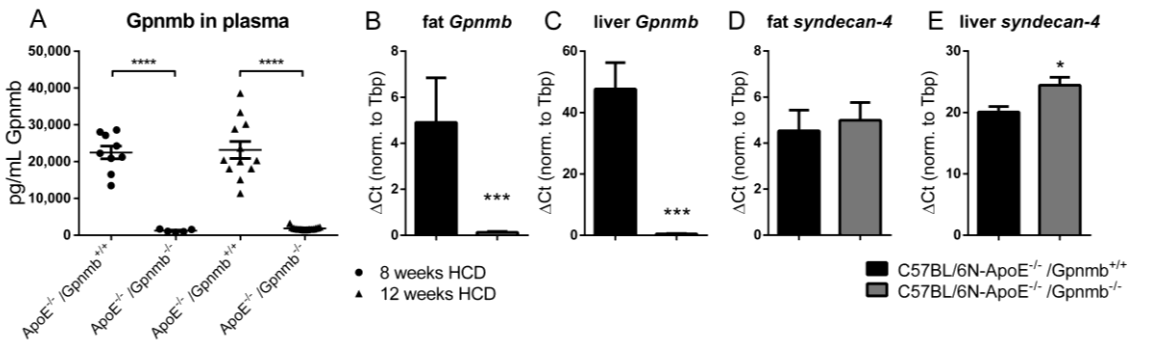

Figure 27: Gpnmb and Gpnmb-receptor syncdecan-4 expression of female, HCD-fed C57BL/6N-ApoE $^{-/-}$ /Gpnmb$^{-/-}$ and C57BL/6N-ApoE$^{-/-}$ /Gpnmb$^{+/+}$ mice.

A) *Measurement of soluble Gpnmb in plasma.* ***D-E)*** *mRNA levels of mice fed a HCD for 12 weeks, measured by qRT-PCR. HCD: high cholesterol diet. n=5-15. Statistical differences were determined by a Two-way ANOVA with Bonferroni posttests (A) or by a non-parametric t-test/Mann Whitney test (B-E); *** p<0.001; **** p<0.0001.*

Atherosclerotic plaques in the aorta are only formed, if the ingested cholesterol levels exceed the uptake capacity of the liver and enough LDL particles remain in the blood stream to accumulate in the aortic wall. Cholesterol is normally below 100 mg/dL in wildtype mice and around 200-500 mg/dL in ApoE$^{-/-}$ mice fed a normal chow [283, 284]. After feeding our animals for several weeks a HCD, they exhibited cholesterol levels of almost 1000 mg/dL (**Figure 28 B**). The composition of cholesterol in healthy animals consists of several times more HDL than LDL [284]. In our animals, the ratio is reversed in favor of LDL, with LDL being about 20-fold more abundant than HDL (**Figure 28 C-D**). However, triglycerides, total cholesterol, HDL and LDL were not altered by the absence of Gpnmb (**Figure 28**). Thus, although a basis for the development of atherosclerosis was established, the cellular uptake of lipids was not influenced by Gpnmb to an extent that affected circulating lipid values.

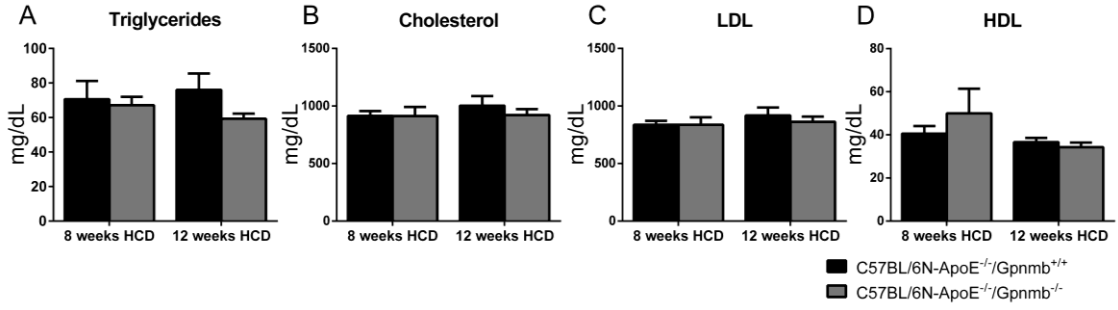

Figure 28: Lipids in plasma of female, HCD-fed C57BL/6N-ApoE $^{-/-}$/Gpnmb$^{-/-}$ and C57BL/6N-ApoE$^{-/-}$ /Gpnmb$^{+/+}$ mice.

HCD: high cholesterol diet. n=5-15. No statistical differences were detected using a Two-way ANOVA with Bonferroni posttests.

6.2.2. Gpnmb did not affect aortic plaque size

We wanted to demonstrate that the formation of atherosclerosis is influenced by the absence of Gpnmb. Although atherosclerosis is a global disease with several aspects, the main determinant of the disease progression are the plaques formed in the vessel wall. Plaques of whole aorta were stained for lipids with OilRedO and the signals appeared where expected [70]. OilRedO signals concentrated at the lower curvature of the aortic arch and at the root of the principal

branches of the thoracic aorta (**Figure 29**). Plaque size increased from 8 to 12 weeks of HCD, however no difference could be detected between the two genotypes (**Figure 29**). In line with that, quantification of plaque size in the aortic root within the heart, using hematoxylin and eosin staining, exhibited no genotype difference (**Figure 30 A, B**). Nevertheless, the composition of a plaque became visible. Whereas the surface of the plaque contained plenty of cells, the layers below showed more fibrosis and necrosis. The necrotic core contained cholesterol crystals and was devoid of nuclei. Fibrosis was visualized using collagen-staining Sirius red (**Figure 30 A**). Again, the quantification did not reveal a statistical difference between the genotypes (**Figure 30 C**). Thus, the main hypothesis, that Gpnmb influences the development of atherosclerosis, has to be rejected so far.

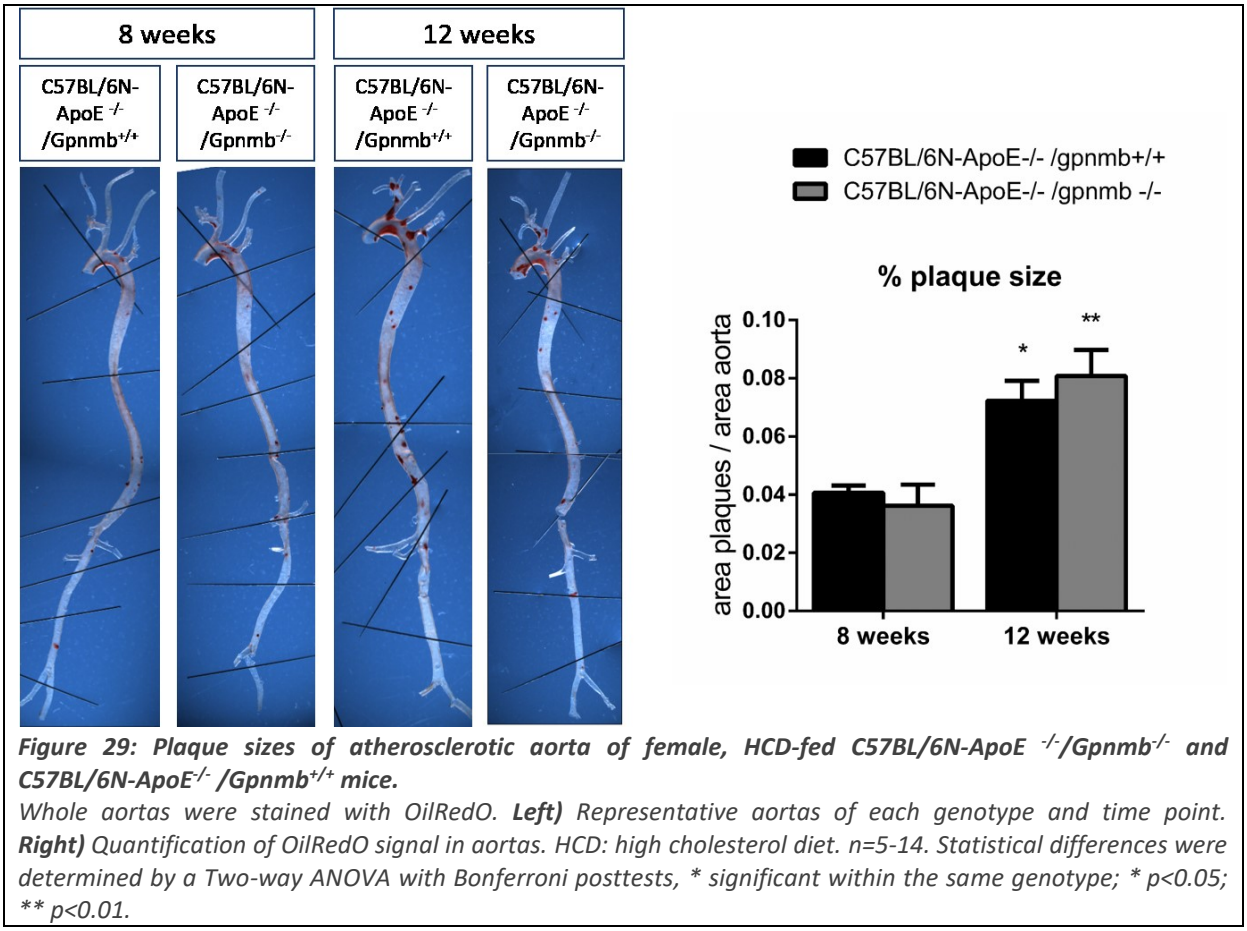

Figure 29: Plaque sizes of atherosclerotic aorta of female, HCD-fed C57BL/6N-ApoE $^{-/-}$/Gpnmb$^{-/-}$ and C57BL/6N-ApoE$^{-/-}$ /Gpnmb$^{+/+}$ mice.

Whole aortas were stained with OilRedO. ***Left)*** *Representative aortas of each genotype and time point.* ***Right)*** *Quantification of OilRedO signal in aortas. HCD: high cholesterol diet. n=5-14. Statistical differences were determined by a Two-way ANOVA with Bonferroni posttests, * significant within the same genotype; * p<0.05; ** p<0.01.*

6.2.1. Gpnmb was expressed in lipid-containing macrophages

Histological sections showed strong signals from macrophage markers CD68 and Galectin-3 (Mac-2) at the surface layer of aortic root plaques (**Figure 31 A-C**). Thus, monocytes/macrophages were crossing the CD31-positive endothelial layer, incorporating lipids until containing large lipid vesicles. Not all of the macrophages contained lipid droplets, suggesting that some have not yet evolved to foam cells. The same vice versa: not all labelled lipid vesicles were located to macrophage. Those single lipid droplet signals appeared mostly in deeper layers, either the once lipid containing foam cells had become apoptotic or necrotic and are not expressing macrophage markers anymore, or other cells contained the lipids in deeper layers. Especially the plaque surface cells showed a pronounced Gpnmb signal (**Figure 31 D-F**). Again, not all CD68- or Mac-2-positive cells were Gpnmb-positive and vice versa, confirming that

only a specific subset of macrophages were expressing Gpnmb [133, 199]. Only few of the CD31-positive endothelial cells were Gpnmb-positive (**Figure 31 E**). CD3-positive T cells were not found to express Gpnmb (picture not shown). Thus, mostly macrophages were expressing Gpnmb but other cells like dendritic cells might be another source of Gpnmb.

To study the influence of Gpnmb on foam cell formation *in vitro*, we fed primary macrophages acetylated LDL. However, expression of Gpnmb was not influenced and shedding of Gpnmb was only slightly increased upon uptake of LDL (**Figure 12**, **Figure 13**), which was verified by immunocytochemistry (**Figure 32**).

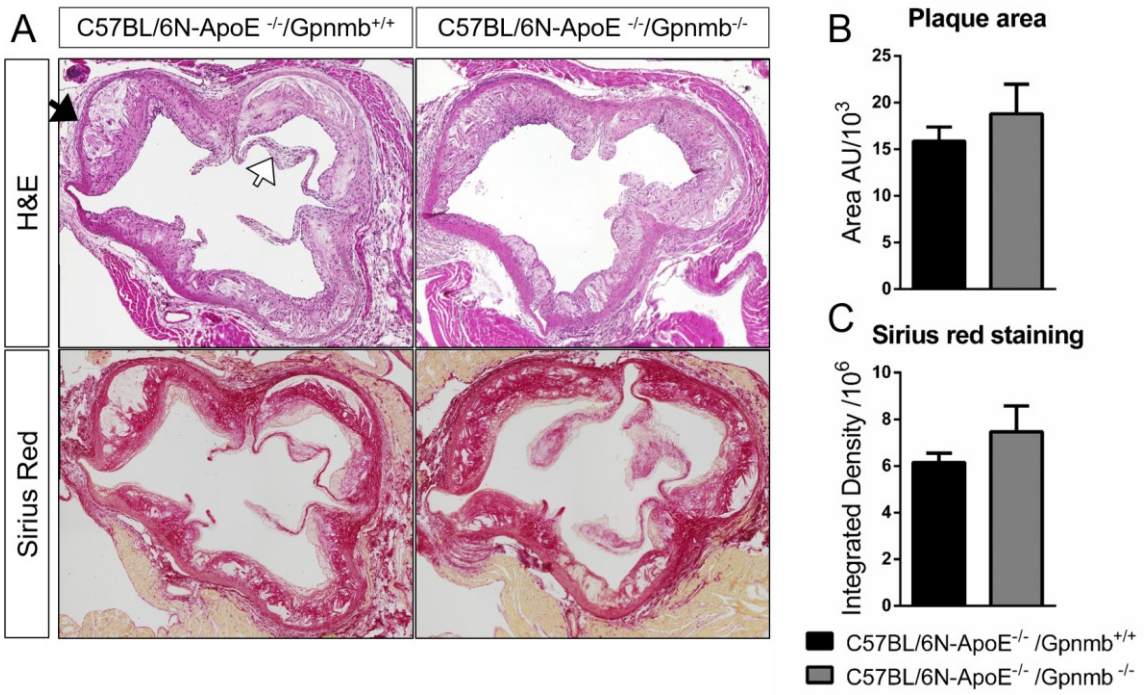

Figure 30: Plaque size and fibrosis of aortic root of female C57BL/6N-ApoE $^{-/-}$/Gpnmb$^{-/-}$ and C57BL/6N-ApoE$^{-/-}$/Gpnmb$^{+/+}$ mice fed a HCD-fed for 12 weeks.

A) *Representative pictures of 5 µm heart sections for quantification.* ***B)*** *Hematoxylin & eosin (H&E) staining was used to measure plaque size.* ***C)*** *Sirius red staining was used to measure fibrosis. Integrated density describes the product of the selected area (the plaques) and mean gray value (the intensity of the signal) and is therefore a product of size and magnitude of fibrosis. Four sections of each of the three animals were analyzed, respectively (n=3). HCD: high cholesterol diet.*

6.2.1. Gpnmb did not alter body weight, but exerted a mild anti-inflammatory effect

Metabolically, Gpnmb had a mild influence on body weight gain during the 12 weeks of HCD. *Gpnmb*-knockout animals were slightly lighter throughout the HCD feeding time period (**Figure 33 A-C**). The composition of body fat, muscle and free water was not altered by Gpnmb (**Figure 33 D-F**).

Looking at the two organs metabolically most active in a diet-induced disease, fat and liver, we found elevated macrophage marker *F4/80* and elevated pro-inflammatory marker *Il6* only in adipose tissue of *Gpnmb*-knockout animals (**Figure 34**). Liver was not affected, and as inflammation thrives by communication, the inflammation was not yet transmitted to circulating cytokine IL-1β levels in plasma. By tendency, the anti-inflammatory marker genes *Arg1* and

Abca1 (the latter being a cholesterol efflux gene) were reduced in adipose tissue of *Gpnmb*-knockout animals, corroborating mild anti-inflammatory properties of Gpnmb.

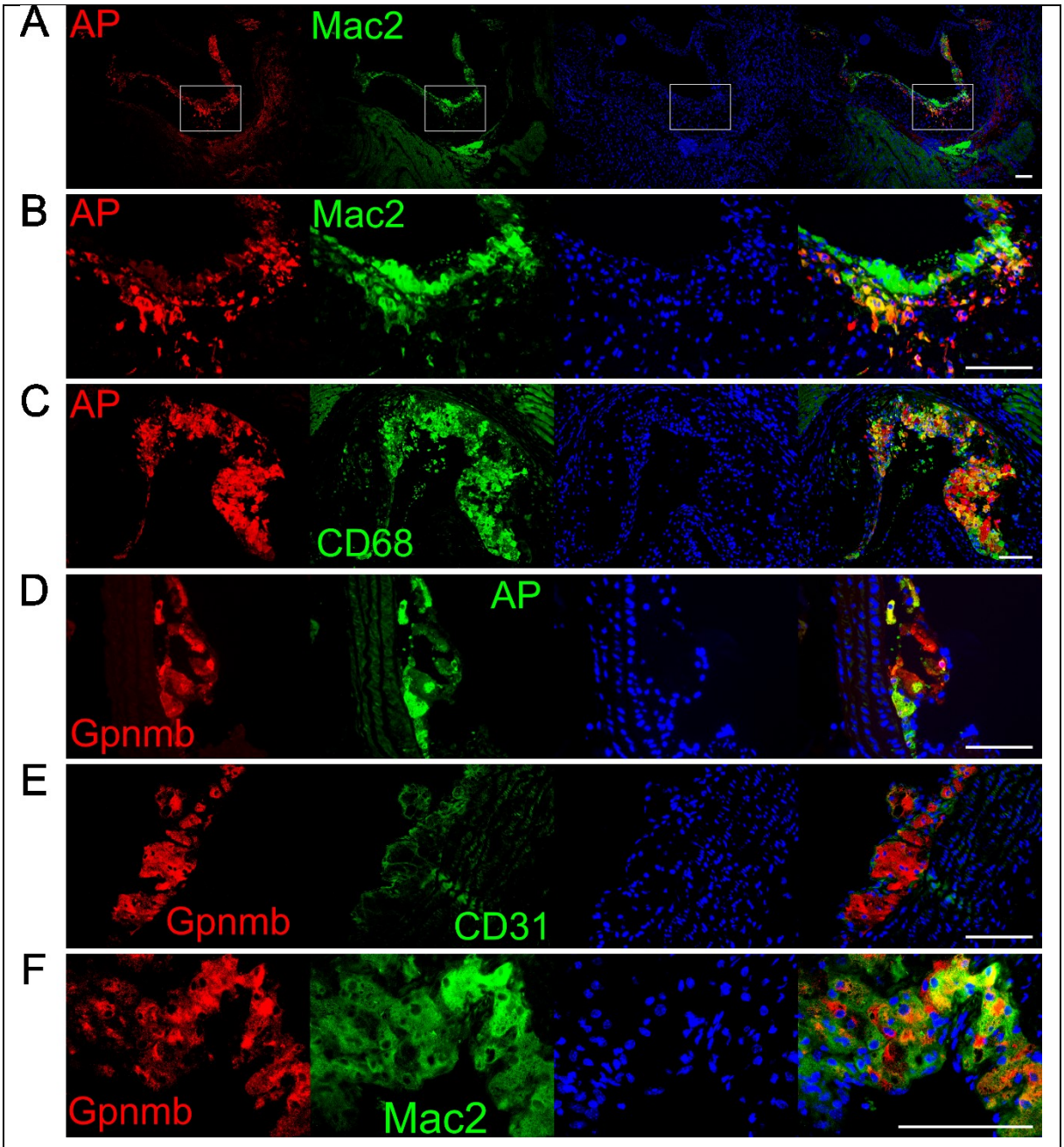

Figure 31: Gpnmb, macrophage and lipid droplet localization in plaques of aortic root of female, HCD-fed C57BL/6N-ApoE$^{-/-}$ /Gpnmb$^{+/+}$ mice.
Immunohistological staining of 5 µm heart sections. ***A)*** *Overview of one valve in the aortic root. A part of the picture* ***(A)*** *is enlarged in* ***(B)****. Macrophages are stained by anti-Mac-2 and anti-CD68 antibodies, lipid droplets by an anti-adipophilin (AP) antibody. The third picture in a row depicts nuclear staining by DAPI in blue, on the right are merged pictures. HCD: high cholesterol diet. Scale bar: 100 µm.*

6.2.2. Gpnmb did not alter liver fibrosis in atherosclerotic mice

Excessive cholesterol metabolism can exceed liver capacity. To assess liver damage and fibrosis, the enzymes ALP, AST and ALT were measured in plasma. However, liver function readings were not altered at 8 or 12 weeks of HCD in our animals (**Figure 35 A-C**). The same applies for the

central lipid regulator *peroxisome proliferator-activated receptor γ* (*Pparγ*) and the expression of collagens that could convey the development of liver fibrosis (**Figure 35 D-F**).

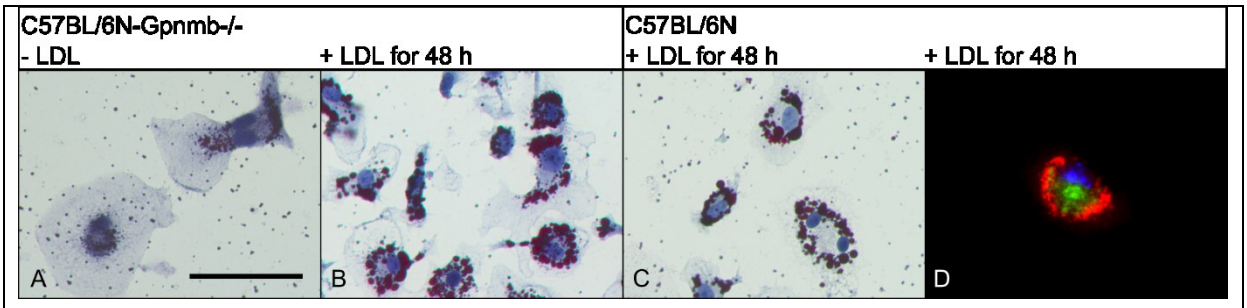

***Figure 32: Uptake of acetylated LDL by macrophages* in vitro.**
Mature C57BL/6N and C57BL/6N-Gpnmb$^{-/-}$-derived macrophages were treated with 20 µg/mL acetylated LDL for 48 h. ***A-C)*** *Lipid droplets are stained by OilRedO (red), nuclei are stained by hematoxylin and eosin (purple).* ***D)*** *Lipid droplets are stained by an anti-adipophilin antibody (red), anti-Gpnmb (green), the nucleus is stained by Hoechst 33342 (blue). Scale bar: 50 µm.*

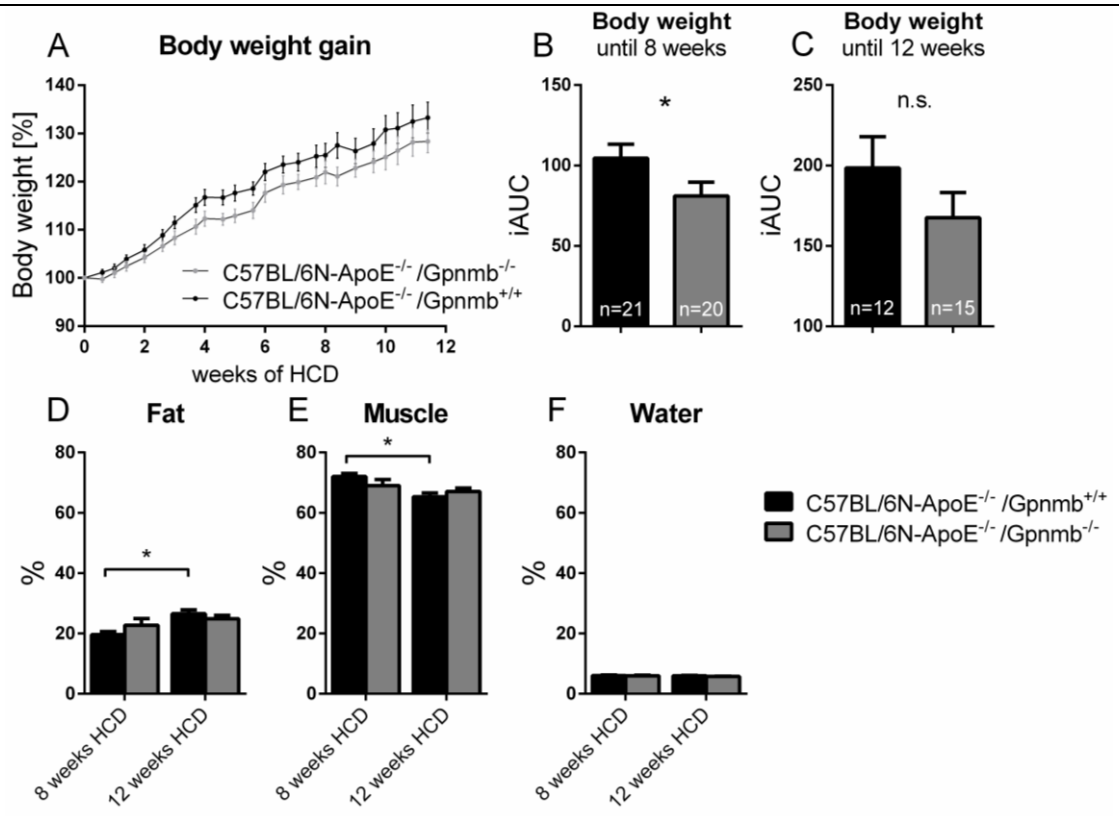

Figure 33: Body weight and body composition (D-F) of female, HCD-fed C57BL/6N-ApoE $^{-/-}$/Gpnmb$^{-/-}$ and C57BL/6N-ApoE$^{-/-}$ /Gpnmb$^{+/+}$ mice.
A-C) *Body weight and its respective integrated area under the curve (iAUC).* ***D-F)*** *Body composition analysis. HCD: high cholesterol diet, n.s.: not significant. n=5-15. Statistical differences were determined by a non-parametric t-test/Mann Whitney test (B, C) or by a Two-way ANOVA with Bonferroni posttests (A, D-F); * p<0.05.*

Taken together, atherosclerosis was induced in ApoE-deficient animals by feeding HCD for several weeks. Gpnmb was highly expressed in macrophages of plaques in aortic root. The function of Gpnmb is so far elusive, as neither atherosclerotic plaque formation nor circulating lipids nor liver fibrosis were impacted by the absence of Gpnmb. However, adipose tissue contained more and more inflammatory macrophages in *Gpnmb*-knockout animals.

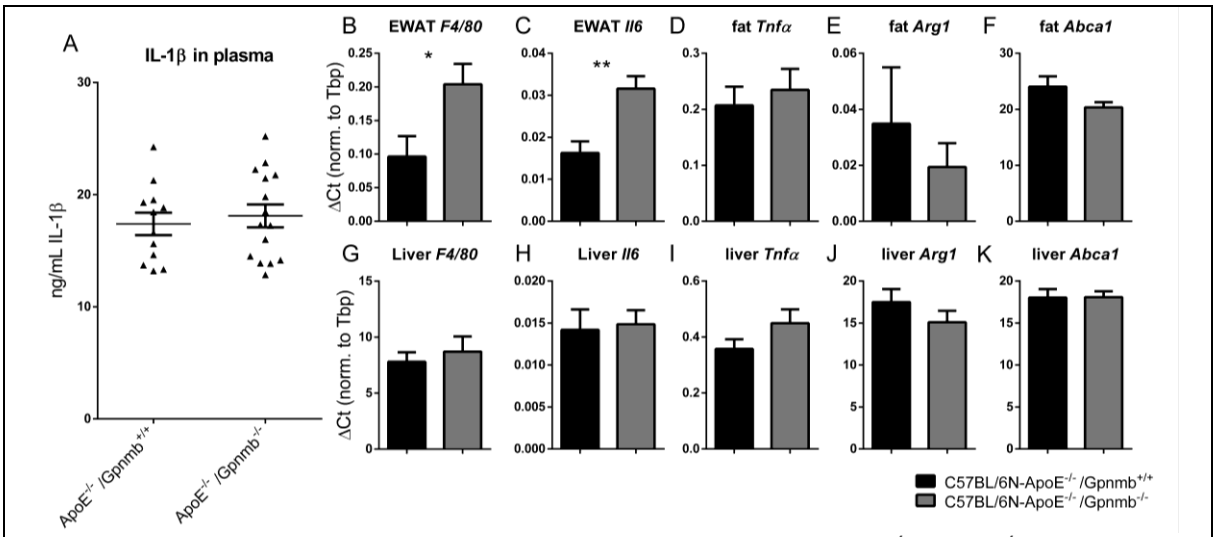

Figure 34: Macrophage and inflammation status of female C57BL/6N-ApoE $^{-/-}$/Gpnmb$^{-/-}$ and C57BL/6N-ApoE$^{-/-}$ /Gpnmb$^{+/+}$ mice fed a HCD for 12 weeks.

A) *IL-1ß measured in plasma by ELISA.* ***B-K)*** *Transcript levels in epididymal adipose tissue* ***(B-F)*** *and liver* ***(G-K)*** *were measured by qRT-PCR. HCD: high cholesterol diet. n=12-15. Statistical differences were determined by a non-parametric t-test/Mann Whitney test; * p<0.05 ;** p<0.01.*

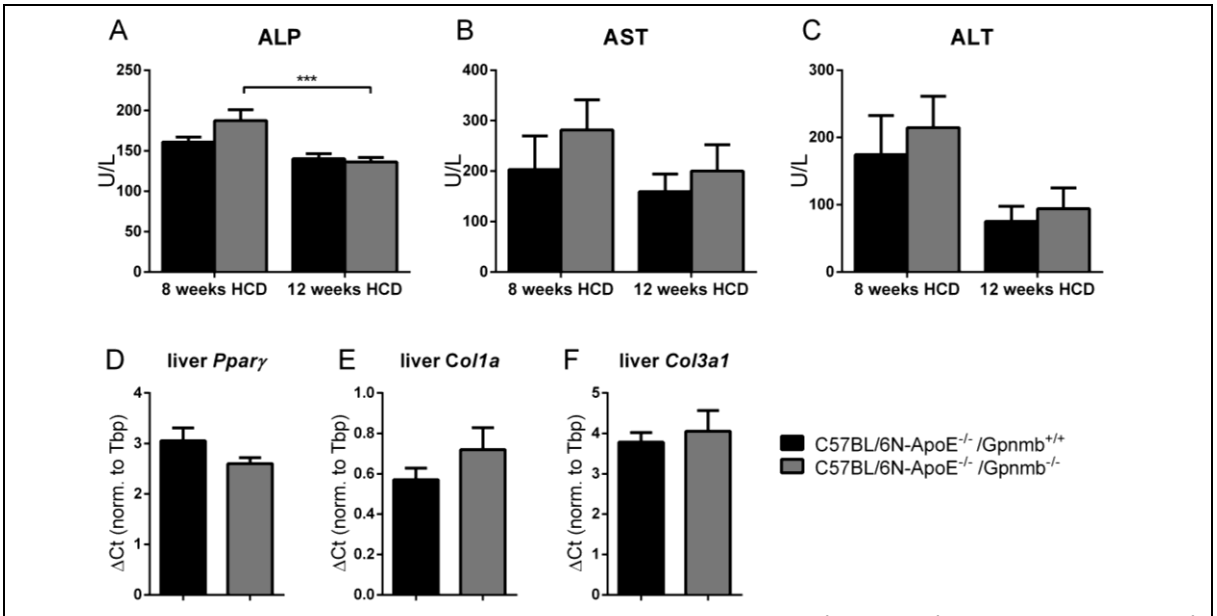

Figure 35: Liver damage markers in female, HCD-fed C57BL/6N-ApoE $^{-/-}$/Gpnmb$^{-/-}$ and C57BL/6N-ApoE$^{-/-}$ /Gpnmb$^{+/+}$ mice.

A-C) *Liver damage markers measured in plasma.* ***D-F)*** *mRNA levels of animals fed a HCD for 12 weeks, measured by qRT-PCR. HCD: high cholesterol diet. n=5-15. Statistical differences were determined by a Two-way ANOVA with Bonferroni posttests (A-C) or by a non-parametric t-test/Mann Whitney test (D-F); *** p<0.001.*

Therefore, atherosclerosis might not be a disease in which the function of Gpnmb is relevant or easily assessable. The only statistical difference between C57BL/6N-ApoE$^{-/-}$/Gpnmb$^{-/-}$ and C57BL/6N-ApoE$^{-/-}$/Gpnmb$^{+/+}$ mice was detected in adipose tissue. This organ is crucial in obesity, another metabolic disease that we studied next.

6.3. Obesity

6.3.1. Gpnmb expression was increased by obesity, but had no influence on body weight

As obesity is associated with chronic, low-grade inflammation, hyperinsulinemia, disrupted glucose metabolism and fatty liver, it is a model for pre-diabetes and liver steatosis in animals [285–287]. Male C57BL/6N and C57BL/6N-Gpnmb$^{-/-}$ mice were fed a high fat diet (HFD, 60% calories from fat) for 16 weeks. Liver and brain *Gpnmb* mRNA were increased by 16 weeks of HFD (**Figure 36 A-B**). Plasma levels of circulating Gpnmb were not altered between lean female and male animals, but increased in males after 16 weeks of HFD (**Figure 36 C-D**). Strikingly, even in *Gpnmb*-knockout animals, a small induction of Gpnmb became detectable after 16 weeks of HFD, suggesting the use of an alternate start codon.

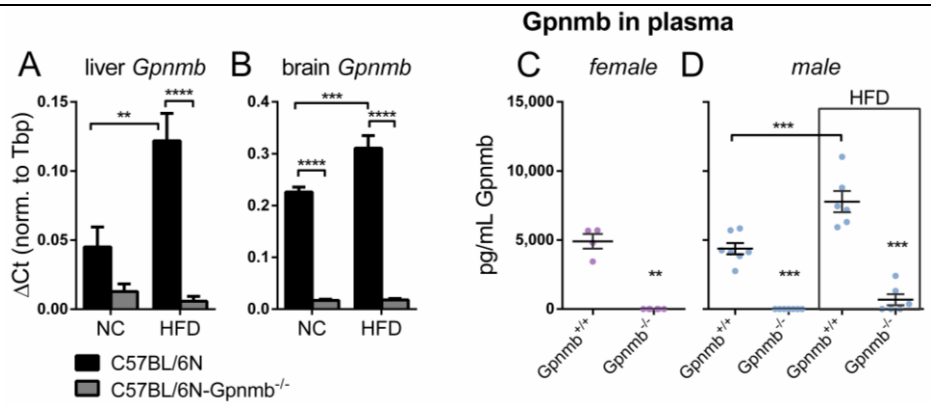

Figure 36: Gpnmb expression of lean or HFD-fed C57BL/6N and C57BL/6N-Gpnmb$^{-/-}$ mice.
A-B) *Gpnmb mRNA levels of male mice, measured by qRT-PCR.* ***C-D)*** *Measurement of soluble Gpnmb in plasma by ELISA. NC: normal chow, HFD: high fat diet. n=6-7. Statistical differences were determined by a non-parametric t-test/Mann Whitney test for female animals (D) and by a Two-way ANOVA with Bonferroni posttests for male animals (A-C, E); ** p<0.01; *** p<0.001; **** p<0.0001.*

Throughout the 16 weeks of feeding HFD, body weight increased similarly in both strains (**Figure 37 A**). The *Gpnmb*-knockout animals were slightly lighter but caught up at the end of the feeding period. Fractions of fat, muscle and water measured in a body composition analysis at the end of the 16 weeks were similar in both strains (**Figure 37 C**). Of note, the body composition analysis showed that the slight decrease of body weight in *Gpnmb*-knockout mice derived rather from a lower amount of muscle mass than less body fat, thus *Gpnmb*-knockout animals should not be considered as having a metabolic advantage. Organ weight of epididymal and brown adipose tissue increased with 16 weeks of HFD, however the weight was not affected by genotype (**Figure 37 D-E**). It should be mentioned that unfortunately both cages of lean, normal chow (NC)-fed *Gpnmb*-knockout animals were fighting. This resulted in a reduced adipose tissue weight compared to their wildtype controls (not significant with One-way ANOVA and posttests as indicated in **Figure 37**, however p=0.0379 when calculated with an isolated two-tailed Mann Whitney t-test), which is also reflected in later analysis.

Blood lipid parameters were measured to check the effect of the diet. Total cholesterol as well as HDL levels were increased after 16 weeks HFD, whereas triglyceride and LDL levels were not affected by food intake (**Figure 37 G-J**). Though atherosclerosis and obesity have in common that they are a lipid-associated diseases with induced low-grade inflammation, the blood lipid

levels reveal a different mechanism of action. Obese animals had 10-fold less cholesterol in blood than atherosclerotic animals. HDL/LDL ratio was, as opposed to atherosclerotic animals, on the HDL side. Total triglycerides were similar in all diseases and conditions. Altogether, atherosclerotic animals had more lipids in the bloodstream than animals that were fed a diet with higher fat content and for a longer period of time.

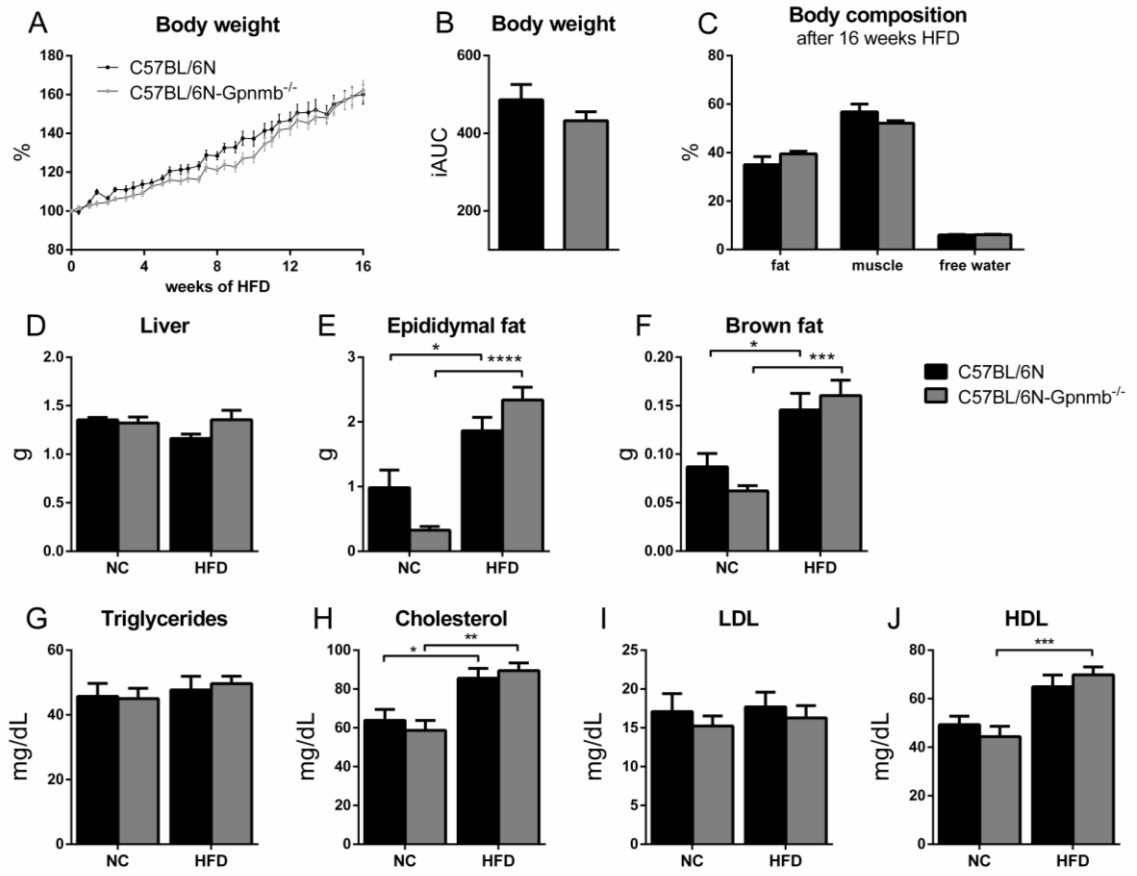

Figure 37: Impact of Gpnmb and 16 weeks of HFD on body weight, organ weight and plasma lipid parameters of lean or HFD-fed, male C57BL/6N and C57BL/6N-Gpnmb$^{-/-}$ mice.
A) *Body weight curve and* ***B)*** *integrated area under the curve of the body weight (iAUC).* ***C)*** *Body composition analysis at the end of the 16 weeks of HFD.* ***D-E)*** *Organ weight.* ***G-J)*** *Blood lipid parameters in plasma. NC: normal chow, HFD: high fat diet. n=6-7. Statistical differences were tested by a Two-way ANOVA with Bonferroni posttests (A, C-J) or by a non-parametric t-test/Mann Whitney test (B); * p<0.05; ** p<0.01; *** p<0.001; **** p<0.0001.*

6.3.2. Gpnmb increased the number of adipose tissue macrophages

Analysis of fixed epididymal adipose tissue sections with hematoxylin and eosin revealed an increased adipocyte diameter by HFD, showing a hypertrophy of adipocytes (**Figure 38 C**). The low body weight of NC-fed *Gpnmb*-knockout animals was reflected in their adipocyte diameter as well. Viewing the sections, *Gpnmb*-knockout animals generally seemed to have more small cells additionally to the adipocytes. Those cells appeared uniform, isolated and widely dispersed between adipocytes in lean *Gpnmb*-knockout mice but formed aggregates completely surrounding adipocytes in obese mice. Those aggregates, so-called crown-like structures (CLS) are described as dead or apoptotic adipocyte surrounded by macrophages, forming a shape that looks like a crown [288]. Indeed, the cells surrounding the adipocyte were CD68-positive

macrophages and expressed Gpnmb in wildtype mice (**Figure 38**). The CLSs occurred in higher frequency in obese *Gpnmb*-knockout animals (**Figure 38 D**), suggesting an inhibitory effect of Gpnmb on macrophage infiltration of adipose tissue. CLSs are a sign of adipose tissue inflammation, which is considered a causative factor for insulin resistance [16, 285, 288].

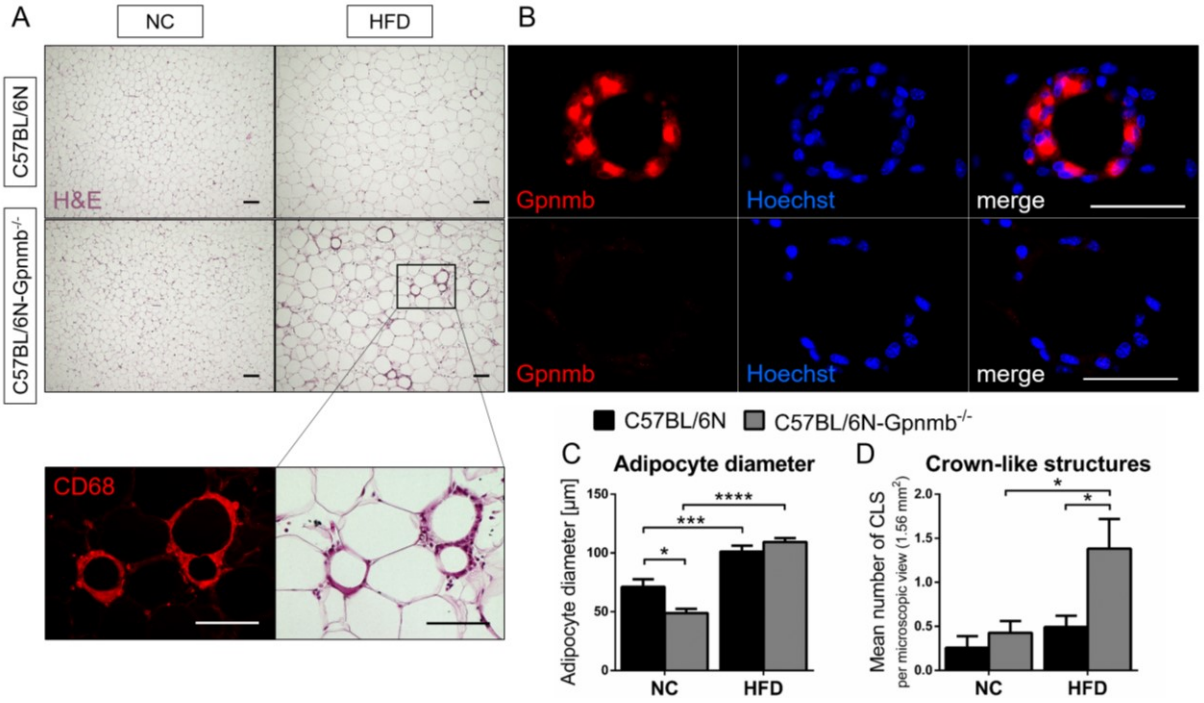

Figure 38: Analysis of epididymal adipose tissue of lean or HFD-fed, male C57BL/6N and C57BL/6N-Gpnmb$^{-/-}$ mice.

A) *Representative pictures of hematoxylin and eosin (H&E) staining and CD68 staining. Scale bar: 100 µm* ***B)*** *Gpnmb in cells of a crown-like structure (CLS). Scale bar: 50 µm.* ***C)*** *On average 37 cells on each of on average 11 microscopic views of 10 µm sections were analyzed per animal.* ***D)*** *On average 11 microscopic views of 10 µm sections were analyzed per animal. NC: normal chow, HFD: high fat diet. n=6-7. Statistical differences were determined by a Two-way ANOVA with Bonferroni posttests; * p<0.05; *** p<0.001; **** p<0.0001.*

6.3.3. Gpnmb ameliorated insulin resistance

HFD induces insulin resistance, which is marked by an impaired clearance of glucose in the blood [285]. When challenged with sugar, blood glucose peaks within 30 min and is removed quickly by insulin-sensitive organs such as muscle, liver and adipose tissue and in addition by an insulin clearing mechanism by liver and kidney [289]. This peak was distinct after an oral glucose dose of 3 g/kg body weight in HFD-fed animals but almost not visible in lean animals (**Figure 39 A**), showing that insulin resistance was induced by HFD. In obese *Gpnmb*-knockout animals, the peak was further increased and glucose clearance delayed compared to wildtype controls. Some of the obese *Gpnmb*-knockout mice still exhibited hyperglycemia (defined as blood glucose >300 mg/dL [290]) 120 min after the oral dose of glucose (**Figure 39 E**). Apparently, the absence of Gpnmb led to a more pronounced insulin resistance. Pro-insulin is cleaved into insulin and C-peptide, so both molecules are secreted in equimolar concentrations. The half-life of insulin and C-peptide is around 5 min and 30 min, respectively [289, 291, 292]. Thus, C-peptide is a more reliable, indirect tool to measure insulin release. In line with glucose levels, insulin and C-peptide levels were increased in HFD-fed, *Gpnmb*-knockout animals (**Figure 39 F-I).** However, all male animals had received an oral dose of glucose more than 2 h before blood extraction for ELISA measurements, which may have influenced insulin and

C-peptide values. Especially obese *Gpnmb*-knockout animals had obviously a different kinetic of postprandial blood glucose excursion. Therefore, another control group was added, female mice of both strains that were fasted for at least 6 h before blood sampling.

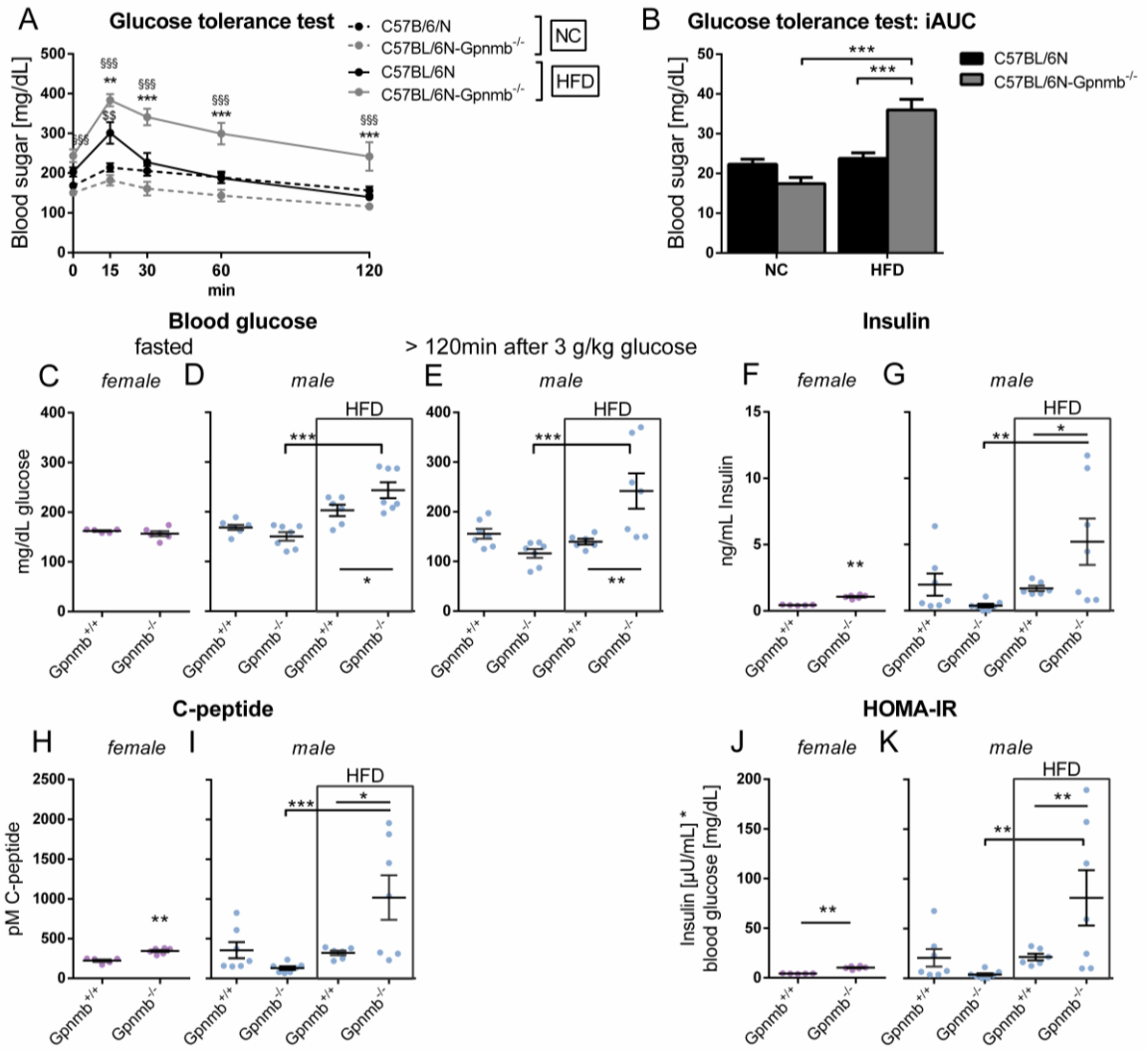

Figure 39: Insulin resistance of lean or HFD-fed C57BL/6N and C57BL/6N-Gpnmb$^{-/-}$ mice.

A) *Blood glucose time line of oral glucose tolerance test conducted in 6 h fasted animals and* ***B)*** *its respective integrated area under the curve (iAUC).* ***C-E)*** *Blood glucose of (A) in comparison to female control animals.* ***F-I)*** *ELISA of insulin and C-peptide in plasma.* ***J-K)*** *Homeostatic model assessment for insulin resistance (HOMA-IR), a product of insulin and fasted blood sugar. NC: normal chow, HFD: high fat diet. n=6-7. Statistical differences were determined by a non-parametric t-test/Mann Whitney test for female animals (C, F, H, J) and by a Two-way ANOVA with Bonferroni posttests for male animals (A, B, D, E, G, I, K).*

*A) * C57BL/6N (16 weeks HFD) vs. C57BL/6N-Gpnmb$^{-/-}$ (16 weeks HFD); $ C57BL/6N (16 weeks HFD) vs. C57BL/6N (NC); § C57BL/6N-Gpnmb$^{-/-}$ (16 weeks HFD) vs. C57BL/6N-Gpnmb$^{-/-}$ (NC). For all graphs: * p<0.05; **/$$ p<0.01; ***/§§§ p<0.001.*

Insulin levels were significantly increased in female *Gpnmb*-knockout animals (**Figure 39 F**), although those animals were still able to maintain similar baseline glucose levels as wildtype controls (**Figure 39 C**). Taken together, already lean *Gpnmb*-knockout animals are at the beginning of insulin resistance that is further enhanced by HFD, as indicated by the homeostatic model assessment for insulin resistance (HOMA-IR) values, an approximating equation to quantify insulin resistance and β-cell function (**Figure 39 J-K**).

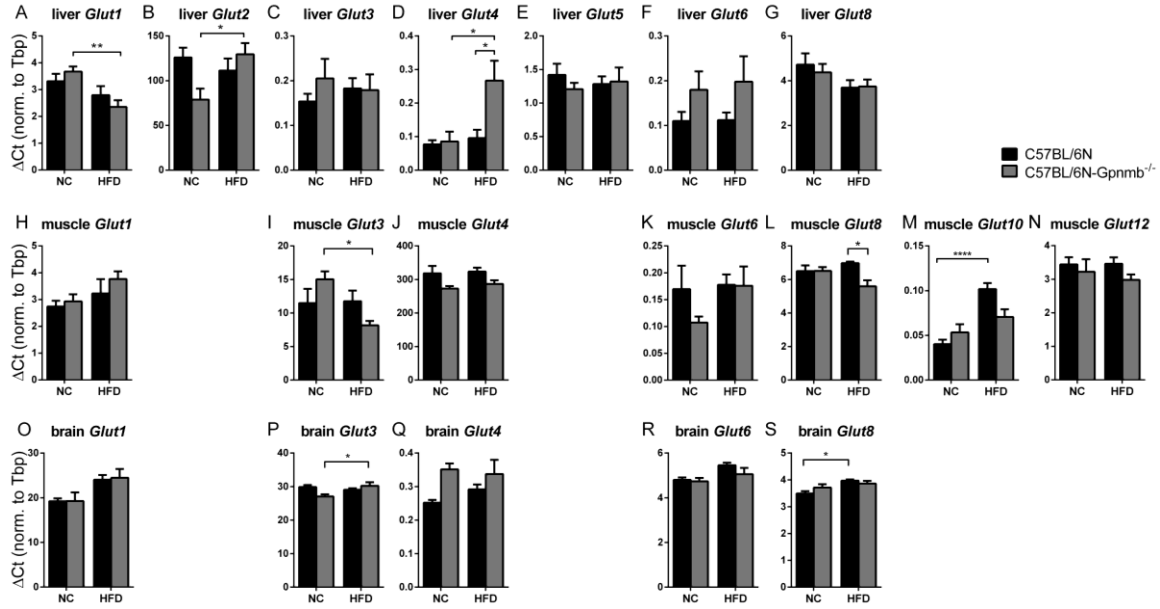

Figure 40: Slc2a/Glut glucose transporters in liver, muscle and brain of lean or HFD-fed C57BL/6N and C57BL/6N-Gpnmb$^{-/-}$ mice.

*Transcript levels were determined by qRT-PCR. Gaps indicate missing Glut isoforms that are either reported to be not expressed in the tissue or measured expression was too low for analysis. NC: normal chow, HFD: high fat diet. n=6-7. Statistical differences were determined by a Two-way ANOVA with Bonferroni posttests; * p<0.05; ** p<0.01; **** p<0.0001.*

6.3.4. Expression of metabolic genes, insulin and glucose receptors

To elucidate the cause for the increased insulin resistance in *Gpnmb*-knockout animals, gene expression of glucose transporters, insulin, insulin-like growth factor 1 (Igf-1) and leptin receptors as well as other metabolic genes were analyzed in liver, muscle and brain tissues.

The glucose transporter family (Gluts/ *Slc2a* genes) consists of different isoforms with tissue-specific expression. Of note, Glut2 is mostly expressed by pancreatic β-cells and liver and serves as a glucose sensor and induction of insulin secretion [31]. Glut4 is the only insulin-dependent Glut that is mainly expressed by liver, skeletal muscle and adipose tissue. Insulin-independent Glut1, -3, -6 and -8 provide the brain with energy [33, 293–297]. In diet-induced obesity, it is reported that Glut4 expression of muscle decreases and Glut2 expression of liver increases [298, 299]. Brain, muscle and liver samples were analyzed for expression of various *Glut* isoforms (**Figure 40**). Most *Glut* isoforms were not affected by HFD or genotype. *Glut4* mRNA is increased in liver of HFD-fed, *Gpnmb*-knockout animals. However, as mentioned, liver is not the primary organ for Glut4 expression. Of interest is the *Glut2* expression in liver that was unchanged in wildtype animals but increased by HFD in *Gpnmb*-knockout animals (**Figure 40 B**), having a similar pattern as glucose and insulin levels (**Figure 39**).

Insulin-, *Igf-1-* and *leptin receptors* were not altered by HFD or the presence of Gpnmb in liver, muscle or brain (**Figure 41**). The only exception was the insulin receptor in brain, which was increased by HFD in both strains, possibly contributing to the impaired glucose tolerance in obese mice (**Figure 39 A**). Leptin receptors *ObRa* (short form) and *ObRb* (long form) showed no sign of leptin resistance in brain (**Figure 41**).

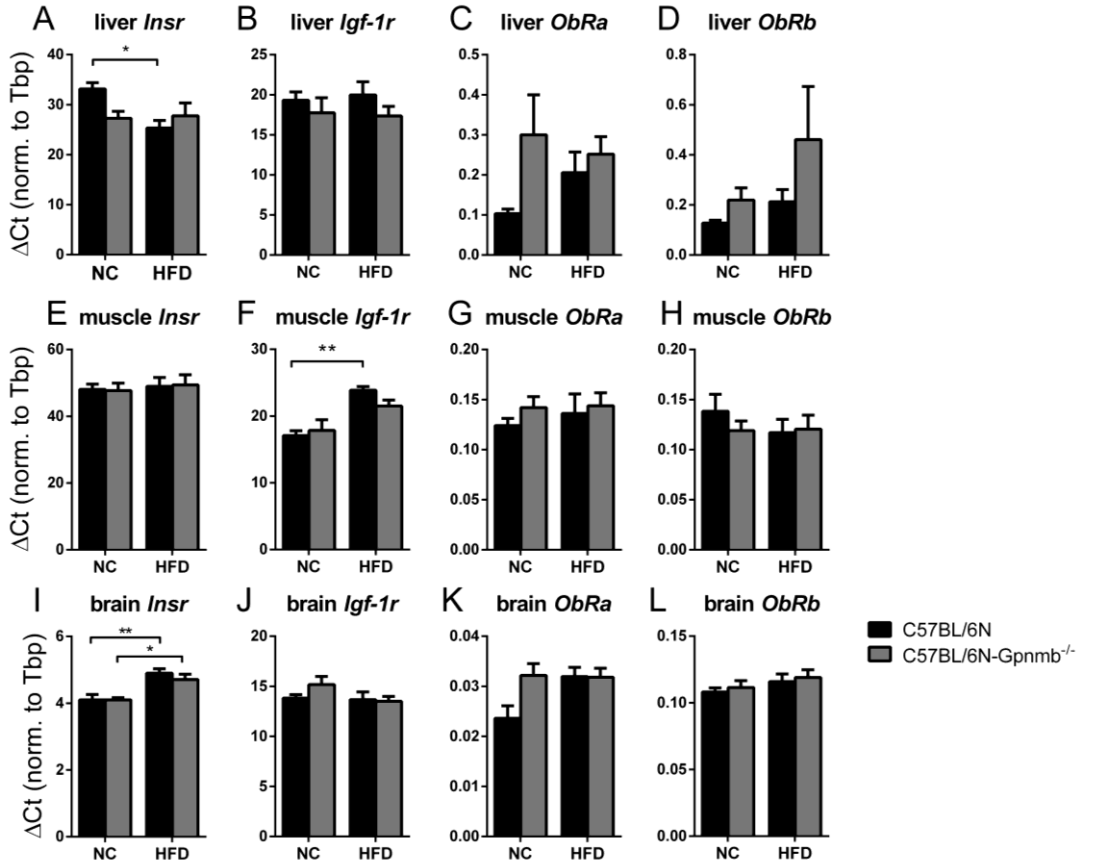

Figure 41: Receptors for insulin, Igf-1 and leptin in liver, muscle and brain of lean or HFD-fed C57BL/6N and C57BL/6N-Gpnmb$^{-/-}$ mice.

*Transcript levels were determined by qRT-PCR. Primers for insulin receptor gene amplify both isoforms INSR-A and INSR-B that differ only in the presence of exon 11. NC: normal chow, HFD: high fat diet. n=6-7. Statistical differences were determined by a Two-way ANOVA with Bonferroni posttests; * p<0.05; ** p<0.01.*

The liver constantly evaluates external cues and adapts its glucose metabolism appropriately. Hyperinsulinemia can result in excessive hepatic glucose production via gluconeogenesis. GSK-3β inhibits glycogen synthesis by inactivating glycogen synthesizing enzymes Gys1 and Gys2. FoxO1 activates genes for gluconeogenesis and glycogenolysis and inhibits adipogenesis [300]. In insulin resistant mice, FoxO1 is constitutively active, resulting in enhanced hepatic glucose production. Insulin phosphorylates and thereby inactivates both GSK-3β and FoxO1 via PI3K and AKT [301–304]. No impact of HFD or presence of Gpnmb on the expression of the glycogenetic genes *Gys1* and *Gys2* as well as gluconeogenetic genes *Gsk-3β* and *FoxO1* was observed on transcriptional level (**Figure 42**). Acetyl-CoA carboxylase (Acc), fatty acid synthase (Fasn) and acyl-CoA desaturase 1 (Scd1) are enzymes in the fatty acid synthesis pathway converting acetyl-CoA to triglycerides. The more expressed or more active those proteins are, the higher is the lipogenesis [305, 306]. From all measured genes regarding either storage or catabolism of glucose, glycogen and lipids, the expression of lipogenic genes like *Scd1*, *Fasn* and *Acc* were reacting the most to the tested conditions. The expression levels of all three genes reflected the glucose, insulin, liver *Glut2*, and to some degree, the body fat levels of the respective animals (**Figure 42 F-H**). While low expression of those lipogenic genes was observed in lean *Gpnmb*-knockout animals, HFD led to a duplication of lipogenic gene expression in obese *Gpnmb*-knockout animals compared to their wildtype controls. In contrast, the mRNA for *carnitine palmitoyltransferase I* (*Cpt1*), a mitochondrial enzyme essential in the β-oxidation of long chain fatty acids, was elevated by HFD only in wildtype animals (**Figure 42 H**).

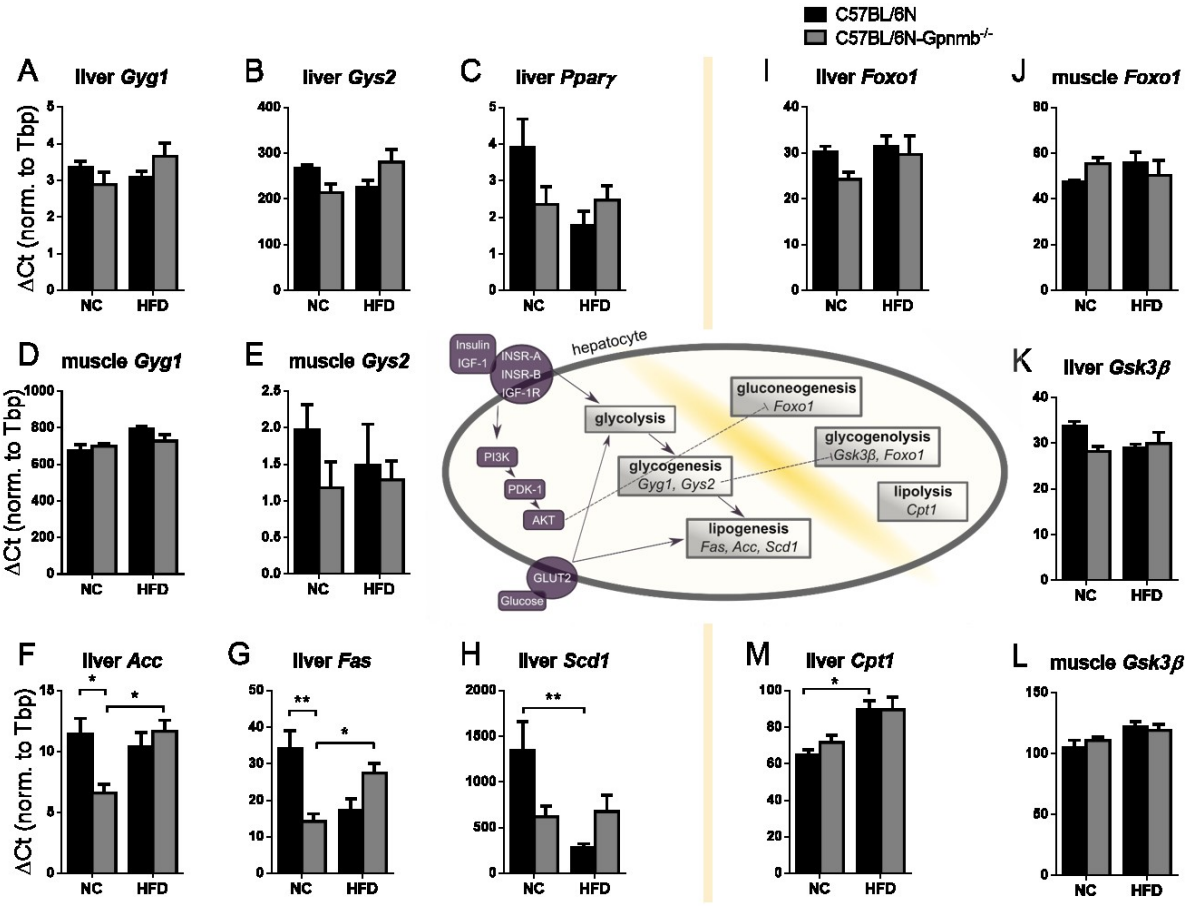

Figure 42: Metabolic enzymes/regulators in muscle and liver tissues of lean or HFD-fed C57BL/6N and C57BL/6N-Gpnmb$^{-/-}$ mice.

*Transcript levels were determined by qRT-PCR. Glucose degradation and storage **(A-E)** as well as lipogenic **(F-H)** mRNA levels are indicated on the left, glucose generation **(I-L)** and lipolysis **(M)** mRNA levels are shown on the right. NC: normal chow, HFD: high fat diet. n=6-7. Statistical differences were determined by a Two-way ANOVA with Bonferroni's multiple comparisons posttests; * p<0.05; ** p<0.01.*

We also evaluated the phosphorylation state of key metabolic enzymes of the liver. Insulin receptor substrate 1 (IRS1) is the most direct enzyme to measure insulin response because it starts several signaling pathways by activating PI3K. Surprisingly, neither an increase in IRS1 expression nor increased phosphorylation could be detected in HFD-fed mice (**Figure 43 A, E-G**) that would be expected in an insulin resistant state [307]. Another key regulator is AKT1/2/3/Protein Kinase B. IRS1 directly reacts to insulin signaling whereas AKT is a signaling molecule that includes other pathways as well. AKT has multiple phosphorylation sites. The phosphoinositide-dependent kinase-1 (PDK1) phosphorylates AKT at threonine 308, however full activation of AKT is achieved by phosphorylation of serine 473 by mTORC2 (rictor mTOR complex) [308–310], which is especially important in diabetes [311]. In contrast to IRS1, AKT responded to HFD, but only in *Gpnmb*-knockout animals and showed the same pattern as the expression of lipogenic genes (**Figure 42 F-H**), with lean *Gpnmb*-knockout mice having a reduced AKT-S473 phosphorylation that was significantly increased by HFD (**Figure 43 A-D**). However, the effect of HFD in general remained subtle.

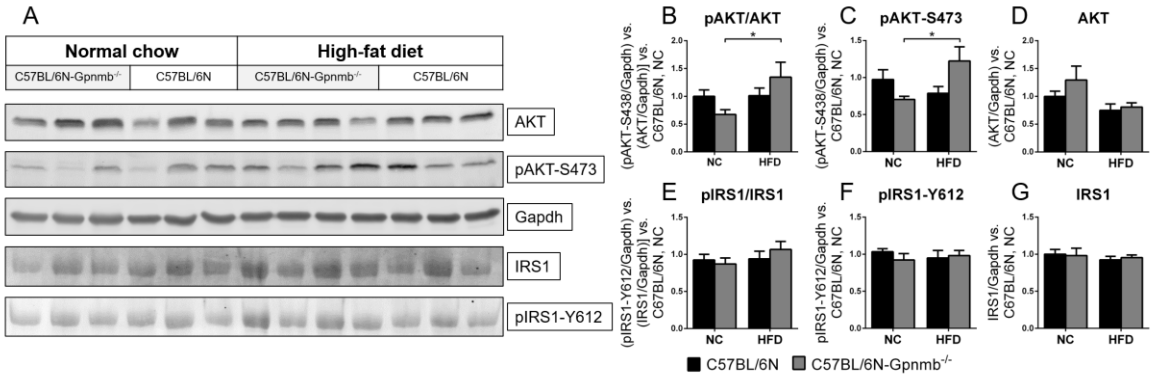

Figure 43: Analysis of insulin downstream targets in liver tissues of lean or HFD-fed C57BL/6N and C57BL/6N-Gpnmb$^{-/-}$ mice.

A) *Representative Western blot of indicated genes.* ***B-G)*** *Quantification of Western blots.* ***B)*** *Proportion of AKT that is phosphorylated at serine 473* ***(C)*** *divided by whole AKT* ***(D)****.* ***E)*** *Proportion of IRS1 that is phosphorylated at tyrosine 612* ***(F)*** *divided by whole IRS1* ***(G)****. NC: normal chow, HFD: high fat diet. n=6-7. Statistical differences were determined by a Two-way ANOVA with Bonferroni posttests; * p<0.05.*

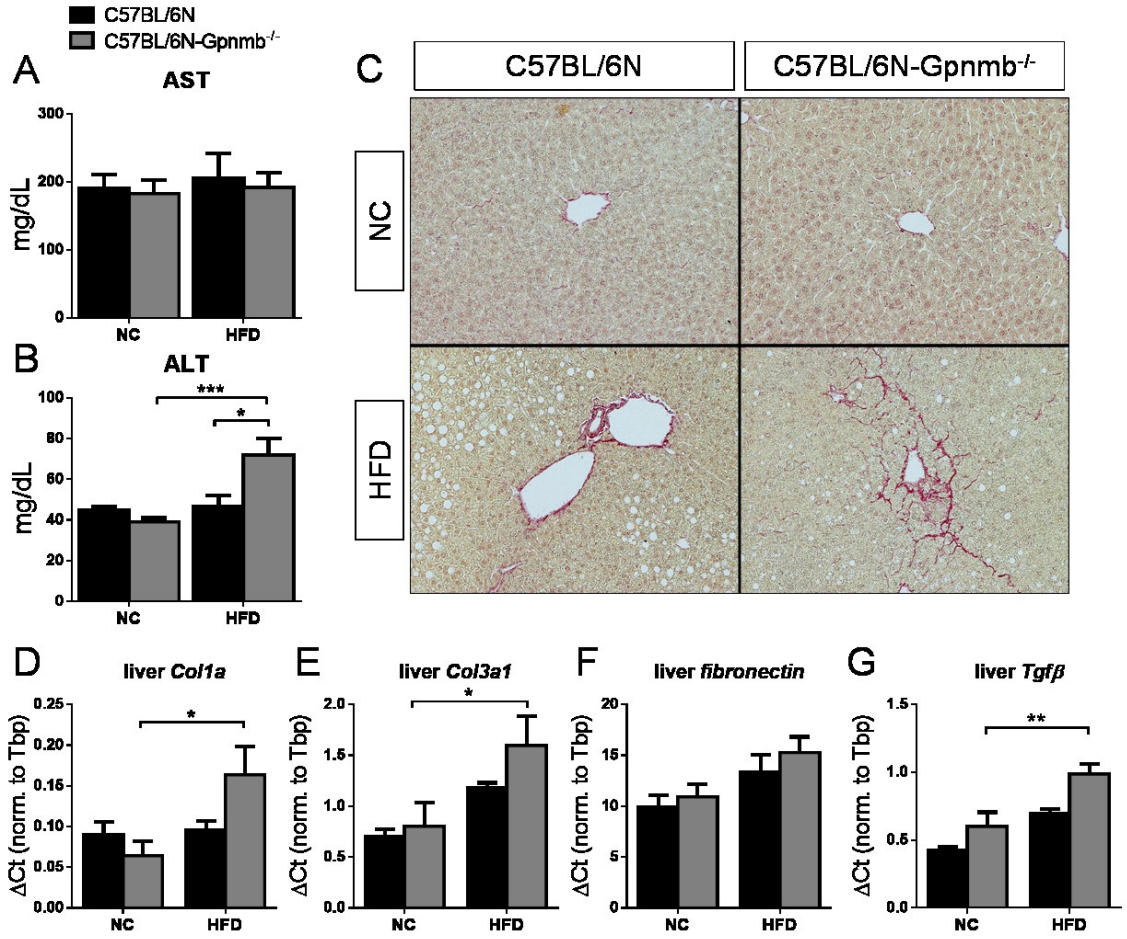

Figure 44: Hepatic fibrosis in male lean or HFD-fed C57BL/6N and C57BL/6N-Gpnmb$^{-/-}$ mice.

A-B) *Liver damage markers in plasma tissue.* ***C)*** *Representative pictures of Sirius red staining of 5 µm liver tissue sections.* ***D-F)*** *Fibrotic mRNA levels in liver, measured by qRT-PCR. AST: aspartate aminotransferase, ALT, alanine aminotransferase, NC: normal chow, HFD: high fat diet. n=6-7. Statistical differences were determined by a Two-way ANOVA with Bonferroni posttests; * p<0.05; ** p<0.01; *** p<0.001.*

6.3.1. Gpnmb suppressed liver fibrosis in obese mice

Obesity typically impairs liver function because the liver metabolizes the ingested fat. Lipids that are not metabolized by the liver are stored in vacuoles instead. This ectopic fat deposition is called steatosis and can lead to inflammation and fibrosis. Histology showed large vacuoles full of fat in liver sections that appeared in both genotypes after 16 weeks of HFD (**Figure 44 C**). Sirius red staining showed deposition of extracellular matrix material that is typical for fibrosis. Fibrotic depositions seemed more pronounced in obese *Gpnmb*-knockout animals, so we tested for liver damage markers in plasma. Only upon hepatic dysfunction, aminotransferases are released into the bloodstream. AST is produced by multiple organs like liver, brain, pancreas, heart, kidneys, lung and skeletal muscle. In contrast, ALT is expressed primarily by the liver and therefore a more specific liver damage marker [176]. An increase of ALT in plasma was seen exclusively in obese *Gpnmb*-knockout animals (**Figure 44 A-B**) and indicated an ameliorating influence of Gpnmb on the development of liver damage. AST remained equal in all conditions, excluding general organ damage. In line with this, fibrotic genes in liver like collagens and *Tgfβ* were upregulated by HFD in *Gpnmb*-knockout but not in wildtype animals (**Figure 44 C-F**).

6.3.2. Gpnmb exerted a mild anti-inflammatory effect in obese mice

Diet-induced obesity is a model disease for chronic low-grade inflammation. Testing macrophage infiltration into liver, muscle and brain tissues, obesity led only in liver to a significant increase of macrophage marker *F4/80* and anti-inflammatory marker *Abca1* gene expression (**Figure 45 A, B**). Scavenger receptor *Cd36* expression can be a sign for specifically metabolic activation of macrophages [23]. However, no major impact of HFD or the absence of Gpnmb could be observed on the expression of *Cd36*. Muscle and brain showed no major macrophage infiltration caused by HFD. Interestingly, the expression of the inflammatory cytokine *Il1β* increased non-significantly in obese *Gpnmb*-knockout animals in all tissues. To summarize, the low-grade inflammation induced by HFD is indeed low and most pronounced in liver with a possible mild anti-inflammatory effect of Gpnmb.

Taken together, obesity was inducing a low-grade inflammation in liver and pre-diabetes with insulin resistance. Although body weight gain as the main determinant of obesity pathology was not affected by the absence of Gpnmb, Gpnmb acted positively on insulin resistance and glucose levels as well as liver fibrosis, possibly via activated AKT.

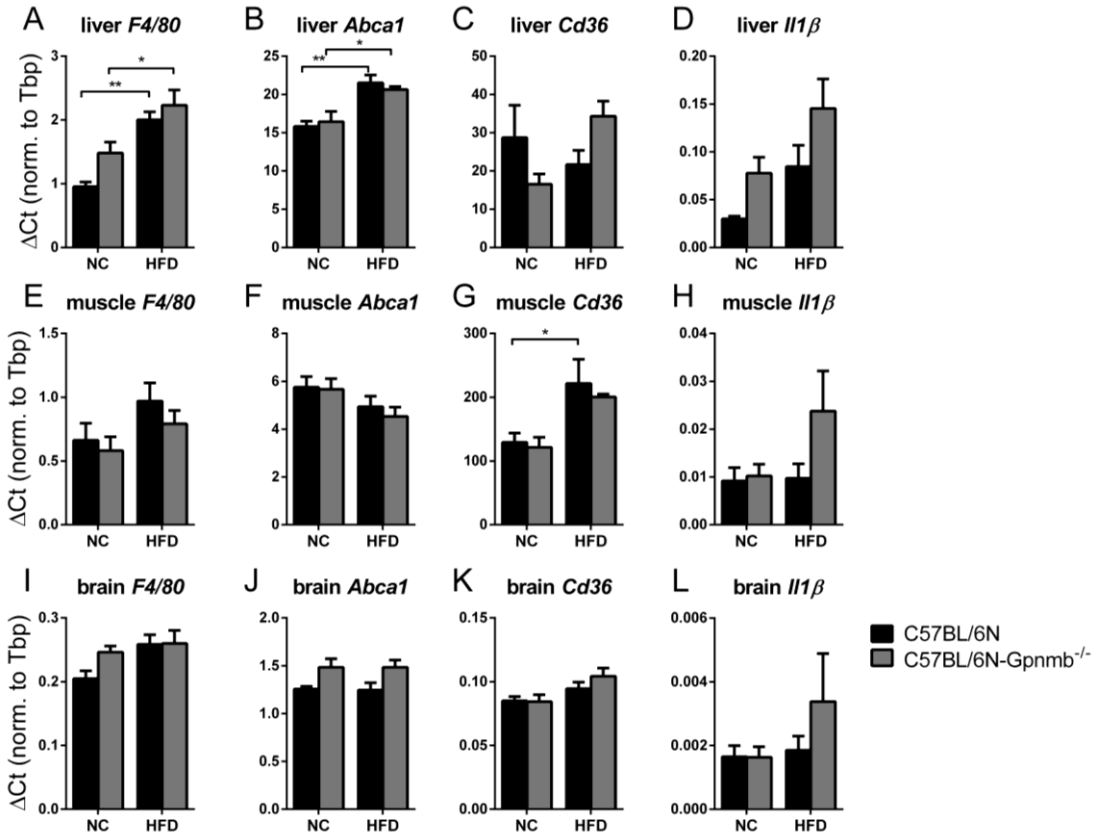

Figure 45: Macrophage and inflammation status in liver, muscle and brain tissues of male lean or HFD-fed C57BL/6N and C57BL/6N-Gpnmb$^{-/-}$ mice.

*Transcript levels were measured by qRT-PCR. NC: normal chow, HFD: high fat diet. n=6-7. Statistical differences were determined by a Two-way ANOVA with Bonferroni posttests; * p<0.05; ** p<0.01.*

7. Discussion

7.1. Molecular forms of Gpnmb

Examining functions of Gpnmb in primary macrophages derived from *Gpnmb*-knockout mice or wildtype controls, a highly variable appearance of Gpnmb in Western blots emerged, suggesting a protein that adapts quickly to different conditions.

7.1.1. Molecular weight of Gpnmb in Western blot

Western blot signals of Gpnmb that are faint or hardly visible became strong after certain treatments. It is thus difficult to unambiguously describe the molecular diversity of Gpnmb on Western blots. In the following, three sections from low to high molecular weight bands detected by Western blot – 0-40 kDa/50-70 kDa/above 90 kDa - are described.

7.1.1.1. Low molecular weight zone

The anti-Gpnmb antibody detects a plethora of low molecular weight bands. The molecular mass of the intracellular C-terminal Gpnmb fragment that remains after cleavage is predicted 17.4 kDa [79]. In Western blot, the C-terminal remnant was detected at 12 and 30 kDa [184], at 36 kDa [165], at 25 and 13kDa [124], at 14 and 20 kDa [92] and at 20 kDa, the latter using a tagged protein [178, 312]. It was reported that the small fragment is translocated into the nucleus where it regulates RNA splicing [110, 312].

We detected especially in eye lysates huge amounts of signals within this range (**Figure 11**). However, the *Gpnmb*-knockout controls showed similar bands at this low molecular weight zone in Western blot, thus this range was not analyzed.

7.1.1.2. Medium molecular weight zone

The molecular weight of Gpnmb based on its sequence is predicted around 65 kDa. In fact, Western blot repeatedly showed a form at 65 kDa that is referred to as the immature/native/unglycosylated form of Gpnmb [90, 93, 109, 110, 184, 232]. A band around this size was even reported as the strongest amongst Gpnmb signals at 36, 68 and 115 kDa [165]. Moreover, shedding produced a 50-70 kDa fragment in microglia [123] and a C-terminal 50 kDa fragment in neuronal cells [110].

Our Western blots reliably showed a band at 65 kDa. A pronounced increase in intensity of the bands between 60-70 kDa after de-glycosylation corroborates the hypothesis that this is in fact the immature form of Gpnmb, confirming de-glycosylation experiments carried out by others [74, 92]. However, a band this size can be detected in both murine *Gpnmb*-knockout strains, DBA/2J and C57BL/6N-Gpnmb$^{-/-}$, questioning a lot of published findings about Gpnmb using the same antibody. It was reported by others that bands at 60 kDa [78] and slightly above and below 50 kDa [74] are unspecific. Possibly, anti-Gpnmb antibodies recognize similar proteins like Pmel17, which can exhibit several bands as well [80]. Another group excluded the ~68 kDa band because it did not respond to treatments [172]. A band at ~65 kDa is therefore not necessarily

unspecific, however a robust method should be used to ensure specificity such as a *Gpnmb*-knockout control or a tagged protein.

7.1.1.3. High molecular weight zone

The high molecular weight zone above 90 kDa was the only area devoid of signal in the *Gpnmb*-knockout lanes. Here, Gpnmb signal still appears in several bands (**Table 35**). The glycosylated forms exhibited a high variation in size and signal strength, influenced by bafilomycin treatment, starvation and inhibition of shedding. Starvation increased the glycosylated band, making it smearier and more diffuse. Bafilomycin introduced an entirely new, strong band below 100 kDa. The existence of several bands suggested extensive co- or post-translational modification. Extensive N-glycosylation has been reported for Gpnmb [80]. Strikingly, there are still at least two bands present after removing N-linked glycans. This was confirmed in other cell types [74]. So far, alternative splicing has been reported only for human GPNMB [89, 90], rendering this option as an explanation for the two bands of mouse-derived Gpnmb used in this study unlikely.

Table 35: Summary of the variety of specific Gpnmb bands repeatedly appearing in Western blot.

WB bands	Size	Glycosylation	Characteristic
Large	100 - 150 kDa	Yes	Highly variable
Middle	Below 100 kDa	Yes	Strongly induced by bafilomycin
Small	Two bands above and below 75 kDa	No	-

Also in other studies, countless possibilities were detected with Gpnmb signal varying in shape, size and number. Not only between studies but even within one and the same study, a high variability of Gpnmb bands was reported dependent on cell types, tissue and treatments [74, 109]. Assigning the bands a certain function was difficult, both in this and in other studies. Nevertheless, the bigger form of the two bands is mostly considered as the mature glycosylated form compared to the premature full-length form that runs below [80, 88]. Pulse-chasing melanoma cells, the lower band at ~100 kDa appeared first, followed by the mature form at ~110 kDa one hour later [80]. This is also cell type-dependent, as in melanocytes, both forms are present from the beginning. Both degrade quickly within a few hours [80].

7.1.2. Glycosylation

Whereas multiple sizes were detected often [80], we detected a gradual increase in Gpnmb size upon starvation and GM6001 treatment that has not been reported so far. GM6001 is a broad-spectrum inhibitor of Mmps that inhibits Gpnmb shedding [80, 92, 171]. GM6001-induced increase is exclusively due to N-glycosylation while starvation-induced Gpnmb still exhibited other modifications. Additionally, starvation did not increase shedding of Gpnmb, suggesting ubiquitination or other modifications that still need to be identified. So far, Gpnmb was not studied in the context of starvation. Glycosylation due to GM6001 treatment in B16-F10 cells is likely cell-specific as treating mouse myoblastic C_2C_{12} cells with GM6001 led to a reduced signal but not to a change in size [92]. Even in a pulse-chase experiment where the synthesis and degradation can be clearly seen, a gradual increase in size within the life cycle of Gpnmb was not detected [80].

Glycosylation altering Gpnmb signal in a cell type- and time-dependent manner has been reported often before [74, 78]. Most reports are in line with our findings, detecting Gpnmb stripped of N-glycans in several bands at ~66-68 and ~70-80 kDa [74, 78, 80, 90, 92]. An *in vitro* cell-free translation of mouse *Gpnmb* cDNA resulted in one band around 70-75 kDa [80].

Glycosylation does not occur *in vitro*, so this is likely to be the native size of Gpnmb. Surprisingly, in cell lysates, several bands above and below were visible but not at the same height as the *in vitro*-translated band, suggesting that this band is not existent in physiological cell states [80]. Interestingly, tunicamycin, an agent blocking the first step of glycoprotein synthesis, decreased intensity of the signal but not the size [93]. Impaired glycosylation might in this case lead to rapid proteasomal degradation of Gpnmb [184].

N-linked oligosaccharides are attached to asparagine residues within a consensus sequence of the core protein. O-linked oligosaccharides on the other hand are attached to any serine or threonine residue within the peptide chain, making it more difficult to predict the modification site. One study removed O-linked glycans from Gpnmb, reducing the size to a similar level as after removing N-linked glycans [93]. Combining both treatments, the size of Gpnmb dropped to 90 kDa. Here unfortunately, the size of de-glycosylated Gpnmb deviated from other studies that observed a drop to 60-80 kDa when removing solely N-glycans. Additionally, not several bands were detected in each condition but only one distinct band in the upper molecular weight zone. Thus, it is difficult to predict, if the two unglycosylated isoforms we detected differ only in O-linked glycans or consist of other modifications as well.

Beyond N- and O-linked glycans, glycosaminoglycans are sometimes considered as a third group of glycosylation. The main categories of glycosaminoglycans are heparin/heparan sulfate, chondroitin sulfate/dermatan sulfate, keratan sulfate and hyaluronic acid. Glycosaminoglycans are mostly attached to an exposed serine of the protein core, resulting in the formation of a proteoglycan [313]. Gpnmb has a chondroitin sulfate [314] and heparin-binding motif. Thereby, it may bind cells or promote cell adhesion by recognizing heparan sulfate proteoglycans [74, 94, 114, 122]. Both Gpnmb receptors, syndecan-4 and CD44, are heparan sulfate proteoglycans permanently and in some conditions, respectively [94, 95, 315]. The structure of heparan sulfate moieties on syndecan-4 determines the binding capacity of Gpnmb and its inhibitory effect on T cells [94]. Three glycosaminoglycan attachment sites are predicted for Gpnmb in the extracellular domain [79]. Thus, Gpnmb might not only recognize heparan sulfates of other proteoglycans, but be one itself. Gpnmb binding to receptors on osteoblasts, T cells, keratinocytes and endothelial cells is abrogated by addition of heparin [74, 78, 114, 122]. Thus, attaching glycosaminoglycans to Gpnmb might modulate binding of Gpnmb to its receptors and be one of the reasons why Gpnmb stably consists of two bands after de-N-glycosylation.

Comparing the literature on that topic with this work, glycosylation is highly plastic and likely indispensable for Gpnmb function. Still, no report was successful in determining when Gpnmb is glycosylated and what it means to the function of the protein.

7.1.3. Shedding

Shedding is the proteolytic removal of membrane protein ectodomains [316]. Although we could show an increased Gpnmb expression after TGFβ treatment, shedding was reduced compared to untreated cells. In contrast, pro-inflammatory macrophages stimulated with LPS and IFNγ showed unaltered Gpnmb expression but doubled Gpnmb shedding, indicating an endocrine function of Gpnmb under pro-inflammatory conditions. This might infer a negative regulation of inflammatory responses, as it was proposed before [134]. It was reported before that Gpnmb shedding does not correlate with Gpnmb expression, indicating that Gpnmb shedding is tightly regulated independently of its expression [124, 156, 221].

Soluble Gpnmb released into the cell culture medium was detected at the same height as Gpnmb of respective whole cell lysates. This suggests that Gpnmb was shed close to its transmembrane domain with the bulk of its protein intact. Thus, bafilomycin, compared to basal conditions, might increase shedding rate of the same shedding site. The sizes of soluble fragments we detected are consistent with reported sizes between 90 and 115 kDa [80, 92, 93, 124, 184, 312]. There are several bands of shed Gpnmb, suggesting shedding at different sites [124]. Three potential cleavage sites of rat Gpnmb were observed [312]. Sheddases so far identified are ADAM10 [92, 118, 124], furin-like proteases [123] and possibly ADAM8 [118]. Moreover, Hoashi *et al.* postulated that shedding is mostly restricted to Gpnmb on the plasma membrane [80].

There are several reasons why we suspected that Gpnmb could be also shed in intracellular vesicles that are released upon a stimulus. (1) Observing that GM6001, inhibiting shedding of Gpnmb, led to an increased glycosylation of Gpnmb, suggested accumulation of glycosylated Gpnmb that is prone to be shed. Indeed, Hoashi *et al.* proposed that only the late-Golgi modified mature form of Gpnmb is shed but not the unmodified one, even if both are transported to the cell membrane [80], indicating that glycosylation is a crucial factor for regulation of shedding. Counterintuitively, the bigger, glycosylated form was more pronounced in the intracellular compartment compared to the plasma membrane fraction [74]. (2) Apart from the 50-70 kDa fragment that was identified exclusively in microglia [123], shedding majorly produced a fragment that has either the same size as the one in the cell lysate (110 kDa or 115kDa) [80, 93] or a slightly smaller one [171, 312]. Finding the same fragment in cell lysates and in medium suggests shedding already inside the cell in vesicles. (3) Pmel17 with a high similarity to Gpnmb is heavily glycosylated in the Golgi, localizes to Lamp1-positive vesicles, is upregulated by bafilomycin and cleaved within vesicles [317]. We suspected that cathepsin B might shed Gpnmb within lysosomes because of the interaction found by mass spectrometry. However, our hypothesis of cathepsin B as the sheddase of Gpnmb turned out wrong.

7.1.4. Bafilomycin effect on Gpnmb

We detected a unique effect of bafilomycin on Gpnmb expression, size and shedding. Other inhibitors had effects that were less pronounced and not significant.

Concanamycin A, which binds and inhibits V-ATPase directly like bafilomycin [318], induced *Gpnmb* transcript to a level half of that induced by bafilomycin and chloroquine [170]. The latter neutralizes the low pH of acidic organelles without targeting the V-ATPase [272], suggesting that the effect of bafilomycin on Gpnmb expression is not V-ATPase-dependent but due to general lysosomal stress [170]. Lysosomal stress was reported several times to be a crucial factor for Gpnmb expression [170, 171, 197, 216, 250]. Still, studying bafilomycin reveals alternative, relatively simple explanations for bafilomycin-mediated Gpnmb upregulation, shedding and degradation besides lysosomal stress. Before going into depth about those, the mechanism of action of bafilomycin will first be explained.

7.1.4.1. Bafilomycin in detail

Bafilomycin is a selective inhibitor of V-ATPases [271]. As a result, intra-vacuolar pH is raised, cytosolic pH is reduced and fusion of autophagosomes and lysosomes is inhibited reversibly and thus, autophagosomes accumulate [270]. Several effects have been found in addition to autophagy-related actions. Bafilomycin is able to reduce the release of pro-inflammatory cytokines [319] and promote receptor-mediated endocytosis [320]. Bafilomycin but not concanamycin A, another inhibitor of V-ATPases, activates glycolysis and reduces oxidative

phosphorylation [321]. Furthermore, apoptosis and DNA fragmentation and thus cell cycle arrest is induced by bafilomycin [321, 322]. We could observe this effect of bafilomycin on apoptosis as well. Moreover, bafilomycin was reported to function as a potassium ionophore and uncouple mitochondrial potential [323], which, compared to lysosomal inhibition, might rather be the reason for apoptosis induction [321]. Indeed, bafilomycin-induced apoptosis was independent of pH or inhibition of V-ATPase [324]. This predominant view was revised again and malfunctioning mitochondria were reported to be a consequence of autophagy failure induced by both bafilomycin and chloroquine [325].

7.1.4.2. Bafilomycin-mediated upregulation of Gpnmb

Interestingly, bafilomycin is able to promote both cell differentiation and apoptosis [324]. The authors speculated that either bafilomycin is not as specific as assumed and targets other structures such as tyrosine kinases, or the V-ATPase has other functions apart from acidifying vacuoles. Bafilomycin was able to differentiate M1 cells into a macrophage-like phagocytic cells independently of lysosomal pH [322]. Bafilomycin induced apoptosis via induction of p53 and Beclin1 [320, 326]. p53, too, can induce both apoptosis and macrophage differentiation [327, 328]. As discussed later, Gpnmb is majorly influenced by differentiation (chapter 7.2.2.1) and might react to pro-differentiating signals of bafilomycin mediated by the eight p53 binding sites upstream of the *Gpnmb* gene [164, 165]. Probably due to its growth-inhibitory function, bafilomycin promotes differentiation only in cells not requiring proliferation [322]. This is true for primary macrophages [329], which makes our observation of increasing proliferation after bafilomycin treatment quite unexpected, as mentioned above.

7.1.4.3. Bafilomycin-mediated shedding of Gpnmb

With a 10-fold increase, bafilomycin influenced Gpnmb shedding to a higher degree than Gpnmb expression, which was increased only 4-fold. Therefore, shedding might underlie a different aspect of bafilomycin action.

Bafilomycin increases free intracellular calcium both by increasing vacuolar pH and thus assimilating intra- and extravacuolar potential [321] and indirectly via p53 [320, 326, 327]. p53 promotes the release of calcium from ER that targets mitochondria, inducing apoptosis [327, 330]. Gpnmb ectodomain shedding is regulated by protein kinase C (PKC) and intracellular calcium signaling pathways [80]. Sheddases are generally known to be upregulated by phorbol esters [121]. PMA is a phorbol ester and imitates diacylglycerol, an activator of PKC. Substances like PMA enhance Gpnmb shedding and the PKC inhibitor staurosporine nullified this enhancing effect of PMA on Gpnmb shedding [80]. So, in combination with bafilomycin it could be used to test this hypothesis. In line with that, staurosporine alone did not elevate the levels of soluble Gpnmb in the medium (**Figure 23**), hinting that PKC and calcium levels might indeed be relevant for Gpnmb shedding. On the other hand, thapsigargin blocks the Ca^{2+}-ATPase from ER and raises cytosolic calcium levels [331]. Thapsigargin was inlcuded in the organelle stressor panel in this study as well, however no increased shedding of Gpnmb was detected. Interestingly, alkalinization of cytosolic pH was needed in addition to promote exocytosis [331], thus both elevated pH plus calcium levels might be necessary to initiate Gpnmb shedding mechanism.

Taken together, bafilomycin-mediated Gpnmb expression is either induced via MITF and lysosomal stress [170], or by the pro-differentiation and apoptosis signal of bafilomycin that is mediated by p53. Cytosolic calcium resulting from altered intracellular potential and the pro-apoptotic signal of bafilomycin might be responsible for Gpnmb shedding.

7.1.4.4. Chloroquine effect

After bafilomycin treatment, *Gpnmb* transcript levels increased 4-fold after 48 h, Gpnmb protein levels increased 7-fold after 24 h and Gpnmb shedding increased 10-fold after 48 h. In contrast, Gpnmb shedding was only doubled with treatment of chloroquine.

If the abovementioned interaction of Gpnmb and bafilomycin was true, we should have seen comparable effects with other lysosomal stressors such as chloroquine, leupeptin and 3-MA. In contrast to this study, other reports detected an equal effect of lysosomal inhibitors on Gpnmb expression. Both bafilomycin and chloroquine led to a 40-fold increase in RNA level after 24 h in RAW macrophages [170]. Gabriel *et al.* used a higher concentration of both substances but shorter time (50 nM bafilomycin and 40 µM of chloroquine for 24 h). Either 20 µM of chloroquine that we used in our study was not sufficient to highly induce Gpnmb or primary macrophages react differently. Probably both is true: Concentrations should be titrated to a similar inhibitory effect in future studies. Regarding cell type, we observed a higher toxicity of bafilomycin on cell lines B16-F10 and NIH-3T3 cells compared to primary macrophages. Bafilomycin concentration had to be reduced for the treatment of cell lines. Therefore, the cell line RAW might react differently to lysosomal inhibitors as well, which results in a higher sensitivity of Gpnmb expression due to chloroquine treatment.

7.1.4.5. Bafilomycin-mediated glycosylation of Gpnmb

Western blot signals suggested that bafilomycin induced a special glycosylation of Gpnmb. The specific bafilomycin-induced size of Gpnmb below 100 kDa is larger than the unglycosylated and smaller than the usual glycosylated forms. Even after removing the N-glycans, bafilomycin-induced Gpnmb still exhibited different protein sizes than basally expressed Gpnmb. Thus, Gpnmb either contained other modifications such as O-linked glycans or specific trimming of the attached glycans occurred. In both ER and Golgi, extensive trimming followed by re-glycosylation occurs until transmembrane proteins are finally released [332]. Additionally, exoglycosidases such as α-fucosidase are localized in lysosomes and removes fucose from N-linked glycans, which is associated with senescent cells [333].

Another possibility is that bafilomycin-induced upregulation of Gpnmb is accompanied by increased misfolding. Both calnexin and calreticulin binding to Gpnmb were promoted after bafilomycin treatment as we detected by mass spectrometry. Moreover, the bafilomycin-specific Gpnmb band in Western blot also accumulates in other conditions when the proteasome is blocked, suggesting a version that is tagged for degradation. Gpnmb, upregulated after bafilomycin treatment, might require extensive chaperone support and is otherwise degraded with an ER-assisted degradation system, which involves cytosolic ubiquitination followed by proteasomal degradation [332]. Bafilomycin blocks V-ATPases that localize and acidify Golgi, endosomes and lysosomes [334, 335]. Thus, by increasing pH in Golgi, bafilomycin might impair the glycosylation process, resulting in insufficient glycosylated Gpnmb. In fact, bafilomycin affects Golgi trafficking [336] and thereby potentially Gpnmb processing. Gpnmb upregulation may therefore result in a non-functional protein, which could explain why we could not detect a salient effect.

7.1.4.6. Bafilomycin-mediated turn-over of Gpnmb

Bafilomycin increased expression, shedding and degradation of Gpnmb, thus the whole life cycle was accelerated. However, proteasomal degradation that we detected upon bafilomycin

treatment was most likely a consequence of more abundant protein, not because of specifically induced degradation. Inhibiting proteasomal degradation with MG132 led to the accumulation of the bafilomycin-specific Gpnmb band just below 100 kDa in untreated and starved cells as well. This suggests ubiquitination of Gpnmb even in steady state, implying a quick turn-over of Gpnmb. Proteasomal inhibition could also direct the degradation pathway towards lysosomal degradation, thus leading to lysosomal Gpnmb accumulation, a condition comparable with bafilomycin treatment. However, another proteasome inhibitor, epoxomicin, led to a time-dependent decrease of Gpnmb level but not to a change in size [92].

A fast turn-over of several hours was observed before [80]. After inhibition of protein synthesis for 1 h, detection of Gpnmb is nearly impossible [171]. The argument that lysosomal inhibitors make Gpnmb more visible simply because of Gpnmb accumulation in lysosomes [171] can be opposed by induction of Gpnmb expression upon bafilomycin treatment. Surprisingly, the strongest cellular Gpnmb signal remained at Golgi even after extended bafilomycin treatment, opposed to the expected re-location to peripheral vesicles. On the other hand, even V-ATPase itself accumulates in Golgi after bafilomycin treatment [337] and Gpnmb can interact with the V-ATPase as we detected by mass spectrometry (chapter 7.6.1), rendering Gpnmb in the Golgi reasonable.

By using bafilomycin and a proteasomal inhibitor, two degradation pathways were blocked which ought to lead to maximum Gpnmb accumulation. However, the toxicity of the substances prohibited extended exposure. Co-immunoprecipitation of ubiquitinated proteins failed to show Gpnmb bands with other treatments than bafilomycin (data not shown). The reason is likely the degree, to which exclusively bafilomycin induced Gpnmb protein levels when administered for a minimum of 24 h.

Taken together, similarly to the effect we see with polarized macrophages, bafilomycin-mediated Gpnmb expression is more salient than its function. Bafilomycin increased both half-life and turn-over of Gpnmb. Comparing different drugs and cell types is obviously necessary to reveal mechanisms of Gpnmb function. Combining treatment of different inhibitors of both protein synthesis and degradation could be applied in future studies to examine the exact turn-over of Gpnmb.

7.2. Cellular Functions

Observing a highly plastic Gpnmb expression, it was of interest if this expression has consequences for the cell. The two main macrophage function phagocytosis and inflammatory polarization were examined.

7.2.1. Phagocytosis and autophagy

Phagocytosis and autophagy are two processes that are closely intertwined as autophagy, the process of degradation of intracellular organelles, is necessary for the degradation of endocytosed particles [338]. Gpnmb was associated with uptake, phagocytosis and degradation of particles because of its presence in lysosomal/endosomal vesicles [72, 78, 80, 80, 130, 137].

7.2.1.1. Phagocytosis

We could not detect an impairment of uptake and degradation of bacterial and yeast particles in primary macrophages lacking Gpnmb. It is possible that general phagocytosis remained unaffected because Gpnmb action is only required in specific tasks. For example, Gpnmb was shown to bind the dermatophytic fungus *Trichophyton rubrum* with high affinity but not *E. coli, Candidal pseudohyphae, Staphylococcus aureus*, group A streptococci or *Pseudomonas aeruginosa* [85], suggesting a specific interaction and explaining why we did not see an impairment of *E. coli* particles in *Gpnmb*-deficient macrophages. This pathogen interaction was furthermore influenced by the glycosylation state of Gpnmb [85]. In our experiments, glycosylation of Gpnmb was highly plastic and differed in each condition; therefore it might not have been in an adequate glycosylation state for binding the particles that were examined.

Binding a pathogen is just the first step in phagocytosis. Gpnmb was furthermore observed to facilitate phagocytosis of apoptotic particles and FITC-microspheres [137, 176]. In detail, Gpnmb was proposed to be necessary for recruitment of the autophagy protein LC3 to the phagosome and for its fusion to the lysosome [137]. Here, Gpnmb specifically enhanced the formation of phagosome rings that were LC3-positive when treating cells with apoptotic bodies and zymosan yeast particles. Our data on the other hand suggest that general degradation of zymosan yeast particles can nevertheless progress.

7.2.1.2. Autophagy

Regular autophagy remained unaffected by the absence of Gpnmb. This is surprising because we observed an upregulation of Gpnmb upon bafilomycin treatment, which inhibits the last step of autophagy and lysosomal degradation [339]. Upregulation of Gpnmb after treatment with other lysosomal inhibitors or autophagy inducers such as chloroquine, concanamycin A and torin1 was reported [170]. Interestingly, the mTOR inhibitor rapamycin did not induce Gpnmb in melanoma cells [171], in RAW macrophages [170], nor in our experiments in BMDMs. However, one study found a decline in Gpnmb expression after rapamycin treatment but only in cells that were characteristic of high mTOR activation [340]. It is a well-known characteristic of rapamycin that different cell types exhibit highly variable sensitivity [276].

Downregulation of mTOR led to an upregulation of Gpnmb in a MITF-dependent manner [170]. MITF regulates starvation-induced autophagy and binds the promoters of lysosomal and autophagosomal genes [341]. Although MITF was reported to induce Gpnmb [132, 138, 147, 160, 170], we did not find increased Gpnmb expression in response to starvation. Our data suggest that the stimulus responsible for Gpnmb induction might not have to be related to the consequential action of Gpnmb. In fact, although Gpnmb expression reacts to mTOR and lysosomal inhibition, Gpnmb is not directly associated with autophagy [170, 197]. This is further supported by the observation that Gpnmb expression had no impact on lysosomal gene expression and biogenesis [160]. Thus, the potential function of Gpnmb in lysosomes remains elusive.

7.2.2. Polarization

Another feature of macrophages is their pro- or anti-inflammatory potential, which is relevant in different phases of an infection. A slight anti-inflammtory effect of Gpnmb on polarization was detected. Interestingly, the most important finding of the polarization experiment was not related to inflammation.

7.2.2.1. Maturation effect

The most striking finding of the polarization experiment was the impact of timing on Gpnmb expression. The biggest difference in Gpnmb expression occurred basally between 4 and 24 h, thus between day six and seven *in vitro*. Gpnmb transcript increased more than 100-fold, likely resulting from maturation and ageing. In comparison, TGFβ led to a roughly 2-fold and bafilomycin to a 4-fold induction of Gpnmb expression. Gpnmb was described before to be induced in differentiated cells [77, 134, 137, 145] and was thus proposed as a maturation marker [77, 134]. BMDMs are thought to be mature after 5-7 days exposure to M-CSF [329]. Thus, Gpnmb levels in a typical 48 h experiment is heavily influenced by time and thus ageing, rendering vehicle controls necessary for each time point. For example, Tajima *et al.* conducted 48 h experiments and observed an upregulation of Gpnmb when applying ERK and AKT inhibitors without providing a vehicle control for each time point [186]. These results should be carefully evaluated assuming a default increase of Gpnmb expression with time.

Gpnmb expression reached a plateau at 24 h/day 7 *in vitro* and remained elevated at 48 h/day 8 where the cells did not look morphologically healthy anymore. The question remains, if Gpnmb upregulation was due to maturation, age, senescence or apoptosis. *In vivo*, macrophages are long-living immune cells and survive for months to years [342]. Therefore, macrophages depend on proteins upregulated in later cellular life. In humans, GPNMB expression emerges in elderly and was listed as part of a frailty biomarker panel [213], suggesting functions of Gpnmb in matured or senescent cells. Interestingly, polarization of tissue macrophages and response to stimuli is altered in elderly compared to young individuals [343], which could be partly due to upregulated Gpnmb expression.

Another hint for a crucial upregulation of Gpnmb on day seven *in vitro* is the difference between *Gpnmb*-knockout cells and wildtype controls. The one base deletion in genomic *Gpnmb* is theoretically not affecting transcription and results in a nonsense protein due to the frame shift. Indeed, *Gpnmb* transcript could be detected in cells derived from *Gpnmb*-knockout animals. Polarizing cells for 4 h, the panel of stimulants induced the exact same pattern of *Gpnmb* expression in wildtype and *Gpnmb*-knockout macrophages. However, 24 h later, *Gpnmb* was more than 100-fold induced in wildtype macrophages whereas *Gpnmb*-deficient cells kept a comparably low expression. *Gpnmb* transcript was obviously more controlled at later time points. Further induction of mRNA expression might have been prevented by nonsense-mediated decay, the mechanism that degrades *Gpnmb* mRNA in DBA/2J mice as well [135, 265]. This suggests a specific upregulation of Gpnmb in mature macrophages.

7.2.2.2. TGFβ induced Gpnmb

Apart from the upregulation of Gpnmb due to maturation, Gpnmb expression did further react to stimulants. So far, literature gives a very inconclusive picture of Gpnmb upregulation due to different cytokines (chapter 1.2.15.2). This work showed a 2-fold upregulation of Gpnmb by TGFβ on mRNA and protein level. Such an upregulation was not detected using other pro- or anti-inflammatory stimulants for 24 or 48 h, confirming the findings of Chung *et al.* [89].

TGFβ is an important cytokine regulating a multitude of cellular processes such as cell growth, cell proliferation, differentiation, and apoptosis and has been associated with diseases associated to ageing [213, 344]. TGFβ recruits macrophages and neutrophils and leads to the deposition of extracellular matrix, contributing to fibrosis [345]. However, this versatile cytokine can both fuel and depress immune responses.

M2c macrophage polarization, induced by TGFβ, is specialized on clearing apoptotic cells [346], a finding that has already been associated with Gpnmb [137]. Gpnmb was described as a "TGF-β family of transmembrane glycoprotein" [347]. *In vivo*, Gpnmb was detected as a target of the oncogene MAFK, a downstream molecule of TGFβ signaling [87]. Another inducer of M2c polarization, IL-10, was shown to strongly induce Gpnmb in human dendritic cells [149, 150]. In line with our data, Gpnmb protein was not detected at early time points (24 h) of this polarization but increased strongly with time. Additionally, IL-10 promoted cell surface presentation of Gpnmb [150], suggesting increased shedding. We found reduced shedding in TGFβ conditions, illustrating the difference of the two M2c-inducers TGFβ and IL-10. On the other hand, even shedding of cell surface Gpnmb is tightly regulated [124, 156, 221]. We could not detect effects of Gpnmb on apoptosis or cell survival upon TGFβ treatment. The effect on gene expression remained mild. To find the potential role of Gpnmb in M2c-polarized macrophages, we conducted interaction proteomics of TGFβ-treated macrophages (**Table 36**). However, in comparison to bafilomycin-treated macrophages, the interaction partners revealed no salient role of Gpnmb in TGFβ-treated cells.

7.2.2.3. Effect of Gpnmb on polarized macrophages

Gpnmb was often proposed as an anti-inflammatory protein and in general, this work can confirm these anti-inflammatory properties of Gpnmb. Still, many marker genes showed no alteration in the absence of Gpnmb. Concluding, Gpnmb exerts only a mild impact on the polarization of macrophages.

An explanation is a potential fine-tuning by Gpnmb rather than it being a major factor of polarization. The influence might only be detectable in a very severe or long-term disease or *in vitro*, in a specific setting of pre-stimulation. Cytokines used in combination can have fundamentally different effects [346]. An illustration thereof is the absence of altered Gpnmb localization upon activation with pro-inflammatory molecules IFNγ and LPS individually; whereas specifically priming overnight with IFNγ and sequential LPS treatment led to an enormous relocation to small vesicles around the nucleus [134]. This shows that Gpnmb adapts its location very specifically to the cellular context and is tightly regulated.

Summarizing the studies on cellular functions, Gpnmb did not influence autophagy, phagocytosis, apoptosis and survival as well as polarization only to a minor level. However, Gpnmb expression, glycosylation and shedding reacted strongly to polarization, stimulation by bafilomycin and differentiation. The latter might have a so far neglected role in Gpnmb studies.

7.3. Atherosclerosis

Atherosclerosis was one of the two examined disease models to study Gpnmb function. We induced atherosclerosis by using *ApoE*-knockout mice and feeding them a high cholesterol diet (HCD) for several weeks. In contrast to obesity, we found no salient phenotype in *Gpnmb*-knockout animals.

7.3.1. Blood lipid parameters

Blood lipid levels did not reveal an impact of Gpnmb after atherogenic diet. LDL levels were about 50 times higher in ApoE-deficient females after HCD than in obese wildtype males after high fat diet (HFD), highlighting the impact of atherogenic food and genotype. However, no

impact of Gpnmb on blood lipid levels could be observed in either diet. Katayama *et al.* observed that Gpnmb significantly reduced cholesterol and LDL levels in HFD-induced obesity, suggesting a role of Gpnmb in atherosclerosis [109]. In their study, the cholesterol and LDL blood levels were induced about 2-3 times higher [109] than we see with our obesity-inducing HFD. This indicates that only elevated blood lipid levels are able to reveal an effect of Gpnmb. However, our atherogenic diet highly elevated cholesterol blood levels without being affected by the absence of Gpnmb, refuting this argument. Moreover, overexpression of Gpnmb had no beneficial effect on blood lipid levels [109]. In contrast, Gpnmb overexpression in rats fed a choline-deficient diet increased cholesterol levels compared to wildtype animals, opposing Katayama *et al.*'s murine data [173]. Those contrary published data together with the findings of unaltered blood lipid levels in atherosclerotic and obese mice of this study renders an impact of Gpnmb on blood lipids rather unlikely.

7.3.2. Lesion development

The equal levels of atherogenic lipids already hinted that Gpnmb might play a minor role in the aortic plaque development. Indeed, whole aorta plaque staining revealed lesion sizes unaffected by the absence of Gpnmb. Measurements of aortic root sections showed similar results. *En face* preparations of aorta were renounced because plaques were not covering the whole aorta, and the probability of undiscovered lesions was low.

Still, Gpnmb was highly expressed in foam cells, which represented the major cell type of Gpnmb-expressing cells in atherosclerotic lesions. Gpnmb was found in foam or lipid-loaded macrophages before, corroborating its relevance in this cell type [137, 148, 170, 197]. Interestingly, we observed that not all foam cells expressed Gpnmb. Thus, it is likely that Gpnmb is relevant only for a specific subtype of plaque-associated macrophages. Observing *in vitro* that reparative macrophages are the main source of Gpnmb expression (chapter 6.1.1), this might be the case *in vivo* as well. It was previously described that only a subtype of macrophages express Gpnmb in other diseases or tissues [123, 133, 179], however its function remained elusive.

Gpnmb may rather be associated with plaque rupture than with plaque formation because plaque size was not altered in this study. For plaque rupture, the development of a fibrous cap is crucial. Examining fibrosis with Sirius red staining of aortic root sections, we detected a trend of Gpnmb ameliorating fibrotic deposition in lesions, possibly via secretion of Mmps. Gpnmb-induced Mmp expression [175] might lead to degradation of extracellular tissue that weakens the plaque and increases the risk of rupture [71]. Thus, Gpnmb would be rather a detrimental factor in this disease. However, this requires further research involving other cell or animal models than mice, which are naturally protected against plaque rupture [348].

7.4. Obesity

7.4.1. The hypothesis

Diet-induced obesity revealed three major effects of Gpnmb in different tissues: (1) liver-associated amelioration of fibrosis, (2) adipose tissue-associated reduction of macrophage content and (3) a global decrease in insulin resistance. Those alterations can be caused either independently by Gpnmb or dependent on each other. The most likely explanation is that Gpnmb contributes to a healthy inflammatory balance in adipose tissue and delays obesity-associated

inflammation and concomitant adipose tissue insulin resistance. This in turn retains insulin sensitivity of other organs, maintaining liver function. In contrast, a deleterious cycle occurs in *Gpnmb*-knockout animals. More and more pro-inflammatory macrophages accelerate the detrimental metabolic switch in adipose tissue, impairing insulin sensitivity. The resulting higher blood glucose levels enhance insulin resistance and lipid production in liver. Hepatic lipids stored in intracellular vesicles impair liver function leading to elevated ALT levels in plasma. Several rationales are in favor of this hypothesis and are listed in the following paragraphs.

7.4.2. Gpnmb in adipose tissue macrophages

The first argument for the hypothesis concerns both Gpnmb and macrophage marker expression in different tissues. First, liver Gpnmb expression was hardly detectable by Western blot and immunohistochemistry (data not shown), whereas in adipose tissue, Gpnmb is strongly expressed by macrophages. Second, staining of adipose tissue revealed more macrophages in obese *Gpnmb*-deficient mice, whereas no difference could be found in transcript levels of macrophage markers in liver, muscle and brain of obese mice. In line with this, atherosclerotic mice showed no salient phenotype except a higher macrophage marker expression with more IL-6 cytokine production in white adipose tissue, corroborating a role of Gpnmb in alleviating adipose tissue inflammation.

Adipose tissue macrophages contribute to lipid trafficking by activating their lysosomal metabolism upon obesity [24]. Macrophages buffer surrounding cells from lipotoxic effects by taking up and catabolizing excess lipids [24]. With increased adiposity, lysosomal degradation is inhibited and thus lipid accumulation increases to reduce the amount of free lipids [24]. Surprisingly, a recent study reported that autophagy is dispensable for the function of adipose tissue macrophages and lipids are transported to lysosomes in a pathway independent of autophagy [24, 349]. We observed that Gpnmb is upregulated *in vitro* by bafilomycin without affecting autophagy. This further supports the hypothesis that Gpnmb is upregulated in adipose tissue macrophages due to lysosomal stress with a function distinct from autophagy.

Therefore, the function of Gpnmb might be associated with recruitment of macrophages or with inflammation of adipose tissue. Both are possible and outlined in the following.

7.4.2.1. Gpnmb recruits macrophages

In leanness, macrophages in adipose tissue are homogenously distributed, isolated and widely dispersed between adipocytes, but form macrophage aggregates in obese mice [15]. Those aggregates are called crown-like structures (CLS) and resemble macrophage syncytia characteristic of other chronic inflammatory diseases such as rheumatoid arthritis. Gpnmb prevented the formation of CLS around adipocytes in this study. Although it was reported that adipocyte size and CLS density correlate [15, 288], *Gpnmb*-knockout and wildtype strains differed significantly in CLS density but not in adipocyte size, suggesting an impact of Gpnmb on macrophage attraction rather than adipocyte metabolism. Macrophages in CLSs surround apoptotic adipocytes [15] suggesting an the influence of Gpnmb on apoptosis. However, at least in macrophage cell culture, Gpnmb did not influence apoptosis.

A higher macrophage content in *Gpnmb*-knockout mice suggests that Gpnmb reduced the macrophage infiltration into adipose tissue. Paradoxically, Gpnmb was so far rather associated with attraction of macrophages. In disease-associated macrophages, Gpnmb correlated in

Alzheimer disease with *Ccl2* and in obesity with *osteopontin* expression, genes relevant for monocyte attraction [148, 170]. Gpnmb-containing tumors recruited more macrophages [83]. Gpnmb expression, although basically highly induced in wounds, is suppressed in genetically induced diabetes (*db/db*) [200]. Despite reduced expression, it improved wound healing compared to *Gpnmb*-deficient mice by recruiting mesenchymal stem cells and enhancing trafficking of M2 macrophages [200]. Macrophage markers were positively correlated with Gpnmb expression in murine adipose tissue [170]. This suggests a positive effect of Gpnmb on the recruitment of macrophages to adipose tissue. Katayama *et al.* were the first to examine this using *Gpnmb*-knockout mice and ruled out a severe impact of Gpnmb on adipose tissue inflammation in obese mice [109], contradicting our hypothesis. A comparison to this study is described in detail in chapter 7.4.4. Those observations speak against a role in recruitment of macrophages. Alleviating inflammation is therefore another mechanism to reduce the macrophage content of adipose tissue.

7.4.2.2. Gpnmb influences the inflammatory environment in adipose tissue

Gpnmb's alleviating role in adipose tissue inflammation fits to most of the literature. However, in our *in vitro* experiments, Gpnmb had only a very mild influence on polarization of macrophages. This anti-inflammatory effect is probably not strong enough to explain the strong reducing effect of Gpnmb on macrophage content in obese animals. Interestingly, a recent publication reveals that the metabolic change of adipose tissue might be caused less by an often reported M1/M2 switch of adipose tissue macrophages, but by the pure number of recruited macrophages upon obesity [24]. One fold of recruited immune cells is associated with a 10-fold increase in TNFα, meaning that every immune cell exponentially influences the inflammatory environment. Thus, the actual degree of inflammation can be higher than the number of recruited immune cells. Phenotyping the macrophage population of adipose tissue revealed that Gpnmb expression is 200-fold induced in obesity-associated adipose tissue macrophages compared to lean mice and, strikingly, equally in M1 and M2 macrophages [350]. This suggests that the observed impact of Gpnmb, increasing numbers of macrophages, is independent of M1/M2 polarization and sufficient to promote adipose tissue inflammation.

7.4.2.3. Gpnmb dampens inflammation via its receptors

Furthermore, Gpnmb might dampen adipose tissue inflammation by binding syndecan-4 on activated T cells and thus exerting a negative effect on inflammation. MDSCs, a cell type specifically expressing Gpnmb, play a beneficial role in type I diabetes in an immune-suppressive manner, possibly by promoting regulatory T cells [351]. Co-injection of inflammatory T cells with MDSCs could prevent diabetes and elevated TGFβ and IL-10 levels compared to injection of inflammatory T cells alone. Not much is known about the expression of syndecan-4 in adipose tissue or regarding insulin resistance. Only one study reports that syndecan-4 is expressed in muscle and adipose tissue and is upregulated after physical exercise [352].

It is already reported that Gpnmb binds to its second receptor CD44 on adipocytes [118]. This, contrary to our findings, increased the lipogenic program and insulin resistance. Gong *et al.* focused on extracellular Gpnmb, which might have other functions than macrophage-associated full-length Gpnmb. CD44 is actually known to be a stem cell marker [353]. However, CD44 expression was also detected in pro-inflammatory macrophages in adipose tissue [354] and was the top candidate implicated in the development of diabetes in rodent and human in an

expression-based genome-wide association study [355]. Its deficiency or blockage improved insulin resistance and adipose tissue inflammation. An anti-inflammatory role of Gpnmb on adipose tissue inflammation via pro-inflammatory CD44 would infer an inhibitory effect of Gpnmb on CD44. In fact, Gpnmb expressed by anti-inflammatory astrocytes attenuated neuroinflammation via CD44 expressed by pro-inflammatory astrocytes [98]. Hyaluronan, a component of extracellular matrix, is the major ligand of CD44 and this interaction is often associated with inflammation [356]. Gpnmb might prevent this interaction by binding CD44 and blocking migration of mesenchymal stem cells or monocytes that would otherwise develop into pro-inflammatory macrophages. This might explain why more macrophages are present in adipose tissue of *Gpnmb*-knockout mice.

7.4.3. Adipose tissue can induce insulin resistance

The second reason supporting the hypothesis that the symptoms of the obese *Gpnmb*-knockout mouse are caused mainly by a lack of Gpnmb in adipose tissue, are reports saying that adipose tissue alone is sufficient to cause global insulin resistance.

The animals of this study had similar body and fat weight, but only *Gpnmb*-knockout mice exhibited impaired insulin sensitivity. In line with this, selectively impaired glucose uptake in adipose tissue increased whole body insulin resistance without affecting adiposity [37, 357]. Although adipose tissue accounts little for global glucose uptake [358, 359], adipose tissue dysfunction is an important contributor to systemic insulin resistance via several mechanisms.

7.4.3.1. Inflammatory molecules

Adipose tissue as an endocrine organ can influence insulin sensitivity in muscle and liver physiology. In detail, several adipocyte-secreted molecules like leptin, adiponectin, resistin, fatty acids, TNFα, MCP-1, ApoE and glucocorticoids influence insulin resistance [360]. Furthermore, macrophages contribute to an immunological switch via cytokine expression such as *Tnfα, Il6, Nos2* [15–17, 288]. Thus, adipose tissue inflammation impacts on insulin sensitivity and secretion, food intake and energy expenditure as reviewed by Kahn in 2019 [36, 361].

7.4.3.2. PAHSAs

Another pathway of communication from adipose tissue to the liver is a special lipid called palmitic acid esters of hydroxystearic acids (PAHSAs). It has anti-diabetic and anti-inflammatory effects and ameliorates glucose homeostasis on different levels, mechanisms and organs [362–364]. For instance, it enhances insulin-stimulated glucose transport and boosts glucose-dependent insulin secretion of pancreatic islets. PAHSAs are made of palmitate, which can induce Gpnmb [170] and has anti-inflammatory properties, which fits to our findings of Gpnmb as an anti-inflammatory molecule in adipose tissue. However, it is not yet known whether PAHSAs induce Gpnmb expression.

7.4.3.3. Glucose transporters

Adipocyte Glut4 expression is crucial for adipose tissue homeostasis and reduced in starvation or obesity [365]. It induces Rbp4, which in turn promotes inflammation of surrounding cells [366–369], causing insulin resistance and glucose intolerance without affecting body weight [370].

We could not see a major influence of Gpnmb on expression of *Glut* isoforms after HFD. Liver *Glut4* expression was elevated in *Gpnmb*-knockout animals; however *Glut4* was expressed at very low levels in liver compared to muscle. Additionally, rather a *Glut* downregulation instead of an upregulation is characteristic to hyperglycemic adaptions [11, 140]. This renders this transporter as the main cause for delayed insulin action in *Gpnmb*-knockout animals unlikely. It was expected to see a downregulated *Glut4* expression in muscle, as this was often reported to be a major contributor of glucose uptake [11, 140, 371]. However, *Glut4* in muscle was only slightly reduced. On the other hand, muscle is a large tissue and minor changes have big consequences. Eventually, the rate of sugar uptake is regulated by the number of available cell surface Gluts.

We detected *in vitro* an interaction of Gpnmb to unconventional myosin-Ic (Myo1c), an actin-based motor protein, detected by mass spectrometry. Myo1c is responsible for Glut4 transport to the membrane [372]. Additionally, Myo1c was found together with Gpnmb in a proteomic approach looking for melanosome-associated genes [125]. Thus, disrupting Glut transport to the cell surface might be another way by which the lack of Gpnmb induces hyperglycemia. However, further characterization of adipose tissue is necessary to unravel the mechanism of Gpnmb in this tissue.

7.4.4. Effect size

Another argument in favor of the hypothesis that Gpnmb mainly influences adipose tissue macrophages, which is followed by insulin resistance and liver fibrosis is the magnitude of the effects we observe. The effect of Gpnmb absence was more pronounced in adipose tissue and in insulin resistance than in liver function readings. Statistically, the effects of Gpnmb on adipose tissue macrophages and insulin resistance were strongly significant whereas differences in liver values like phosphorylated AKT (pAKT) and ALT levels as well as fibrotic and lipogenic gene expression were barely significant. Nevertheless, the liver fibrosis results are corroborated by several other reports [109, 172, 173]. Others conclude as well that Gpnmb had a very mild effect on the development of steatosis [109]. Thus, this might be a true but secondary effect.

7.4.5. Involvement of pancreas

The previous four chapters listed arguments for a sole influence of Gpnmb on adipose tissue macrophages. However, there was one striking finding that questions this hypothesis. We detected elevated insulin plasma levels with normal glucose levels in female lean *Gpnmb*-knockout animals. This suggests the pancreas as the starting point. However, preliminary immunohistological stainings of this organ showed intact pancreatic β-islets in both strains. Gpnmb has not been connected to the pancreas so far. On the other hand, hyperinsulinemia can compensate hyperglycemia, thus Gpnmb reducing high blood sugar would be the starting point. Hyperglycemia however can be caused by many versatile factors like regulation of Glut expression (chapter 7.4.3.3).

7.4.6. Signaling of insulin resistance

7.4.6.1. Insulin resistance paradox

HFD does not necessarily increase fasted blood glucose levels in wildtype animals [373] an effect that was confirmed using our wildtype mice with fasted blood glucose levels around 180 mg/dL.

Apparently, these animals had mechanisms to prevent or delay insulin resistance that were disrupted in the absence of Gpnmb. Thus, the elevated Gpnmb plasma levels detected in patients with type II diabetes compared to patients with normal glucose tolerance might be a protective compensatory adaptation [109]. In line with that, treating insulin resistant mice with an inhibitor of glycosphingolipid synthesis lowered both Gpnmb expression and the degree of insulin resistance [250].

As a consequence of obesity, hepatic metabolic gene expression should be altered. Surprisingly, the hepatic transcript levels of genes involved in metabolism of glucose or glycogen were not changed between lean and obese mice, suggesting a post-transcriptional or –translational regulation. In contrast, obesity had an effect on genes involved in hepatic lipid metabolism. To put in simple, the lipolytic gene *Cpt1* increased from leanness to obesity, whereas lipogenic genes showed the opposite, a decrease from leanness to obesity. Grouping the three lipogenic genes *Scd1*, *Acc* and *Fasn* into one category, those three lipogenic genes decreased from leanness to obesity which is prevented in the absence of Gpnmb.

NC-fed *Gpnmb*-knockout animals were special because the respective cages developed rivalry fights. Thus, those mice were very lean and could not produce lipids, thus the expression of their lipogenic genes was half of their wildtype controls. Therefore, this group served maybe less as a control for lean *Gpnmb*-knockout mice but rather as positive control for a mouse that is largely deprived of fat, with low insulin levels and an activated immune system involved in wound healing.

Nevertheless, obese *Gpnmb*-knockout animals exhibited on the one hand insulin resistance and on the other hand high lipogenic transcript levels, which looks like a paradox. In fact, it is a well-known insulin resistance paradox, resulting in a fatal triad of hyperinsulinemia, hyperglycemia, and hypertriglyceridemia [29], which is explained in the following. The function of insulin in liver of healthy individuals is to store energy in form of glycogen and fatty acids. Therefore, insulin represses gluconeogenesis via Foxo1 but promotes lipogenesis via Srebp1c, Acc and Fasn [29]. In hepatic insulin resistance, insulin loses its suppressive function on gluconeogenesis, leading to elevated hepatic glucose production and plasma glucose levels as well as the need for more insulin [374]. Paradoxically, insulin does not lose its promoting function on the lipogenic pathway [29]. Thus, it still enhances fatty acid synthesis, leading to hepatic steatosis [29, 249]. An explanation for this paradox might be the concentrations of insulin required for the different effects [11]. Thus, the insulin resistance paradox is taking effect in *Gpnmb*-knockout animals. Unaffected by insulin resistance, lipogenesis was enhanced in *Gpnmb*-knockout animals and thus reflected elevated insulin levels. However, we did not observe elevated plasma lipid levels in *Gpnmb*-knockout animals. Apparently, hepatic lipids were not released but stored in hepatocytes, causing liver damage and fibrosis shown by ALT levels.

7.4.6.2. AKT signaling

AKT signaling is a crucial mediator of insulin signals. Gpnmb has been reported to induce and inhibit AKT phosphorylation and to be up- or downregulated upon AKT activation (chapter 1.2.14.2). We observed reversed pAKT levels of *Gpnmb*-knockout and wildtype animals in leanness and obesity. *Gpnmb*-knockout animals exhibited lower pAKT levels in leanness and higher pAKT levels in obesity compared to wildtype controls. The examined S473-pAKT phosphorylation site was positively associated with Gpnmb before [119, 185]. This confirms the findings of lean animals. In liver, insulin signals through S473-pAKT phosphorylation, resulting in elevated pAKT levels in obesity [249]. Unfortunately, the animals in both cages used as NC-fed

Gpnmb-knockout mice were fighting and exhibited wounds and very low body fat content. Thus, their insulin levels were accordingly low. It is likely that low pAKT levels of NC-fed *Gpnmb*-knockout mice are a reflection of their low insulin levels rather than deriving from the absence of Gpnmb. In contrast, only obese *Gpnmb*-knockout but not wildtype animals exhibited high insulin levels that were reflected in promoted phosphorylation levels of AKT explaining the inversed pAKT levels in obesity.

The two AKT phosphorylations at T308 and S473 are independent of each other, but both are required for full AKT activity [375]. The AKT phosphorylation at T308 was checked in this experiment but the antibody signal was qualitatively ambiguous. We did not observe an influence of Gpnmb or obesity on IRS1 phosphorylation levels. Nevertheless, Gpnmb might still signal via another phosphorylation site or another organ through IRS1 or 2 [11, 298]. Since we did not find alterations in IRS1 activation, Gpnmb might influence S473-pAKT via mTORC2 [308–310].

7.4.7. Comparison with related studies

The two studies experimentally related to this work [109, 118] overlap in some parts and contradict in others. Liver fibrosis, adipose tissue inflammation and insulin resistance are the factors that are either common or discrepant. Gong *et al.* observed contradicting data on the effect of Gpnmb on insulin resistance [118], however the design differed in several ways. We agree with Katayama *et al.* on the beneficial role of Gpnmb on liver fibrosis but disagree on its role in adipose tissue inflammation [109]. With finding a role of Gpnmb in ameliorating insulin resistance and adipose tissue inflammation, this study adds a third option to complete the picture.

7.4.7.1. Gong *et al.*

We observed Gpnmb as ameliorating agent in insulin resistance. However, this contradicts the main finding of Gong *et al.* [118]. Proposing Gpnmb as an upstream molecule of AKT and mTORC1, Gong *et al.* observed a enhancing effect of Gpnmb on insulin resistance and fatty acid accumulation in adipocytes [118]. Although proposed otherwise, Gpnmb inducing fatty acid accumulation in adipocytes might not be as deleterious as assumed. After all, this is the main function of adipocytes. Thereby, Gpnmb might contribute to a healthy instead of an inflammatory environment. Additionally, Glut4 expression in adipose tissue is normally downregulated in obese animals compared to lean mice [11, 251]. Thus, Gpnmb inducing glucose transporters Glut1 and 4 in adipocytes [118] would be beneficial. In all their work, Gong *et al.* concentrated on soluble Gpnmb. However, soluble and full-length Gpnmb might have different functions as we detected increased Gpnmb expression in reparative macrophages but increased production of soluble Gpnmb in inflammatory macrophages *in vitro*. Instead of downregulation or knockout, Gpnmb function was blocked using an antibody [118]. However, blocking Gpnmb using an antibody can modify Gpnmb phosphorylation and induce maturation and a higher inflammatory potential of the Gpnmb-expressing cell [85]. Thus, using antibodies to neutralize Gpnmb is a double-edged sword.

It should be mentioned that we agree with Gong *et al.* regarding the negative influence of Gpnmb on lipogenic gene expression, although they prominently report a positive association of lipogenic genes *Acc*, *Fasn*, *ATP-citrate lyase* (*Acl*), *long-chain fatty acyl elongase* (*Lce*) and *acetyl-CoA synthetase* (*Acs*) and Gpnmb in white adipose tissue [118]. Interestingly, an inverse regulation was found in liver and adipose tissue. In line with our findings, a high hepatic Gpnmb

expression was associated with downregulation of lipogenic genes in liver [118]. This was confirmed in rats, where liver but not adipose tissue of diabetic animals showed elevated lipogenesis suggesting that liver is the cause of elevated circulating blood lipids and bigger fat cells [376].

7.4.7.2. Katayama *et al.*

Katayama *et al.* had a comparable experimental setup to this work regarding mouse model and diet [109]. However, the effect on adipose tissue inflammation was absent and the effect on insulin and glucose tolerance was mild [109]. Two possible reasons may cause this absence of insulin resistance. (1) Compared to 16 weeks of this study, the duration of only five weeks was potentially too short to establish effects of Gpnmb. Still, the magnitude of induction of soluble Gpnmb in serum by obesity was similar in both studies, increasing from 2.91 to 3.85 ng/mL [109] and increasing from 5 to 8 ng/mL in this study. Thus, the time factor is probably not relevant. (2) At first glance, the high fat high sugar diet (D12331, researchdiets) is similar to our HFD (MD.06414 envigo). However, having a closer look, the major difference is neither the amount of sugar (21.4 vs. 25% kcal, respectively) nor fat (58 vs. 60%, respectively) but the composition of fat. Whereas the high fat high sugar diet was mostly composed of coconut oil, our HFD was mostly composed of lard. Lard but not coconut oil effectively induces insulin resistance [377]. Looking at the fatty acid profile (**Figure 46**), the most striking difference are the substantial amounts of palmitic acid in lard, which are three times increased compared to coconut oil [378]. It is the starting substance of ceramide, sphingosine and S1P. Gpnmb is known to react either directly to those lipids or indirectly via the lysosomal stress that is caused by those lipids (see chapter 1.3.9) [216, 250]. Thus, adipose tissue macrophages might benefit from Gpnmb when lysosomes are persistently overloaded with lipids, which is only revealed with a lard-based diet. On the other hand, both fat sources are able to induce liver steatosis that both this and Katayama *et al.*'s study detected [377].

	Soybean oil	Lard	Coconut oil
Saturated	14	40	90
Lauric	—	—	48
Myristic	—	2	16
Palmitic	10	27	9
Caprylic	—	—	8
Capric	—	—	7
Stearic	4	11	2
Unsaturated	81	59	9
Oleic	23	44	7
Linoleic	51	11	2
Linolenic	7	—	—
Palmitoleic	—	4	—
Other	5	1	1

Figure 46: Percentage of fatty acids in soybean oil, lard and coconut oil *[378].*

Summarizing the chapter regarding obesity, Gpnmb deficiency induces hyperglycemia/hyperinsulinemia with a reasonable starting point of increasing the macrophage numbers in adipose tissue. Promoted adipose tissue inflammation might impair insulin sensitivity. Eventually, high insulin levels increase hepatic AKT phosphorylation and lipogenesis. Liver function is impaired, plasma ALT levels rise and liver fibrosis ensues. The remaining pivotal issue for this study remains to be the question of the hen and the egg, if there is first hyperglycemia or hyperinsulinemia and which one is caused by Gpnmb.

7.5. Liver fibrosis

7.5.1. Influence of insulin resistance on liver fibrosis

The following chapter covers results from both atherosclerosis and obesity regarding liver fibrosis. HFD induced F4/80 expression in liver, proving the induction of hepatitis in our study. In line with other reports, Gpnmb reduced liver damage and expression of extracellular matrix genes [109, 172, 173]. NASH, characterized by ectopic fat deposition, inflammation, liver cell damage and fibrosis [236, 237], was fully induced only in *Gpnmb*-knockout animals. Insulin levels and development of NASH are closely interconnected. Insulin resistance, hypertension and elevated levels of ALT are independent predictors of NASH [379]. Hyperinsulinemia and insulin resistance is present in patients with mild or severe NAFLD/NASH, independent of obesity, diabetes mellitus, and hyperlipidemia [380–382]. Especially insulin resistance of normoweight NASH patients led to the conclusion that insulin resistance might be the key driver for NASH [380]. This makes it possible that NASH in the *Gpnmb*-knockout animals is a secondary effect due to insulin resistance. In contrast, Gpnmb ameliorated NASH induced by a choline-deficient diet [173]. This diet is a way to induce NASH by inhibiting fatty acid oxidation in hepatocytes without affecting weight gain or insulin sensitivity [286], suggesting a direct effect of Gpnmb on liver fibrosis and not via the detour of insulin resistance.

7.5.2. Influence of diet, time and gender on liver fibrosis

Liver fibrosis was reported to be ameliorated [109, 172, 173], promoted [176] or not affected [118] by Gpnmb. We examined two diseases that cause liver fibrosis, atherosclerosis [286] and obesity [109], but only in obesity liver fibrosis was affected by the presence of Gpnmb. This adds one more study to the controversial role of Gpnmb in liver fibrosis.

Factors for this discrepancy could be diet composition, time or gender, which are outlined in the following. In general, the lipid composition of the diet has a major effect on the development of symptoms [383, 384]. Fat derived from lard (HFD) enhances whereas butter fat (HCD) prevents hepatic necrosis [385], which might explain why we can detect a beneficial effect of Gpnmb on ALT release after HFD but not after HCD.

Twelve weeks of atherosclerosis compared to 16 weeks of obesity might not have been enough to show detectable differences of liver damage markers in blood. However, ALT levels of atherosclerotic mice were similar or even higher than those of obese mice, showing that liver damage was present but not affected by the *Gpnmb* genotype. Moreover, ALT levels of atherosclerotic mice slightly decreased from 8 to 12 weeks of HCD, suggesting that adaption to the diet occurred and an extension of time would have not revealed an effect of Gpnmb absence.

The third factor, gender, turned out to be quite interesting. Atherosclerotic mice were female but obese mice were male, thus comprising two factors and making it hardly legit to compare liver fibrosis. Originally, it was not intended to examine a gender effect of Gpnmb. It is nevertheless considered in the following because there is an interesting study examining gender differences in NASH [347]. IKKβ deficiency in hepatocytes aggravated Western diet-induced NASH in male but not in female mice, which was associated with a high upregulation of Gpnmb in male but not in female liver tissues [347]. Moreover, male mice developed a more severe liver fibrosis, inflammation and higher ALT levels in plasma. In wildtype animals, the same trend of the aforementioned symptoms including Gpnmb expression was seen but not as dramatic [347]. In

the condition where Gpnmb was upregulated, sulfotransferase family E1 (Sult1e1), a protein inactivating estrogen, was upregulated as well [347]. Gpnmb might either be suppressed by estrogen or upregulated by androgens. In fact, it was reported that androgen can regulate Gpnmb expression, however in opposite way: It decreased *Gpnmb* promoter activity and gene expression in prostatic carcinoma cells [165]. It would be interesting to know, if this mechanism applies to non-cancerous cells as well. The studies observing an ameliorating effect of Gpnmb on fibrosis used male animals [109, 172, 173]. Thus, especially male mice might benefit from Gpnmb expression via a mechanism that could involve sex hormones. Unfortunately, one group that detected a net promotion of fibrosis by Gpnmb did not describe the sex [176].

7.5.3. Liver inflammation

Distinct macrophage subsets can execute complementary functions [386]. Interestingly, the sequence of matrix deposition and matrix resolution is sequentially reversed in liver fibrosis compared to other injuries [27]. The reported effects of Gpnmb, such as wound healing [200], increasing [176] or reducing [173] hepatic stellate cells, down- (this work) or upregulating fibrotic genes [173] as well as Mmp induction [82, 92, 172, 172, 174, 176–179] fit to both categories, making it difficult to assign a distinct role to Gpnmb.

Whereas this study showed a prominent role of Gpnmb on liver fibrosis in obese mice, an impact on macrophage recruitment and liver inflammation could not be detected. Thus, Gpnmb might not be relevant for inflammatory hepatic macrophages. Additionally, although *Gpnmb* mRNA increased 3-fold in liver of obese wildtype mice, Gpnmb was hardly detectable on protein level (not shown). Thereby, Gpnmb may not influence the liver by being locally expressed but by a hormonal effect of the soluble form generated elsewhere in the body and acting on liver cells in a dampening manner.

This was suggested before by Katayama *et al.* who observed a hepatic effect of extracellular Gpnmb produced by adipocytes [109]. In contrast, it was also reported that hepatocytes [118] or liver macrophages [176] are the main source of local Gpnmb expression. A hepatic Gpnmb production was also observed in an atherosclerosis experiment, concomitant with a rise in liver macrophage markers [250]. Unfortunately, the exact cell type was not investigated. Thus, the liver fibrosis issue remains heavily contradictory.

Taken together, the Gpnmb-mediated amelioration of liver fibrosis can result from indirect effect of insulin resistance, hepatic Gpnmb regulated by sex hormones, or extracellular Gpnmb.

7.6. Proteomics

Discovering potential binding partners of Gpnmb by performing interaction proteomics together with the MDC Proteomics core facility, several pathways were discovered that may explain some of the phenotypes found in the *Gpnmb*-knockout mice and could be followed up in future studies in order to better understand the cellular functions of Gpnmb. Most of them have not been associated with Gpnmb so far and further question, if Gpnmb is a single or a multi-functional protein. The proteins that were discovered by mass spectrometry as potential interaction partners are displayed in bold letters in the following.

7.6.1. Lysosomal proteins

Binding of **cathepsin B** indicated an interaction with Gpnmb resulting in proteolysis of Gpnmb. The experimental data suggested otherwise showing no decrease of soluble Gpnmb in cell culture medium upon inhibition of cathepsin B. An explanation of the detected interaction is the same as for other lysosomal proteins that were detected by mass spectrometry. Gpnmb, accumulating in lysosomes after bafilomycin treatment, was stuck in close spatial relationship with proteins that only interact in this special condition. Bafilomycin in contrast to TGFβ is no endogenous stimulus. Thus, bafilomycin might have created an artificial condition that does not occur in a normal cell state. Gpnmb bound to other lysosome-specific proteins like lysosomal protective protein (**PPGB**), **CD68** and **V-ATPase**. Of note, Gpnmb interacts with the cytosolic subunit A of the V-ATPase whereas bafilomycin interacts with its transmembrane V_o subunit [387]. If Gpnmb is naturally associated with the V-ATPase, it might have caused the compensatory upregulation of Gpnmb upon V-ATPase inhibition with bafilomycin. However, the reasons outlined in chapter 7.1.4 are more likely.

7.6.2. Ribosomal proteins

Fifteen ribosomal proteins bound to Gpnmb, 12 of them were recognized by KEGG analysis. The ribosome contains more than 50 ribosomal proteins whose individual functions are not completely resolved [388]. Extraribosomal functions in apoptosis and cell cycle were reported for 6 and 5 of the ribosomal proteins, respectively, that were bound by Gpnmb [389]. These extraribosomal actions can be dependent on p53. Upon nucleolar stress caused by stressors such as DNA damage or starvation, ribosomal proteins are released from the nucleoli and activate p53 in a transcriptional, post-transcriptional and post-translational manner. For example, **L26** binds to the 5'-UTR of *Tp53* mRNA facilitating its translation. Gpnmb might activate p53 via ribosomal proteins, and p53 in turn promotes Gpnmb expression [164, 165] creating a positive feedback loop.

7.6.3. Actin network

Binding of Gpnmb to several motor and cytoskeleton proteins was observed. This may be due to regular trafficking of Gpnmb. Another possibility of Gpnmb as an active player in cytoskeleton regulation is illustrated in the following.

One of the top hits of binding Gpnmb was coronin-1C (**Coro1c**). Type I coronins (1A–C) are a very conserved family of F-actin binding proteins and have thereby functions in cell proliferation, cytokinesis, endocytosis, secretion and pinocytosis [390, 391]. The absence of Coro1c leads to long actin filaments [392] and affects wound healing [391], cancer invasion and metastasis [393]. Coro1c not only binds to F-actin but also modulates it by inhibiting the actin-related protein (**Arp**) 2/**3**-mediated actin branching and by promoting the disassembly of branched actin networks [390]. The Arp2/3 complex provides the force for cell motility and consists of 7 subunits, some of which are more prone to inhibition by coronins [390, 392]. Especially actin-related protein 2/3 complex subunit 5 (**Arpc5**) mediates the negative effects of coronins on actin polymerization [392]. Coronin and **cofilin** act in concert to disassemble actin filaments [390, 394]. This creates new pointed ends to which the stabilizing agent tropomyosin can bind, promoting mobility [395]. Tropomyosin (Tpm) in turn acts in concert with tropomodulin (Tmod), which inhibits actin elongation at the pointed end. Both have many isoforms that exhibit a huge variety of interactions and contribute to rather short actin filaments

[396]. The stress fiber-associated **Tpm4** displayed rapid dynamics on actin filaments and compared to other isoforms did not efficiently protect filaments from cofilin [397, 398]. Taken together, Gpnmb bound proteins are involved in the rapid turn-over of the actin cytoskeleton.

Summarizing the interactions, Gpnmb bound to Coro1c, Arp3, Arpc5, cofilin-1, Tpm4 and Tmod1 especially upon bafilomycin treatment. Bafilomycin is able to downregulate invasion and migration, both of which are actin-dependent mechanisms [337]. Interestingly, V-ATPase containing vesicles are re-distributed in migrating cells and co-localize with F-actin in leading edges.

Coro1c is an unspecific target of tyrosine kinase inhibitors imatinib and nilotinib, [190], both of which strongly upregulated Gpnmb [132]. A role of Gpnmb in migration, wound healing and phagocytosis was suggested before [137, 176, 200]. Although migration was mostly proposed as an effect of extracellular, soluble Gpnmb, it was shown that the kringle-like domain of Gpnmb was integral to maintain cortical actin fibers whereas deletion of this domain resulted in activated stress fiber formation, altering motility and cell migration [84]. Additionally, Coro1c was associated with fibronectin receptors syndecan-4 and $\alpha_5\beta_1$ integrin, both of which are Gpnmb receptors, in the protrusion of cells [399]. Gpnmb influencing the regulation of actin cytoskeleton turn-over and thus migration may explain the central finding of the *in vivo* experiments of more macrophages in adipose tissue of obese and atherosclerotic *Gpnmb*-knockout mice.

7.6.4. Atherosclerosis-associated proteins

Interestingly, binding to **LDL receptor** and **ApoE** occurred exclusively under bafilomycin treatment and might confirm the review of van der Lienden *et al.* that suggested a role of Gpnmb in lysosomal dysfunction in lipid storage diseases [197]. Additionally, Gpnmb expression correlated to ApoE levels in a model for Alzheimer disease, where lipid-loaded microglia where the source of Gpnmb expression [148]. In our atherosclerosis experiment, the absence of Gpnmb might not have exerted any effect on plaque development because we used a mouse model lacking an essential interaction partner of Gpnmb, ApoE.

Furthermore, Gpnmb bound to the macrophage-specific protein **CD68** that is a scavenger receptor for modified LDL in plaque-associated macrophages [400]. We did a co-staining in atherosclerotic plaques and found a co-localization of CD68 and Gpnmb in some but not all macrophages. Gpnmb has been suggested to be in a co-expression network with CD68 in a systems genetics approach, suggesting that they confer a similar function [158].

7.6.5. ER chaperones

BiP, **calreticulin** and **calnexin** are known to be ER-localized chaperones [401], thus supporting that Gpnmb is a glycoprotein requiring assistance in folding and glycosylation. Calreticulin is the soluble orthologue of calnexin in the ER. Calnexin was shown to bind Gpnmb before [109]. So far, only *BiP* mRNA was reported to bind Gpnmb, facilitating *BiP* splicing [110]. Interestingly, calreticulin, calnexin and BiP together with Gpnmb were identified in an approach aimed to identify melanosomal proteins [125]. Furthermore, a partial co-localization of calnexin and Gpnmb was detected surprisingly in the cellular periphery [130]. Thus, the three proteins might have a function beyond their role as chaperones. Apart from the category “protein processing in ER”, KEGG analysis suggested two of the chaperones to play a role in both “antigen processing and presentation” (see below) as well as “phagosome formation”. An influence of Gpnmb on

phagocytosis has been observed before [137]. However, as mentioned above (chapter 7.2.1), Gpnmb might not influence phagocytosis in general but a part that is specialized on specific pathogens.

7.6.6. Antigen processing

KEGG analysis revealed a potential role of Gpnmb in antigen processing and presentation. Gpnmb was found to bind to **H2-D1**, **H2-K1**, both parts of the MHC class I complex, and the accessory protein **β2-microglobuli**. Antigens are presented by MHC class II on specialized antigen-presenting cells like monocytes, macrophages and dendritic cells. Antigens on MHC class I are presented on almost all nucleated cells and serve the detection of intracellular pathogens. Thus, Gpnmb might facilitate discriminating between self and foreign. However, Tomihari *et al.* knocked down Gpnmb in B16-F10 melanoma cells, a cell line high in endogenous Gpnmb expression. Analyzing these cells by flow cytometry revealed no difference in ovalbumin peptide-loaded H-2K^{b} or H-2D^{b} with or without Gpnmb [157]. This indicates that the Gpnmb peptides detected by mass spectrometry might have been carried by MHC class I as part of the general presentation of self-peptides to T cells. Carriage of Gpnmb peptides by MHC class I was already predicted by computer modeling [79].

Appendix

Table 36: Proteins identified by mass spectrometry attached to Gpnmb.
*Enrichment factor "**xx**" means a score of greater than LogFC score of 3 (wildtype vs. Gpnmb-knockout samples), "**x**" means a score of 1-3, "**~**"means a score of 0-1, "**-**" means that knockout control was binding more than wildtype sample. Order is alphabetical. Listed are the "https://www.uniprot.org/" recommended names and abbreviations of the detected proteins.*

Uniprot ID	**Protein**		**Vehicle**	**TGFβ**	**Baf**
P08226	**ApoE**	Apolipoprotein E		**-**	**x**
Q99JY9	**Arp3**	Actin-related protein 3	**x**	**-**	**xx**
Q9CPW4	**Arpc5**	Actin-related protein 2/3 complex subunit 5	**~**	**~**	**xx**
O55143-2	**At2a2**	Sarcoplasmic/endoplasmic reticulum calcium ATPase 2			**x**
P01887	**B2mg**	B-2-microglobulin			**x**
P20029	**Bip**	Endoplasmic reticulum chaperone BiP	**x**	**x**	**x**
P14211	**Calr**	Calreticulin			**xx**
P35564	**Calx**	Calnexin		**xx**	**xx**
P10605	**Catb**	Cathepsin B	**~**	**~**	**x**
P31996-2	**Cd68**	Macrosialin (Isoform Short)			**x**
P18760	**Cof1**	Cofilin-1	**~**	**x**	**x**
Q9WUM	**Cor1c**	Coronin-1C	**x**	**-**	**xx**
Q9JHU4	**Dyhc1**	Cytoplasmic dynein 1 heavy chain 1	**~**	**x**	**~**
Q9EQP2	**Ehd4**	EH domain-containing protein 4	**~**	**x**	**x**
P08113	**Enpl**	Endoplasmin	**~**	**~**	**x**
P08752	**Gnai2**	Guanine nucleotide-binding protein G(i) subunit α-2	**x**		**x**
Q99P91	**Gpnmb**	**Transmembrane glycoprotein NMB**	**xx**	**xx**	**xx**
P01899	**H2-D1**	H-2 class I histocompatibility antigen, D-B α chain			**xx**
P01901	**H2-K1**	H-2 class I histocompatibility antigen, K-B α chain			**xx**
P35951	**Ldlr**	Low-density lipoprotein receptor			**xx**
P16045	**Leg1**	Galectin-1	**x**	**x**	**x**
P19973	**Lsp1**	Lymphocyte-specific protein 1	**x**	**x**	**xx**
Q3THE2	**Ml12b**	Myosin regulatory light chain 12B	**x**	**0**	**x**
A1L314	**Mpeg1**	Macrophage-expressed gene 1 protein	**-**	**~**	**x**
Q9WTI7-2	**Myo1c**	Unconventional myosin-Ic		**x**	**xx**
P70248	**Myo1f**	Unconventional myosin-If	**~**	**x**	**x**
O35375-5	**Nrp2**	Neuropilin-2 (Isoform B0)			**x**
P09405	**Nucl**	Nucleolin	**~**	**x**	**x**
P29341	**Pabp1**	Polyadenylate-binding protein 1		**x**	**x**
P27773	**Pdia3**	Protein disulfide-isomerase A3			**x**
Q61233	**Lcp1**	Plastin-2	**xx**	**~**	**x**
P16675	**Ppgb**	Lysosomal protective protein	**-**	**-**	**x**
P35278	**Rab5c**	Ras-related protein RABC1	**x**		**x**
O23657	**Rabc1**	Ras-related protein RABC1			**x**
Q05144	**Rac2**	Ras-related C3 botulinum toxin substrate 2	**x**	**x**	**x**
P62827	**Ran**	GTP-binding nuclear protein Ran	**~**	**~**	**x**
Q9QUI0	**Rhoa**	Transforming protein RhoA		**x**	**x**
P53026	**Rl10a**	60S ribosomal protein L10a	**~**	**~**	**~**

Q9CPR4	**Rl17**	60S ribosomal protein L17	**~**	**~**	**~**
P61255	**Rl26**	60S ribosomal protein L26	**~**	**~**	**x**
P41105	**Rl28**	60S ribosomal protein L28	**~**	**~**	**x**
P62889	**Rl30**	60S ribosomal protein L30	**~**	**~**	**~**
O55142	**Rl35a**	60S ribosomal protein L35a		**~**	**x**
Q9D8E6	**Rl4**	60S ribosomal protein L4	**~**	**~**	**~**
P47911	**Rl6**	60S ribosomal protein L6	**~**	**x**	**x**
P62918	**Rl8**	60S ribosomal protein L8	**~**	**x**	**~**
P62281	**Rs11**	40S ribosomal protein S11	**~**	**~**	**x**
P14131	**Rs16**	40S ribosomal protein S16	**x**	**x**	**x**
P62849-2	**Rs24**	40S ribosomal protein S24 Isoform 2	**~**	**~**	**x**
P62983	**Rs27a**	Ubiquitin-40S ribosomal protein S27a	**~**	**~**	**x**
P62908	**Rs3**	40S ribosomal protein S3	**~**	**~**	**~**
P62082	**Rs7**	40S ribosomal protein S7	**~**	**x**	**x**
P07091	**S10a4**	S100-A4		**-**	**x**
P14069	**S10a6**	S100-A6	**~**	**x**	**x**
O08992	**Sdcb1**	Syntenin-1			**x**
P05213	**Tba1b**	Tubulin α-1B	**~**	**~**	**~**
P68372	**Tbb4b**	Tubulin β-4B chain	**~**	**~**	**x**
P49813	**Tmod1**	Tropomodulin-1			**xx**
Q6IRU2	**Tpm4**	Tropomyosin α-4 chain		**x**	**xx**
P50516	**Vata**	V-type proton ATPase catalytic subunit A	**x**	**~**	**x**
Q60930	**Vdac2**	Voltage-dependent anion-selective channel protein 2	**x**	**x**	**-**

References

[1] Farsang, C.; Naditch-Brule, L.; Perlini, S.; Zidek, W.; Kjeldsen, S.E. and GOOD investigators: Inter-regional comparisons of the prevalence of cardiometabolic risk factors in patients with hypertension in Europe: the GOOD survey, Journal of Human Hypertension, **23** (2009), no. 5, pp. 316–324.

[2] Ford, E.S.; Li, C. and Zhao, G.: Prevalence and correlates of metabolic syndrome based on a harmonious definition among adults in the US, Journal of Diabetes, **2** (2010), no. 3, pp. 180–193.

[3] Samson, S.L. and Garber, A.J.: Metabolic syndrome, Endocrinology and Metabolism Clinics of North America, **43** (2014), no. 1, pp. 1–23.

[4] Catapano, A.L.; Graham, I.; De Backer, G.; Wiklund, O.; Chapman, M.J.; Drexel, H.; Hoes, A.W.; Jennings, C.S.; *et al.*: 2016 ESC/EAS Guidelines for the Management of Dyslipidaemias, European Heart Journal, **37** (2016), no. 39, pp. 2999–3058.

[5] De Backer, G.; Ambrosioni, E.; Borch-Johnsen, K.; Brotons, C.; Cifkova, R.; Dallongeville, J.; Ebrahim, S.; Faergeman, O.; *et al.*: European guidelines on cardiovascular disease prevention in clinical practiceThird Joint Task Force of European and other Societies on Cardiovascular Disease Prevention in Clinical Practice (constituted by representatives of eight societies and by invited experts), European Heart Journal, **24** (2003), no. 17, pp. 1601–1610.

[6] Knowler, W.C.; Barrett-Connor, E.; Fowler, S.E.; Hamman, R.F.; Lachin, J.M.; Walker, E.A. and Nathan, D.M.: Reduction in the incidence of type 2 diabetes with lifestyle intervention or metformin, The New England journal of medicine, **346** (2002), no. 6, pp. 393–403.

[7] Mendrick, D.L.; Diehl, A.M.; Topor, L.S.; Dietert, R.R.; Will, Y.; La Merrill, M.A.; Bouret, S.; Varma, V.; Hastings, K.L.; Schug, T.T.; Emeigh Hart, S.G. and Burleson, F.G.: Metabolic Syndrome and Associated Diseases: From the Bench to the Clinic, Toxicological Sciences, **162** (2018), no. 1, pp. 36–42.

[8] Tilg, H. and Kaser, A.: Gut microbiome, obesity, and metabolic dysfunction, The Journal of Clinical Investigation, **121** (2011), no. 6, pp. 2126–2132.

[9] Reilly Muredach P. and Rader Daniel J.: The Metabolic Syndrome, Circulation, **108** (2003), no. 13, pp. 1546–1551.

[10] Gregor, M.F. and Hotamisligil, G.S.: Inflammatory mechanisms in obesity, Annual Review of Immunology, **29** (2011), pp. 415–445.

[11] Kahn, B.B. and Flier, J.S.: Obesity and insulin resistance, Journal of Clinical Investigation, **106** (2000), no. 4, pp. 473–481.

[12] Sierra Rojas, J.X.; García-San Frutos, M.; Horrillo, D.; Lauzurica, N.; Oliveros, E.; Carrascosa, J.M.; Fernández-Agulló, T. and Ros, M.: Differential Development of Inflammation and Insulin Resistance in Different Adipose Tissue Depots Along Aging in Wistar Rats: Effects of Caloric Restriction, The Journals of Gerontology. Series A, Biological Sciences and Medical Sciences, (2015).

[13] Chen, Y.; Zhu, J.; Lum, P.Y.; Yang, X.; Pinto, S.; MacNeil, D.J.; Zhang, C.; Lamb, J.; *et al.*: Variations in DNA elucidate molecular networks that cause disease, Nature, **452** (2008), no. 7186, pp. 429–435.

[14] Yang, X.; Deignan, J.L.; Qi, H.; Zhu, J.; Qian, S.; Zhong, J.; Torosyan, G.; Majid, S.; *et al.*: Validation of candidate causal genes for obesity that affect shared metabolic pathways and networks, Nature Genetics, **41** (2009), no. 4, pp. 415–423.

[15] Weisberg, S.P.; McCann, D.; Desai, M.; Rosenbaum, M.; Leibel, R.L. and Ferrante, A.W.: Obesity is associated with macrophage accumulation in adipose tissue, The Journal of Clinical Investigation, **112** (2003), no. 12, pp. 1796–1808.

[16] Xu, H.; Barnes, G.T.; Yang, Q.; Tan, G.; Yang, D.; Chou, C.J.; Sole, J.; Nichols, A.; Ross, J.S.; Tartaglia, L.A. and Chen, H.: Chronic inflammation in fat plays a crucial role in the development of obesity-related insulin resistance, The Journal of Clinical Investigation, **112** (2003), no. 12, pp. 1821–1830.

[17] Lumeng, C.N.; Bodzin, J.L. and Saltiel, A.R.: Obesity induces a phenotypic switch in adipose tissue macrophage polarization, The Journal of Clinical Investigation, **117** (2007), no. 1, pp. 175–184.

[18] Odegaard, J.I. and Chawla, A.: Pleiotropic actions of insulin resistance and inflammation in metabolic homeostasis, Science (New York, N.Y.), **339** (2013), no. 6116, pp. 172–177.

[19] Komohara, Y.; Fujiwara, Y.; Ohnishi, K.; Shiraishi, D. and Takeya, M.: Contribution of Macrophage Polarization to Metabolic Diseases, Journal of Atherosclerosis and Thrombosis, **23** (2016), no. 1, pp. 10–17.

[20] Olefsky, J.M. and Glass, C.K.: Macrophages, Inflammation, and Insulin Resistance, Annual Review of Physiology, **72** (2010), no. 1, pp. 219–246.

[21] Wen, H.; Gris, D.; Lei, Y.; Jha, S.; Zhang, L.; Huang, M.T.-H.; Brickey, W.J. and Ting, J.P.-Y.: Fatty acid-induced NLRP3-ASC inflammasome activation interferes with insulin signaling, Nature Immunology, **12** (2011), no. 5, pp. 408–415.

[22] Oh, J.; Riek, A.E.; Weng, S.; Petty, M.; Kim, D.; Colonna, M.; Cella, M. and Bernal-Mizrachi, C.: Endoplasmic reticulum stress controls M2 macrophage differentiation and foam cell formation, The Journal of Biological Chemistry, **287** (2012), no. 15, pp. 11629–11641.

[23] Kratz, M.; Coats, B.R.; Hisert, K.B.; Hagman, D.; Mutskov, V.; Peris, E.; Schoenfelt, K.Q.; Kuzma, J.N.; Larson, I.; Billing, P.S.; Landerholm, R.W.; Crouthamel, M.; Gozal, D.; Hwang, S.; Singh, P.K. and Becker, L.: Metabolic dysfunction drives a mechanistically distinct proinflammatory phenotype in adipose tissue macrophages, Cell Metabolism, **20** (2014), no. 4, pp. 614–625.

[24] Xu, X.; Grijalva, A.; Skowronski, A.; van Eijk, M.; Serlie, M.J. and Ferrante, A.W.: Obesity Activates a Program of Lysosomal-Dependent Lipid Metabolism in Adipose Tissue Macrophages Independently of Classic Activation, Cell metabolism, **18** (2013), no. 6, pp. 816–830.

[25] Caspar-Bauguil, S.; Kolditz, C.-I.; Lefort, C.; Vila, I.; Mouisel, E.; Beuzelin, D.; Tavernier, G.; Marques, M.-A.; Zakaroff-Girard, A.; Pecher, C.; Houssier, M.; Mir, L.; Nicolas, S.; Moro, C. and Langin, D.: Fatty acids from fat cell lipolysis do not activate an inflammatory response but are stored as triacylglycerols in adipose tissue macrophages, Diabetologia, (2015), pp. 1–10.

[26] Nishimura, S.; Manabe, I.; Nagasaki, M.; Eto, K.; Yamashita, H.; Ohsugi, M.; Otsu, M.; Hara, K.; Ueki, K.; Sugiura, S.; Yoshimura, K.; Kadowaki, T. and Nagai, R.: CD8+ effector T cells contribute to macrophage recruitment and adipose tissue inflammation in obesity, Nature Medicine, **15** (2009), no. 8, pp. 914–920.

[27] Wynn, T.A.; Chawla, A. and Pollard, J.W.: Origins and Hallmarks of Macrophages: Development, Homeostasis, and Disease, Nature, **496** (2013), no. 7446, pp. 445–455.

[28] Neels, J.G. and Olefsky, J.M.: Inflamed fat: what starts the fire?, The Journal of Clinical Investigation, **116** (2006), no. 1, pp. 33–35.

[29] Brown, M.S. and Goldstein, J.L.: Selective versus Total Insulin Resistance: A Pathogenic Paradox, Cell Metabolism, **7** (2008), no. 2, pp. 95–96.

[30] Vigneri, R.; Goldfine, I.D. and Frittitta, L.: Insulin, insulin receptors, and cancer, Journal of Endocrinological Investigation, **39** (2016), no. 12, pp. 1365–1376.

[31] Thorens, B.; Sarkar, H.K.; Kaback, H.R. and Lodish, H.F.: Cloning and functional expression in bacteria of a novel glucose transporter present in liver, intestine, kidney, and β-pancreatic islet cells, Cell, **55** (1988), no. 2, pp. 281–290.

[32] Schürmann, A.: Glucose Transporters: Their Abnormalities and Significance in Type 2 Diabetes and Cancer, Frontiers in Diabetes, KARGER, Basel, 2008, pp. 71–83.

[33] Mueckler, M. and Thorens, B.: The SLC2 (GLUT) family of membrane transporters, Molecular Aspects of Medicine, **34** (2013), no. 2, pp. 121–138.

[34] Huang, S. and Czech, M.P.: The GLUT4 glucose transporter, Cell Metabolism, **5** (2007), no. 4, pp. 237–252.

[35] Zierath, J.R.; He, L.; Gumà, A.; Odegoard Wahlström, E.; Klip, A. and Wallberg-Henriksson, H.: Insulin action on glucose transport and plasma membrane GLUT4 content in skeletal muscle from patients with NIDDM, Diabetologia, **39** (1996), no. 10, pp. 1180–1189.

[36] Kim, Y.B.; Nikoulina, S.E.; Ciaraldi, T.P.; Henry, R.R. and Kahn, B.B.: Normal insulin-dependent activation of Akt/protein kinase B, with diminished activation of phosphoinositide 3-kinase, in muscle in type 2 diabetes, The Journal of Clinical Investigation, **104** (1999), no. 6, pp. 733–741.

[37] Abel, E.D.; Peroni, O.; Kim, J.K.; Kim, Y.-B.; Boss, O.; Hadro, E.; Minnemann, T.; Shulman, G.I. and Kahn, B.B.: Adipose-selective targeting of the GLUT4 gene impairs insulin action in muscle and liver, Nature, **409** (2001), no. 6821, p. 729.

[38] Zisman, A.; Peroni, O.D.; Abel, E.D.; Michael, M.D.; Mauvais-Jarvis, F.; Lowell, B.B.; Wojtaszewski, J.F.P.; Hirshman, M.F.; Virkamaki, A.; Goodyear, L.J.; Kahn, C.R. and Kahn, B.B.: Targeted disruption of the glucose transporter 4 selectively in muscle causes insulin resistance and glucose intolerance, Nature Medicine, **6** (2000), no. 8, pp. 924–928.

[39] Gisterå, A. and Hansson, G.K.: The immunology of atherosclerosis, Nature Reviews Nephrology, **13** (2017), no. 6, pp. 368–380.

[40] Stary Herbert C.; Chandler A. Bleakley; Dinsmore Robert E.; Fuster Valentin; Glagov Seymour; Insull William; Rosenfeld Michael E.; Schwartz Colin J.; Wagner William D. and Wissler Robert W.: A Definition of Advanced Types of Atherosclerotic Lesions and a Histological Classification of Atherosclerosis, Circulation, **92** (1995), no. 5, pp. 1355–1374.

[41] Davignon Jean and Ganz Peter: Role of Endothelial Dysfunction in Atherosclerosis, Circulation, **109** (2004), no. 23_suppl_1, pp. III–27.

[42] Favero, G.; Paganelli, C.; Buffoli, B.; Rodella, L.F. and Rezzani, R.: Endothelium and its alterations in cardiovascular diseases: life style intervention, BioMed Research International, **2014** (2014), p. 801896.

[43] Burtea, C.; Laurent, S.; Murariu, O.; Rattat, D.; Toubeau, G.; Verbruggen, A.; Vansthertem, D.; Vander Elst, L. and Muller, R.N.: Molecular imaging of alpha v beta3 integrin expression in atherosclerotic plaques with a mimetic of RGD peptide grafted to Gd-DTPA, Cardiovascular Research, **78** (2008), no. 1, pp. 148–157.

[44] Badimon, L. and Vilahur, G.: LDL-cholesterol versus HDL-cholesterol in the atherosclerotic plaque: inflammatory resolution versus thrombotic chaos, Annals of the New York Academy of Sciences, **1254** (2012), no. 1, pp. 18–32.

[45] Rubbo, H.; Trostchansky, A.; Botti, H. and Batthyány, C.: Interactions of nitric oxide and peroxynitrite with low-density lipoprotein, Biological Chemistry, **383** (2002), nos. 3–4, pp. 547–552.

[46] Weber, C. and Noels, H.: Atherosclerosis: current pathogenesis and therapeutic options, Nature Medicine, **17** (2011), no. 11, pp. 1410–1422.

[47] Rajagopalan, S.; Kurz, S.; Münzel, T.; Tarpey, M.; Freeman, B.A.; Griendling, K.K. and Harrison, D.G.: Angiotensin II-mediated hypertension in the rat increases vascular superoxide production via membrane NADH/NADPH oxidase activation. Contribution to alterations of vasomotor tone, The Journal of Clinical Investigation, **97** (1996), no. 8, pp. 1916–1923.

[48] Yokoyama, M.; Inoue, N. and Kawashima, S.: Role of the vascular NADH/NADPH oxidase system in atherosclerosis, Annals of the New York Academy of Sciences, **902** (2000), pp. 241–247; discussion 247-248.

[49] Kalinowski, L. and Malinski, T.: Endothelial NADH/NADPH-dependent enzymatic sources of superoxide production: relationship to endothelial dysfunction, Acta Biochimica Polonica, **51** (2004), no. 2, pp. 459–469.

[50] Samsam Shariat, S.Z.A.; Mostafavi, S.A. and Khakpour, F.: Antioxidant Effects of Vitamins C and E on the Low-Density Lipoprotein Oxidation Mediated by Myeloperoxidase, Iranian Biomedical Journal, **17** (2013), no. 1, pp. 22–28.

[51] Wang, Y.; Chun, O.K. and Song, W.O.: Plasma and Dietary Antioxidant Status as Cardiovascular Disease Risk Factors: A Review of Human Studies, Nutrients, **5** (2013), no. 8, pp. 2969–3004.

[52] Gleissner, C.A.; Leitinger, N. and Ley, K.: Effects of native and modified low-density lipoproteins on monocyte recruitment in atherosclerosis, Hypertension (Dallas, Tex.: 1979), **50** (2007), no. 2, pp. 276–283.

[53] Greaves, D.R. and Gordon, S.: The macrophage scavenger receptor at 30 years of age: current knowledge and future challenges, Journal of Lipid Research, **50 Suppl** (2009), pp. S282-286.

[54] Badimón, L.; Vilahur, G. and Padró, T.: Lipoproteins, platelets and atherothrombosis, Revista Espanola De Cardiologia, **62** (2009), no. 10, pp. 1161–1178.

[55] Moore, K.; Sheedy, F. and Fisher, E.: Macrophages in atherosclerosis: a dynamic balance, Nature reviews. Immunology, **13** (2013), no. 10, pp. 709–721.

[56] Chen, C. and Khismatullin, D.B.: Oxidized Low-Density Lipoprotein Contributes to Atherogenesis via Co-activation of Macrophages and Mast Cells, PLOS ONE, **10** (2015), no. 3, p. e0123088.

[57] Zhou, X.; Paulsson, G.; Stemme, S. and Hansson, G.K.: Hypercholesterolemia is associated with a T helper (Th) 1/Th2 switch of the autoimmune response in atherosclerotic apo E-knockout mice, The Journal of Clinical Investigation, **101** (1998), no. 8, pp. 1717–1725.

[58] Mach, F.; Sauty, A.; Iarossi, A.S.; Sukhova, G.K.; Neote, K.; Libby, P. and Luster, A.D.: Differential expression of three T lymphocyte-activating CXC chemokines by human atheroma-associated cells, The Journal of Clinical Investigation, **104** (1999), no. 8, pp. 1041–1050.

[59] Grundy Scott M.; Cleeman James I.; Merz C. Noel Bairey; Brewer H. Bryan; Clark Luther T.; Hunninghake Donald B.; Pasternak Richard C.; Smith Sidney C. and Stone Neil J.: Implications of Recent Clinical Trials for the National Cholesterol Education Program Adult Treatment Panel III Guidelines, Circulation, **110** (2004), no. 2, pp. 227–239.

[60] Bobryshev, Y.V.; Ivanova, E.A.; Chistiakov, D.A.; Nikiforov, N.G. and Orekhov, A.N.: Macrophages and Their Role in Atherosclerosis: Pathophysiology and Transcriptome Analysis, BioMed Research International, **2016** (2016).

[61] Kadl, A.; Meher, A.K.; Sharma, P.R.; Lee, M.Y.; Doran, A.C.; Johnstone, S.R.; Elliott, M.R.; Gruber, F.; Han, J.; Chen, W.; Kensler, T.; Ravichandran, K.S.; Isakson, B.E.; Wamhoff, B.R. and Leitinger, N.: Identification of a Novel Macrophage Phenotype That Develops in Response to Atherogenic Phospholipids via Nrf2, Circulation Research, **107** (2010), no. 6, pp. 737–746.

[62] Fisher, E.A.: Regression of Atherosclerosis: The Journey From the Liver to the Plaque and Back, Arteriosclerosis, Thrombosis, and Vascular Biology, **36** (2016), no. 2, pp. 226–235.

[63] Llodrá, J.; Angeli, V.; Liu, J.; Trogan, E.; Fisher, E.A. and Randolph, G.J.: Emigration of monocyte-derived cells from atherosclerotic lesions characterizes regressive, but not progressive, plaques, Proceedings of the National Academy of Sciences of the United States of America, **101** (2004), no. 32, pp. 11779–11784.

[64] Trogan, E.; Feig, J.E.; Dogan, S.; Rothblat, G.H.; Angeli, V.; Tacke, F.; Randolph, G.J. and Fisher, E.A.: Gene expression changes in foam cells and the role of chemokine receptor CCR7 during atherosclerosis regression in ApoE-deficient mice, Proceedings of the National Academy of Sciences of the United States of America, **103** (2006), no. 10, pp. 3781–3786.

[65] Liao, X.; Sluimer, J.C.; Wang, Y.; Subramanian, M.; Brown, K.; Pattison, J.S.; Robbins, J.; Martinez, J. and Tabas, I.: Macrophage Autophagy Plays a Protective Role in Advanced Atherosclerosis, Cell Metabolism, **15** (2012), no. 4, pp. 545–553.

[66] von Zychlinski, A.; Williams, M.; McCormick, S. and Kleffmann, T.: Absolute quantification of apolipoproteins and associated proteins on human plasma lipoproteins, Journal of Proteomics, **106** (2014), pp. 181–190.

[67] Mahley, R.W.; Weisgraber, K.H. and Huang, Y.: Apolipoprotein E: structure determines function, from atherosclerosis to Alzheimer's disease to AIDS, Journal of Lipid Research, **50** (2009), no. Suppl, pp. S183–S188.

[68] de Nijs, T.; Sniderman, A. and de Graaf, J.: ApoB versus non-HDL-cholesterol: diagnosis and cardiovascular risk management, Critical Reviews in Clinical Laboratory Sciences, **50** (2013), no. 6, pp. 163–171.

[69] Jawien, J.: The role of an experimental model of atherosclerosis: apoE-knockout mice in developing new drugs against atherogenesis, Current Pharmaceutical Biotechnology, **13** (2012), no. 13, pp. 2435–2439.

[70] Nakashima, Y.; Plump, A.S.; Raines, E.W.; Breslow, J.L. and Ross, R.: ApoE-deficient mice develop lesions of all phases of atherosclerosis throughout the arterial tree, Arteriosclerosis and Thrombosis: A Journal of Vascular Biology, **14** (1994), no. 1, pp. 133–140.

[71] Libby, P.; Ridker, P.M. and Maseri, A.: Inflammation and atherosclerosis, Circulation, **105** (2002), no. 9, pp. 1135–1143.

[72] Weterman, M.A.; Ajubi, N.; van Dinter, I.M.; Degen, W.G.; van Muijen, G.N.; Ruitter, D.J. and Bloemers, H.P.: nmb, a novel gene, is expressed in low-metastatic human melanoma cell lines and xenografts, International Journal of Cancer, **60** (1995), no. 1, pp. 73–81.

[73] Bächner, D.; Schröder, D. and Gross, G.: mRNA expression of the murine glycoprotein (transmembrane) nmb (Gpnmb) gene is linked to the developing retinal pigment epithelium and iris, Brain Research. Gene Expression Patterns, **1** (2002), nos. 3–4, pp. 159–165.

[74] Shikano, S.; Bonkobara, M.; Zukas, P.K. and Ariizumi, K.: Molecular cloning of a dendritic cell-associated transmembrane protein, DC-HIL, that promotes RGD-dependent adhesion of endothelial cells through recognition of heparan sulfate proteoglycans, The Journal of Biological Chemistry, **276** (2001), no. 11, pp. 8125–8134.

[75] Turque, N.; Denhez, F.; Martin, P.; Planque, N.; Bailly, M.; Bègue, A.; Stéhelin, D. and Saule, S.: Characterization of a new melanocyte-specific gene (QNR-71) expressed in v-myc-transformed quail neuroretina, The EMBO journal, **15** (1996), no. 13, pp. 3338–3350.

[76] Safadi, Fayez.F.; Xu, J.; Smock, S.L.; Rico, M.C.; Owen, T.A. and Popoff, S.N.: Cloning and characterization of osteoactivin, a novel cDNA expressed in osteoblasts, Journal of Cellular Biochemistry, **84** (2002), no. 1, pp. 12–26.

[77] Bandari, P.S.; Qian, J.; Yehia, G.; Joshi, D.D.; Maloof, P.B.; Potian, J.; Oh, H.S.; Gascon, P.; Harrison, J.S. and Rameshwar, P.: Hematopoietic growth factor inducible neurokinin-1 type: a transmembrane protein that is similar to neurokinin 1 interacts with substance P, Regulatory Peptides, **111** (2003), nos. 1–3, pp. 169–178.

[78] Tomihari, M.; Hwang, S.-H.; Chung, J.-S.; Cruz, P.D. and Ariizumi, K.: Gpnmb is a melanosome-associated glycoprotein that contributes to melanocyte/keratinocyte adhesion in a RGD-dependent fashion, Experimental dermatology, **18** (2009), no. 7, pp. 586–595.

[79] Selim, A.A.: Osteoactivin bioinformatic analysis: prediction of novel functions, structural features, and modes of action, Medical Science Monitor: International Medical Journal of Experimental and Clinical Research, **15** (2009), no. 2, pp. MT19-33.

[80] Hoashi, T.; Sato, S.; Yamaguchi, Y.; Passeron, T.; Tamaki, K. and Hearing, V.J.: Glycoprotein nonmetastatic melanoma protein b, a melanocytic cell marker, is a melanosome-specific and proteolytically released protein, FASEB journal: official publication of the Federation of American Societies for Experimental Biology, **24** (2010), no. 5, pp. 1616–1629.

[81] Chung, J.-S.; Sato, K.; Dougherty, I.I.; Cruz, P.D. and Ariizumi, K.: DC-HIL is a negative regulator of T lymphocyte activation, Blood, **109** (2007), no. 10, pp. 4320–4327.

[82] Bhattacharyya, S.; Feferman, L.; Sharma, G. and Tobacman, J.K.: Increased GPNMB, phospho-ERK1/2, and MMP-9 in cystic fibrosis in association with reduced arylsulfatase B, Molecular Genetics and Metabolism, **124** (2018), no. 2, pp. 168–175.

[83] Maric, G.; Annis, M.G.; Dong, Z.; Rose, A. a. N.; Ng, S.; Perkins, D.; MacDonald, P.A.; Ouellet, V.; Russo, C. and Siegel, P.M.: GPNMB cooperates with neuropilin-1 to promote mammary tumor growth and engages integrin α5β1 for efficient breast cancer metastasis, Oncogene, **34** (2015), no. 43, pp. 5494–5504.

[84] Xie, R.; Okita, Y.; Ichikawa, Y.; Muhammad, F.A.; Huynh Dam, K.T.; Tran, S.P.T. and Kato, M.: Role of the kringle-like domain in Glycoprotein NMB for its tumorigenic potential, Cancer Science, (2019).

[85] Chung, J.-S.; Yudate, T.; Tomihari, M.; Akiyoshi, H.; Cruz, P.D. and Ariizumi, K.: Binding of DC-HIL to Dermatophytic Fungi Induces Tyrosine Phosphorylation and Potentiates Antigen Presenting Cell Function, The Journal of Immunology, **183** (2009), no. 8, pp. 5190–5198.

[86] Lin, A.; Li, C.; Xing, Z.; Hu, Q.; Liang, K.; Han, L.; Wang, C.; Hawke, D.H.; Wang, S.; Zhang, Y.; Wei, Y.; Ma, G.; Park, P.K.; Zhou, J.; Zhou, Y.; Hu, Z.; Zhou, Y.; Marks, J.R.; Liang, H.; Hung, M.-C.; Lin, C. and Yang, L.: The LINK-A lncRNA activates normoxic HIF1α signalling in triple-negative breast cancer, Nature Cell Biology, **18** (2016), no. 2, pp. 213–224.

[87] Okita, Y.; Kimura, M.; Xie, R.; Chen, C.; Shen, L.T.-W.; Kojima, Y.; Suzuki, H.; Muratani, M.; Saitoh, M.; Semba, K.; Heldin, C.-H. and Kato, M.: The transcription factor MAFK induces EMT and malignant progression of triple-negative breast cancer cells through its target GPNMB, Science Signaling, **10** (2017), no. 474.

[88] Yang, C.-F.; Lin, S.-P.; Chiang, C.-P.; Wu, Y.-H.; H'ng, W.S.; Chang, C.-P.; Chen, Y.-T. and Wu, J.-Y.: Loss of GPNMB Causes Autosomal-Recessive Amyloidosis Cutis Dyschromica in Humans, American Journal of Human Genetics, **102** (2018), no. 2, pp. 219–232.

[89] Chung, J.-S.; Bonkobara, M.; Tomihari, M.; Cruz, P.D. and Ariizumi, K.: The DC-HIL/syndecan-4 pathway inhibits human allogeneic T cell responses, European journal of immunology, **39** (2009), no. 4, pp. 965–974.

[90] Tse, K.F.; Jeffers, M.; Pollack, V.A.; McCabe, D.A.; Shadish, M.L.; Khramtsov, N.V.; Hackett, C.S.; Shenoy, S.G.; *et al*.: CR011, a fully human monoclonal antibody-auristatin E conjugate, for the treatment of melanoma, Clinical Cancer Research: An Official Journal of the American Association for Cancer Research, **12** (2006), no. 4, pp. 1373–1382.

[91] Zhang, P.; Liu, W.; Zhu, C.; Yuan, X.; Li, D.; Gu, W.; Ma, H.; Xie, X. and Gao, T.: Silencing of GPNMB by siRNA Inhibits the Formation of Melanosomes in Melanocytes in a MITF-Independent Fashion, PLoS ONE, **7** (2012), no. 8.

[92] Furochi, H.; Tamura, S.; Mameoka, M.; Yamada, C.; Ogawa, T.; Hirasaka, K.; Okumura, Y.; Imagawa, T.; Oguri, S.; Ishidoh, K.; Kishi, K.; Higashiyama, S. and Nikawa, T.: Osteoactivin fragments produced by ectodomain shedding induce MMP-3 expression via ERK pathway in mouse NIH-3T3 fibroblasts, FEBS letters, **581** (2007), no. 30, pp. 5743–5750.

[93] Abdelmagid, S.M.; Barbe, M.F.; Rico, M.C.; Salihoglu, S.; Arango-Hisijara, I.; Selim, A.H.; Anderson, M.G.; Owen, T.A.; Popoff, S.N. and Safadi, F.F.: Osteoactivin, an anabolic factor that regulates osteoblast differentiation and function, Experimental cell research, **314** (2008), no. 13, pp. 2334–2351.

[94] Chung, J.-S.; Shiue, L.H.; Duvic, M.; Pandya, A.; Cruz, P.D. and Ariizumi, K.: Sézary syndrome cells overexpress syndecan-4 bearing distinct heparan sulfate moieties that suppress T-cell activation by binding DC-HIL and trapping TGF-beta on the cell surface, Blood, **117** (2011), no. 12, pp. 3382–3390.

[95] Esko, J.D. and Selleck, S.B.: Order Out of Chaos: Assembly of Ligand Binding Sites in Heparan Sulfate, Annual Review of Biochemistry, **71** (2002), no. 1, pp. 435–471.

[96] Anderson, M.G.; Smith, R.S.; Hawes, N.L.; Zabaleta, A.; Chang, B.; Wiggs, J.L. and John, S.W.M.: Mutations in genes encoding melanosomal proteins cause pigmentary glaucoma in DBA/2J mice, Nature Genetics, **30** (2002), no. 1, pp. 81–85.

[97] Murthy, M.N.; Blauwendraat, C.; Guelfi, S.; Hardy, J.; Lewis, P.A. and Trabzuni, D.: Increased brain expression of GPNMB is associated with genome wide significant risk for Parkinson's disease on chromosome 7p15.3, Neurogenetics, **18** (2017), no. 3, pp. 121–133.

[98] Neal, M.L.; Boyle, A.M.; Budge, K.M.; Safadi, F.F. and Richardson, J.R.: The glycoprotein GPNMB attenuates astrocyte inflammatory responses through the CD44 receptor, Journal of Neuroinflammation, **15** (2018), no. 1, p. 73.

[99] Chang, D.; Nalls, M.A.; Hallgrímsdóttir, I.B.; Hunkapiller, J.; van der Brug, M.; Cai, F.; Kerchner, G.A.; Ayalon, G.; Bingol, B.; Sheng, M.; Hinds, D.; Behrens, T.W.; Singleton, A.B.; Bhangale, T.R. and Graham, R.R.: A meta-analysis of genome-wide association studies identifies 17 new Parkinson's disease risk loci, Nature genetics, **49** (2017), no. 10, pp. 1511–1516.

[100] Nalls, M.A.; Pankratz, N.; Lill, C.M.; Do, C.B.; Hernandez, D.G.; Saad, M.; DeStefano, A.L.; Kara, E.; *et al*., International Parkinson's Disease Genomics Consortium (IPDGC); Parkinson's Study Group (PSG) Parkinson's Research: The Organized GENetics Initiative (PROGENI); 23andMe; GenePD; NeuroGenetics Research Consortium (NGRC); Hussman Institute of Human Genomics (HIHG); Ashkenazi Jewish Dataset Investigator; Cohorts for Health and Aging Research in Genetic Epidemiology (CHARGE); North American Brain Expression Consortium (NABEC); United Kingdom Brain Expression Consortium (UKBEC); Greek Parkinson's Disease Consortium; Alzheimer Genetic Analysis Group; Ikram, M.A.; Ioannidis, J.P.A.; Hadjigeorgiou, G.M.; Bis, J.C.; Martinez, M.; Perlmutter, J.S.; Goate, A.; Marder, K.; *et al*.: Large-scale meta-analysis of genome-wide association data identifies six new risk loci for Parkinson's disease, Nature Genetics, **46** (2014), no. 9, pp. 989–993.

[101] International Parkinson's Disease Genomics Consortium (IPDGC) and Wellcome Trust Case Control Consortium 2 (WTCCC2): A two-stage meta-analysis identifies several new loci for Parkinson's disease, PLoS genetics, **7** (2011), no. 6, p. e1002142.

[102] Meng, S.; Song, F.; Chen, H.; Gao, X.; Amos, C.I.; Lee, J.E.; Wei, Q.; Qureshi, A.A. and Han, J.: No association between Parkinson's disease alleles and the risk of melanoma, Cancer epidemiology, biomarkers & prevention : a publication of the American Association for Cancer Research, cosponsored by the American Society of Preventive Oncology, **21** (2012), no. 1, pp. 243–245.

[103] Xu, Y.; Chen, Y.; Ou, R.; Wei, Q.-Q.; Cao, B.; Chen, K. and Shang, H.-F.: No association of GPNMB rs156429 polymorphism with Parkinson's disease, amyotrophic lateral sclerosis and multiple system atrophy in Chinese population, Neuroscience Letters, **622** (2016), pp. 113–117.

[104] Wang, L.; Li, N.-N.; Lu, Z.-J.; Li, J.-Y.; Peng, J.-X.; Duan, L.-R. and Peng, R.: Association of three candidate genetic variants in ACMSD/TMEM163, GPNMB and BCKDK /STX1B with sporadic Parkinson's disease in Han Chinese, Neuroscience Letters, **703** (2019), pp. 45–48.

[105] Wu, H.-C.; Chen, C.-M.; Chen, Y.-C.; Fung, H.-C.; Chang, K.-H. and Wu, Y.-R.: DLG2, but not TMEM229B, GPNMB, and ITGA8 polymorphism, is associated with Parkinson's disease in a Taiwanese population, Neurobiology of Aging, **64** (2018), pp. 158.e1-158.e6.

[106] Sjöblom, T.; Jones, S.; Wood, L.D.; Parsons, D.W.; Lin, J.; Barber, T.D.; Mandelker, D.; Leary, R.J.; *et al*.: The consensus coding sequences of human breast and colorectal cancers, Science (New York, N.Y.), **314** (2006), no. 5797, pp. 268–274.

[107] Mota, A.; Triviño, J.C.; Rojo-Sebastian, A.; Martínez-Ramírez, Á.; Chiva, L.; González-Martín, A.; Garcia, J.F.; Garcia-Sanz, P. and Moreno-Bueno, G.: Intra-tumor heterogeneity in TP53 null High Grade Serous Ovarian Carcinoma progression, BMC Cancer, **15** (2015).

[108] Ono, Y.; Chiba, S.; Yano, H.; Nakayama, N.; Saio, M.; Tsuruma, K.; Shimazawa, M.; Iwama, T. and Hara, H.: Glycoprotein nonmetastatic melanoma protein B (GPNMB) promotes the progression of brain glioblastoma via Na+/K+-ATPase, Biochemical and Biophysical Research Communications, **481** (2016), nos. 1–2, pp. 7–12.

[109] Katayama, A.; Nakatsuka, A.; Eguchi, J.; Murakami, K.; Teshigawara, S.; Kanzaki, M.; Nunoue, T.; Hida, K.; Wada, N.; Yasunaka, T.; Ikeda, F.; Takaki, A.; Yamamoto, K.; Kiyonari, H.; Makino, H. and Wada, J.: Beneficial impact of Gpnmb and its significance as a biomarker in nonalcoholic steatohepatitis, Scientific Reports, **5** (2015), p. 16920.

[110] Noda, Y.; Tsuruma, K.; Takata, M.; Ishisaka, M.; Tanaka, H.; Nakano, Y.; Nagahara, Y.; Shimazawa, M. and Hara, H.: GPNMB Induces BiP Expression by Enhancing Splicing of BiP Pre-mRNA during the Endoplasmic Reticulum Stress Response, Scientific Reports, **7** (2017), no. 1, p. 12160.

[111] Rameshwar, P.: Implication of possible therapies targeted for the tachykinergic system with the biology of neurokinin receptors and emerging related proteins, Recent patents on CNS drug discovery, **2** (2007), no. 1, pp. 79–84.

[112] Ishiguro, K.; Kadomatsu, K.; Kojima, T.; Muramatsu, H.; Iwase, M.; Yoshikai, Y.; Yanada, M.; Yamamoto, K.; Matsushita, T.; Nishimura, M.; Kusugami, K.; Saito, H. and Muramatsu, T.: Syndecan-4 Deficiency Leads to High Mortality of Lipopolysaccharide-injected Mice, Journal of Biological Chemistry, **276** (2001), no. 50, pp. 47483–47488.

[113] Averbeck, M.; Gebhardt, C.; Anderegg, U.; Termeer, C.; Sleeman, J.P. and Simon, J.C.: Switch in syndecan-1 and syndecan-4 expression controls maturation associated dendritic cell motility, Experimental Dermatology, **16** (2007), no. 7, pp. 580–589.

[114] Chung, J.-S.; Dougherty, I.; Cruz, P.D. and Ariizumi, K.: Syndecan-4 mediates the coinhibitory function of DC-HIL on T cell activation, Journal of Immunology (Baltimore, Md.: 1950), **179** (2007), no. 9, pp. 5778–5784.

[115] Yamashita, Y.; Oritani, K.; Miyoshi, E.K.; Wall, R.; Bernfield, M. and Kincade, P.W.: Syndecan-4 Is Expressed by B Lineage Lymphocytes and Can Transmit a Signal for Formation of Dendritic Processes, The Journal of Immunology, **162** (1999), no. 10, pp. 5940–5948.

[116] Ramani, V.; Teshima, T.; Tamura, K.; Chung, J.-S.; Kobayashi, M.; Cruz, P.D. and Ariizumi, K.: Melanoma-Derived Soluble DC-HIL/GPNMB Promotes Metastasis by Excluding T-Lymphocytes from the Pre-Metastatic Niches, The Journal of Investigative Dermatology, **138** (2018), no. 11, pp. 2443–2451.

[117] Akiyoshi, H.; Chung, J.-S.; Tomihari, M.; Cruz, P.D. and Ariizumi, K.: Depleting syndecan-4+ T lymphocytes using toxin-bearing dendritic cell-associated heparan sulfate proteoglycan-dependent integrin ligand: a new opportunity for treating activated T cell-driven disease, Journal of Immunology (Baltimore, Md.: 1950), **184** (2010), no. 7, pp. 3554–3561.

[118] Gong, X.-M.; Li, Y.-F.; Luo, J.; Wang, J.-Q.; Wei, J.; Wang, J.-Q.; Xiao, T.; Xie, C.; Hong, J.; Ning, G.; Shi, X.-J.; Li, B.-L.; Qi, W. and Song, B.-L.: Gpnmb secreted from liver promotes lipogenesis in white adipose tissue and aggravates obesity and insulin resistance, Nature Metabolism, **1** (2019), no. 5, p. 570.

[119] Yu, B.; Sondag, G.; Malcuit, C.; Kim, M.-H. and Safadi, F.F.: Macrophage-Associated Osteoactivin/GPNMB Mediates Mesenchymal Stem Cell Survival, Proliferation, and Migration via a CD44-Dependent Mechanism, Journal of Cellular Biochemistry, (2015).

[120] Sondag, G.R.; Mbimba, T.S.; Moussa, F.M.; Novak, K.; Yu, B.; Jaber, F.A.; Abdelmagid, S.M.; Geldenhuys, W.J. and Safadi, F.F.: Osteoactivin inhibition of osteoclastogenesis is mediated through CD44-ERK signaling, Experimental & Molecular Medicine, **48** (2016), no. 9, p. e257.

[121] Hooper, N.M.; Karran, E.H. and Turner, A.J.: Membrane protein secretases, The Biochemical Journal, **321 (Pt 2)** (1997), pp. 265–279.

[122] Moussa, F.M.; Hisijara, I.A.; Sondag, G.R.; Scott, E.M.; Frara, N.; Abdelmagid, S.M. and Safadi, F.F.: Osteoactivin promotes osteoblast adhesion through HSPG and αvβ1 integrin, Journal of Cellular Biochemistry, **115** (2014), no. 7, pp. 1243–1253.

[123] Kawahara, K.; Hirata, H.; Ohbuchi, K.; Nishi, K.; Maeda, A.; Kuniyasu, A.; Yamada, D.; Maeda, T.; Tsuji, A.; Sawada, M. and Nakayama, H.: The novel monoclonal antibody 9F5 reveals expression of a fragment of GPNMB/osteoactivin processed by furin-like protease(s) in a subpopulation of microglia in neonatal rat brain, Glia, **64** (2016), no. 11, pp. 1938–1961.

[124] Rose, A.A.N.; Annis, M.G.; Dong, Z.; Pepin, F.; Hallett, M.; Park, M. and Siegel, P.M.: ADAM10 releases a soluble form of the GPNMB/Osteoactivin extracellular domain with angiogenic properties, PloS One, **5** (2010), no. 8.

[125] Basrur, V.; Yang, F.; Kushimoto, T.; Higashimoto, Y.; Yasumoto, K.; Valencia, J.; Muller, J.; Vieira, W.D.; Watabe, H.; Shabanowitz, J.; Hearing, V.J.; Hunt, D.F. and Appella, E.: Proteomic Analysis of Early Melanosomes: Identification of Novel Melanosomal Proteins, Journal of Proteome Research, **2** (2003), no. 1, pp. 69–79.

[126] Chi, A.; Valencia, J.C.; Hu, Z.-Z.; Watabe, H.; Yamaguchi, H.; Mangini, N.J.; Huang, H.; Canfield, V.A.; Cheng, K.C.; Yang, F.; Abe, R.; Yamagishi, S.; Shabanowitz, J.; Hearing, V.J.; Wu, C.; Appella, E. and Hunt, D.F.: Proteomic and bioinformatic characterization of the biogenesis and function of melanosomes, Journal of Proteome Research, **5** (2006), no. 11, pp. 3135–3144.

[127] Kwon, B.S.; Halaban, R.; Ponnazhagan, S.; Kim, K.; Chintamaneni, C.; Bennett, D. and Pickard, R.T.: Mouse silver mutation is caused by a single base insertion in the putative cytoplasmic domain of Pmel 17, Nucleic Acids Research, **23** (1995), no. 1, pp. 154–158.

[128] Hellström, A.R.; Watt, B.; Fard, S.S.; Tenza, D.; Mannström, P.; Narfström, K.; Ekesten, B.; Ito, S.; Wakamatsu, K.; Larsson, J.; Ulfendahl, M.; Kullander, K.; Raposo, G.; Kerje, S.; Hallböök, F.; Marks, M.S. and Andersson, L.:

Inactivation of Pmel Alters Melanosome Shape But Has Only a Subtle Effect on Visible Pigmentation, PLOS Genetics, **7** (2011), no. 9, p. e1002285.

[129] McGlinchey, R.P. and Lee, J.C.: Why Study Functional Amyloids? Lessons from the Repeat Domain of Pmel17, Journal of Molecular Biology, **430** (2018), no. 20, pp. 3696–3706.

[130] Theos, A.C.; Watt, B.; Harper, D.C.; Janczura, K.J.; Theos, S.C.; Herman, K.E. and Marks, M.S.: The PKD domain distinguishes the trafficking and amyloidogenic properties of the pigment cell protein PMEL and its homologue GPNMB, Pigment Cell & Melanoma Research, **26** (2013), no. 4, pp. 470–486.

[131] Kushimoto, T.; Basrur, V.; Valencia, J.; Matsunaga, J.; Vieira, W.D.; Ferrans, V.J.; Muller, J.; Appella, E. and Hearing, V.J.: A model for melanosome biogenesis based on the purification and analysis of early melanosomes, Proceedings of the National Academy of Sciences of the United States of America, **98** (2001), no. 19, pp. 10698–10703.

[132] Gutknecht, M.; Geiger, J.; Joas, S.; Dörfel, D.; Salih, H.R.; Müller, M.R.; Grünebach, F. and Rittig, S.M.: The transcription factor MITF is a critical regulator of GPNMB expression in dendritic cells, Cell communication and signaling: CCS, **13** (2015), p. 19.

[133] Szulzewsky, F.; Pelz, A.; Feng, X.; Synowitz, M.; Markovic, D.; Langmann, T.; Holtman, I.R.; Wang, X.; Eggen, B.J.L.; Boddeke, H.W.G.M.; Hambardzumyan, D.; Wolf, S.A. and Kettenmann, H.: Glioma-associated microglia/macrophages display an expression profile different from M1 and M2 polarization and highly express Gpnmb and Spp1, PloS One, **10** (2015), no. 2, p. e0116644.

[134] Ripoll, V.M.; Irvine, K.M.; Ravasi, T.; Sweet, M.J. and Hume, D.A.: Gpnmb is induced in macrophages by IFN-gamma and lipopolysaccharide and acts as a feedback regulator of proinflammatory responses, Journal of Immunology (Baltimore, Md.: 1950), **178** (2007), no. 10, pp. 6557–6566.

[135] Anderson, M.G.; Nair, K.S.; Amonoo, L.A.; Mehalow, A.; Trantow, C.M.; Masli, S. and John, S.W.: GpnmbR150X allele must be present in bone marrow derived cells to mediate DBA/2J glaucoma, BMC Genetics, **9** (2008), p. 30.

[136] Haralanova-Ilieva, B.; Ramadori, G. and Armbrust, T.: Expression of osteoactivin in rat and human liver and isolated rat liver cells, Journal of Hepatology, **42** (2005), no. 4, pp. 565–572.

[137] Li, B.; Castano, A.P.; Hudson, T.E.; Nowlin, B.T.; Lin, S.-L.; Bonventre, J.V.; Swanson, K.D. and Duffield, J.S.: The melanoma-associated transmembrane glycoprotein Gpnmb controls trafficking of cellular debris for degradation and is essential for tissue repair, The FASEB Journal, **24** (2010), no. 12, pp. 4767–4781.

[138] Loftus, S.K.; Antonellis, A.; Matera, I.; Renaud, G.; Baxter, L.L.; Reid, D.; Wolfsberg, T.G.; Chen, Y.; Wang, C.; NISC Comparative Sequencing Program; Prasad, M.K.; Bessling, S.L.; McCallion, A.S.; Green, E.D.; Bennett, D.C. and Pavan, W.J.: Gpnmb is a melanoblast-expressed, MITF-dependent gene, Pigment Cell & Melanoma Research, **22** (2009), no. 1, pp. 99–110.

[139] Baerveldt, E.M.; Onderdijk, A.J.; Kurek, D.; Kant, M.; Florencia, E.F.; Ijpma, A.S.; van der Spek, P.J.; Bastiaans, J.; Jansen, P.A.; van Kilsdonk, J.W.J.; Laman, J.D. and Prens, E.P.: Ustekinumab improves psoriasis-related gene expression in noninvolved psoriatic skin without inhibition of the antimicrobial response, The British Journal of Dermatology, **168** (2013), no. 5, pp. 990–998.

[140] Choi, M.-S.; Kim, Y.-J.; Kwon, E.-Y.; Ryoo, J.Y.; Kim, S.R. and Jung, U.J.: High-fat diet decreases energy expenditure and expression of genes controlling lipid metabolism, mitochondrial function and skeletal system development in the adipose tissue, along with increased expression of extracellular matrix remodelling- and inflammation-related genes, The British Journal of Nutrition, **113** (2015), no. 6, pp. 867–877.

[141] Huang, J.-J.; Ma, W.-J. and Yokoyama, S.: Expression and immunolocalization of Gpnmb, a glioma-associated glycoprotein, in normal and inflamed central nervous systems of adult rats, Brain and Behavior, **2** (2012), no. 2, pp. 85–96.

[142] Rose, A.A.N.; Grosset, A.-A.; Dong, Z.; Russo, C.; Macdonald, P.A.; Bertos, N.R.; St-Pierre, Y.; Simantov, R.; Hallett, M.; Park, M.; Gaboury, L. and Siegel, P.M.: Glycoprotein nonmetastatic B is an independent prognostic indicator of recurrence and a novel therapeutic target in breast cancer, Clinical Cancer Research: An Official Journal of the American Association for Cancer Research, **16** (2010), no. 7, pp. 2147–2156.

[143] Rose, A.A.N.; Biondini, M.; Curiel, R. and Siegel, P.M.: Targeting GPNMB with glembatumumab vedotin: Current developments and future opportunities for the treatment of cancer, Pharmacology & Therapeutics, **179** (2017), pp. 127–141.

[144] Nikawa, T.; Ishidoh, K.; Hirasaka, K.; Ishihara, I.; Ikemoto, M.; Kano, M.; Kominami, E.; Nonaka, I.; Ogawa, T.; Adams, G.R.; Baldwin, K.M.; Yasui, N.; Kishi, K. and Takeda, S.: Skeletal muscle gene expression in space-flown rats, FASEB journal: official publication of the Federation of American Societies for Experimental Biology, **18** (2004), no. 3, pp. 522–524.

[145] Ahn, J.H.; Lee, Y.; Jeon, C.; Lee, S.-J.; Lee, B.-H.; Choi, K.D. and Bae, Y.-S.: Identification of the genes differentially expressed in human dendritic cell subsets by cDNA subtraction and microarray analysis, Blood, **100** (2002), no. 5, pp. 1742–1754.

[146] Chung, J.-S.; Tamura, K.; Akiyoshi, H.; Cruz, P.D. and Ariizumi, K.: The DC-HIL/syndecan-4 pathway regulates autoimmune responses through myeloid-derived suppressor cells, Journal of Immunology (Baltimore, Md.: 1950), **192** (2014), no. 6, pp. 2576–2584.

[147] Ripoll, V.M.; Meadows, N.A.; Raggatt, L.-J.; Chang, M.K.; Pettit, A.R.; Cassady, A.I. and Hume, D.A.: Microphthalmia transcription factor regulates the expression of the novel osteoclast factor GPNMB, Gene, **413** (2008), nos. 1–2, pp. 32–41.

[148] Hüttenrauch, M.; Ogorek, I.; Klafki, H.; Otto, M.; Stadelmann, C.; Weggen, S.; Wiltfang, J. and Wirths, O.: Glycoprotein NMB: a novel Alzheimer's disease associated marker expressed in a subset of activated microglia, Acta Neuropathologica Communications, **6** (2018).

[149] Knödler, A.; Schmidt, S.M.; Bringmann, A.; Weck, M.M.; Brauer, K.M.; Holderried, T. a. W.; Heine, A.-K.; Grünebach, F. and Brossart, P.: Post-transcriptional regulation of adapter molecules by IL-10 inhibits TLR-mediated activation of antigen-presenting cells, Leukemia, **23** (2009), no. 3, pp. 535–544.

[150] Schwarzbich, M.-A.; Gutknecht, M.; Salih, J.; Salih, H.R.; Brossart, P.; Rittig, S.M. and Grünebach, F.: The immune inhibitory receptor osteoactivin is upregulated in monocyte-derived dendritic cells by BCR-ABL tyrosine kinase inhibitors, Cancer immunology, immunotherapy: CII, **61** (2012), no. 2, pp. 193–202.

[151] Kobayashi, M.; Chung, J.-S.; Beg, M.; Arriaga, Y.; Verma, U.; Courtney, K.; Mansour, J.; Haley, B.; Khan, S.; Horiuchi, Y.; Ramani, V.; Harker, D.; Gopal, P.; Araghizadeh, F.; Cruz, P.D. and Ariizumi, K.: Blocking Monocytic Myeloid-Derived Suppressor Cell Function via Anti-DC-HIL/GPNMB Antibody Restores the In Vitro Integrity of T Cells from Cancer Patients, Clinical Cancer Research: An Official Journal of the American Association for Cancer Research, **25** (2019), no. 2, pp. 828–838.

[152] Cao, L.Y.; Chung, J.-S.; Teshima, T.; Feigenbaum, L.; Cruz, P.D.; Jacobe, H.T.; Chong, B.F. and Ariizumi, K.: Myeloid-derived Suppressor Cells in Psoriasis Are an Expanded Population Exhibiting Diverse T cell-Suppressor Mechanisms, The Journal of investigative dermatology, **136** (2016), no. 9, pp. 1801–1810.

[153] Chung, J.-S.; Tamura, K.; Cruz, P.D. and Ariizumi, K.: DC-HIL-expressing myelomonocytic cells are critical promoters of melanoma growth, The Journal of Investigative Dermatology, **134** (2014), no. 11, pp. 2784–2794.

[154] Turrentine, J.; Chung, J.-S.; Nezafati, K.; Tamura, K.; Harker-Murray, A.; Huth, J.; Sharma, R.R.; Harker, D.B.; Ariizumi, K. and Cruz, P.D.: DC-HIL+ CD14+ HLA-DRno/low Cells Are a Potential Blood Marker and Therapeutic Target for Melanoma, The Journal of investigative dermatology, **134** (2014), no. 11, pp. 2839–2842.

[155] Hwang, S.M.; Kang, J.H.; Kim, B.K.; Uhm, T.G.; Kim, H.J.; Lee, H.-H.; Binas, B. and Chung, I.Y.: GPNMB promotes proliferation of developing eosinophils, Journal of Biochemistry, **162** (2017), no. 2, pp. 85–91.

[156] Roth, M.; Barris, D.M.; Piperdi, S.; Kuo, V.; Everts, S.; Geller, D.; Houghton, P.; Kolb, E.A.; Hawthorne, T.; Gill, J. and Gorlick, R.: Targeting Glycoprotein NMB With Antibody-Drug Conjugate, Glembatumumab Vedotin, for the Treatment of Osteosarcoma, Pediatric Blood & Cancer, **63** (2016), no. 1, pp. 32–38.

[157] Tomihari, M.; Chung, J.-S.; Akiyoshi, H.; Cruz, P.D. and Ariizumi, K.: DC-HIL/Gpnmb promotes growth of melanoma in mice by inhibiting the activation of tumor-reactive T cells, Cancer research, **70** (2010), no. 14, pp. 5778–5787.

[158] Lu, Y.; Zhou, D.; Lu, H.; Xu, F.; Yue, J.; Tong, J. and Lu, L.: Investigating a downstream gene of Gpnmb using the systems genetics method, Molecular Vision, **25** (2019), pp. 222–236.

[159] Haraszti, T.; Trantow, C.M.; Hedberg-Buenz, A.; Grunze, M. and Anderson, M.G.: Spectral analysis by XANES reveals that GPNMB influences the chemical composition of intact melanosomes, Pigment Cell & Melanoma Research, **24** (2011), no. 1, pp. 187–196.

[160] Bhattacharyya, S.; Feferman, L. and Tobacman, J.K.: Inhibition of Phosphatase Activity Follows Decline in Sulfatase Activity and Leads to Transcriptional Effects through Sustained Phosphorylation of Transcription Factor MITF, PLoS ONE, **11** (2016), no. 4.

[161] Rose, A.A.N.; Annis, M.G.; Frederick, D.T.; Biondini, M.; Dong, Z.; Kwong, L.; Chin, L.; Keler, T.; Hawthorne, T.; Watson, I.R.; Flaherty, K.T. and Siegel, P.M.: MAPK Pathway Inhibitors Sensitize BRAF-Mutant Melanoma to an Antibody-Drug Conjugate Targeting GPNMB, Clinical Cancer Research: An Official Journal of the American Association for Cancer Research, **22** (2016), no. 24, pp. 6088–6098.

[162] Oh, S.-M.; Shin, J.-S.; Kim, I.-K.; Kim, J.-H.; Moon, J.-S.; Lee, S.-K. and Lee, J.-H.: Therapeutic Effects of HIF-1α on Bone Formation around Implants in Diabetic Mice Using Cell-Penetrating DNA-Binding Protein, Molecules (Basel, Switzerland), **24** (2019), no. 4.

[163] Jeon, M.; Shin, Y.; Jung, J.; Jung, U.-W.; Lee, J.-H.; Moon, J.-S.; Kim, I.; Shin, J.-S.; Lee, S.-K. and Song, J.S.: HIF1A overexpression using cell-penetrating DNA-binding protein induces angiogenesis in vitro and in vivo, Molecular and Cellular Biochemistry, **437** (2018), nos. 1–2, pp. 99–107.

[164] Metz, R.L.; Yehia, G.; Fernandes, H.; Donnelly, R.J. and Rameshwar, P.: Cloning and characterization of the 5' flanking region of the HGFIN gene indicate a cooperative role among p53 and cytokine-mediated transcription factors: relevance to cell cycle regulation, Cell Cycle (Georgetown, Tex.), **4** (2005), no. 2, pp. 315–322.

[165] Tsui, K.-H.; Chang, Y.-L.; Feng, T.-H.; Chang, P.-L. and Juang, H.-H.: Glycoprotein transmembrane nmb: an androgen-downregulated gene attenuates cell invasion and tumorigenesis in prostate carcinoma cells, The Prostate, **72** (2012), no. 13, pp. 1431–1442.

[166] Metz, R.L.; Patel, P.S.; Hameed, M.; Bryan, M. and Rameshwar, P.: Role of human HGFIN/nmb in breast cancer, Breast cancer research: BCR, **9** (2007), no. 5, p. R58.

[167] Athwal, V.S.; Pritchett, J.; Martin, K.; Llewellyn, J.; Scott, J.; Harvey, E.; Zaitoun, A.M.; Mullan, A.F.; Zeef, L.A.H.; Friedman, S.L.; Irving, W.L.; Hanley, N.A.; Guha, I.N. and Hanley, K.P.: SOX9 regulated matrix proteins are increased in patients serum and correlate with severity of liver fibrosis, Scientific Reports, **8** (2018), no. 1, p. 17905.

[168] Abdelmagid, S.M.; Barbe, M.F.; Arango-Hisijara, I.; Owen, T.A.; Popoff, S.N. and Safadi, F.F.: Osteoactivin acts as downstream mediator of BMP-2 effects on osteoblast function, Journal of Cellular Physiology, **210** (2007), no. 1, pp. 26–37.

[169] Tol, M.J.; van der Lienden, M.J.C.; Gabriel, T.L.; Hagen, J.J.; Scheij, S.; Veenendaal, T.; Klumperman, J.; Donker-Koopman, W.E.; Verhoeven, A.J.; Overkleeft, H.; Aerts, J.M.; Argmann, C.A. and van Eijk, M.: HEPES activates a MiT/TFE-dependent lysosomal-autophagic gene network in cultured cells: A call for caution, Autophagy, **14** (2018), no. 3, pp. 437–449.

[170] Gabriel, T.L.; Tol, M.J.; Ottenhof, R.; Roomen, C. van; Aten, J.; Claessen, N.; Hooibrink, B.; Weijer, B. de; Serlie, M.J.; Argmann, C.; Elsenburg, L. van; Aerts, J.M.F.G. and Eijk, M. van: Lysosomal Stress in Obese Adipose Tissue Macrophages Contributes to MITF-Dependent Gpnmb Induction, Diabetes, **63** (2014), no. 10, pp. 3310–3323.

[171] Qian, X.; Mills, E.; Torgov, M.; LaRochelle, W.J. and Jeffers, M.: Pharmacologically enhanced expression of GPNMB increases the sensitivity of melanoma cells to the CR011-vcMMAE antibody-drug conjugate, Molecular Oncology, **2** (2008), no. 1, pp. 81–93.

[172] Ogawa, T.; Nikawa, T.; Furochi, H.; Kosyoji, M.; Hirasaka, K.; Suzue, N.; Sairyo, K.; Nakano, S.; Yamaoka, T.; Itakura, M.; Kishi, K. and Yasui, N.: Osteoactivin upregulates expression of MMP-3 and MMP-9 in fibroblasts infiltrated into denervated skeletal muscle in mice, American Journal of Physiology - Cell Physiology, **289** (2005), no. 3, pp. C697–C707.

[173] Abe, H.; Uto, H.; Takami, Y.; Takahama, Y.; Hasuike, S.; Kodama, M.; Nagata, K.; Moriuchi, A.; Numata, M.; Ido, A. and Tsubouchi, H.: Transgenic expression of osteoactivin in the liver attenuates hepatic fibrosis in rats, Biochemical and Biophysical Research Communications, **356** (2007), no. 3, pp. 610–615.

[174] Furochi, H.; Tamura, S.; Takeshima, K.; Hirasaka, K.; Nakao, R.; Kishi, K. and Nikawa, T.: Overexpression of osteoactivin protects skeletal muscle from severe degeneration caused by long-term denervation in mice, The journal of medical investigation: JMI, **54** (2007), nos. 3–4, pp. 248–254.

[175] Arosarena, O.A.; Barr, E.W.; Thorpe, R.; Yankey, H.; Tarr, J.T. and Safadi, F.F.: Osteoactivin regulates head and neck squamous cell carcinoma invasion by modulating matrix metalloproteases, Journal of Cellular Physiology, **233** (2018), no. 1, pp. 409–421.

[176] Kumagai, K.; Tabu, K.; Sasaki, F.; Takami, Y.; Morinaga, Y.; Mawatari, S.; Hashimoto, S.; Tanoue, S.; Kanmura, S.; Tamai, T.; Moriuchi, A.; Uto, H.; Tsubouchi, H. and Ido, A.: Glycoprotein Nonmetastatic Melanoma B (Gpnmb)-Positive Macrophages Contribute to the Balance between Fibrosis and Fibrolysis during the Repair of Acute Liver Injury in Mice, PloS One, **10** (2015), no. 11, p. e0143413.

[177] Shi, F.; Duan, S.; Cui, J.; Yan, X.; Li, H.; Wang, Y.; Chen, F.; Zhang, L.; Liu, J. and Xie, X.: Induction of matrix metalloproteinase-3 (MMP-3) expression in the microglia by lipopolysaccharide (LPS) via upregulation of glycoprotein nonmetastatic melanoma B (GPNMB) expression, Journal of molecular neuroscience: MN, **54** (2014), no. 2, pp. 234–242.

[178] Tonogai, I.; Takahashi, M.; Yukata, K.; Sato, R.; Nikawa, T.; Yasui, N. and Sairyo, K.: Osteoactivin attenuates skeletal muscle fibrosis after distraction osteogenesis by promoting extracellular matrix degradation/remodeling, Journal of Pediatric Orthopedics. Part B, **24** (2015), no. 2, pp. 162–169.

[179] Järve, A.; Mühlstedt, S.; Qadri, F.; Nickl, B.; Schulz, H.; Hübner, N.; Özcelik, C. and Bader, M.: Adverse left ventricular remodeling by glycoprotein nonmetastatic melanoma protein B in myocardial infarction, FASEB journal: official publication of the Federation of American Societies for Experimental Biology, **31** (2017), no. 2, pp. 556–568.

[180] Roux, P.P. and Blenis, J.: ERK and p38 MAPK-Activated Protein Kinases: a Family of Protein Kinases with Diverse Biological Functions, Microbiology and Molecular Biology Reviews, **68** (2004), no. 2, pp. 320–344.

[181] Cicenas, J.; Zalyte, E.; Rimkus, A.; Dapkus, D.; Noreika, R. and Urbonavicius, S.: JNK, p38, ERK, and SGK1 Inhibitors in Cancer, Cancers, **10** (2018), no. 1, p. 1.

[182] Abdelmagid, S.M.; Sondag, G.R.; Moussa, F.M.; Belcher, J.Y.; Yu, B.; Stinnett, H.; Novak, K.; Mbimba, T.; Khol, M.; Hankenson, K.D.; Malcuit, C. and Safadi, F.F.: Mutation in Osteoactivin Promotes Receptor Activator of NFκB Ligand (RANKL)-mediated Osteoclast Differentiation and Survival but Inhibits Osteoclast Function, Journal of Biological Chemistry, **290** (2015), no. 33, pp. 20128–20146.

[183] Sasaki, F.; Kumagai, K.; Uto, H.; Takami, Y.; Kure, T.; Tabu, K.; Nasu, Y.; Hashimoto, S.; Kanmura, S.; Numata, M.; Moriuchi, A.; Sakiyama, T.; Tsubouchi, H. and Ido, A.: Expression of glycoprotein nonmetastatic melanoma protein B in macrophages infiltrating injured mucosa is associated with the severity of experimental colitis in mice, Molecular Medicine Reports, **12** (2015), no. 5, pp. 7503–7511.

[184] Tanaka, H.; Shimazawa, M.; Kimura, M.; Takata, M.; Tsuruma, K.; Yamada, M.; Takahashi, H.; Hozumi, I.; Niwa, J.; Iguchi, Y.; Nikawa, T.; Sobue, G.; Inuzuka, T. and Hara, H.: The potential of GPNMB as novel neuroprotective factor in amyotrophic lateral sclerosis, Scientific Reports, **2** (2012), p. 573.

[185] Ono, Y.; Tsuruma, K.; Takata, M.; Shimazawa, M. and Hara, H.: Glycoprotein nonmetastatic melanoma protein B extracellular fragment shows neuroprotective effects and activates the PI3K/Akt and MEK/ERK pathways via the Na^+/K^+-ATPase, Scientific Reports, **6** (2016), p. 23241.

[186] Tajima, J.Y.; Futamura, M.; Gaowa, S.; Mori, R.; Tanahashi, T.; Tanaka, Y.; Matsuhashi, N.; Takahashi, T.; Yamaguchi, K.; Miyazaki, T. and Yoshida, K.: Clinical Significance of Glycoprotein Non-metastatic B and Its Association with EGFR/HER2 in Gastrointestinal Cancer, Journal of Cancer, **9** (2018), no. 2, pp. 358–366.

[187] Kanematsu, M.; Futamura, M.; Takata, M.; Gaowa, S.; Yamada, A.; Morimitsu, K.; Morikawa, A.; Mori, R.; Hara, H. and Yoshida, K.: Clinical significance of glycoprotein nonmetastatic B and its association with HER2 in breast cancer, Cancer Medicine, **4** (2015), no. 9, pp. 1344–1355.

[188] Xu, W.; Yang, Z. and Lu, N.: A new role for the PI3K/Akt signaling pathway in the epithelial-mesenchymal transition, Cell Adhesion & Migration, **9** (2015), no. 4, pp. 317–324.

[189] Faderl, S.; Talpaz, M.; Estrov, Z.; O'Brien, S.; Kurzrock, R. and Kantarjian, H.M.: The Biology of Chronic Myeloid Leukemia, http://dx.doi.org/10.1056/NEJM199907153410306, https://www.nejm.org/doi/full/10.1056/NEJM199907153410306, accessed 10 May 2019.

[190] Hantschel, O.; Rix, U. and Superti-Furga, G.: Target spectrum of the BCR-ABL inhibitors imatinib, nilotinib and dasatinib, Leukemia & Lymphoma, **49** (2008), no. 4, pp. 615–619.

[191] Jin, R.; Jin, Y.-Y.; Tang, Y.-L.; Yang, H.-J.; Zhou, X.-Q. and Lei, Z.: GPNMB silencing suppresses the proliferation and metastasis of osteosarcoma cells by blocking the PI3K/Akt/mTOR signaling pathway, Oncology Reports, **39** (2018), no. 6, pp. 3034–3040.

[192] Maric, G.; Annis, M.G.; MacDonald, P.A.; Russo, C.; Perkins, D.; Siwak, D.R.; Mills, G.B. and Siegel, P.M.: GPNMB augments Wnt-1 mediated breast tumor initiation and growth by enhancing PI3K/AKT/mTOR pathway signaling and β-catenin activity, Oncogene, (2019), p. 1.

[193] Mialet-Perez, J. and Vindis, C.: Autophagy in health and disease: focus on the cardiovascular system, Essays in Biochemistry, **61** (2017), no. 6, pp. 721–732.

[194] Mattson, M.P.; Longo, V.D. and Harvie, M.: Impact of intermittent fasting on health and disease processes, Ageing Research Reviews, **39** (2017), pp. 46–58.

[195] Ravanan, P.; Srikumar, I.F. and Talwar, P.: Autophagy: The spotlight for cellular stress responses, Life Sciences, **188** (2017), pp. 53–67.

[196] Tanida, I.: Autophagosome formation and molecular mechanism of autophagy, Antioxidants & Redox Signaling, **14** (2011), no. 11, pp. 2201–2214.

[197] van der Lienden, M.J.C.; Gaspar, P.; Boot, R.; Aerts, J.M.F.G. and van Eijk, M.: Glycoprotein Non-Metastatic Protein B: An Emerging Biomarker for Lysosomal Dysfunction in Macrophages, International Journal of Molecular Sciences, **20** (2018), no. 1.

[198] Murray, P.J.; Allen, J.E.; Biswas, S.K.; Fisher, E.A.; Gilroy, D.W.; Goerdt, S.; Gordon, S.; Hamilton, J.A.; Ivashkiv, L.B.; Lawrence, T.; Locati, M.; Mantovani, A.; Martinez, F.O.; Mege, J.-L.; Mosser, D.M.; Natoli, G.; Saeij, J.P.; Schultze, J.L.; Shirey, K.A.; Sica, A.; Suttles, J.; Udalova, I.; van Ginderachter, J.A.; Vogel, S.N. and Wynn, T.A.: Macrophage activation and polarization: nomenclature and experimental guidelines, Immunity, **41** (2014), no. 1, pp. 14–20.

[199] Ramachandran, P.; Pellicoro, A.; Vernon, M.A.; Boulter, L.; Aucott, R.L.; Ali, A.; Hartland, S.N.; Snowdon, V.K.; Cappon, A.; Gordon-Walker, T.T.; Williams, M.J.; Dunbar, D.R.; Manning, J.R.; van Rooijen, N.; Fallowfield, J.A.; Forbes, S.J. and Iredale, J.P.: Differential Ly-6C expression identifies the recruited macrophage phenotype, which orchestrates the regression of murine liver fibrosis, Proceedings of the National Academy of Sciences of the United States of America, **109** (2012), no. 46, pp. E3186-3195.

[200] Yu, B.; Alboslemy, T.; Safadi, F. and Kim, M.-H.: Glycoprotein Nonmelanoma Clone B Regulates the Crosstalk between Macrophages and Mesenchymal Stem Cells toward Wound Repair, The Journal of Investigative Dermatology, **138** (2018), no. 1, pp. 219–227.

[201] Hudson, A.L.; Parker, N.R.; Khong, P.; Parkinson, J.F.; Dwight, T.; Ikin, R.J.; Zhu, Y.; Chen, J.; Wheeler, H.R. and Howell, V.M.: Glioblastoma Recurrence Correlates With Increased APE1 and Polarization Toward an Immuno-Suppressive Microenvironment, Frontiers in Oncology, **8** (2018), p. 314.

[202] Zhou, L.; Zhuo, H.; Ouyang, H.; Liu, Y.; Yuan, F.; Sun, L.; Liu, F. and Liu, H.: Glycoprotein non-metastatic melanoma protein b (Gpnmb) is highly expressed in macrophages of acute injured kidney and promotes M2 macrophages polarization, Cellular Immunology, **316** (2017), pp. 53–60.

[203] Schlichting, N.; Dehne, T.; Mans, K.; Endres, M.; Stuhlmüller, B.; Sittinger, M.; Kaps, C. and Ringe, J.: Suitability of porcine chondrocyte micromass culture to model osteoarthritis in vitro, Molecular Pharmaceutics, **11** (2014), no. 7, pp. 2092–2105.

[204] Freeman, G.J.; Long, A.J.; Iwai, Y.; Bourque, K.; Chernova, T.; Nishimura, H.; Fitz, L.J.; Malenkovich, N.; Okazaki, T.; Byrne, M.C.; Horton, H.F.; Fouser, L.; Carter, L.; Ling, V.; Bowman, M.R.; Carreno, B.M.; Collins, M.; Wood, C.R. and Honjo, T.: Engagement of the PD-1 immunoinhibitory receptor by a novel B7 family member leads to negative regulation of lymphocyte activation, The Journal of Experimental Medicine, **192** (2000), no. 7, pp. 1027–1034.

[205] Latchman, Y.; Wood, C.R.; Chernova, T.; Chaudhary, D.; Borde, M.; Chernova, I.; Iwai, Y.; Long, A.J.; Brown, J.A.; Nunes, R.; Greenfield, E.A.; Bourque, K.; Boussiotis, V.A.; Carter, L.L.; Carreno, B.M.; Malenkovich, N.; Nishimura, H.; Okazaki, T.; Honjo, T.; Sharpe, A.H. and Freeman, G.J.: PD-L2 is a second ligand for PD-1 and inhibits T cell activation, Nature Immunology, **2** (2001), no. 3, pp. 261–268.

[206] Chen, L. and Flies, D.B.: Molecular mechanisms of T cell co-stimulation and co-inhibition, Nature reviews. Immunology, **13** (2013), no. 4, pp. 227–242.

[207] Leach, D.R.; Krummel, M.F. and Allison, J.P.: Enhancement of Antitumor Immunity by CTLA-4 Blockade, Science, **271** (1996), no. 5256, pp. 1734–1736.

[208] Peach, R.J.; Bajorath, J.; Naemura, J.; Leytze, G.; Greene, J.; Aruffo, A. and Linsley, P.S.: Both Extracellular Immunoglobin-like Domains of CD80 Contain Residues Critical for Binding T Cell Surface Receptors CTLA-4 and CD28, Journal of Biological Chemistry, **270** (1995), no. 36, pp. 21181–21187.

[209] Chung, J.-S.; Cruz, P.D. and Ariizumi, K.: Inhibition of T-cell activation by syndecan-4 is mediated by CD148 through protein tyrosine phosphatase activity, European Journal of Immunology, **41** (2011), no. 6, pp. 1794–1799.

[210] Lin, J. and Weiss, A.: The tyrosine phosphatase CD148 is excluded from the immunologic synapse and down-regulates prolonged T cell signaling, The Journal of Cell Biology, **162** (2003), no. 4, pp. 673–682.

[211] Tian, F.; Liu, C.; Wu, Q.; Qu, K.; Wang, R.; Wei, J.; Meng, F.; Liu, S. and Chang, H.: Upregulation of glycoprotein nonmetastatic B by colony-stimulating factor-1 and epithelial cell adhesion molecule in hepatocellular carcinoma cells, Oncology Research, **20** (2013), no. 8, pp. 341–350.

[212] Grempler, R.; Wolff, M.; Simon, E.; Schmid, R.; Eisele, C.; Rieber, K.; Fischer, E.; Mettel, S.; Gabrielyan, O.; Delic, D.; Luippold, G. and Redeman, N.: Discovery and translation of a target engagement marker for AMP-activated protein kinase (AMPK), PloS One, **13** (2018), no. 5, p. e0197849.

[213] Cardoso, A.L.; Fernandes, A.; Aguilar-Pimentel, J.A.; de Angelis, M.H.; Guedes, J.R.; Brito, M.A.; Ortolano, S.; Pani, G.; Athanasopoulou, S.; Gonos, E.S.; Schosserer, M.; Grillari, J.; Peterson, P.; Tuna, B.G.; Dogan, S.; Meyer, A.; van Os, R. and Trendelenburg, A.-U.: Towards frailty biomarkers: Candidates from genes and pathways regulated in aging and age-related diseases, Ageing Research Reviews, **47** (2018), pp. 214–277.

[214] Patel-Chamberlin, M.; Wang, Y.; Satirapoj, B.; Phillips, L.M.; Nast, C.C.; Dai, T.; Watkins, R.A.; Wu, X.; Natarajan, R.; Leng, A.; Ulanday, K.; Hirschberg, R.R.; Lapage, J.; Nam, E.J.; Haq, T. and Adler, S.G.: Hematopoietic growth

factor inducible neurokinin-1 (Gpnmb/Osteoactivin) is a biomarker of progressive renal injury across species, Kidney International, **79** (2011), no. 10, pp. 1138–1148.

[215] Cluzeau, C.V.M.; Watkins-Chow, D.E.; Fu, R.; Borate, B.; Yanjanin, N.; Dail, M.K.; Davidson, C.D.; Walkley, S.U.; Ory, D.S.; Wassif, C.A.; Pavan, W.J. and Porter, F.D.: Microarray expression analysis and identification of serum biomarkers for Niemann–Pick disease, type C1, Human Molecular Genetics, **21** (2012), no. 16, pp. 3632–3646.

[216] Marques, A.R.A.; Gabriel, T.L.; Aten, J.; van Roomen, C.P.A.A.; Ottenhoff, R.; Claessen, N.; Alfonso, P.; Irún, P.; Giraldo, P.; Aerts, J.M.F.G. and van Eijk, M.: Gpnmb Is a Potential Marker for the Visceral Pathology in Niemann-Pick Type C Disease, PloS One, **11** (2016), no. 1, p. e0147208.

[217] Kramer, G.; Wegdam, W.; Donker-Koopman, W.; Ottenhoff, R.; Gaspar, P.; Verhoek, M.; Nelson, J.; Gabriel, T.; Kallemeijn, W.; Boot, R.G.; Laman, J.D.; Vissers, J.P.C.; Cox, T.; Pavlova, E.; Moran, M.T.; Aerts, J.M. and van Eijk, M.: Elevation of glycoprotein nonmetastatic melanoma protein B in type 1 Gaucher disease patients and mouse models, FEBS open bio, **6** (2016), no. 9, pp. 902–913.

[218] Murugesan, V.; Liu, J.; Yang, R.; Lin, H.; Lischuk, A.; Pastores, G.; Zhang, X.; Chuang, W.-L. and Mistry, P.K.: Validating glycoprotein non-metastatic melanoma B (gpNMB, osteoactivin), a new biomarker of Gaucher disease, Blood Cells, Molecules & Diseases, **68** (2018), pp. 47–53.

[219] Zigdon, H.; Savidor, A.; Levin, Y.; Meshcheriakova, A.; Schiffmann, R. and Futerman, A.H.: Identification of a biomarker in cerebrospinal fluid for neuronopathic forms of Gaucher disease, PloS One, **10** (2015), no. 3, p. e0120194.

[220] Omura, S.; Kawai, E.; Sato, F.; Martinez, N.E.; Chaitanya, G.V.; Rollyson, P.A.; Cvek, U.; Trutschl, M.; Alexander, J.S. and Tsunoda, I.: Bioinformatics multivariate analysis determined a set of phase-specific biomarker candidates in a novel mouse model for viral myocarditis, Circulation. Cardiovascular Genetics, **7** (2014), no. 4, pp. 444–454.

[221] Lin, L.-Y.; Chun Chang, S.; O'Hearn, J.; Hui, S.T.; Seldin, M.; Gupta, P.; Bondar, G.; Deng, M.; Jauhiainen, R.; Kuusisto, J.; Laakso, M.; Sinsheimer, J.S.; Deb, A.; Rau, C.; Ren, S.; Wang, Y.; Lusis, A.J.; Wang, J.J. and Huertas-Vazquez, A.: Systems Genetics Approach to Biomarker Discovery: GPNMB and Heart Failure in Mice and Humans, G3 (Bethesda, Md.), **8** (2018), no. 11, pp. 3499–3506.

[222] Pollack, V.A.; Alvarez, E.; Tse, K.F.; Torgov, M.Y.; Xie, S.; Shenoy, S.G.; MacDougall, J.R.; Arrol, S.; Zhong, H.; Gerwien, R.W.; Hahne, W.F.; Senter, P.D.; Jeffers, M.E.; Lichenstein, H.S. and LaRochelle, W.J.: Treatment parameters modulating regression of human melanoma xenografts by an antibody-drug conjugate (CR011-vcMMAE) targeting GPNMB, Cancer Chemotherapy and Pharmacology, **60** (2007), no. 3, pp. 423–435.

[223] Ott, P.A.; Pavlick, A.C.; Johnson, D.B.; Hart, L.L.; Infante, J.R.; Luke, J.J.; Lutzky, J.; Rothschild, N.E.; Spitler, L.E.; Cowey, C.L.; Alizadeh, A.R.; Salama, A.K.; He, Y.; Hawthorne, T.R.; Bagley, R.G.; Zhang, J.; Turner, C.D. and Hamid, O.: A phase 2 study of glembatumumab vedotin, an antibody-drug conjugate targeting glycoprotein NMB, in patients with advanced melanoma, Cancer, **125** (2019), no. 7, pp. 1113–1123.

[224] Bendell, J.; Saleh, M.; Rose, A.A.N.; Siegel, P.M.; Hart, L.; Sirpal, S.; Jones, S.; Green, J.; Crowley, E.; Simantov, R.; Keler, T.; Davis, T. and Vahdat, L.: Phase I/II study of the antibody-drug conjugate glembatumumab vedotin in patients with locally advanced or metastatic breast cancer, Journal of Clinical Oncology: Official Journal of the American Society of Clinical Oncology, **32** (2014), no. 32, pp. 3619–3625.

[225] Yardley, D.A.; Weaver, R.; Melisko, M.E.; Saleh, M.N.; Arena, F.P.; Forero, A.; Cigler, T.; Stopeck, A.; Citrin, D.; Oliff, I.; Bechhold, R.; Loutfi, R.; Garcia, A.A.; Cruickshank, S.; Crowley, E.; Green, J.; Hawthorne, T.; Yellin, M.J.; Davis, T.A. and Vahdat, L.T.: EMERGE: A Randomized Phase II Study of the Antibody-Drug Conjugate Glembatumumab Vedotin in Advanced Glycoprotein NMB-Expressing Breast Cancer, Journal of Clinical Oncology: Official Journal of the American Society of Clinical Oncology, **33** (2015), no. 14, pp. 1609–1619.

[226] Tray, N.; Adams, S. and Esteva, F.J.: Antibody-drug conjugates in triple negative breast cancer, Future Oncology (London, England), **14** (2018), no. 25, pp. 2651–2661.

[227] Okita, Y.; Chen, C. and Kato, M.: Cell-surface GPNMB and induction of stemness, Oncotarget, **9** (2018), no. 99, pp. 37289–37290.

[228] Hanemaaijer, S.H.; van Gijn, S.E.; Oosting, S.F.; Plaat, B.E.C.; Moek, K.L.; Schuuring, E.M.; van der Laan, B.F.A.M.; Roodenburg, J.L.N.; van Vugt, M.A.T.M.; van der Vegt, B. and Fehrmann, R.S.N.: Data-Driven prioritisation of antibody-drug conjugate targets in head and neck squamous cell carcinoma, Oral Oncology, **80** (2018), pp. 33–39.

[229] Li, H.; Xiao, Y.; Wu, C.-C.; Yang, L.-L.; Cao, L.-Y.; Chen, D.-R.; Zhou, J.-J.; Zhang, W.-F. and Sun, Z.-J.: High expression of GPNMB predicts poor prognosis in head and neck squamous cell carcinoma, Histology and Histopathology, (2019), p. 18084.

[230] Ashktorab, H.; Rahi, H.; Nouraie, M.; Shokrani, B.; Lee, E.; Haydari, T.; Laiyemo, A.O.; Siegel, P. and Brim, H.: GPNMB methylation: a new marker of potentially carcinogenic colon lesions, BMC cancer, **18** (2018), no. 1, p. 1068.

[231] Belone, A. de F.F.; Rosa, P.S.; Trombone, A.P.F.; Fachin, L.R.V.; Guidella, C.C.; Ura, S.; Barreto, J.A.; Pinilla, M.G.; de Carvalho, A.F.; Carraro, D.M.; Soares, F.A. and Soares, C.T.: Genome-Wide Screening of mRNA Expression in Leprosy Patients, Frontiers in Genetics, **6** (2015), p. 334.

[232] Frara, N.; Abdelmagid, S.M.; Sondag, G.R.; Moussa, F.M.; Yingling, V.R.; Owen, T.A.; Popoff, S.N.; Barbe, M.F. and Safadi, F.F.: Transgenic Expression of Osteoactivin/gpnmb Enhances Bone Formation In Vivo and Osteoprogenitor Differentiation Ex Vivo, Journal of Cellular Physiology, **231** (2016), no. 1, pp. 72–83.

[233] Abdelmagid, S.M.; Belcher, J.Y.; Moussa, F.M.; Lababidi, S.L.; Sondag, G.R.; Novak, K.M.; Sanyurah, A.S.; Frara, N.A.; Razmpour, R.; Del Carpio-Cano, F.E. and Safadi, F.F.: Mutation in osteoactivin decreases bone formation in vivo and osteoblast differentiation in vitro, The American Journal of Pathology, **184** (2014), no. 3, pp. 697–713.

[234] Fader, K.A.; Nault, R.; Raehtz, S.; McCabe, L.R. and Zacharewski, T.R.: 2,3,7,8-Tetrachlorodibenzo-p-dioxin dose-dependently increases bone mass and decreases marrow adiposity in juvenile mice, Toxicology and Applied Pharmacology, **348** (2018), pp. 85–98.

[235] Nahrendorf, M.; Pittet, M.J. and Swirski, F.K.: Monocytes: protagonists of infarct inflammation and repair after myocardial infarction, Circulation, **121** (2010), no. 22, pp. 2437–2445.

[236] Brunt, E.M.: Nonalcoholic steatohepatitis, Seminars in Liver Disease, **24** (2004), no. 1, pp. 3–20.

[237] Machado, M.V. and Cortez-Pinto, H.: Non-alcoholic fatty liver disease: What the clinician needs to know, World Journal of Gastroenterology : WJG, **20** (2014), no. 36, pp. 12956–12980.

[238] Nakamura, A.; Ishii, A.; Ohata, C. and Komurasaki, T.: Early induction of osteoactivin expression in rat renal tubular epithelial cells after unilateral ureteral obstruction, Experimental and Toxicologic Pathology: Official Journal of the Gesellschaft Fur Toxikologische Pathologie, **59** (2007), no. 1, pp. 53–59.

[239] Moloney, E.B.; Moskites, A.; Ferrari, E.J.; Isacson, O. and Hallett, P.J.: The glycoprotein GPNMB is selectively elevated in the substantia nigra of Parkinson's disease patients and increases after lysosomal stress, Neurobiology of Disease, **120** (2018), pp. 1–11.

[240] Nagahara, Y.; Shimazawa, M.; Tanaka, H.; Ono, Y.; Noda, Y.; Ohuchi, K.; Tsuruma, K.; Katsuno, M.; Sobue, G. and Hara, H.: Glycoprotein nonmetastatic melanoma protein B ameliorates skeletal muscle lesions in a SOD1G93A mouse model of amyotrophic lateral sclerosis, Journal of Neuroscience Research, **93** (2015), no. 10, pp. 1552–1566.

[241] Lynch, D.V. and Dunn, T.M.: An introduction to plant sphingolipids and a review of recent advances in understanding their metabolism and function, New Phytologist, **161** (2004), no. 3, pp. 677–702.

[242] Yang, Q.; Vijayakumar, A. and Kahn, B.B.: Metabolites as regulators of insulin sensitivity and metabolism, Nature Reviews. Molecular Cell Biology, **19** (2018), no. 10, pp. 654–672.

[243] Alam, Md.S.; Getz, M.; Safeukui, I.; Yi, S.; Tamez, P.; Shin, J.; Velázquez, P. and Haldar, K.: Genomic Expression Analyses Reveal Lysosomal, Innate Immunity Proteins, as Disease Correlates in Murine Models of a Lysosomal Storage Disorder, PLoS ONE, **7** (2012), no. 10.

[244] Mistry, P.K.; Liu, J.; Sun, L.; Chuang, W.-L.; Yuen, T.; Yang, R.; Lu, P.; Zhang, K.; Li, J.; Keutzer, J.; Stachnik, A.; Mennone, A.; Boyer, J.L.; Jain, D.; Brady, R.O.; New, M.I. and Zaidi, M.: Glucocerebrosidase 2 gene deletion rescues type 1 Gaucher disease, Proceedings of the National Academy of Sciences of the United States of America, **111** (2014), no. 13, pp. 4934–4939.

[245] Aburasayn, H.; Al Batran, R. and Ussher, J.R.: Targeting ceramide metabolism in obesity, American Journal of Physiology. Endocrinology and Metabolism, **311** (2016), no. 2, pp. E423-435.

[246] Bruce, C.R.; Risis, S.; Babb, J.R.; Yang, C.; Kowalski, G.M.; Selathurai, A.; Lee-Young, R.S.; Weir, J.M.; Yoshioka, K.; Takuwa, Y.; Meikle, P.J.; Pitson, S.M. and Febbraio, M.A.: Overexpression of sphingosine kinase 1 prevents ceramide accumulation and ameliorates muscle insulin resistance in high-fat diet-fed mice, Diabetes, **61** (2012), no. 12, pp. 3148–3155.

[247] Fayyaz, S.; Henkel, J.; Japtok, L.; Krämer, S.; Damm, G.; Seehofer, D.; Püschel, G.P. and Kleuser, B.: Involvement of sphingosine 1-phosphate in palmitate-induced insulin resistance of hepatocytes via the S1P2 receptor subtype, Diabetologia, **57** (2014), no. 2, pp. 373–382.

[248] Holland, W.L.; Miller, R.A.; Wang, Z.V.; Sun, K.; Barth, B.M.; Bui, H.H.; Davis, K.E.; Bikman, B.T.; Halberg, N.; Rutkowski, J.M.; Wade, M.R.; Tenorio, V.M.; Kuo, M.-S.; Brozinick, J.T.; Zhang, B.B.; Birnbaum, M.J.; Summers,

S.A. and Scherer, P.E.: Receptor-mediated activation of ceramidase activity initiates the pleiotropic actions of adiponectin, Nature Medicine, **17** (2011), no. 1, pp. 55–63.

[249] Bijl, N.; Sokolović, M.; Vrins, C.; Langeveld, M.; Moerland, P.D.; Ottenhoff, R.; Roomen, C.P.A.A. van; Claessen, N.; Boot, R.G.; Aten, J.; Groen, A.K.; Aerts, J.M.F.G. and Eijk, M. van: Modulation of glycosphingolipid metabolism significantly improves hepatic insulin sensitivity and reverses hepatic steatosis in mice, Hepatology, **50** (2009), no. 5, pp. 1431–1441.

[250] Lombardo, E.; van Roomen, C.P.A.A.; van Puijvelde, G.H.; Ottenhoff, R.; van Eijk, M.; Aten, J.; Kuiper, J.; Overkleeft, H.S.; Groen, A.K.; Verhoeven, A.J.; Aerts, J.M.F.G. and Bietrix, F.: Correction of Liver Steatosis by a Hydrophobic Iminosugar Modulating Glycosphingolipids Metabolism, PLoS ONE, **7** (2012), no. 10.

[251] Eijk, M. van; Aten, J.; Bijl, N.; Ottenhoff, R.; Roomen, C.P.A.A. van; Dubbelhuis, P.F.; Seeman, I.; Vlugt, K.G. der; Overkleeft, H.S.; Arbeeny, C.; Groen, A.K. and Aerts, J.M.F.G.: Reducing Glycosphingolipid Content in Adipose Tissue of Obese Mice Restores Insulin Sensitivity, Adipogenesis and Reduces Inflammation, PLOS ONE, **4** (2009), no. 3, p. e4723.

[252] Aureli, M.; Samarani, M.; Murdica, V.; Mauri, L.; Loberto, N.; Bassi, R.; Prinetti, A. and Sonnino, S.: Gangliosides and cell surface ganglioside glycohydrolases in the nervous system, Advances in Neurobiology, **9** (2014), pp. 223–244.

[253] Alvarez-Llamas, G.; Szalowska, E.; de Vries, M.P.; Weening, D.; Landman, K.; Hoek, A.; Wolffenbuttel, B.H.R.; Roelofsen, H. and Vonk, R.J.: Characterization of the human visceral adipose tissue secretome, Molecular & cellular proteomics: MCP, **6** (2007), no. 4, pp. 589–600.

[254] Blüher, M.: Adipokines - removing road blocks to obesity and diabetes therapy, Molecular Metabolism, **3** (2014), no. 3, pp. 230–240.

[255] Dahlman, I.; Elsen, M.; Tennagels, N.; Korn, M.; Brockmann, B.; Sell, H.; Eckel, J. and Arner, P.: Functional annotation of the human fat cell secretome, Archives of Physiology and Biochemistry, **118** (2012), no. 3, pp. 84–91.

[256] Makowski, L.; Boord, J.B.; Maeda, K.; Babaev, V.R.; Uysal, K.T.; Morgan, M.A.; Parker, R.A.; Suttles, J.; Fazio, S.; Hotamisligil, G.S. and Linton, M.F.: Lack of macrophage fatty-acid–binding protein aP2 protects mice deficient in apolipoprotein E against atherosclerosis, Nature medicine, **7** (2001), no. 6, pp. 699–705.

[257] Xu, J.; Jüllig, M.; Middleditch, M.J. and Cooper, G.J.S.: Modelling atherosclerosis by proteomics: Molecular changes in the ascending aortas of cholesterol-fed rabbits, Atherosclerosis, **242** (2015), no. 1, pp. 268–276.

[258] Kattoor, A.J.; Pothineni, N.V.K.; Palagiri, D. and Mehta, J.L.: Oxidative Stress in Atherosclerosis, Current Atherosclerosis Reports, **19** (2017), no. 11, p. 42.

[259] Rios, F.J.; Touyz, R.M. and Montezano, A.C.: Isolation and Differentiation of Murine Macrophages, Methods in Molecular Biology (Clifton, N.J.), **1527** (2017), pp. 297–309.

[260] Tomida, M.; Yamamoto-Yamaguchi, Y. and Hozumi, M.: Purification of a factor inducing differentiation of mouse myeloid leukemic M1 cells from conditioned medium of mouse fibroblast L929 cells., Journal of Biological Chemistry, **259** (1984), no. 17, pp. 10978–10982.

[261] Hjerpe, R.; Aillet, F.; Lopitz-Otsoa, F.; Lang, V.; England, P. and Rodriguez, M.S.: Efficient protection and isolation of ubiquitylated proteins using tandem ubiquitin-binding entities, EMBO Reports, **10** (2009), no. 11, pp. 1250–1258.

[262] Hubner, N.C.; Bird, A.W.; Cox, J.; Splettstoesser, B.; Bandilla, P.; Poser, I.; Hyman, A. and Mann, M.: Quantitative proteomics combined with BAC TransgeneOmics reveals in vivo protein interactions, The Journal of Cell Biology, **189** (2010), no. 4, pp. 739–754.

[263] Howell, G.R.; Libby, R.T.; Marchant, J.K.; Wilson, L.A.; Cosma, I.M.; Smith, R.S.; Anderson, M.G. and John, S.W.M.: Absence of glaucoma in DBA/2J mice homozygous for wild-type versions of Gpnmb and Tyrp1, BMC genetics, **8** (2007), p. 45.

[264] Piedrahita, J.A.; Zhang, S.H.; Hagaman, J.R.; Oliver, P.M. and Maeda, N.: Generation of mice carrying a mutant apolipoprotein E gene inactivated by gene targeting in embryonic stem cells., Proceedings of the National Academy of Sciences of the United States of America, **89** (1992), no. 10, pp. 4471–4475.

[265] Maquat, L.E.: Nonsense-mediated mRNA decay in mammals, Journal of Cell Science, **118** (2005), no. Pt 9, pp. 1773–1776.

[266] Richardson, C.D.; Ray, G.J.; DeWitt, M.A.; Curie, G.L. and Corn, J.E.: Enhancing homology-directed genome editing by catalytically active and inactive CRISPR-Cas9 using asymmetric donor DNA, Nature Biotechnology, **34** (2016), no. 3, pp. 339–344.

[267] Renaud, J.-B.; Boix, C.; Charpentier, M.; De Cian, A.; Cochennec, J.; Duvernois-Berthet, E.; Perrouault, L.; Tesson, L.; Edouard, J.; Thinard, R.; Cherifi, Y.; Menoret, S.; Fontanière, S.; de Crozé, N.; Fraichard, A.; Sohm, F.; Anegon, I.; Concordet, J.-P. and Giovannangeli, C.: Improved Genome Editing Efficiency and Flexibility Using Modified Oligonucleotides with TALEN and CRISPR-Cas9 Nucleases, Cell Reports, **14** (2016), no. 9, pp. 2263–2272.

[268] Cong, L.; Ran, F.A.; Cox, D.; Lin, S.; Barretto, R.; Habib, N.; Hsu, P.D.; Wu, X.; Jiang, W.; Marraffini, L.A. and Zhang, F.: Multiplex genome engineering using CRISPR/Cas systems, Science (New York, N.Y.), **339** (2013), no. 6121, pp. 819–823.

[269] Vierbuchen, T.; Ostermeier, A.; Pang, Z.P.; Kokubu, Y.; Südhof, T.C. and Wernig, M.: Direct conversion of fibroblasts to functional neurons by defined factors, Nature, **463** (2010), no. 7284, pp. 1035–1041.

[270] Yamamoto, A.; Tagawa, Y.; Yoshimori, T.; Moriyama, Y.; Masaki, R. and Tashiro, Y.: Bafilomycin A1 prevents maturation of autophagic vacuoles by inhibiting fusion between autophagosomes and lysosomes in rat hepatoma cell line, H-4-II-E cells, Cell Structure and Function, **23** (1998), no. 1, pp. 33–42.

[271] Yoshimori, T.; Yamamoto, A.; Moriyama, Y.; Futai, M. and Tashiro, Y.: Bafilomycin A1, a specific inhibitor of vacuolar-type H(+)-ATPase, inhibits acidification and protein degradation in lysosomes of cultured cells, The Journal of Biological Chemistry, **266** (1991), no. 26, pp. 17707–17712.

[272] Pasquier, B.: Autophagy inhibitors, Cellular and Molecular Life Sciences, **73** (2016), no. 5, pp. 985–1001.

[273] Bechor, S.; Nachmias, D.; Elia, N.; Haim, Y.; Vatarescu, M.; Leikin-Frenkel, A.; Gericke, M.; Tarnovscki, T.; Las, G. and Rudich, A.: Adipose tissue conditioned media support macrophage lipid-droplet biogenesis by interfering with autophagic flux, Biochimica Et Biophysica Acta. Molecular and Cell Biology of Lipids, **1862** (2017), no. 9, pp. 1001–1012.

[274] Wu, Y.-T.; Tan, H.-L.; Shui, G.; Bauvy, C.; Huang, Q.; Wenk, M.R.; Ong, C.-N.; Codogno, P. and Shen, H.-M.: Dual role of 3-methyladenine in modulation of autophagy via different temporal patterns of inhibition on class I and III phosphoinositide 3-kinase, The Journal of Biological Chemistry, **285** (2010), no. 14, pp. 10850–10861.

[275] Cnop, M.; Abdulkarim, B.; Bottu, G.; Cunha, D.A.; Igoillo-Esteve, M.; Masini, M.; Turatsinze, J.-V.; Griebel, T.; Villate, O.; Santin, I.; Bugliani, M.; Ladriere, L.; Marselli, L.; McCarthy, M.I.; Marchetti, P.; Sammeth, M. and Eizirik, D.L.: RNA sequencing identifies dysregulation of the human pancreatic islet transcriptome by the saturated fatty acid palmitate, Diabetes, **63** (2014), no. 6, pp. 1978–1993.

[276] Mukhopadhyay, S.; Frias, M.A.; Chatterjee, A.; Yellen, P. and Foster, D.A.: The Enigma of Rapamycin Dosage, Molecular Cancer Therapeutics, **15** (2016), no. 3, pp. 347–353.

[277] Halter, D.; Neumann, S.; Dijk, S.M. van; Wolthoorn, J.; Mazière, A.M. de; Vieira, O.V.; Mattjus, P.; Klumperman, J.; Meer, G. van and Sprong, H.: Pre- and post-Golgi translocation of glucosylceramide in glycosphingolipid synthesis, J Cell Biol, **179** (2007), no. 1, pp. 101–115.

[278] Guida, M.C.; Hermle, T.; Graham, L.A.; Hauser, V.; Ryan, M.; Stevens, T.H. and Simons, M.: ATP6AP2 functions as a V-ATPase assembly factor in the endoplasmic reticulum, Molecular Biology of the Cell, **29** (2018), no. 18, pp. 2156–2164.

[279] Kinouchi, K.; Ichihara, A.; Sano, M.; Sun-Wada, G.-H.; Wada, Y.; Kurauchi-Mito, A.; Bokuda, K.; Narita, T.; Oshima, Y.; Sakoda, M.; Tamai, Y.; Sato, H.; Fukuda, K. and Itoh, H.: The (Pro)renin Receptor/ATP6AP2 is Essential for Vacuolar H+-ATPase Assembly in Murine Cardiomyocytes, Circulation Research, **107** (2010), no. 1, pp. 30–34.

[280] Kinouchi, K.; Ichihara, A.; Sano, M.; Sun-Wada, G.-H.; Wada, Y.; Ochi, H.; Fukuda, T.; Bokuda, K.; Kurosawa, H.; Yoshida, N.; Takeda, S.; Fukuda, K. and Itoh, H.: The role of individual domains and the significance of shedding of ATP6AP2/(pro)renin receptor in vacuolar H(+)-ATPase biogenesis, PloS One, **8** (2013), no. 11, p. e78603.

[281] Yuan, N.; Song, L.; Zhang, S.; Lin, W.; Cao, Y.; Xu, F.; Fang, Y.; Wang, Z.; Zhang, H.; Li, X.; Wang, Z.; Cai, J.; Wang, J.; Zhang, Y.; Mao, X.; Zhao, W.; Hu, S.; Chen, S. and Wang, J.: Bafilomycin A1 targets both autophagy and apoptosis pathways in pediatric B-cell acute lymphoblastic leukemia, Haematologica, **100** (2015), no. 3, pp. 345–356.

[282] Belmokhtar, C.A.; Hillion, J. and Ségal-Bendirdjian, E.: Staurosporine induces apoptosis through both caspase-dependent and caspase-independent mechanisms, Oncogene, **20** (2001), no. 26, pp. 3354–3362.

[283] Hinder, L.M.; Vincent, A.M.; Hayes, J.M.; McLean, L.L. and Feldman, E.L.: Apolipoprotein E Knockout as the Basis for Mouse Models of Dyslipidemia-Induced Neuropathy, Experimental neurology, **239** (2013), pp. 102–110.

[284] Plump, A.S.; Smith, J.D.; Hayek, T.; Aalto-Setälä, K.; Walsh, A.; Verstuyft, J.G.; Rubin, E.M. and Breslow, J.L.: Severe hypercholesterolemia and atherosclerosis in apolipoprotein E-deficient mice created by homologous recombination in ES cells, Cell, **71** (1992), no. 2, pp. 343–353.

[285] van der Heijden, R.A.; Sheedfar, F.; Morrison, M.C.; Hommelberg, P.P.H.; Kor, D.; Kloosterhuis, N.J.; Gruben, N.; Youssef, S.A.; de Bruin, A.; Hofker, M.H.; Kleemann, R.; Koonen, D.P.Y. and Heeringa, P.: High-fat diet induced obesity primes inflammation in adipose tissue prior to liver in C57BL/6j mice, Aging, **7** (2015), no. 4, pp. 256–268.

[286] Ibrahim, S.H.; Hirsova, P.; Malhi, H. and Gores, G.J.: Animal Models of Nonalcoholic Steatohepatitis: Eat, Delete, and Inflame, Digestive diseases and sciences, **61** (2016), no. 5, pp. 1325–1336.

[287] Kneer, K.; Green, M.B.; Meyer, J.; Rich, C.B.; Minns, M.S. and Trinkaus-Randall, V.: High fat diet induces pre-type 2 diabetes with regional changes in corneal sensory nerves and altered P2X7 expression and localization, Experimental eye research, **175** (2018), pp. 44–55.

[288] Murano, I.; Barbatelli, G.; Parisani, V.; Latini, C.; Muzzonigro, G.; Castellucci, M. and Cinti, S.: Dead adipocytes, detected as crown-like structures, are prevalent in visceral fat depots of genetically obese mice, Journal of Lipid Research, **49** (2008), no. 7, pp. 1562–1568.

[289] Duckworth, W.C.; Bennett, R.G. and Hamel, F.G.: Insulin Degradation: Progress and Potential, Endocrine Reviews, **19** (1998), no. 5, pp. 608–624.

[290] Jürgens, H.S.; Neschen, S.; Ortmann, S.; Scherneck, S.; Schmolz, K.; Schüler, G.; Schmidt, S.; Blüher, M.; Klaus, S.; Perez-Tilve, D.; Tschöp, M.H.; Schürmann, A. and Joost, H.-G.: Development of diabetes in obese, insulin-resistant mice: essential role of dietary carbohydrate in beta cell destruction, Diabetologia, **50** (2007), no. 7, pp. 1481–1489.

[291] Jones, A.G. and Hattersley, A.T.: The clinical utility of C-peptide measurement in the care of patients with diabetes, Diabetic Medicine, **30** (2013), no. 7, pp. 803–817.

[292] Venugopal, S.K. and Jialal, I.: C Peptide, StatPearls, StatPearls Publishing, Treasure Island (FL), 2019.

[293] Byrne, F.L.; Olzomer, E.M.; Brink, R. and Hoehn, K.L.: Knockout of glucose transporter GLUT6 has minimal effects on whole body metabolic physiology in mice, American Journal of Physiology. Endocrinology and Metabolism, **315** (2018), no. 2, pp. E286–E293.

[294] Leybaert, L.: Neurobarrier Coupling in the Brain: A Partner of Neurovascular and Neurometabolic Coupling?:, Journal of Cerebral Blood Flow & Metabolism, (2016).

[295] Sankar, R.; Thamotharan, S.; Shin, D.; Moley, K.H. and Devaskar, S.U.: Insulin-responsive glucose transporters-GLUT8 and GLUT4 are expressed in the developing mammalian brain, Brain Research. Molecular Brain Research, **107** (2002), no. 2, pp. 157–165.

[296] Schmidt, S.; Joost, H.-G. and Schürmann, A.: GLUT8, the enigmatic intracellular hexose transporter, American Journal of Physiology. Endocrinology and Metabolism, **296** (2009), no. 4, pp. E614-618.

[297] Simpson, I.A.; Carruthers, A. and Vannucci, S.J.: Supply and demand in cerebral energy metabolism: the role of nutrient transporters, Journal of Cerebral Blood Flow and Metabolism: Official Journal of the International Society of Cerebral Blood Flow and Metabolism, **27** (2007), no. 11, pp. 1766–1791.

[298] Mabhida, S.E.; Johnson, R.; Ndlovu, M.; Louw, J.; Opoku, A. and Mosa, R.A.: Molecular basis of the anti-hyperglycemic activity of RA-3 in hyperlipidemic and streptozotocin-induced type 2 diabetes in rats, Diabetology & Metabolic Syndrome, **11** (2019), p. 27.

[299] Martínez-Fernández, L.; González-Muniesa, P.; Laiglesia, L.M.; Sáinz, N.; Prieto-Hontoria, P.L.; Escoté, X.; Odriozola, L.; Corrales, F.J.; Arbones-Mainar, J.M.; Martínez, J.A. and Moreno-Aliaga, M.J.: Maresin 1 improves insulin sensitivity and attenuates adipose tissue inflammation in ob/ob and diet-induced obese mice, The FASEB Journal, (2017).

[300] Zhang, W.; Patil, S.; Chauhan, B.; Guo, S.; Powell, D.R.; Le, J.; Klotsas, A.; Matika, R.; Xiao, X.; Franks, R.; Heidenreich, K.A.; Sajan, M.P.; Farese, R.V.; Stolz, D.B.; Tso, P.; Koo, S.-H.; Montminy, M. and Unterman, T.G.: FoxO1 regulates multiple metabolic pathways in the liver: effects on gluconeogenic, glycolytic, and lipogenic gene expression, The Journal of Biological Chemistry, **281** (2006), no. 15, pp. 10105–10117.

[301] Biggs, W.H.; Meisenhelder, J.; Hunter, T.; Cavenee, W.K. and Arden, K.C.: Protein kinase B/Akt-mediated phosphorylation promotes nuclear exclusion of the winged helix transcription factor FKHR1, Proceedings of the National Academy of Sciences, **96** (1999), no. 13, pp. 7421–7426.

[302] Cross, D.A.; Alessi, D.R.; Vandenheede, J.R.; McDowell, H.E.; Hundal, H.S. and Cohen, P.: The inhibition of glycogen synthase kinase-3 by insulin or insulin-like growth factor 1 in the rat skeletal muscle cell line L6 is blocked by wortmannin, but not by rapamycin: evidence that wortmannin blocks activation of the mitogen-activated protein kinase pathway in L6 cells between Ras and Raf, The Biochemical Journal, **303 (Pt 1)** (1994), pp. 21–26.

[303] Cross, D.A.; Alessi, D.R.; Cohen, P.; Andjelkovich, M. and Hemmings, B.A.: Inhibition of glycogen synthase kinase-3 by insulin mediated by protein kinase B, Nature, **378** (1995), no. 6559, pp. 785–789.

[304] Huaman, C.; Caron, S.; Briand, O.; Dehondt, H.; Duplan, I.; Kuipers, F.; Hennuyer, N.; Clavey, V. and Staels, B.: The human hepatocyte cell lines IHH and HepaRG: Models to study glucose, lipid and lipoprotein metabolism, Archives of physiology and biochemistry, **118** (2012), pp. 102–11.

[305] Matsuzaka, T.; Shimano, H.; Yahagi, N.; Amemiya-Kudo, M.; Okazaki, H.; Tamura, Y.; Iizuka, Y.; Ohashi, K.; Tomita, S.; Sekiya, M.; Hasty, A.; Nakagawa, Y.; Sone, H.; Toyoshima, H.; Ishibashi, S.; Osuga, J. and Yamada, N.: Insulin-Independent Induction of Sterol Regulatory Element-Binding Protein-1c Expression in the Livers of Streptozotocin-Treated Mice, Diabetes, **53** (2004), no. 3, pp. 560–569.

[306] Sanders, F. and Griffin, J.: De novo lipogenesis in the liver in health and disease: More than just a shunting yard for glucose, Biological reviews of the Cambridge Philosophical Society, **91** (2015).

[307] Frias, F. de T.; Rocha, K.C. e; Mendonça, M. de; Murata, G.M.; Araujo, H.N.; Sousa, L.G.O. de; Sousa, É. de; Hirabara, S.M.; Leite, N. de C.; Carneiro, E.M.; Curi, R.; Silveira, L.R. and Rodrigues, A.C.: Fenofibrate reverses changes induced by high-fat diet on metabolism in mice muscle and visceral adipocytes, Journal of Cellular Physiology, **233** (2018), no. 4, pp. 3515–3528.

[308] Dangelmaier, C.; Manne, B.K.; Liverani, E.; Jin, J.; Bray, P. and Kunapuli, S.P.: PDK1 selectively phosphorylates Thr(308) on Akt and contributes to human platelet functional responses, Thrombosis and haemostasis, **111** (2014), no. 3, pp. 508–517.

[309] Downward, J.: Mechanisms and consequences of activation of protein kinase B/Akt, Current Opinion in Cell Biology, **10** (1998), no. 2, pp. 262–267.

[310] Sarbassov, D.D.; Guertin, D.A.; Ali, S.M. and Sabatini, D.M.: Phosphorylation and Regulation of Akt/PKB by the Rictor-mTOR Complex, Science, **307** (2005), no. 5712, pp. 1098–1101.

[311] Maria, Z.; Campolo, A.R. and Lacombe, V.A.: Diabetes Alters the Expression and Translocation of the Insulin-Sensitive Glucose Transporters 4 and 8 in the Atria, PLOS ONE, **10** (2015), no. 12, p. e0146033.

[312] Utsunomiya, K.; Owaki, K.; Okumura, Y.; Yano, M.; Oto, T.; Suzuki, E.; Tamura, S.; Abe, T.; Kohno, S.; Ohno, A.; Hirasaka, K.; Teshima-Kondoh, S. and Nikawa, T.: An intracellular fragment of osteoactivin formed by ectodomain shedding translocated to the nucleoplasm and bound to RNA binding proteins, Bioscience, Biotechnology, and Biochemistry, **76** (2012), no. 12, pp. 2225–2229.

[313] Sasisekharan, R.; Raman, R. and Prabhakar, V.: Glycomics Approach to Structure-Function Relationships of Glycosaminoglycans, Annual Review of Biomedical Engineering, **8** (2006), no. 1, pp. 181–231.

[314] Miyazaki, T.; Miyauchi, S.; Anada, T.; Tawada, A. and Suzuki, O.: Chondroitin Sulfate-E Binds to Both Osteoactivin and Integrin αVβ3 and Inhibits Osteoclast Differentiation, Journal of Cellular Biochemistry, **116** (2015), no. 10, pp. 2247–2257.

[315] Bernfield, M.; Götte, M.; Park, P.W.; Reizes, O.; Fitzgerald, M.L.; Lincecum, J. and Zako, M.: Functions of Cell Surface Heparan Sulfate Proteoglycans, Annual Review of Biochemistry, **68** (1999), no. 1, pp. 729–777.

[316] Lichtenthaler, S.F.; Lemberg, M.K. and Fluhrer, R.: Proteolytic ectodomain shedding of membrane proteins in mammals-hardware, concepts, and recent developments, The EMBO journal, **37** (2018), no. 15.

[317] Berson, J.F.; Harper, D.C.; Tenza, D.; Raposo, G. and Marks, M.S.: Pmel17 Initiates Premelanosome Morphogenesis within Multivesicular Bodies, Molecular Biology of the Cell, **12** (2001), no. 11, pp. 3451–3464.

[318] Huss, M.; Ingenhorst, G.; König, S.; Gassel, M.; Dröse, S.; Zeeck, A.; Altendorf, K. and Wieczorek, H.: Concanamycin A, the specific inhibitor of V-ATPases, binds to the V(o) subunit c, The Journal of Biological Chemistry, **277** (2002), no. 43, pp. 40544–40548.

[319] Wang, S.; Liu, F.; Zeng, Z.; Yang, H. and Jiang, H.: The Protective Effect of Bafilomycin A1 Against Cobalt Nanoparticle-Induced Cytotoxicity and Aseptic Inflammation in Macrophages In Vitro, Biological Trace Element Research, **169** (2016), no. 1, pp. 94–105.

[320] Xu, J.; Feng, H.T.; Wang, C.; Yip, K.H.M.; Pavlos, N.; Papadimitriou, J.M.; Wood, D. and Zheng, M.H.: Effects of Bafilomycin A1: an inhibitor of vacuolar H (+)-ATPases on endocytosis and apoptosis in RAW cells and RAW cell-derived osteoclasts, Journal of Cellular Biochemistry, **88** (2003), no. 6, pp. 1256–1264.

[321] Zhdanov, A.V.; Dmitriev, R.I. and Papkovsky, D.B.: Bafilomycin A1 activates respiration of neuronal cells via uncoupling associated with flickering depolarization of mitochondria, Cellular and Molecular Life Sciences, **68** (2011), no. 5, pp. 903–917.

[322] Kinoshita, K.; Hidaka, H. and Ohkuma, S.: Induction of phagocytic activity of M1 cells by an inhibitor of vacuolar FT-ATPase, bafilomycin A1, FEBS Letters, **337** (1994), no. 3, pp. 221–225.

[323] Teplova, V.V.; Tonshin, A.A.; Grigoriev, P.A.; Saris, N.-E.L. and Salkinoja-Salonen, M.S.: Bafilomycin A1 is a potassium ionophore that impairs mitochondrial functions, Journal of Bioenergetics and Biomembranes, **39** (2007), no. 4, p. 321.

[324] Kinoshita, K.; Waritani, T.; Noto, M.; Takizawa, K.; Minemoto, Y.; Nishikawa, Y. and Ohkuma, S.: Bafilomycin A1 induces apoptosis in PC12 cells independently of intracellular pH, FEBS letters, **398** (1996), no. 1, pp. 61–66.

[325] Redmann, M.; Benavides, G.A.; Berryhill, T.F.; Wani, W.Y.; Ouyang, X.; Johnson, M.S.; Ravi, S.; Barnes, S.; Darley-Usmar, V.M. and Zhang, J.: Inhibition of autophagy with bafilomycin and chloroquine decreases mitochondrial quality and bioenergetic function in primary neurons, Redox Biology, **11** (2016), pp. 73–81.

[326] Xie, Z.; Xie, Y.; Xu, Y.; Zhou, H.; Xu, W. and Dong, Q.: Bafilomycin A1 inhibits autophagy and induces apoptosis in MG63 osteosarcoma cells, Molecular Medicine Reports, **10** (2014), no. 2, pp. 1103–1107.

[327] Giorgi, C.; Bonora, M.; Sorrentino, G.; Missiroli, S.; Poletti, F.; Suski, J.M.; Galindo Ramirez, F.; Rizzuto, R.; Di Virgilio, F.; Zito, E.; Pandolfi, P.P.; Wieckowski, M.R.; Mammano, F.; Del Sal, G. and Pinton, P.: p53 at the endoplasmic reticulum regulates apoptosis in a Ca2+-dependent manner, Proceedings of the National Academy of Sciences of the United States of America, **112** (2015), no. 6, pp. 1779–1784.

[328] Matas, D.; Milyavsky, M.; Shats, I.; Nissim, L.; Goldfinger, N. and Rotter, V.: p53 is a regulator of macrophage differentiation, Cell Death and Differentiation, **11** (2004), no. 4, pp. 458–467.

[329] Hume, D.A. and Gordon, S.: Optimal conditions for proliferation of bone marrow-derived mouse macrophages in culture: the roles of CSF-1, serum, Ca2+, and adherence, Journal of Cellular Physiology, **117** (1983), no. 2, pp. 189–194.

[330] Mattson, M.P. and Chan, S.L.: Calcium orchestrates apoptosis, Nature Cell Biology, **5** (2003), no. 12, p. 1041.

[331] Alfonso, A.; Cabado, A.G.; Vieytes, M.R. and Botana, L.M.: Calcium-pH crosstalks in rat mast cells: cytosolic alkalinization, but not intracellular calcium release, is a sufficient signal for degranulation, British Journal of Pharmacology, **130** (2000), no. 8, pp. 1809–1816.

[332] Bieberich, E.: Synthesis, processing, and function of N-glycans in N-glycoproteins, Advances in neurobiology, **9** (2014), pp. 47–70.

[333] Hildebrand, D.G.; Lehle, S.; Borst, A.; Haferkamp, S.; Essmann, F. and Schulze-Osthoff, K.: α-Fucosidase as a novel convenient biomarker for cellular senescence, Cell Cycle, **12** (2013), no. 12, pp. 1922–1927.

[334] Demaurex, N.: pH Homeostasis of cellular organelles, News in Physiological Sciences: An International Journal of Physiology Produced Jointly by the International Union of Physiological Sciences and the American Physiological Society, **17** (2002), pp. 1–5.

[335] Oot, R.A.; Couoh-Cardel, S.; Sharma, S.; Stam, N.J. and Wilkens, S.: Breaking up and making up: The secret life of the vacuolar H+ -ATPase, Protein Science: A Publication of the Protein Society, **26** (2017), no. 5, pp. 896–909.

[336] Palokangas, H.; Ying, M.; Väänänen, K. and Saraste, J.: Retrograde transport from the pre-Golgi intermediate compartment and the Golgi complex is affected by the vacuolar H+-ATPase inhibitor bafilomycin A1, Molecular Biology of the Cell, **9** (1998), no. 12, pp. 3561–3578.

[337] Licon-Munoz, Y.; Michel, V.; Fordyce, C.A. and Parra, K.J.: F-actin reorganization by V-ATPase inhibition in prostate cancer, Biology Open, **6** (2017), no. 11, pp. 1734–1744.

[338] Galluzzi, L.; Baehrecke, E.H.; Ballabio, A.; Boya, P.; Bravo-San Pedro, J.M.; Cecconi, F.; Choi, A.M.; Chu, C.T.; *et al.*: Molecular definitions of autophagy and related processes, The EMBO Journal, **36** (2017), no. 13, pp. 1811–1836.

[339] Mauvezin, C. and Neufeld, T.P.: Bafilomycin A1 disrupts autophagic flux by inhibiting both V-ATPase-dependent acidification and Ca-P60A/SERCA-dependent autophagosome-lysosome fusion, Autophagy, **11** (2015), no. 8, pp. 1437–1438.

[340] Tyburczy, M.E.; Kotulska, K.; Pokarowski, P.; Mieczkowski, J.; Kucharska, J.; Grajkowska, W.; Roszkowski, M.; Jozwiak, S. and Kaminska, B.: Novel proteins regulated by mTOR in subependymal giant cell astrocytomas of patients with tuberous sclerosis complex and new therapeutic implications, The American Journal of Pathology, **176** (2010), no. 4, pp. 1878–1890.

[341] Möller, K.; Sigurbjornsdottir, S.; Arnthorsson, A.O.; Pogenberg, V.; Dilshat, R.; Fock, V.; Brynjolfsdottir, S.H.; Bindesboll, C.; Bessadottir, M.; Ogmundsdottir, H.M.; Simonsen, A.; Larue, L.; Wilmanns, M.; Thorsson, V.; Steingrimsson, E. and Ogmundsdottir, M.H.: MITF has a central role in regulating starvation-induced autophagy in melanoma, Scientific Reports, **9** (2019).

[342] Varol, C.; Mildner, A. and Jung, S.: Macrophages: development and tissue specialization, Annual Review of Immunology, **33** (2015), pp. 643–675.

[343] Jackaman, C.; Tomay, F.; Duong, L.; Abdol Razak, N.B.; Pixley, F.J.; Metharom, P. and Nelson, D.J.: Aging and cancer: The role of macrophages and neutrophils, Ageing Research Reviews, **36** (2017), pp. 105–116.

[344] Ikushima, H. and Miyazono, K.: TGF-β signal transduction spreading to a wider field: a broad variety of mechanisms for context-dependent effects of TGF-β, Cell and Tissue Research, **347** (2012), no. 1, pp. 37–49.

[345] Wahl, S.M.: Transforming growth factor-β: innately bipolar, Current Opinion in Immunology, **19** (2007), no. 1, pp. 55–62.

[346] Zizzo, G.; Hilliard, B.A.; Monestier, M. and Cohen, P.L.: Efficient clearance of early apoptotic cells by human macrophages requires M2c polarization and MerTK induction, Journal of Immunology (Baltimore, Md.: 1950), **189** (2012), no. 7, pp. 3508–3520.

[347] Matsushita, N.; Hassanein, M.T.; Martinez-Clemente, M.; Lazaro, R.; French, S.W.; Xie, W.; Lai, K.; Karin, M. and Tsukamoto, H.: Gender difference in NASH susceptibility: Roles of hepatocyte Ikkβ and Sult1e1, PLoS ONE, **12** (2017), no. 8.

[348] Schwartz, S.M.; Galis, Z.S.; Rosenfeld, M.E. and Falk, E.: Plaque rupture in humans and mice, Arteriosclerosis, Thrombosis, and Vascular Biology, **27** (2007), no. 4, pp. 705–713.

[349] Grijalva, A.; Xu, X. and Ferrante, A.W.: Autophagy Is Dispensable for Macrophage-Mediated Lipid Homeostasis in Adipose Tissue, Diabetes, **65** (2016), no. 4, pp. 967–980.

[350] Gabriel, T.L.; Mirzaian, M.; Hooibrink, B.; Ottenhoff, R.; van Roomen, C.; Aerts, J.M.F.G. and van Eijk, M.: Induction of Sphk1 activity in obese adipose tissue macrophages promotes survival, PLoS ONE, **12** (2017), no. 7.

[351] Yin, B.; Ma, G.; Yen, C.-Y.; Zhou, Z.; Wang, G.X.; Divino, C.M.; Casares, S.; Chen, S.-H.; Yang, W.-C. and Pan, P.-Y.: Myeloid-derived suppressor cells prevent type 1 diabetes in murine models, Journal of Immunology (Baltimore, Md.: 1950), **185** (2010), no. 10, pp. 5828–5834.

[352] Lee, S.; Kolset, S.O.; Birkeland, K.I.; Drevon, C.A. and Reine, T.M.: Acute exercise increases syndecan-1 and -4 serum concentrations, Glycoconjugate Journal, **36** (2019), no. 2, pp. 113–125.

[353] Morath, I.; Hartmann, T.N. and Orian-Rousseau, V.: CD44: More than a mere stem cell marker, The International Journal of Biochemistry & Cell Biology, **81** (2016), no. Pt A, pp. 166–173.

[354] Liu, L.F.; Kodama, K.; Wei, K.; Tolentino, L.L.; Choi, O.; Engleman, E.G.; Butte, A.J. and McLaughlin, T.: The receptor CD44 is associated with systemic insulin resistance and proinflammatory macrophages in human adipose tissue, Diabetologia, **58** (2015), no. 7, pp. 1579–1586.

[355] Kodama, K.; Horikoshi, M.; Toda, K.; Yamada, S.; Hara, K.; Irie, J.; Sirota, M.; Morgan, A.A.; Chen, R.; Ohtsu, H.; Maeda, S.; Kadowaki, T. and Butte, A.J.: Expression-based genome-wide association study links the receptor CD44 in adipose tissue with type 2 diabetes, Proceedings of the National Academy of Sciences of the United States of America, **109** (2012), no. 18, pp. 7049–7054.

[356] Lee-Sayer, S.S.M.; Dong, Y.; Arif, A.A.; Olsson, M.; Brown, K.L. and Johnson, P.: The Where, When, How, and Why of Hyaluronan Binding by Immune Cells, Frontiers in Immunology, **6** (2015).

[357] Carvalho, E.; Kotani, K.; Peroni, O.D. and Kahn, B.B.: Adipose-specific overexpression of GLUT4 reverses insulin resistance and diabetes in mice lacking GLUT4 selectively in muscle, American Journal of Physiology-Endocrinology and Metabolism, **289** (2005), no. 4, pp. E551–E561.

[358] James, D.E.; Burleigh, K.M. and Kraegen, E.W.: Time Dependence of Insulin Action in Muscle and Adipose Tissue in the Rat In Vivo: An Increasing Response in Adipose Tissue with Time, Diabetes, **34** (1985), no. 10, pp. 1049–1054.

[359] Mårin, P.; Rebuffé-Scrive, M.; Smith, U. and Björntorp, P.: Glucose uptake in human adipose tissue, Metabolism: Clinical and Experimental, **36** (1987), no. 12, pp. 1154–1160.

[360] Kershaw, E.E. and Flier, J.S.: Adipose Tissue as an Endocrine Organ, The Journal of Clinical Endocrinology & Metabolism, **89** (2004), no. 6, pp. 2548–2556.

[361] Kahn, B.B.: Adipose Tissue, Inter-Organ Communication, and the Path to Type 2 Diabetes: The 2016 Banting Medal for Scientific Achievement Lecture, Diabetes, **68** (2019), no. 1, pp. 3–14.

[362] Lee, J.; Moraes-Vieira, P.M.; Castoldi, A.; Aryal, P.; Yee, E.U.; Vickers, C.; Parnas, O.; Donaldson, C.J.; Saghatelian, A. and Kahn, B.B.: Branched Fatty Acid Esters of Hydroxy Fatty Acids (FAHFAs) Protect against Colitis by Regulating Gut Innate and Adaptive Immune Responses, Journal of Biological Chemistry, **291** (2016), no. 42, pp. 22207–22217.

[363] Syed, I.; Lee, J.; Moraes-Vieira, P.M.; Donaldson, C.J.; Sontheimer, A.; Aryal, P.; Wellenstein, K.; Kolar, M.J.; Nelson, A.T.; Siegel, D.; Mokrosinski, J.; Farooqi, I.S.; Zhao, J.J.; Yore, M.M.; Peroni, O.D.; Saghatelian, A. and

Kahn, B.B.: Palmitic Acid Hydroxystearic Acids Activate GPR40, Which Is Involved in Their Beneficial Effects on Glucose Homeostasis, Cell Metabolism, **27** (2018), no. 2, pp. 419-427.e4.

[364] Hammarstedt, A.; Syed, I.; Vijayakumar, A.; Eliasson, B.; Gogg, S.; Kahn, B.B. and Smith, U.: Adipose tissue dysfunction is associated with low levels of the novel Palmitic Acid Hydroxystearic Acids, Scientific Reports, **8** (2018), no. 1, p. 15757.

[365] Pedersen, O.; Kahn, C.R. and Kahn, B.B.: Divergent regulation of the Glut 1 and Glut 4 glucose transporters in isolated adipocytes from Zucker rats, The Journal of Clinical Investigation, **89** (1992), no. 6, pp. 1964–1973.

[366] Kraus, B.J.; Sartoretto, J.L.; Polak, P.; Hosooka, T.; Shiroto, T.; Eskurza, I.; Lee, S.-A.; Jiang, H.; Michel, T. and Kahn, B.B.: Novel role for retinol-binding protein 4 in the regulation of blood pressure, FASEB journal: official publication of the Federation of American Societies for Experimental Biology, **29** (2015), no. 8, pp. 3133–3140.

[367] Lee, S.-A.; Yuen, J.J.; Jiang, H.; Kahn, B.B. and Blaner, W.S.: Adipocyte-specific overexpression of retinol-binding protein 4 causes hepatic steatosis in mice, Hepatology (Baltimore, Md.), **64** (2016), no. 5, pp. 1534–1546.

[368] Yang, Q.; Graham, T.E.; Mody, N.; Preitner, F.; Peroni, O.D.; Zabolotny, J.M.; Kotani, K.; Quadro, L. and Kahn, B.B.: Serum retinol binding protein 4 contributes to insulin resistance in obesity and type 2 diabetes, Nature, **436** (2005), no. 7049, pp. 356–362.

[369] Norseen, J.; Hosooka, T.; Hammarstedt, A.; Yore, M.M.; Kant, S.; Aryal, P.; Kiernan, U.A.; Phillips, D.A.; Maruyama, H.; Kraus, B.J.; Usheva, A.; Davis, R.J.; Smith, U. and Kahn, B.B.: Retinol-Binding Protein 4 Inhibits Insulin Signaling in Adipocytes by Inducing Proinflammatory Cytokines in Macrophages through a c-Jun N-Terminal Kinase- and Toll-Like Receptor 4-Dependent and Retinol-Independent Mechanism, Molecular and Cellular Biology, **32** (2012), no. 10, pp. 2010–2019.

[370] Moraes-Vieira, P.M.; Yore, M.M.; Dwyer, P.M.; Syed, I.; Aryal, P. and Kahn, B.B.: RBP4 activates antigen-presenting cells, leading to adipose tissue inflammation and systemic insulin resistance, Cell metabolism, **19** (2014), no. 3, pp. 512–526.

[371] DeFronzo, R.A.; Jacot, E.; Jequier, E.; Maeder, E.; Wahren, J. and Felber, J.P.: The Effect of Insulin on the Disposal of Intravenous Glucose: Results from Indirect Calorimetry and Hepatic and Femoral Venous Catheterization, Diabetes, **30** (1981), no. 12, pp. 1000–1007.

[372] Boguslavsky, S.; Chiu, T.; Foley, K.P.; Osorio-Fuentealba, C.; Antonescu, C.N.; Bayer, K.U.; Bilan, P.J. and Klip, A.: Myo1c binding to submembrane actin mediates insulin-induced tethering of GLUT4 vesicles, Molecular Biology of the Cell, **23** (2012), no. 20, pp. 4065–4078.

[373] Trefts, E.; Hughey, C.C.; Lantier, L.; Lark, D.S.; Boyd, K.L.; Pozzi, A.; Zent, R. and Wasserman, D.H.: Energy Metabolism Couples Hepatocyte Integrin-linked Kinase to Liver Glucoregulation and the Postabsorptive Response of Mice in an Age-dependent Manner, American Journal of Physiology-Endocrinology and Metabolism, (2019).

[374] Sparks, J.D. and Sparks, C.E.: Insulin regulation of triacylglycerol-rich lipoprotein synthesis and secretion, Biochimica Et Biophysica Acta, **1215** (1994), nos. 1–2, pp. 9–32.

[375] Alessi, D.R.; Andjelkovic, M.; Caudwell, B.; Cron, P.; Morrice, N.; Cohen, P. and Hemmings, B.A.: Mechanism of activation of protein kinase B by insulin and IGF-1., The EMBO Journal, **15** (1996), no. 23, pp. 6541–6551.

[376] Martin, R.J.: Invivo lipogenesis and enzyme levels in adipose and liver tissues from pair-fed genetically obese and lean rats, Life Sciences, **14** (1974), no. 8, pp. 1447–1453.

[377] Buettner, R.; Parhofer, K.G.; Woenckhaus, M.; Wrede, C.E.; Kunz-Schughart, L.A.; Schölmerich, J. and Bollheimer, L.C.: Defining high-fat-diet rat models: metabolic and molecular effects of different fat types, Journal of Molecular Endocrinology, **36** (2006), no. 3, pp. 485–501.

[378] Rendina-Ruedy, E. and Smith, B.J.: Methodological considerations when studying the skeletal response to glucose intolerance using the diet-induced obesity model, BoneKEy Reports, **5** (2016).

[379] Dixon, J.B.; Bhathal, P.S. and O'Brien, P.E.: Nonalcoholic fatty liver disease: predictors of nonalcoholic steatohepatitis and liver fibrosis in the severely obese, Gastroenterology, **121** (2001), no. 1, pp. 91–100.

[380] Chitturi, S.; Abeygunasekera, S.; Farrell, G.C.; Holmes-Walker, J.; Hui, J.M.; Fung, C.; Karim, R.; Lin, R.; Samarasinghe, D.; Liddle, C.; Weltman, M. and George, J.: NASH and insulin resistance: Insulin hypersecretion and specific association with the insulin resistance syndrome, Hepatology (Baltimore, Md.), **35** (2002), no. 2, pp. 373–379.

[381] Cömert, B.; Mas, M.R.; Erdem, H.; Dinc, A.; Saglamkaya, U.; Cigerim, M.; Kuzhan, O.; Unal, T. and Kocabalkan, F.: Insulin resistance in non-alcoholic steatohepatitis, Digestive and Liver Disease: Official Journal of the Italian

Society of Gastroenterology and the Italian Association for the Study of the Liver, **33** (2001), no. 4, pp. 353–358.

[382] Lee, J.H.; Rhee, P.L.; Lee, J.K.; Lee, K.T.; Kim, J.J.; Koh, K.C.; Paik, S.W.; Rhee, J.C. and Choi, K.W.: Role of hyperinsulinemia and glucose intolerance in the pathogenesis of nonalcoholic fatty liver in patients with normal body weight, The Korean Journal of Internal Medicine, **13** (1998), no. 1, pp. 12–14.

[383] Kakimoto, P.A. and Kowaltowski, A.J.: Effects of high fat diets on rodent liver bioenergetics and oxidative imbalance, Redox Biology, **8** (2016), pp. 216–225.

[384] Stephenson, K.; Kennedy, L.; Hargrove, L.; Demieville, J.; Thomson, J.; Alpini, G. and Francis, H.: Updates on Dietary Models of Nonalcoholic Fatty Liver Disease: Current Studies and Insights, Gene Expression, **18** (2018), no. 1, pp. 5–17.

[385] Gyorgy, P. and Goldblatt, H.: Further observations on the production and prevention of dietary hepatic injury in rats, The Journal of Experimental Medicine, **89** (1949), no. 2, pp. 245–268.

[386] Duffield, J.S.; Forbes, S.J.; Constandinou, C.M.; Clay, S.; Partolina, M.; Vuthoori, S.; Wu, S.; Lang, R. and Iredale, J.P.: Selective depletion of macrophages reveals distinct, opposing roles during liver injury and repair, Journal of Clinical Investigation, **115** (2005), no. 1, pp. 56–65.

[387] Huss, M. and Wieczorek, H.: Inhibitors of V-ATPases: old and new players, Journal of Experimental Biology, **212** (2009), no. 3, pp. 341–346.

[388] Chang, K.-C.; Wen, J.-D. and Yang, L.-W.: Functional Importance of Mobile Ribosomal Proteins, BioMed Research International, **2015** (2015), p. 539238.

[389] Xu, X.; Xiong, X. and Sun, Y.: The role of ribosomal proteins in the regulation of cell proliferation, tumorigenesis, and genomic integrity, Science China Life Sciences, **59** (2016), no. 7, pp. 656–672.

[390] Chan, K.T.; Creed, S.J. and Bear, J.E.: Unraveling the enigma: progress towards understanding the coronin family of actin regulators, Trends in Cell Biology, **21** (2011), no. 8, pp. 481–488.

[391] Rosentreter, A.; Hofmann, A.; Xavier, C.-P.; Stumpf, M.; Noegel, A.A. and Clemen, C.S.: Coronin 3 involvement in F-actin-dependent processes at the cell cortex, Experimental Cell Research, **313** (2007), no. 5, pp. 878–895.

[392] Abella, J.V.G.; Galloni, C.; Pernier, J.; Barry, D.J.; Kjær, S.; Carlier, M.-F. and Way, M.: Isoform diversity in the Arp2/3 complex determines actin filament dynamics, Nature Cell Biology, **18** (2016), no. 1, pp. 76–86.

[393] Shao, J.; Zhang, H. and Wang, Z.: Coronin 1c and F-actin Promote Metastasis of Breast Cancer, Medical Science Monitor: International Medical Journal of Experimental and Clinical Research, **24** (2018), pp. 5980–5987.

[394] Cai, L.; Marshall, T.W.; Uetrecht, A.C.; Schafer, D.A. and Bear, J.E.: Coronin 1B coordinates Arp2/3 complex and cofilin activities at the leading edge, Cell, **128** (2007), no. 5, pp. 915–929.

[395] Hsiao, J.Y.; Goins, L.M.; Petek, N.A. and Mullins, R.D.: Arp2/3 complex and cofilin modulate binding of tropomyosin to branched actin networks, Current biology: CB, **25** (2015), no. 12, pp. 1573–1582.

[396] Colpan, M.; Moroz, N.A. and Kostyukova, A.S.: Tropomodulins and Tropomyosins: Working as a Team, Journal of muscle research and cell motility, **34** (2013), no. 0, pp. 247–260.

[397] Gateva, G.; Kremneva, E.; Reindl, T.; Kotila, T.; Kogan, K.; Gressin, L.; Gunning, P.W.; Manstein, D.J.; Michelot, A. and Lappalainen, P.: Tropomyosin Isoforms Specify Functionally Distinct Actin Filament Populations In Vitro, Current Biology, **27** (2017), no. 5, pp. 705–713.

[398] Janco, M.; Bonello, T.T.; Byun, A.; Coster, A.C.F.; Lebhar, H.; Dedova, I.; Gunning, P.W. and Böcking, T.: The impact of tropomyosins on actin filament assembly is isoform specific, Bioarchitecture, **6** (2016), no. 4, pp. 61–75.

[399] Williamson, R.C.; Cowell, C.A.M.; Reville, T.; Roper, J.A.; Rendall, T.C.S. and Bass, M.D.: Coronin-1C Protein and Caveolin Protein Provide Constitutive and Inducible Mechanisms of Rac1 Protein Trafficking, The Journal of Biological Chemistry, **290** (2015), no. 25, pp. 15437–15449.

[400] Zeibig, S.; Büttcher, M.; Goebel, S.; Pauli, J.; Hunger, A.; Ungerer, M.; Gawaz, M. and Münch, G.: The Scavenger Receptor CD68 Regulates Platelet Mediated Oxidized Low-Density Lipoprotein (oxLDL) Deposition in Atherosclerotic Vessels at an Early Stage of Atherosclerosis in *LDLR-/-/<ApoBec<sup>-/-<sup>* Mice | Cell Physiol Biochem, Cellular Physiology & Biochemistry, **52** (2019), no. 4, pp. 681–695.

[401] McCaffrey, K. and Braakman, I.: Protein quality control at the endoplasmic reticulum, Essays In Biochemistry, **60** (2016), no. 2, pp. 227–235.

Abbreviations

3-MA	3-methyladenine
aa	Amino acid(s)
ABCA1	ABC transporter 1
Abca1	ATP-binding cassette subfamily A member 1
Abcg1	ATP-binding cassette sub-family G member 1
Abl	Tyrosine-protein kinase Abl1
ACAT1	Acyl-CoA cholesterol acyltransferase 1
Acc	Acetyl-CoA carboxylase
Acl	ATP-citrate lyase
acLDL	Acetylated LDL
Acs	Acetyl-CoA synthetase
ADAM	A disintegrin and metalloprotease
ALP	Alkaline phosphatase
ALS	Amyotrophic lateral sclerosis
ALT	Alanine aminotransferase
ANOVA	Analysis of variance
AP	Adaptor protein
AP-1	Activator protein 1
aP2	Adipocyte fatty-acid–binding protein
ApoB-100	Apolipoprotein B-100
ApoE	Apolipoprotein E
APS	Ammonium persulfate
Arg1	Arginase 1
Arp2/3	Actin-related protein 2/3
Arpc5	Actin-related protein 2/3 complex subunit 5
Arsb	Lysosomal enzyme Arylsulfatase B
AST	Aspartate aminotransferase
ATG	AuTophaGy-related genes
ATP	adenosine triphosphate
ATP6ap2	V-ATPase associated protein 2
Atp6v0d2	V-ATPase V_0 subunit d2
Baf	Bafilomycin
Bcr	Breakpoint cluster region protein
BFA	Brefeldin A
bFGF	Basic fibroblast growth factor
BiP	Binding immunoglobulin protein
BMDM	Bone marrow-derived macrophages
Bmp-2	Bone morphogenetic protein 2
BSA	Bovine serum albumin
CAMK4	Calcium/Calmodulin-dep- kinase 4
Cas9	Crispr-associated
Ccl3	C-C motif chemokine 3
CCl_4	Carbon tetrachloride
Cd36	Cluster of differentiation 36
cDNA	Complementary DNA
CLS	Crown-like structures
CoA	Coenzyme A
Col	Collagen
Coro	Coronin
Cpt1	Carnitine Palmitoyltransferase 1A
CQ	Chloroquine
Crispr	Clustered regularly interspaced short palindromic repeats
CTLA-4	Cytotoxic T-lymphocyte protein 4
DAPI	4, 6-diamidino-2-phenylindole

DC-HIL	Dendritic Cell-associated, heparan sulfate proteoglycans-dependent integrin ligand
ddH_2O	Double-distilled water
DEPC	Diethylpyrocarbonate
DMEM	Dulbecco's modified Eagle's medium
DMSO	Dimethyl sulfoxide
DNA	Deoxyribonucleic acid
DNase	Deoxyribonuclease
dNTPs	Deoxyribonucleotides
DTT	1,4-Dithiothreitol
EAE	Experimental autoimmune encephalomyelitis
EDTA	Ethylenediaminetetraacetic acid
EEA	Early endosome antigen
Eef1a-1	Elongation factor 1-α-1
EGF	Epidermal growth factor
EGFP	Enhanced green fluorescent protein
EGFR	Epidermal growth factor receptor
ELISA	Enzyme-linked Immunosorbent Assays
ER	Endoplasmatic reticulum
ERK	Extracellular signal-regulated kinases
FACS	Flow cytometry
Fasn	Fatty-acid synthase
FGF2	Fibroblast growth factor 2
FITC	Fluorescein isothyiocyanate
Foxo1	Forkhead box protein O1
fw	Forward
Gapdh	Glyceraldehyde-3-phosphate dehydrogenase
GBA	Glucocerebrosidase
GCA	Golgicide A
GFAP	Glial fibrillary acidic protein
GlcCer	Glucosylceramide
Glut	Glucose transporter
GM130	130 kDa cis-Golgi matrix protein
GM-CSF	Granulocyte-macrophage colony-stimulating factor
GPI	Glycosylphosphatidylinositol
Gpnmb	Glycoprotein nonmetastatic melanoma protein b
Gsk-3β	Glycogen synthase kinase-3β
Gyg1	Glycogenin-1
Gys2	Glycogen [starch] synthase, liver
H&E	Hematoxylin and eosin
HB-EGF	Heparin-binding EGF-like growth factor
HBSS	Hank's balanced salt solution
HCD	High cholesterol diet
HDL	High-density lipoprotein
HDR	Homology-directed repair
HEK293	Human embryonic kidney cells
HEPES	4-(2-hydroxyethyl)-1-piperazineethanesulfonic acid
HFD	High fat diet
HGFIN	Hematopoietic Growth Factor-Inducible Neurokinin-1 type
Hif-1α	Hypoxia-inducible factor 1-α
HOMA-IR	Homeostatic model assessment for insulin resistance
ICC	Immunocytochemistry
IFN	Interferon
Igf-1	Insulin-like growth factor 1
Igf-1r	Insulin-like growth factor 1 receptor
IHC	Immunohistochemistry
IKK β	Inhibitor of κb kinase β
IL	Interleukin
iNOS	Nitric oxide synthase, inducible

Insr	Insulin receptor
IP	Immunoprecipitation
IRS1	Insulin receptor substrate 1
ITAM	Immunoreceptor tyrosine-based activation motif
JNK	Jun N-terminal protein kinase
KEGG	Kyoto Encyclopedia of Genes and Genomes
KLD	Kringle-like domain
LacCer	Lactosylceramide
LaGeSo	Landesamt for Gesundheit und Soziales
Lamp	Lysosome-associated membrane glycoprotein
LC3/Atg8	Microtubule-associated protein 1 light chain 3
Lce	Long-chain fatty acyl elongase
LDL	Low-density lipoprotein
Leup	Leupeptin
LPS	Lipopolysaccharides
LXR	Liver-X-receptor
LysoGL-1	Glucosylsphingosine
M	Marker
mAb	Monoclonal antibody
Mac-2	Galectin-3
MAPK	Mitogen-activated protein kinase
MCP-1	Monocyte chemoattractant protein 1
M-CSF	Macrophage colony-stimulating factor
MDC	Max Delbrück Centrum for Molecular Medicine in the Helmholtz Association
MDDC	Monocyte-derived dendritic cell
MDSC	Myeloid-derived suppressor cell
MEK	Mitogen-activated protein/extracellular signal-regulated kinase kinase
$MgCl_2$	Magnesium chloride
MHC	Major histocompatibility complex
Mitf	Microphthalmia-associated transcription factor
M-MLV	Moloney Murine Leukemia Virus
Mmp	Matrix metalloproteinase
mRNA	Messenger ribonucleic acid
MSH	Melanocyte-stimulating hormone
mTOR	Mammalian target of rapamycin
mTORC	mTOR complex
Myo1c	Unconventional myosin-Ic
n	Number of animals/independent experiments
NADH	Nicotinamide adenine dinucleotide
NADPH	Nicotinamide adenine dinucleotide phosphate
NAFLD	Non-alcoholic fatty liver disease
NASH	Non-alcoholic steatohepatitis
NC	Normal chow
Nceh	Neutral cholesterol ester hydrolases
n.d.	Not detected
NFATc1	Nuclear factor of activated T-cells cytoplasmic 1
NF-κB	Nuclear factor-κB
NHEJ	Nonhomologous end joining
NMR	Nuclear magnetic resonance
NO	Nitric oxide
Nos2	Nitric oxide synthase, inducible
NPD	Niemann-Pick disease
NQ	8-hydroxy-5-nitrochinoline
n.s.	Not significant
ObRa	Leptin receptor
ObRb	Leptin receptor
OLETF rat	Otsuka Long-Evans Tokushima Fatty rat
oxLDL	oxidized LDL

p.	Protein sequence
pAb	Polyclonal antibody
Pahsas	Palmitic acid esters of hydroxy stearic acids
pAKT	Phosphorylated AKT
Palm	Palmitate
PAM	Protospacer-adjacent motif
PBMC	Peripheral blood mononuclear cells
PBMC-DDC	Peripheral blood mononuclear cell-derived dendritic cells
PBS	Phosphate buffered saline
PBST	PBS containing 0.1% Triton X-100
PCR	Polymerase chain reaction
PD-1	Programmed death 1
Pdgf	platelet-derived growth factor
Pdgfr-α	Platelet-derived growth factor receptor-α
PDK1	Phosphoinositide-dependent kinase-1
PFA	Paraformaldehyde
PI3K	Phosphoinositide 3' kinase
PKC	Protein kinase C
PKD	Polycystic kidney disease domain
PMA	Phorbol 12-myristate 13-acetate
Pmel17	Melanocyte protein Pmel
Pparγ	Peroxisome proliferator-activated receptor γ
PPGB	Lysosomal protective protein
proBNP	Pro brain natriuretic peptide
PVDF	Polyvinylidene difluoride
qRT-PCR	Quantitative Real-Time PCR
RANKL	Receptor activator of NF-κB ligand
Rap	Rapamycin
Rbp4	Retinol-binding protein 4
RGD	Arginine-Glycine-Aspartate
RIPA	Radioimmunoprecipitation assay
RNA	Ribonucleic acid
RNase	Ribonuclease
ROS	Reactive oxygen species
RPMI	Roswell Park Memorial Institute
RT	Reverse transcription
rv	Reverse
RXR	Retinoid X receptor
S1P	Sphingosine-1-phosphate
Scd1	Acyl-CoA desaturase 1
SDS	Sodium dodecylsulfate
SDS-PAGE	SDS-Polyacrylamide gel electrophoresis
sgRNA	Single-guide RNA
siRNA	Short interfering RNA
Slc2a	Solute carrier family
SOD1	Superoxide dismutase
Spink1	Serine protease inhibitor, Kazal type 1
SRA	Scavenger receptor A
Srb1	Scavenger receptor class B member 1
Srebp-1c	Sterol regulatory element-binding protein 1c
ssDNA	Single-stranded DNA
STAT6	Signal transducer and transcription activator 6
Sult1e1	Sulfotransferase family E1
TAE	Tris-acetate-EDTA
Tbp	TATA box-binding protein-like protein 1 (Tbpl1)
TBST	Tris-buffered saline containing 0.5% Tween
TCR	T cell receptor
TE	Tris-EDTA

TEMED	Tetramethylethylendiamine
TGFβ	Transforming growth factor β
TGFβR	Tgfβ receptor
T_H	T helper
Thaps	Thapsigargin
Timp-1	Tissue inhibitor of metalloproteinase-1
TLR	Toll-like receptor
Tmod	Tropomodulin
TMT	Tandem Mass Tag
Tnfα	Tumor necrosis factor-α
Tpm	Tropomyosin
Tris	Tris(hydroxymethyl)aminomethane
Trp1	Tyrosinase-related protein 1
TUBE	Tandem Ubiquitin Binding Entity
Tyr	Tyrosinase
UTR	Untranslated region
UV	Ultraviolet
V-ATPase	Vacuolar H^+-ATPase
VCAM-1	Vascular cell adhesion molecule 1
VEGF	Vascular endothelial growth factor
Veh	Vehicle
VLDL	Very low-density lipoprotein
vs.	Versus
w/w	Weight per weight
WB	Western blot

Symbols and Units

%	Percent
*g	Relative centrifugal force
°C	Degree Celcius
A	Ampère
AU	Arbitrary units
bp	Base pair
FI	Fluorescence intensity
g	Gramm
h	Hour
kb	Kilobase
kDa	Kilodalton
kg	Kilogramm
M	Molar
mA	Milliampère
min	Minute
mL	Milliliter
mM	Millimolar
mV	Millivolt
ng	Nanogramm
nm	Nanometer
pmol	Picomole
rpm	Rotations per minute
sec	Second
U	Unit
V	Volt
µL	Microliter
µm	Micrometer
µM	Micromolar

List of Figures

List of Tables

Eidesstattliche Erklärung zur Selbstständigkeit

Hiermit erkläre ich, dass ich die vorliegende Arbeit selbstständig und nur unter der Verwendung der angegebenen Quellen und Hilfsmittel angefertigt habe. Alle Materialien oder Dienstleistungen, die ich von Dritten erhalten habe, sind als solche gekennzeichnet.

Ich versichere, dass ich mich nicht anderswertig um einen Doktorgrad beworben habe oder einen entsprechenden Doktortitel bereits besitze.

Die Promotionsordnung der Mathematisch-Naturwissenschaftlichen Fakultät I vom 27. Juni 2012 der Humboldt-Universität zu Berlin ist mir bekannt.

_____

Bernadette Nickl / Berlin, August 2019